M.Sc. in Mechanical Engineering Thesis

Thermal Analysis and Multi-Objective Optimization of Cascaded and Advanced Absorption Refrigeration Technologies

Submitted By

Yasin Khan

201011015

Supervised By

Prof. Dr. Mohammad Monjurul Ehsan

Department of Mechanical and Production Engineering (MPE)

Islamic University of Technology (IUT)

Gazipur-1704, Bangladesh

May, 2024

Thermal Analysis and Multi-Objective Optimization of Cascaded and Advanced Absorption Refrigeration Technologies

by

Yasin Khan

Student No.: 201011015

A dissertation submitted in partial fulfillment of the requirements for the degree of

MASTER OF SCIENCE (M.Sc.) IN MECHANICAL ENGINEERING

in the

Faculty of Engineering and Technology (FET)

of the

Islamic University of Technology (IUT), Bangladesh

May 2024

turnitin

Similarity Report ID: oid:22779:59960495

PAPER NAME

Thermal Analysis and Multi-objective Optimization of Cascaded and Advanced Absorption Refrigeration technologies

WORD COUNT

53644 Words

CHARACTER COUNT

307547 Characters

PAGE COUNT

231 Pages

FILE SIZE

49.9MB

SUBMISSION DATE

May 25, 2024 3:03 PM GMT+6

REPORT DATE

May 25, 2024 3:07 PM GMT+6

18% Overall Similarity

The combined total of all matches, including overlapping sources, for each database.

- 12% Internet database
- 14% Publications database
- Crossref database
- Crossref Posted Content database

Excluded from Similarity Report

- Submitted Works database
- Bibliographic material

Yasin Khan

checked & verified

Summary

Candidate's Declaration

It is hereby declared that neither this thesis nor any part of it has been submitted elsewhere for the award of any degree or diploma.

Signature of the Candidate

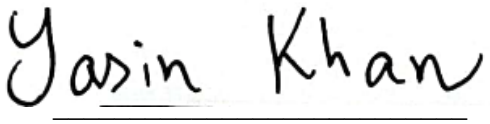

Yasin Khan

Student No.: 201011015
Academic Year: 2020-2021
Date: 23rd May, 2024

Department of Mechanical and Production Engineering (MPE)
Islamic University of Technology (IUT), OIC
Board Bazar, Gazipur-1704
Dhaka, Bangladesh

Signature of the Supervisor

Dr. Mohammad Monjurul Ehsan

Professor

Department of Mechanical and Production Engineering (MPE)
Islamic University of Technology (IUT), OIC
Board Bazar, Gazipur-1704
Dhaka, Bangladesh

Recommendation of the Board of Examiners

The thesis titled "***Thermal Analysis and Multi-Objective Optimization of Cascaded and Advanced Absorption Refrigeration Technologies"*** submitted by Yasin Khan, Student number: 201011015 has been found as satisfactory and accepted partial fulfillment of the requirements for the degree of Master of Science in Mechanical Engineering on 23rd May, 2024.

BOARD OF EXAMINERS

1. (Supervisor) Chairman

Prof. Dr. Mohammad Monjurul Ehsan

Designation: Professor

Address: MPE Department, IUT, Board Bazar, Gazipur-1704.

2. (Ex-Officio) Member

Prof. Dr. Md. Hamidur Rahman

Designation: Professor and Head

Address: MPE Department, IUT, Board Bazar, Gazipur-1704.

3. (Internal) Member

Prof. Dr. Md. Rezwanul Karim

Designation: Professor

Address: MPE Department, IUT, Board Bazar, Gazipur-1704.

4. (External) Member

Prof. Dr. Mohammad Zoynal Abedin

Designation: Professor

Department of Mechanical Engineering

Dhaka University of Engineering & Technology (DUET)
Gazipur, Bangladesh.

Dedication

This thesis is wholeheartedly dedicated to my family, whose unwavering support and love have been the cornerstone of my journey. To my mother, whose sacrifices and strength have inspired me at every turn, and to my wife, whose belief in me has been unfaltering. Your patience, understanding, and encouragement have been my guiding lights. To my father, for instilling in me the values of hard work and perseverance, and to my siblings, for their endless humor and support. You all have contributed in immeasurable ways; this accomplishment is as much yours as it is mine.

Acknowledgments

I extend my deepest appreciation to Allah (SWT) for bestowing upon me the strength and wisdom necessary to complete this thesis both punctually and effectively. This journey has been shaped significantly by numerous individuals, each contributing to the achievements chronicled in this dissertation.

Foremost, my heartfelt thanks to Prof. Dr. Mohammad Monjurul Ehsan, my mentor throughout my M.Sc. studies. Under his guidance, I ventured into new territories of research, always supported me and directed me back on track whenever I veered away. Dr. Ehsan saw potential in me even when I doubted myself, offering unwavering support and mentorship that were crucial for the realization of this dissertation and its accompanying publications. His passion for research and genuine care for his student's success render him an exemplary advisor.

I am also deeply grateful to my friend, Md. Walid Faruq who not only introduced me to the realm of refrigeration but also shared valuable insights and guidance along the way. My appreciation extends to my friend Mahdi Hafi Nabil and my co-researcher, S.M. Naqibul Islam, for their support during the publication process. I owe a debt of gratitude to all faculty members of the MPE department, whose research culture and fervor made this endeavor possible. The encouragement and wisdom of my teachers, colleagues, and brothers have been indispensable. A note of my heartfelt gratitude to everyone at IUT, with a special mention to my dorm and office roommates.

Lastly, my family's unwavering support has been my cornerstone. From urging me to complete my work sooner to purchasing necessary software subscriptions for my research, their role has been instrumental.

My M.Sc. journey, with its highs and lows, from moments of confusion to the triumph of a successful code execution, has been an enriching experience that I will forever cherish.

Yasin Khan

May 2024

Board Bazar, Gazipur- 1704, Dhaka

Table of Contents

List of Figures

List of Tables

List of Symbols

Abbreviation

COP	Coefficient of performance
Ex_{eff}	Exergy efficiency
RAC	Recompression absorption cycle
CARC	Compression absorption refrigeration cycle
EEVCR	Ejector enhanced vapor compression cooling cycle
CRAC	Compression recompression absorption cycle
ECAC	Ejector compression absorption cycle
EICAC	Ejector injection compression absorption cycle
E-CRAC	Ejector compression recompression absorption cycle
EI-CRAC	Ejector enhanced injection recompression absorption cycle
BVIC	Basic vapor injection cycle
EVIC	Ejector enhanced vapor injection cycle
VCR	Vapor compression refrigeration cycle
ARC	Absorption refrigeration cycle
RAC	Recompression absorption cycle
SE-RAC	Solution Ejector enhanced Recompression Absorption Cycle
VI-RAC	Vapor Injection enhanced Recompression Absorption Cycle
RE-RAC	Refrigerant Ejector enhanced Recompression Absorption Cycle
HTC	High-temperature cycle
LTC	Low-temperature cycle
FT	Flash tank cycle
FTSC	Combined flash tank, sub-cooler cycle
DESC	Double expansion sub-cooler cycle
SC	Sub-cooler cycle
EER	Cooling energy efficiency ratio
HFC	Hydrofluorocarbon
ODP	Ozone depletion potential
GWP	Global warming potential
RHX	Refrigerant heat exchanger
CHX	Cascade heat exchanger
SHX	Solution heat exchanger
ANN	Artificial Neural Network
GA	Genetic Algorithm

Symbols

h	Enthalpy [kJ / kg]
P	Pressure [kPa]
a	Area [m^2]
c	Velocity [m/s]
s	Entropy [kJ / (kg K)]
T	Temperature [°C]
$\dot{Ex}$	Exergy [kJ / kg]
$\dot{Q}$	Heat transfer rate [kW]
$\dot{W}$	Rate of work [kW]

$\dot{Ex}_D$	Exergy destruction rate [kW]
ΔP	Pressure drop
ΔT	Temperature difference
mn	Motive nozzle of ejector
sn	Suction nozzle of ejector
m	Mixing chamber of ejector
d	Diffuser of ejector
R_p	Ejector pressure lift ratio

Greek Symbols

η	Efficiency
ρ	Density [kg/m^3]
φ	Area ratio of the mixing chamber
Δ	Difference
ω	Entrainment ratio
ε	Effectiveness of heat exchanger

Subscript

1,2,3,4….	State points
0	Dead state point
is	isentropic
i	inlet
e	outlet
tot	total
gen	Generator
evp	Evaporator
exp	Expansion valve
comp	Compressor
cond	Condenser
abs	Absorber
ext	External
int	Internal

Abstract

This thesis presents an in-depth analysis of advanced modifications of absorption refrigeration systems, with the primary aim of enabling these systems to operate at reduced evaporator temperatures while achieving higher performance. This detailed study marks a significant advancement in refrigeration technology, specifically in the realm of cascade compression absorption refrigeration systems and the advancement of standalone ARC. The goals of this research are to collectively address critical challenges faced by traditional refrigeration cycles, such as energy inefficiency, high compressor power requirements, and environmental concerns, through a comprehensive approach.

The research encompasses the development and simulation of sophisticated cascade compression-absorption refrigeration setups and novel stand-alone absorption system frameworks. Initially, the study focuses on the integration of modified ARC (Absorption Refrigeration Cycle) and advanced RAC (Recompression Absorption Cycle) with enhanced VCRs, incorporated with an ejector to develop advanced proposed novel cascaded configurations: Ejector Compression Absorption Cycle (ECAC), Ejector Injection Compression Absorption Cycle (EICAC), Ejector-Compression Recompression Absorption Cycle (E-CRAC) And Ejector enhanced vapor-Injection Compression Recompression Absorption Cycle (EI-CRAC). Furthermore, the study pioneers the adaptation of novel stand-alone absorption system frameworks, incorporating ejector-injection and recompression technologies to develop Refrigerant Ejector enhanced Recompression Absorption Cycle (RE-RAC) and Vapor Injection enhanced Recompression Absorption Cycle (VI-RAC). Both the advanced cascaded and stand-alone configurations undergo extensive analysis from energy and exergy perspectives, coupled with multi-objective optimization. Utilizing Artificial Neural Network (ANN)-based predictive models, the research meticulously assesses thermal performance, establishing optimal operating conditions and identifying operational limits. This comprehensive evaluation offers profound insights into the systems' behaviors across a spectrum of conditions, enriching our understanding of their potential and constraints in various application scenarios.

The findings reveal that the proposed systems significantly outperform traditional systems in terms of Coefficient of Performance (COP) and exergy efficiency. Specifically, ECAC and EICAC systems achieve approximately 15% and 6% higher COP, respectively, compared to conventional

cascade systems when using the R41-LiBr/H2O refrigerant. Additionally, EICAC and ECAC show significant improvements in exergy efficiency, up to 20% and 10%, respectively, with optimal performance around 77℃ generator temperature. Furthermore, the research explores RAC based proposed cascaded systems: one basic CRAC and two advanced configurations: E-CRAC and EI-CRAC. They significantly outperform the traditional CARC system, with the COP being nearly three times higher. EI-CRAC and E-CRAC show a COP enhancement of about 10% and 20%, respectively, along with an increase in exergy efficiency of 15% and 25% over CRAC, indicating superior efficiency in cooling operations. Finally, this research introduces novel stand-alone recompression absorption refrigeration systems integrating ejector-injection setup to replace expansion valves (RE-RAC and VI-RAC). RE-RAC and VI-RAC significantly outperform conventional ARC and RAC systems. The COP of RE-RAC and VI-RAC is 76% and 63% higher than the conventional RAC system, respectively, despite RE-RAC requiring more external heat generation due to VI-RAC's additional compressor demands.

This research contributes novel insights into the field of refrigeration by analyzing the integration of advanced absorption and compression technologies, providing a pathway for the development of more efficient and environmentally friendly refrigeration systems. The comprehensive analysis from both energetic and exergetic perspectives offers valuable guidance for future improvement and optimization, potentially revolutionizing cooling applications with lower environmental impact. Implementing these systems in real-life scenarios, such as power plants and various industries (e.g., textile, manufacturing, steel), can enhance waste heat utilization by achieving lower evaporator and generator temperatures with higher performance, making them suitable for efficiently using low-grade energy.

Chapter 1: Introduction

1.1 Refrigeration system

Technological advancements and accelerating population growth have fueled a critical demand for more efficient and environmentally sustainable refrigeration technologies. Refrigeration systems are crucial in modern life, significantly impacting our living conditions, food preservation, and coping with extreme weather. These systems play a vital role in maintaining healthy living environments and are key to global economic stability, primarily by preserving food. By slowing down metabolic processes, refrigeration effectively hinders the growth of harmful microorganisms in food, allowing for safe storage without relying on chemical preservatives. Refrigeration plays a vital role in both domestic activities and numerous industrial processes, such as natural gas liquefaction, chilled water provision, pharmaceutical storage, and freezing procedures [1]. The field of application of refrigeration and cooling technology is illustrated in **Figure. 1-1.**

***Figure. 1-1**: Field of application of Refrigeration and Cooling* [2]

According to IEA, cooling will account for 30% of worldwide power consumption by 2050 [3]. This dependence on energy production primarily fueled by fossil fuels [4] exacerbates

environmental concerns, including global warming, CO2 emissions, ozone depletion, and pollution associated with chlorofluorocarbons (CFCs) [5], [6] With the rapid industrialization and increasing quality of life around the world, the demand for energy is surging. To meet this growing need, it's essential to enhance and modify these systems to use electricity more efficiently. This will ensure that refrigeration systems can continue to provide their crucial benefits while minimizing their environmental impact and energy consumption.

1.2 Methods of Refrigeration

The methods of refrigeration can be classified into several categories based on the techniques and principles they employ. These include:

1. **Cyclic Refrigeration**

   a) Mechanical Compression Refrigeration:

   - **Principle:** This method employs a vapor-compression cycle, which involves compressing a refrigerant, condensing it into a liquid, expanding it, and then evaporating it to absorb heat.
   - **Components:** Key components include a compressor, condenser, expansion valve, and evaporator.
   - **Applications:** Widely used in household refrigerators, air conditioners, and large-scale cooling facilities.

   b) Absorption Refrigeration:

   - **Principle:** This method relies on the absorption of a refrigerant by a liquid absorbent; the combined fluid is then separated under heat, and the refrigerant is condensed and evaporated to cause cooling.
   - **Components:** The main components include an absorber, generator, pump, condenser, and evaporator.
   - **Applications:** Suitable for situations where heat is more readily available than electricity, such as industrial waste heat recovery systems.

2. **Non-Cyclic Refrigeration:**

   a) Evaporative Cooling:

   - **Principle:** Utilizes the heat absorbed by water as it evaporates to lower the temperature of the air.
   - **Components:** Consists of a water source, absorbent pads or surfaces, and a fan.
   - **Applications:** Common in dry climates for cooling buildings and in industrial processes.

   b) Ice and Dry Ice: These traditional methods rely on the latent heat of fusion or sublimation to absorb heat. Ice melts at 0°C (32°F), absorbing heat from its surroundings, while dry ice (solid carbon dioxide) sublimates directly from a solid to a gas at -78°C (-109°F), providing even greater cooling power.

3. **Other Methods:**

   a) Thermoelectric Refrigeration:

   - **Principle:** Based on the Peltier effect, where heat is absorbed or released when an electric current passes through two different materials. The illustration is shown in **Figure 1-2** [7].

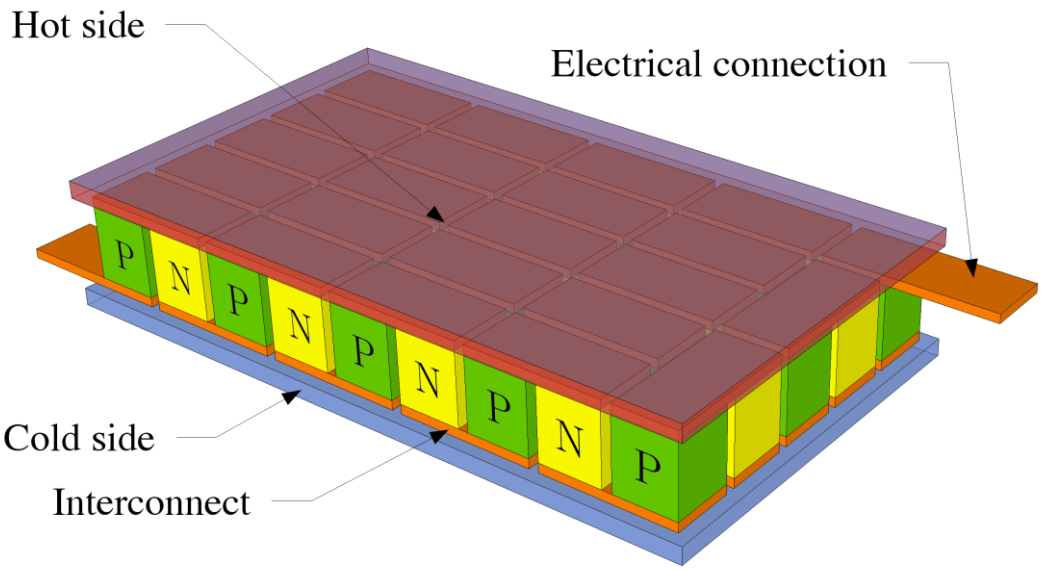

***Figure 1-2**: Illustration of Thermoelectric Refrigeration System* [8]

- **Components:** It mainly consists of Peltier modules and heat sinks.
- **Applications:** Used in small cooling applications like portable coolers and for cooling electronic components.

b) Magnetic Refrigeration:

- **Principle:** Operates on the magnetocaloric effect, where certain materials heat up in the presence of a magnetic field and cool down when removed from it.

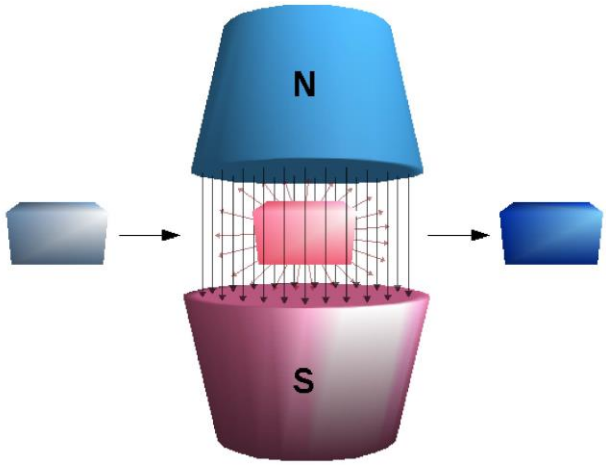

***Figure 1-3**: Illustration of Magnetic Refrigeration System* [9]

- **Components:** Involves a magnetocaloric material, a magnetic field source, and a heat transfer fluid.
- **Applications:** Still in experimental stages, with potential for energy-efficient, environmentally friendly cooling.

c) Cryogenic or Gas Refrigeration:

- **Principle:** Employs the Joule-Thomson effect, where a gas, typically helium or hydrogen, is expanded and cooled.
- **Components:** Includes a high-pressure gas cylinder, expansion valve, and heat exchangers.
- **Applications:** Used for ultra-low temperature applications such as in liquefying gases and in scientific research.

d) Steam Jet Refrigeration:

- **Principle:** Based on the principle of water evaporation under low pressure, which causes cooling.
- **Components:** Consists of a steam ejector, condenser, evaporator, and a boiler or steam generator.
- **Applications:** Often used in industries for cooling large volumes of water or in air conditioning systems for buildings.

e) Thermoacoustic Refrigeration:

- **Principle:** Utilizes sound waves in a gas to create temperature differences and achieve cooling. The principal is illustrated in **Figure 1-4**. [10]

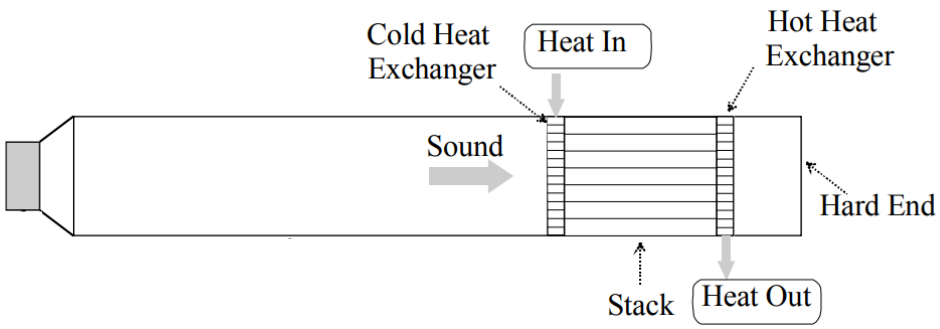

***Figure 1-4**: Illustration of Thermo-acoustic Refrigeration Technology* [10]

- **Components:** Mainly involves a resonator, a stack of plates or tubes, and a sound driver.
- **Applications:** Emerging technology with potential for environmentally friendly refrigeration.

Each of these methods has its unique advantages, limitations, and areas of application, reflecting the diversity and innovation in the field of refrigeration technology.

1. 3 Conventional Cyclic Cooling Systems

Vapor Compression Refrigeration system (VCR) is considered as the most prevalent refrigeration system, given its capacity for diverse utilization, simplicity, and cost-effectiveness. An illustration of simple VCR technology is shown in **Figure 1-5**. While effective, VCR is also notorious for its significantly high electricity consumption and the use of harmful refrigerants that contribute to ozone layer depletion and global warming [11]. Over the years, researchers have developed a plethora of strategies to enhance the Coefficient of Performance (COP) of vapor compression refrigeration systems and make it suitable across different pressure ratios. One approach is utilizing cascade refrigeration systems (CRS), particularly for low-temperature cooling applications. Also, research and studies have been made to reconfigure the system, introducing subcooling prior to expansion, employing vapor injection [12], and replacing the throttle valve with an expander for work recovery. Among these, ejector equipped systems have been proven to be the most sustainable, considering energetic and exergetic performance [13] [14].

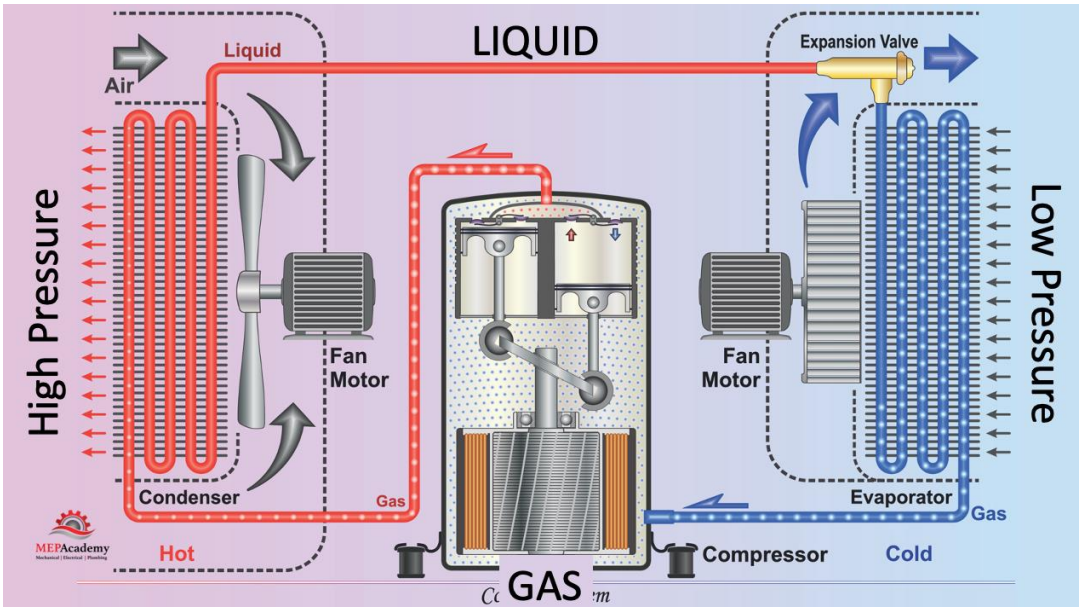

***Figure 1-5**: Illustration of Vapor Compression Refrigeration (VCR) Technology* [15]

The Absorption Refrigeration Cycle (ARC) illustrated in **Figure 1-6** marked a critical shift in the field of refrigeration, offering a fundamentally different principle of operation compared to Vapor Compression Refrigeration (VCR) system. ARC operates based on a solution's ability to absorb a refrigerant, where an absorber-generator assembly replaces the compressor, and heat, rather than

mechanical energy, becomes the primary energy input [16]. This change allows the possibility of using waste or solar heat, making it a potentially more sustainable alternative.

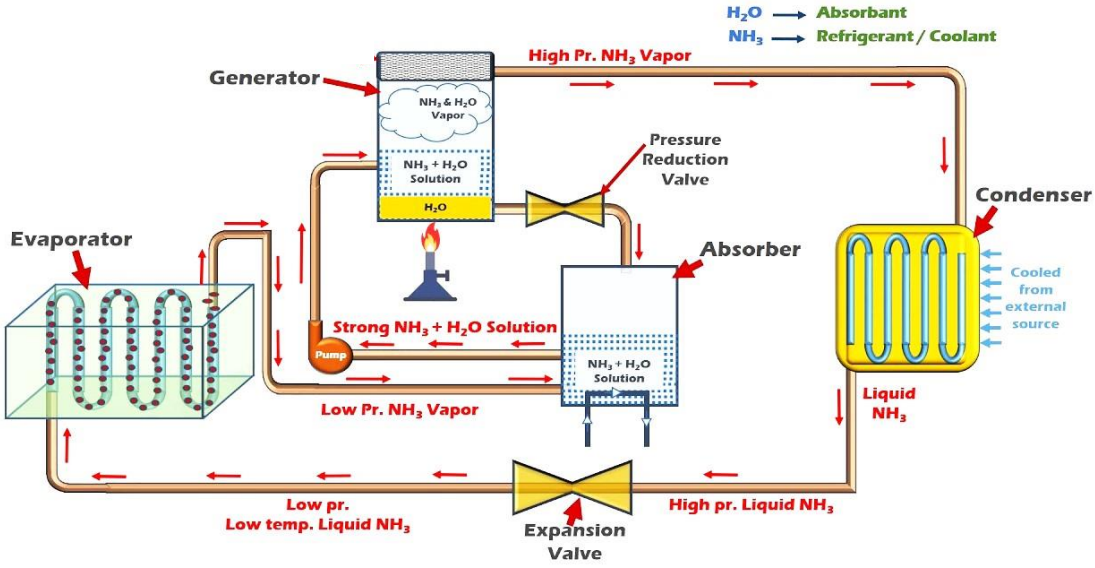

Figure 1-6: *Illustration of Vapor Absorption Refrigeration Cycle (ARC)*[17]

However, despite the promise and potential of the ARC, it is not without its limitations. In particular, the lower Coefficient of Performance (COP) compared to VCR system due to the utilization of low-grade heat, issues of salt crystallization of solution at the absorber inlet stream, and the limitations of water being frozen when evaporator temperature is below freezing temperature of water are significant challenges to be tackled.

1.4 Potential of Cascaded Compression-Absorption System

To address the respective limitations of the VCR and ARC systems while harnessing their individual strengths, the concept of a Combined or Cascaded Compression Absorption Refrigeration Cycle (CARC) was proposed [18]. The configuration permits the system to ensure cooling at lower evaporator temperature due to the use of VCR technology at low temperature cycle (LTC) and significant reduction of compressor's energy consumption due to the use of ARC system at high temperature cycle (HTC) [19]. In the traditional cascaded compression-absorption refrigeration cycle (CARC), a single-effect ARC and a simple VCR are integrated through a cascade heat exchanger. However, this system has several limitations, such as energy waste during throttling in the expansion valve [16], lower heat removal in simple ARC, and the need for a single-stage compressor in VCR [16] resulting in a relatively higher compressor power requirement.

1.5 Scope and Motivation of This Research

The absorption cooling system is a thermally powered refrigeration method using low-grade energy sources. Compared to traditional systems, ARC offers eco-friendly refrigerants, improved waste energy use through heat recovery from various sources, and reduced cycling losses, enhancing flexibility. Studies show ARC can recycle about 50% of unused energy from industries [20]. However, drawbacks include a lower COP, evaporator operational temperature limitations, and potential crystallization at low temperatures. So, enabling ARC system to reach lower evaporator temperature with higher performance is the motivation of this research.

The integration of Absorption Refrigeration Cycle (ARC) with another cycle (i.e., VCR/advanced VCR) can facilitate the system to reach a lower temperature and improve the overall *COP* [21], [22], [23]. Despite the advancements, the literature indicates a significant potential for further enhancement in cascade absorption systems. Investigations have been carried out on traditional Compression Absorption Refrigeration Cycles (CARC), which typically combine a single-effect ARC with a basic VCR via a cascade heat exchanger. However, there is a noticeable gap in the comprehensive analysis of systems integrating advanced ARCs with VCRs. This research aims to bridge this gap by undertaking a comprehensive analysis of cascading various advanced configurations of ARCs and VCRs and contrasting these with conventional systems. It endeavors to contribute novel insights into this field through the development of sophisticated configurations.

The primary goal of this research is to delve into this potential field by integrating a modified ARC and advanced RAC (Recompression Absorption System) with an enhanced VCR, incorporated with an ejector to develop advanced proposed novel configurations: Ejector Compression Absorption Cycle (ECAC), Ejector Injection Compression Absorption Cycle (EICAC), Ejector-Compression Recompression Absorption Cycle (E-CRAC) And Ejector Enhanced Vapor-Injection Compression Recompression Absorption Cycle (EI-CRAC).

Moreover, in a basic ARC system, a significant amount of heat is released in the condenser, presenting an opportunity for heat recovery [24]. Furthermore, the pressure in the generator is determined by the condenser pressure, which cannot be reduced. The RAC (Recompression absorption cycle) has been introduced to harness the rejected heat and enhance the efficiency of the ARC. In the recompression system, ammonia from the generator is recompressed to release heat and condense. This results in higher condensation pressure and Pressure ratio, R_p than basic

ARC [25]. Directly reducing the high pressure of the condensed subcooled ammonia through isenthalpic expansion in a single expansion valve leads to significant energy and exergy losses [26]. In conventional VCR systems, where the pressure ratio is comparably high, replacing the expansion valve and recovering lost energy have been addressed by introducing ejector and vapor injection technologies [11]. These innovations have shown promise in enhancing system efficiency. In this regard, ejector and vapor injection technology have been incorporated in the refrigerant section of the stand-alone RAC cycle to develop proposed advanced recompression absorption systems: Refrigerant Ejector Enhanced Recompression Absorption Cycle (RE-RAC) and Vapor Injection Enhanced Recompression Absorption Cycle (VI-RAC), respectively in this study to develop a stand-alone modification of ARC capable of achieving higher performance at lower evaporator temperature.

1.6 Research Objectives with Specific Aims

The primary aim of the research is **"To enable the Absorption refrigeration system to operate at reduced evaporator temperatures with higher performance."** To achieve this, the study initially focuses on developing and simulating advanced novel cascaded compression-absorption refrigeration setups. By integrating advanced absorption technologies with enhanced Vapor Compression Refrigeration Systems (VCR's), this approach aims to achieve feasible cooling temperatures while enhancing both energetic and exergetic performance at reduced evaporator temperatures.

Furthermore, the study pioneers the adaptation of novel stand-alone absorption system frameworks, incorporating ejector-injection and recompression technologies. This innovation permits the single-effect system to operate at lower evaporator temperatures while simultaneously achieving a higher COP. Both the advanced cascaded and single-effect configurations undergo extensive analysis from energy and exergy perspectives, coupled with multi-objective optimization. Utilizing Artificial Neural Network (ANN)-based predictive models, the research meticulously assesses thermal performance, establishing optimal operating conditions and identifying operational limits. This comprehensive evaluation offers profound insights into the systems' behaviors across a spectrum of conditions, enriching our understanding of their potential and constraints in various application scenarios. The specific objectives are listed below:

i. To model and simulate advanced cascade compression absorption refrigeration technologies to reach feasible cooling temperature (-50℃ to 0℃) providing higher energetic and exergetic performance.
ii. To model and simulate advanced absorption refrigeration cycle equipped with ejector and recompression technologies to reach lower evaporator temperature (-20℃ to 0℃).
iii. To conduct a comprehensive thermal performance assessment of the proposed systems and employ Artificial Neural Network (ANN) based prediction models for multi-objective optimization.

1.7 Significance of This Research

This comprehensive study marks a significant advancement in refrigeration technology, specifically in the realm of cascade compression absorption refrigeration systems and advancement of ARC. The objective of this research collectively addresses critical challenges faced by traditional refrigeration cycles, such as energy inefficiency, high compressor power requirements, and environmental concerns. To fulfill and implement the first objective, a modified Absorption Refrigeration Cycle (ARC) is combined with an improved Vapor Compression Refrigeration (VCR) system, leading to the development of advanced systems like ECAC and EICAC. This research further delves into the field of cascaded compression absorption system by integrating a Recompression Absorption System (RAC) with an enhanced VCR equipped with ejector, resulting in the innovative E-CRAC and EI-CRAC systems. Finally, this research proposes feasible upgrade of standalone single effect ARC by incorporating recompression technology with ejector and injection setup, leading to the development of RE-RAC and VI-RAC systems. These advancements collectively mark a significant leap forward in refrigeration technology.

The cumulative effect of these analysis is a substantial advancement in optimizing the energy and exergy efficiency of refrigeration systems. This collective work not only provides a technical roadmap for developing more efficient refrigeration systems but also contributes to environmental sustainability by proposing systems that are potentially more eco-friendly due to lower greenhouse gas emissions and reduced energy consumption. Moreover, the research embodies a holistic approach to refrigeration technology, encompassing detailed comparative and parametric analyses, first and second law efficiency assessments, and advanced modeling techniques like Artificial Neural Networks (ANNs) and Genetic Algorithms for optimization. This comprehensive analysis

ensures that the proposed systems are not only theoretically sound but also practically viable, offering insights into their real-world applicability and scalability.

This research marks a significant upgrade in existing refrigeration technology, aligning with global sustainability and environmental goals. It introduces more energy-efficient methods by refining traditional refrigeration cycles with innovations like ejectors, vapor injection, and recompression techniques. These advancements are set to influence future refrigeration system designs across various industries, contributing to global energy conservation and environmental protection efforts, and showcasing the ongoing evolution in refrigeration technology towards a more sustainable future.

1.7 Thesis Structure

The thesis study is meticulously organized to explore advanced refrigeration systems through a comprehensive structure, as presented in **Figure 1-7**. It begins with an introduction that sets the stage by delineating the background and the significance of the research. It seamlessly transitions into an extensive literature review that scrutinizes the advancement in Vapor Compression Refrigeration (VCR) systems, modifications of Absorption Refrigeration Cycles (ARC), and the development and analysis of cascaded compression absorption systems.

The study then progresses to a detailed system description, contrasting conventional systems with the proposed innovative designs that include ARC and RAC based cascaded compression absorption systems, and advanced standalone RAC systems equipped with ejector-injection technology. The research methodology is robust, featuring a mix of governing equations, mathematical and ejector modeling, optimization methodologies rooted in machine learning, and a comprehensive mathematical framework that lays out the systemic flow of the study. A rigorous validation process underpins the integrity of the study, evaluating conventional and advanced absorption and VCR-based systems alongside cascade compression technology through multiple lenses, including those with refrigerant pairs like LiBr-H_2O and NH_3-H_2O.

The heart of the thesis lies in the results and discussion section, which is structured into dedicated subsections that offer a thorough analysis of ARC and RAC based cascaded systems, alongside standalone RAC systems.

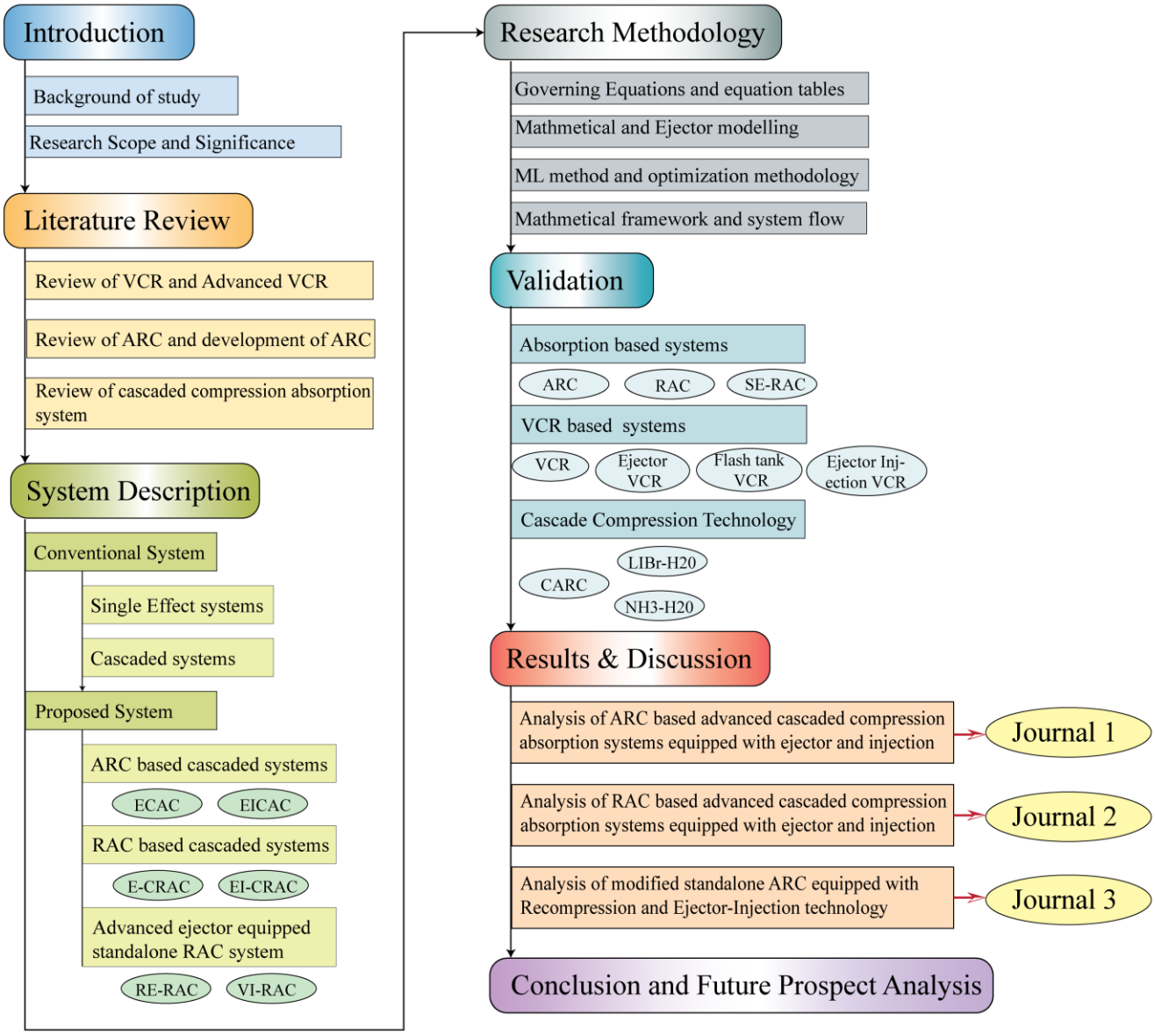

***Figure 1-7**: Structure and outline of the thesis work.*

Each subsection provides a detailed parametric study, alongside a comparative evaluation, integrating multi-objective optimization viewed through the lens of the first and second laws of thermodynamics. The comprehensive nature of these analyses is further enhanced by concise summaries of the corresponding subsections. These sections are crafted with the aim of contributing to peer-reviewed journals, indicating a forward-thinking approach that aims to share findings with the broader academic community. Finally, the thesis culminates with a conclusion and an analysis of future prospects, weaving together the study's findings and laying out a pathway for subsequent research endeavors in the field of refrigeration cycles.

Chapter 2: Literature Review

2.1 Introduction

The refrigeration industry plays an essential part in modern society. Not only does it provide comfortable and healthy living surroundings, but it's also essential for food storage and surviving severe weather conditions. Specifically, food preservation is essential to global economic growth and stability. Metabolic activities are slowed down to prevent the proliferation of microorganisms in order to preserve food. This is simply achievable through cooling or freezing, without the addition of preservatives [27]. One of the primary goals in the field of refrigeration is the development of low-temperature cooling systems that use environmentally friendly, compatible refrigerants with optimal performance in response to the rising demand for cost-effective, safe, and effective refrigeration systems [27]. Researchers in this field have recently moved their attention to discovering alternative working fluids for these systems to combat global warming and ozone layer depletion [28]. Refrigerants have been identified as a significant contributor to global warming and ozone layer depletion [28], [29]. Moreover, almost all modern conveniences require electricity to function; electricity can be thought of as the lifeblood of progress. It's no secret that as the world rapidly industrializes and the quality of life steadily rises, so does the demand for power [30], [31]. The application of refrigeration and air conditioning systems contributes significantly to world energy consumption because these systems require external energy to complete their cycles. Modifications and enhancements of these thermal power consumption systems are necessary to meet the rising demand, as they will enable these systems to utilize electricity more effectively to create the desired result.

2.2 Study on Traditional VCR System and Cascaded VCR Systems

The vapor compression system is a widely accepted refrigeration method because of its simplicity, versatility, and cost-effectiveness. The most common applications of vapor compression refrigeration cycle (VCR) are in liquefying natural gas (108 K or -165°C), household refrigeration, the use of cooled water to supplement industrial procedures (-2°C to -35°C), medicines storage (-50°C to -35°C), and cryogenic processes (below -100°C) [16]. Although the VCR system has many applications and advantages, it has some drawbacks whenorking at low temperatures . A major drawback of low-temperature applications is that the VCR's thermal efficiency reduces when the

evaporator temperature is low, which leads to increase of compressor cost because of high pressure drop [32]. Compressing the refrigerant between high pressure and solidification temperature is challenging. Johnson et al. [32] mentioned two limitation of single-stage vapor compression refrigeration system. First, if the pressure drop is too low, compression becomes too expensive. Second, following compression, the refrigerant's pressure must be below its critical pressure to ensure two-phase condensation. In addition, refrigerants mainly used in a VCR system (either CFCs or HCFCs) are hazardous to the environment and may leak when the system pressures exceed atmospheric pressure by a significant magnitude [33]. For above mentioned reasons, simple VCR is not a viable solution for cryogenic processes and other very low temperature applications from a thermodynamic and cost perspective.

A solution to this issue is the utilization of two-stage or three-stage cascade refrigeration systems (CRS) that are capable of performing cooling operations at moderately low temperatures [34], [35]. The system has the ability to operate between both desirable lower evaporator temperature and higher condensation temperature. Several research has been carried out to optimize and reconfigure individual subsystems of CRS, ensuring their safe and effective operation across various applications, taking into account both energetic and economic perspectives [11].

2.3 Study on the Improvement and Progress of VCR System

In traditional VCR system, the isenthalpic expansion of the refrigerant often leads to significant thermodynamic inefficiencies [36]. These inefficiencies become more pronounced for higher pressure ratio, where irreversibility and entropy generation in compressor operation can compromise system reliability. Numerous approaches have been explored to mitigate the mentioned issues as follows: utilizing subcooling cycles with diverse heat exchangers [37], [38], expansion loss restoration processes employing expanders and ejectors [39], and multi-pressure stage cycles that utilize different refrigerant injection techniques [12]. **Table 2-1** presents a comprehensive overview of the significant studies conducted on the progress and development of VCR technology. Based on the literature review findings, it can be inferred that ejector-enhanced VCR (E-VCR) systems exhibit more efficient performance in low-temperature range refrigeration application than conventional VCRs. Moreover, their significant energy release in the condenser makes them well-suited for cascading with other systems. These aspects highlight their potential for further research and development.

***Table 2-1**. A comprehensive overview of studies conducted on the advancement of VCR technology.*

Proposed Modification	Year	Key Features	Temperature range	Remarks	Reference
Introducing Internal heat exchanger (IHX)	2019	• Experimental study introducing a liquid-suction heat exchanger (SLHX) • Refrigerant used: R290	-40℃ to 70℃	• The potential for savings on energy usage and improved COP can extend up to 27.69% and 38.29%, respectively. • The utilization of R290 additionally contributes to the mitigation of the degradation of the ozone layer and global warming.	D. M. Nasuton et al. [37]
	2019	• Experimental study incorporating internal heat exchanger (IHX) • Refrigerant used: R134a & R513A • Investigated various evaporating and condensing conditions.	-15℃ to 40℃	• R513A increases the refrigeration capability by 5.6%, whereas R134a shoots it up to 3%. • R513A's COP increases by 8% and R134a's by 4% because of the modest electrical consumption reduction. • Empirical data suggests using a high-efficiency intermediate heat exchanger (IHX) for R513A, especially in large compression ratio situations, as long as the output temperature is beneath critical levels.	A. Mota-Babilon et al. [38]
Vapor Injection Technology	2011	• Experimental study comparing the capacity of air-source heat pumps. • Refrigerant used: Air. • Compared cycles: Flash tank (FT) cycle, combined flash tank and sub-cooler (FTSC)	-15℃ to 20℃	• The optimum injection proportion for each cycle option was between 0.2 to 0.3, corresponding to the highest heating capacity. • The overall heating capacities of the FT, FTSC, and DESC systems were 14.5%, 6.3%, and 3.9% higher, each in order compared to the SC system.	J. Heo et al. [40]

		cycle and a double expansion sub-cooler (DESC) cycle.		However, the average COP for all other cycles was very similar.	
	2013	• Experimental study on improved vapor injection refrigeration. • Refrigerant used: R32. • Assessed cooling & heating capability, cooling EER and heating COP.	25℃ to 30℃	• The setup effectively decreases the exit temperatures for cooling and heating operations. • The heating capability is 3% to 9% greater than the single-stage system. Cooling EER, and heating COP are influenced by the refrigerant intermediate pressure and operating conditions. • The optimal range for relative vapor injection mass lies between 12% and 16% to achieve the most favorable cooling and heating performance.	X. Shuxue et al. [41]
Ejector enhanced VCR	2018	• Thermodynamic and numerical investigation. • Refrigerant employed: Zeotropic mixture of R290 & R600a	-30℃ to 55℃	• System COP and cooling ability might be enhanced by 22% and 63.73%. • The EEVCR cycle had a 70% greater COP and cooling capacity than a modified ejector expansion cycle.	M. Elakhdar et al. [39]
	2022	• Numerical energy and exergy analysis on two-stage compression/ejector refrigeration system • Refrigerant used: Transcritical CO_2 • An ejector was used between the heat exchanger and intercooler.	-44℃ to 71℃	• 69.88% of the system's exergy degradation is internal, proposing that the irreversibility of components is the leading cause. • The high-pressure compressor has the most avertible inherent exergy loss, making it the most amenable to optimization. • The system also has a COP of 0.41 under optimal operating conditions and 0.61 during unavoidable processes.	D. Yang et al. [42]

	• Assessed energy performance and exergy destruction		• Ejector, low-pressure, and high-pressure compressor efficiencies of 0.4 to 0.8 boost system exergy efficiency by 5.78%, 36.2%, and 50%. System exergy efficiency dictates a 4.25 MPa intermediate pressure and 8.75 MPa discharge pressure.	
2022	• Exergy analysis on an ejector improved dual-phase evaporation sole-degree VCR • Traditional and modern exergy analysis • Refrigerant used: Transcritical CO_2	9.5℃ to 55℃	• COP of innovative system improves from ejector cycle by 12.1%, dual-phase evaporation by 6.9%, and basic refrigeration by 22.0%. • The exergy investigation demonstrates that the TSEC-E system is capable of reducing the exergy loss during the expansion process by 49.6% and the exergy loss in evaporators by 21.5% compared to the reference cycle. • While the TSEC-E system can be used with different refrigerants, it is particularly well-suited for the CO2 transcritical cycle due to its enhanced effectiveness.	X. Cao et al. [43]
2015	• Thermodynamic analysis of an EVIC • Improving the efficiency by incorporating an ejector connected to a flash tank • Refrigerant used: R22, R290, and R32 • Comparison between the EVIC and BVIC.	-35℃ to 10℃	• Relative to the BVIC, the EVIC with R22, R290, and R32 exhibits 2.5–3.12%, 3.21–3.71%, and 2.91–3.11% better COP, 6.0–8.4%, 7.3–10.2%, and 6.7–8.2% better thermal volume potential. • At the same time, the EVIC reduces compressor output temperature significantly.	X. Wang et al. [14]

Ejector integrated vapor injection technology (EVIC)	2022	• Energic and exergetic analysis on ejector-expansion subcooler vapor-injection refrigeration system • Refrigerant used: Transcritical CO_2 • Enhancing the operational efficiency of CO_2 refrigeration systems	-30℃ to 45℃	• The COP of the proposed cycle exhibits an improvement of approximately 17.9-29.4% compared to the subcooler vapor-injection and ejector-expansion coolant systems. • Similarly, the exergy performance enhances by about 14-28.2%. • Furthermore, it is observed that the reliability of the proposed cycle is particularly enhanced under conditions of low cooling temperature and high surrounding temperature.	M. Q. Zeng et al. [44]
	2023	• Energetic and exergetic analysis on ejector - injection cascade refrigeration system • Enhancing efficiency by integrating an electronic expansion valve with a constant compression ratio (EEVCC) and a variable intercooling fluid temperature (VICFT).	-30℃ to 33℃	• The efficiency of the suggested system is dependent upon pressure drop at ejector and the condensation temperature in the lower circuit. • When the evaporator temperature is set at -60 ℃, the proposed system exhibits an 8.571% increase in the COP and a 7.241% improvement in exergy efficiency compared to the conventional cascade refrigeration system. • The investigation of seven pairs of coolants reveals that R170 and R601 exhibit the highest performance at low-temperature conditions (LTC) and high-temperature conditions (HTC), respectively.	M. Walid Faruque et al. [11]

2.4 Study and Prospects of ARC system

Many studies have been performed searching for substitutes for environmentally hazardous coolants such as CFCs and HCFCs. There is a persistent effort to advance new technologies that can function without these refrigerants, and the issue of power usage is progressively becoming a topic of debate. The practicality of Absorption Refrigeration Cycle (ARC) has been proven as a feasible method for effectively addressing these issues [45]. The absorption cooling system is a thermally powered refrigeration method using low-grade energy sources. Compared to traditional systems, ARC offers eco-friendly refrigerants, improved waste energy use through heat recovery from various sources, and reduced cycling losses, enhancing flexibility. Studies show ARC can recycle about 50% of unused energy from industries [20]. However, drawbacks include a lower COP, operational temperature limitations, and potential crystallization at low temperatures. The *COP* of an ARC system is comparatively lower than that of a standard conventional refrigeration system due to the lower pressure ratio and usage of low-grade energy [46]. The conventional cooling cycle involves converting work to produce cooling effect, while the ARC system utilizes heat directly to drive the process. Besides, the evaporator and absorber pressure are the same in an ARC system, posing a limitation of *COP* improvement. In the context of an ARC system, when the concentration of the water-based coolant is excessively high, or the temperature is significantly reduced, the temperature is possibly transitioning into the crystallization curve, leading to potential crystallization and subsequent disruption of machine performance [47]. So, the evaporator pressure cannot be lowered since it results in a substantially low temperature in the absorber for a particular refrigerant [48].

Numerous methodologies have been investigated to enhance the thermal efficiency of advanced ARC systems. Nikbakhti et al. [45] investigated various improvements of the ARC system to improve its overall efficiency. These strategies encompass utilizing heat recovery techniques, advancements in cycle approach, integration of supplementary sub-components, optimization of innovative functional configurations, and enhancement of working conditions. **Table 2-2** presents a comprehensive overview of the notable studies conducted on the advancement of ARC technology.

The double and triple-effect ARC system exhibits higher *COP* than the conventional ARC system but has some drawbacks [49]. The generator activation temperature for double and triple-effect

ARC systems is high, so the generator load is also high. Besides, the double and triple-effect ARC system is very complex, and their operation cost is also high [50]. On the other hand, in Recompression absorption cycle (RAC), the internal heat exchanger can be utilized, as a result, the condenser can be eliminated from the refrigeration system. Due to the elimination of the condenser in a RAC, the generator's activation temperature reduces, so the generator load reduces and enhances the *COP* simultaneously [24]. Besides, integrating an ejector in an ARC system can widen the cooling system's working pressure and temperature range [51]. Employing an ejector facilitates the rise of the absorber pressure and lessens the evaporator temperature. Recently, the RAC system combined with a solution ejector has been developed and exhibits higher system performance among all the discussed systems [25]. So, it is possible to combine the RAC system and different associate techniques and investigate their system performance and efficiency.

***Table 2-2**: Development on the advancement of absorption refrigeration cycle (ARC)*

Proposed Modification	Reference	Year	Objective	Refrigerants	Temp Range	Remarks
ARC with NH_3-H_2O	Raghuvanshi et al. [52]	2011	• Lower Evaporator Temperature	NH_3-H_2O	2.5°C to 50°C	• COP decreases with increasing generator, absorber, and condenser temperature. • COP increases with decreasing evaporator temperature.
Double effect absorption system	R. Gomri et al. [53]	2009	• Enhance COP • Reduce irreversibility.	LiBr - H_2O	-4°C to 39°C	• COP ranges from 0.73 to 0.79 for single-stage ARC, while it's 1.22 to 1.41 for dual-stage ARC. • Enhancement of exergy efficiency from 23.2% to 25.1% for double-effect ARC
	D Colorado et al.	2015	• Enhance COP • Reduce irreversibility. • Economic analysis	R134a-LiBr /H_2O and	-	• COP enhances about 50% for dual stage ARC • CO_2-LiBr /H_2O exhibits higher COP up to 45% than R134a-LiBr /H_2O

	[54]			CO_2-LiBr /H_2O		• 39% reduced thermal load for R134a-LiBr /H_2O • 17% reduced exergy destruction for R134a-LiBr /H_2O
	M. U. Arshad et al. [55]	2020	• Optimization of series and parallel arrangements • Enhancement of COP • Reducing yearly cost	LiBr - H_2O	4°C to 30°C	• Parallel configurations demonstrated a 6.45% rise in exergy efficiency and a 9.1% increase in COP. • Optimization resulted in 11.68% and 13.73% enhancement in exergy efficiency and COP for series configuration and 21% and 6% for parallel configuration.
Triple effect absorption system	R. Maryam i et al. [56]	2017	• Evaluating the influence of various parameters on COP, thermal load, and exergy.	LiBr-H_2O	4°C to 39°C	• COP enhances with rising evaporator temperature. • COP reduces with rising absorber temperature. • Better COP and exergy efficiency in triple effect ARC than half effect ARC.
	Md. Azhar et al. [57]	2017	• Optimization of operating condition • Enhancement of COP • Reducing the required amount of secondary heat	LiBr - H_2O	4°C to 30°C	• For a specified operation condition, COP of triple effect ARC is 132% higher, and gas requirement is decreased to 122%
	A. Solank et al.	2020	• Investigate the impact of different	LiBr - H_2O	5°C to 40°C	• Exergy efficiency is enhanced with rising generator temperature at a constant absorber temperature (40°C)

	[58]		components on COP and irreversibility			• COP and exergy efficiency enhances with rising evaporator temperature.
Recompression absorption system	Ahmad Dousti et al. [59]	2015	• Enhancement of COP • Reducing heat load at the generator	LiBr - H_2O	0°C to 35°C	• First and second law efficiency is better for RARC than Arc. • Reduced generator load • RARC can operate at lower generator temperatures with a higher-pressure ratio • Utilization of low temperature heat source
	A. Razmi et al. [24]	2018	• Enhancement of COP • Thermal analysis	LiBr-H_2O	10°C to 35°C	• Higher efficiency, about four times more of RARC than ARC • Crystallization possibility is lower than conventional ARC
	A. Razmi et al [60]	2020	• Enhancement of COP • Multi-objective modification	LiBr-H_2O	10°C to 35°C	• Proposed RARC system has a COP of 4.83 and exergy efficiency of 34.84% • A considerable sustainability index of 1.53 • At optimal conditions COP and exergy of RARC enhances up to 4.88% and 37.43% • Payback period is less than 4 years.
Integrating ejector in ARC	C.Vereda et al. [61]	2014	• Enhance the efficiency of single-phase ARC	$LiNO_3$ - H_2O	0°C to 40°C	• Reduced activation temperature • Utilizes low-temperature remaining heat
	A. M. Abed et al.[51]	2015	•Enhanced heat recovery system	NH_3-H_2O	-15°C to 50°C	• About 12.2% enhancement of COP • Reducing the thermal load

			• Reducing Evaporator temperature • Enhancement of COP			• Enhanced refrigeration effect
	Xiao et al. [62]	2019	• Enhancement of absorption technology • Finding a replacement for the solution pump • Enhancement of COP	NH_3/$LiNO_3$ and NH_3/NaSCN	-5°C to 55°C	• Increased efficiency due to utilizing an ejector instead of a mechanical pump • Maximum COP of 0.6354 • COP enhances up to a certain limit with increasing generator temperature and then reduces. • Ejector enhances efficiency by increasing absorber pressure. • Reduced absorber exit temperature decreases thermal load
	A. Dhahi Gharir et al. [63]	2023	• Enhancement of COP • Reduction of thermal load	NH_3-H_2O		• Flash tank among evaporator and condenser increases the ejector's entrainment ratio • Enhanced refrigeration capacity • Reduced thermal load • Energy efficiency increases up to 17.8% • Exergy efficiency enhanced by up to 11.12% • Reduced Cost
Recompression with solution ejector	Ahmad Zarei et al. [25]	2023	• Enhancement of *COP* • Reducing energy consumption	NH_3-H_2O	2°C to 30°C	• Ejector enhances *COP* & Ex_{eff} • The ECT-ARC exhibits a 191.2% better *COP*. • Decreased reliance of the *COP* on the evaporator temperature.

2.5 Investigation on Cascaded Compression-Absorption Refrigeration Cycle (CARC)

The achievement of both higher coefficient of performance (*COP*) and lower refrigeration temperature in the case of ARC presents a challenge because of the conflicting nature and inherent trade-off between them. However, integrating absorption refrigeration cycle (ARC) alongside a different cycle, such as a vapor compression refrigeration (VCR) or advanced VCRs, presents a promising avenue for overcoming these limitations. By leveraging the strengths of each cycle, such as VCR's efficiency at lower temperatures and ARC's industry compatibility and green operation, a cascaded system can achieve both lower temperatures and improved COP, offering a practical and sustainable solution for diverse cooling needs.[19], [64], [65].

Han et al. [66] introduced a hybrid compression absorption refrigeration cycle operating on a medium temperature range and used a waste heat recovery system as the heat source. The system achieved a maximum COP of 1.04 and the lowest operational system temperature of 10 °C. Yu et al. [67] examined a cascaded ARC configuration focused on optimizing the system. As a result of their optimization efforts, exergy destruction reduced to 24.44% compared to the primary system, with a reduced cost rate. Cimsit et al. [68] and Cimsit & Ozturk [69] proposed the incorporation of a cascade heat exchanger in a simple VCR system with variable refrigerant flow (VAR). The implementation improved the COP and the ability to achieve lower temperatures. The system with $LiBr/H_2O$ solution at the absorption system and NH_3 at the vapor compression cycle had a COP of 0.592, 33% greater than that with NH_3/H_2O. The cascade system reduced electricity usage by 48-51% compared to a standard VCR. Xu et al. [70]conducted a simulation and experimental validation of a novel cascade absorption-compression cycle that achieved exceptionally low temperatures. Also, the prospect of CARC in industrial aspect is prominent. ARC in HTC enables the system to be integrated with industrial waste heat recuperation and VCR as LTC enables the system to be operated in lower evaporator temperature. Chen et al. [71] introduced a novel CARC system consisting of three subsystems. The system demonstrated the capability to reach temperatures as low as -55℃. Additionally, study from Razmi et.al demonstrates that integrating a novel cogeneration system with CARC can simultaneously generate 2280 kW of electrical energy and 416.7 kW of cooling capacity, boosting the round trip efficiency to 65.15% and significantly reducing environmental impact [72]. The following literature indicates ample

opportunity for further advancements within the domain of cascade absorption systems at low-temperature applications.

2.6 Chapter Conclusion

The literature review vividly illustrates the critical importance of innovation and technological advancement in the refrigeration sector, driven by the increasing need for efficient and environmentally sustainable cooling solutions. Traditional vapor compression refrigeration (VCR) systems, while widely used due to their simplicity and effectiveness, encounter substantial challenges when operating at low temperatures, including reduced thermodynamic efficiency and environmental damage due to the refrigerants they employ. The absorption refrigeration cycle (ARC) emerges as a promising alternative, offering a greener solution despite its lower performance (*COP*). However, the real frontier of progress lies in the exploration and development of advanced systems that combine the strengths of VCR and ARC through cascading techniques. This approach not only addresses the inherent limitations of each system but also opens up new avenues for achieving higher energy efficiency and reduced environmental impact. The continuous pursuit of research and innovation in cascading VCR and ARC systems, alongside the development of alternative modification of absorption configurations, represents a dynamic and evolving field aimed at meeting the complex demands of modern refrigeration needs.

Chapter 3: System Details and Overview

3.1 Traditional refrigeration systems

Traditional refrigeration systems primarily utilize vapor compression and absorption cycles for cooling. Modifications to these cycles, such as the integration of internal heat exchangers, have become common, significantly enhancing efficiency by recycling heat within the system. Additionally, these two systems are often cascaded in certain applications to combine their strengths, ensuring more effective and energy-efficient refrigeration, particularly in settings demanding lower temperatures or specialized cooling needs.

3.1.1 Conventional Single Effect Absorption and Vapor Compression Technology

The vapor compression cycle, extensively employed in both household and commercial refrigeration, operates on a series of phases involving a refrigerant. Initially, this refrigerant is compressed by a mechanical compressor, increasing its pressure and temperature. This hot, high-pressure gas then travels to a condenser, a type of heat exchanger, where it releases its heat to the surroundings and condenses into a liquid. This heat release is a critical step as it transforms the state of the refrigerant. The now-cooled, high-pressure liquid refrigerant moves to an expansion valve where its pressure is reduced, leading to a drop in temperature. Following this, it enters the evaporator, where it absorbs heat from the refrigerator's interior. This absorption causes the refrigerant to evaporate, turning back into a low-pressure gas, which is then sucked back into the compressor, repeating the cycle. This continuous process of compression, heat release, expansion, and heat absorption effectively maintain a low temperature inside the refrigerator as shown in **Figure 3-1(a)**.

Absorption refrigeration systems, in contrast, operate quite distinctively. They are often fueled by external heat sources such as natural gas, solar energy, or waste heat, instead of electricity. Normally LiBr- H_2O is used in ARC for the simplicity of integrating in cascaded systems. NH_3-H_2O is also used to reach lower evaporator temperatures. In LiBr/H_2O system, H_2O is the refrigerant, while in NH_3/H_2O system, NH_3 (ammonia) is used as the refrigerant. The heat source is applied to this refrigerant-absorbent mixture, causing the refrigerant to boil off. The vaporized refrigerant then travels to a condenser, similar to the vapor compression system, where it releases heat and condenses into a liquid. This liquid refrigerant subsequently goes through an expansion

valve and into an evaporator, where it absorbs heat from the surroundings, providing the cooling effect. The low-pressure refrigerant vapor is then reabsorbed by the secondary fluid, completing the cycle. This system's notable feature is the absence of a mechanical compressor, as the cycle is driven by the heat source. Illustration of this system is depicted in **Figure 3-1(b)**. The absorption refrigeration system is particularly advantageous in situations where heat is readily available, or electrical power is limited, making it a versatile option for various applications. Both systems, with their unique mechanisms, are fundamental in the field of refrigeration, providing efficient cooling solutions across a range of temperatures and conditions.

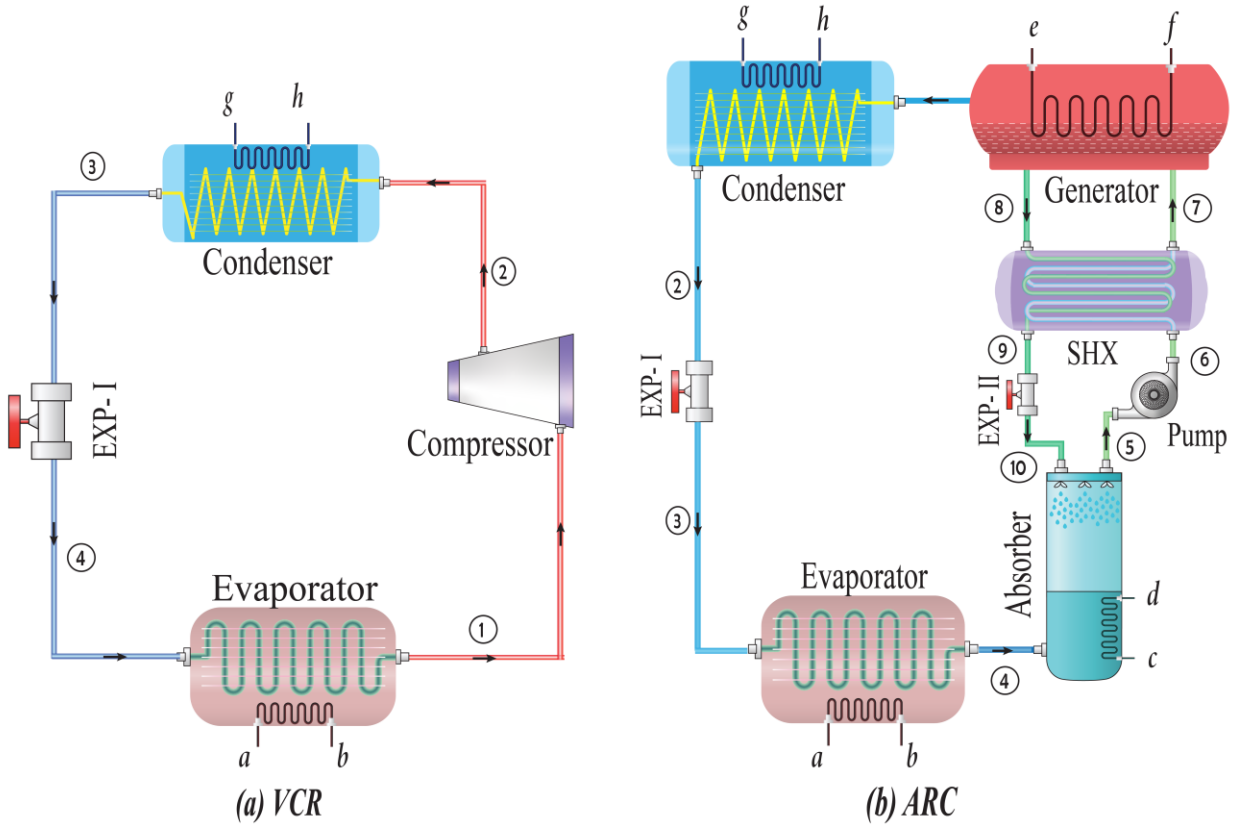

***Figure 3-1**: Schematic diagram of the traditional (a) Vapor Compression Cycle (VCR) and (b) Vapor Absorption Refrigeration Cycle (ARC)* [17].

3.1.2 Conventional Single- Effect Recompression Absorption Technology

In a basic ARC system, a significant amount of heat is released in the condenser, presenting an opportunity for heat recovery [24]. Furthermore, the pressure in the generator is determined by the condenser pressure, which cannot be reduced. This is because, to effectively reject heat, the condenser temperature must exceed the ambient temperature [12]. The RAC has been introduced to harness the rejected heat and enhance the efficiency of the ARC. As depicted in **Figure 3-2(a)**,

an auxiliary booster compressor is placed between the generator (at state 7) and the condenser (at state 8) within this recompression setup. This configuration allows for a reduced generator pressure in comparison to the conventional ARC, facilitating operation at a lower generator temperature [60]. Notably, there is no necessity for an additional sizeable condenser.

Normally LiBr-H_2O is utilized in RAC to use in cascaded systems for feasibility in integration. Similarly, NH_3-H_2O can also be employed in RAC systems to achieve lower evaporator temperatures, making it a preferred choice for analyzing the performance of single-effect standalone systems. The refrigerant (ammonia or water), post-compression and at elevated pressure-temperature, circulates through the generator for condensation. The heat rejected during this phase is harnessed in the generator to warm the NH_3-H_2O strong solution (weak solution in case of LiBr- H_2O), enabling the extraction of pure refrigerant (ammonia or water) from stream 7. Within the generator, the residual weak NH_3-H_2O solution (strong solution in case of LiBr- H_2O) of high temperature is discharged as stream 4 and conveys its heat to pre-warm the strong NH_3-H_2O solution of stream 2 (weak solution in case of LiBr- H_2O). Subsequently, this solution undergoes a single valve expansion to diminish its pressure before entering the absorber (state 6). Therefore, through this efficient gen-cond heat exchanger setup, the external heat load required for the generator is considerably reduced. Following condensation, stream 8 transitions to a saturated liquid state as stream 9. This stream is then directed through RHX to exchange heat internally and become a subcooled liquid of stream 10. Then it's channeled through the throttling valve to reduce its pressure. The refrigerant (ammonia or water), now at reduced pressure and temperature, traverses the evaporator, drawing heat from the refrigerated environment and thus transforming into a saturated vapor, identified as stream 12. This low temperature vapor takes heat in the RHX and becomes superheated before entering the absorber. Within the absorber, the superheated refrigerant is combined with the expanded weak NH_3-H_20 solution (strong solution in case of LiBr- H_2O), which operates at the evaporator pressure. The solution is cooled to become a strong solution and exits as stream 1 (weak solution in case of LiBr- H_2O). This solution is then pumped to generator pressure (state 2), receives heat in SHX, and enters the generator as stream 3, and the cycle continuous.

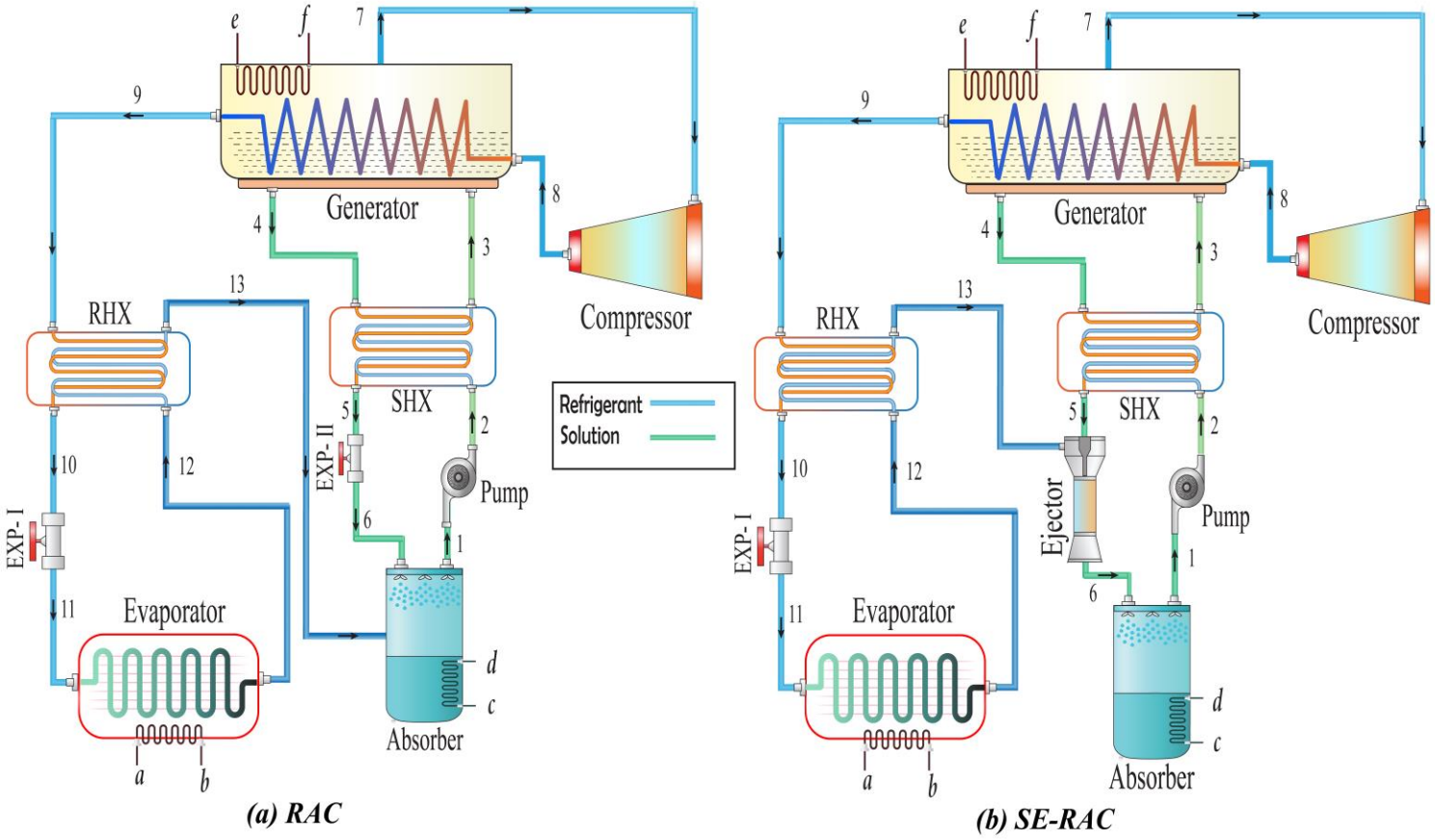

Figure 3-2: *Schematic diagram of the conventional (a) Recompression Absorption Cycle (RAC) and (b)Solution Ejector enhanced Recompression absorption cycle (SE-RAC)* [25], [73]

The Solution Ejector Enhanced Recompression Absorption Cycle (SE-RAC), as illustrated in **Figure 3-2 (b)**, represents an advanced modification of the traditional RAC technology. It benefits from higher absorber pressure and saves energy by mixing refrigerant (ammonia or water) vapor with the weak solution (strong solution in case of LiBr- H_2O) before entering the absorber [25]. Uniquely, this cycle operates across four pressure levels. In which an ejector is employed in place of the solution expansion valve (EXP-II of RAC) before the absorber to recover energy loss during the expansion. Stream 13 of refrigerant vapor from the evaporator and stream 9 of weak NH_3-H_2O solution from the generator (strong solution in case of LiBr- H_2O) is mixed to produce a strong solution of stream 6 (weak solution in case of LiBr- H_2O) and directed to the absorber. Due to the mixing, it allows the absorber to operate at a higher pressure than the evaporator's condition. This dynamic effectively reduces the requisite pumping power, circulation ratio, and external generator load.

3.1.3 Conventional Cascaded Compression Absorption Refrigeration Technology

Implementation of ARC has become a more environmentally friendly substitute for VCR systems. Despite its higher energy efficiency, this system is subject to limitations arising from its low permissible working pressure and low coefficient of performance (*COP*) compared to vapor compression cycles. Furthermore, the phenomenon of water freezing when the evaporator temperature falls below the solidification point of water, coupled with the occurrence of salt crystal formation within the solution, can hamper the system's operational efficiency of the system.

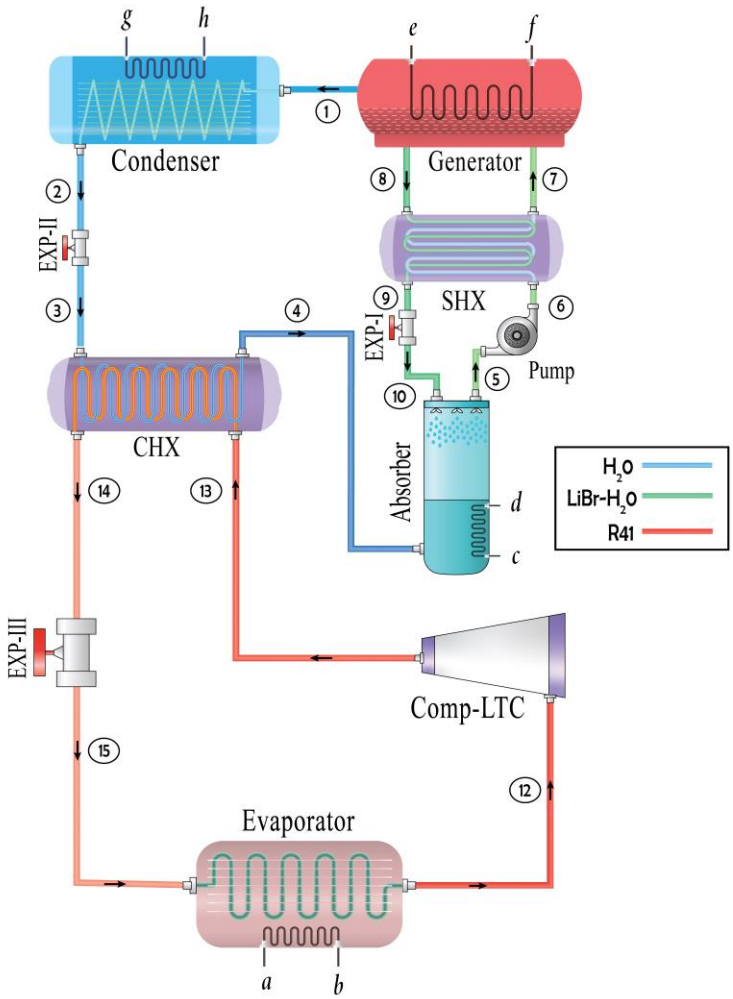

***Figure 3-3**: Schematic diagram of the traditional Compression-Absorption Refrigeration Cycle (CARC)* [74].

To solve the associated problem, Cimsit [18], [69] et al. suggested to cascade a simple VCR with a conventional ARC by incorporating a cascade heat exchanger which will act as a condenser for LTC (VCR) and evaporator for HTC (ARC) as shown in **Figure 3-3**. This inclusion will allow the system to operate with a low evaporator temperature by using VCR as the LTC and the compressor

power input will be reduced by using ARC as the HTC. Normally, LiBr- H_2O is used in RAC and ARC based cascaded systems because of feasibility in integration. In the LTC suitable refrigerants has to be selected based on environmental concerns and performance.

However, the proposed method involves significant power wastage during the expansion process in the expansion valve [16], inadequate thermal energy absorption in conventional ARC [68], and excessive compressor power requirement because of using a single-stage compressor [16]. Thus, it is crucial to continue investigating novel and inventive ways to improve absorption cycle efficiency while acknowledging and resolving these constraints to make them a more viable refrigeration system alternative.

3.2 Proposed Advanced Refrigeration Systems

To address the limitations of traditional systems and implement the first objective of this research, a modified Absorption Refrigeration Cycle (ARC) is combined with an improved Vapor Compression Refrigeration (VCR) system, leading to the development of advanced systems like ECAC and EICAC. This research further delves into the field of cascaded compression absorption system by integrating a Recompression Absorption System (RAC) with an enhanced VCR equipped with ejector, resulting in the innovative E-CRAC and EI-CRAC systems. Finally, this research proposes feasible upgrade of standalone single effect ARC by incorporating recompression technology with ejector and injection setup, leading to the development of RE-RAC and VI-RAC systems. These advancements collectively mark a significant leap forward in refrigeration technology. in RAC and ARC based cascaded systems, LiBr- H_2O as HTC with R41 as LTC is used because of feasibility in integration. But NH_3-H_2O is used in the single effect RAC and ARC analysis to reach lower evaporator temperatures.

3.2.1 ARC Based Proposed Cascaded Compression Absorption Systems Equipped with Ejector.

This study primarily concentrates on resolving the issues of traditional compression absorption cycle by cascading a modified ARC with an improved VCR to achieve enhanced thermal performance. At the evaporator outflow of ARC-HTC, an RHX (refrigerant heat exchanger) can be incorporated to improve the absorption cycle. This integration enables the refrigerant from evaporator outlet to be superheated by the heat provided by subcooled refrigerant of condenser

outlet. With the enthalpy of the liquid reducing, the cooling capacity increases; hence the *COP* enhances [75]. LiBr-H_2O is utilized in ARC-HTC due to its feasibility for use in cascaded systems, alongside R41 in the low-temperature circuit (LTC) owing to its environmental viability. In LiBr/H_2O system, H_2O is the refrigerant, while in NH_3/H_2O system, NH_3 (ammonia) is used as the refrigerant.

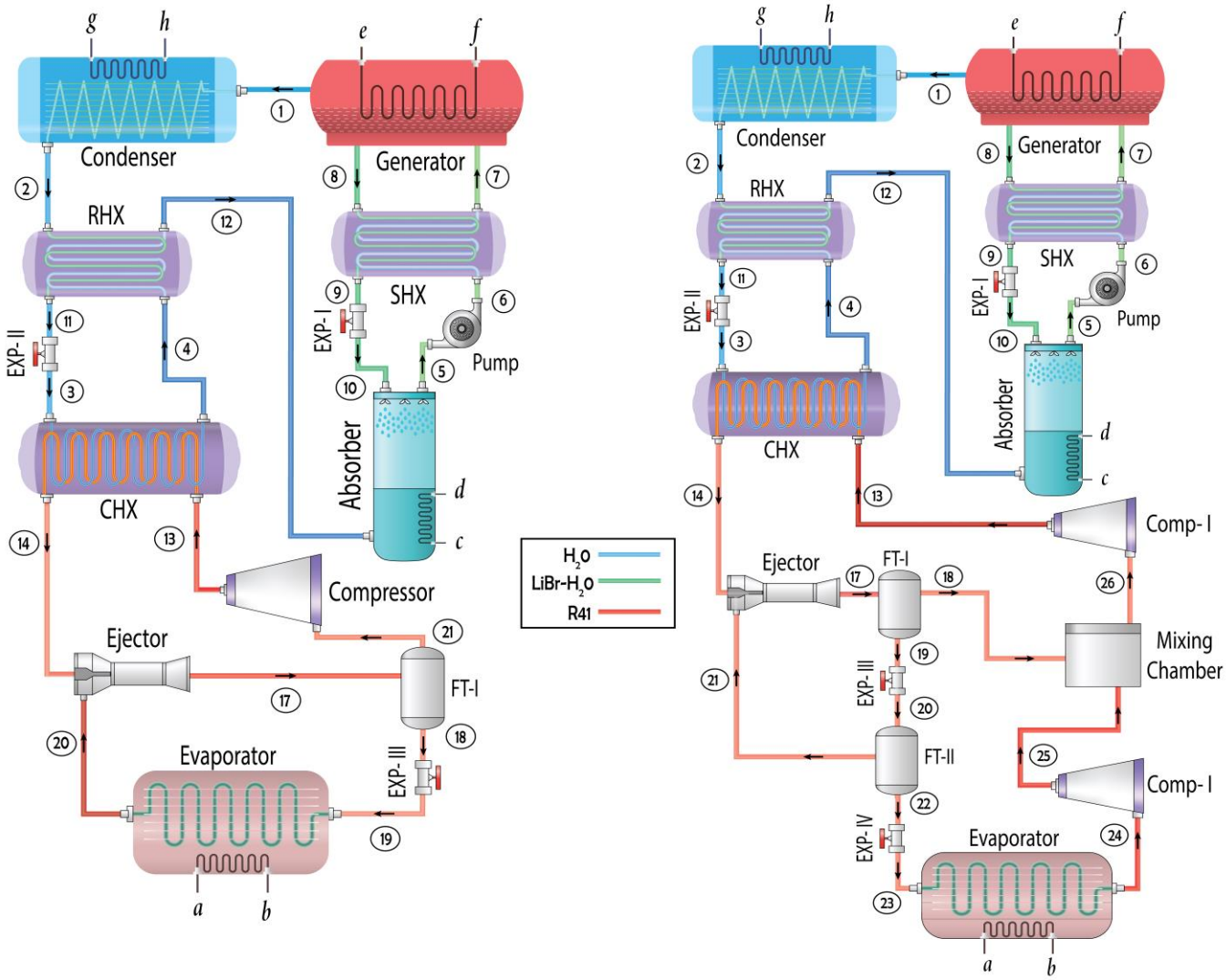

Figure 3-4: *Schematic diagram of the proposed novel (a) Ejector Compression Absorption Cycle (ECAC) and (b) Ejector Injection Compression Absorption Cycle (EICAC).*

In this study, two novel ARC based cascade systems are proposed in which the modified absorption cycle is cascaded with advanced ejector-based VCR systems. **Figure 3-4(a) & Figure 3-4(b)** illustrate the proposed novel Ejector Compression Absorption Cycle (ECAC) and Ejector Injection Compression Absorption Cycle (EICAC), respectively to overcome the limitations of

Conventional Compression Absorption Refrigeration Cycle (CARC). Ejector-based refrigeration systems reduce the energy loss in the expansion valve significantly by ensuring a near isentropic throttle process. Recent advancement in the field of ejector refrigeration system facilitates vapor injection in a two-stage refrigeration system which ensures a higher cooling effect.

An ejector-enhanced expansion cycle is employed in the ECAC as the LTC, as depicted in **Figure 3-4(a).** The diffuser, nozzle, and mixing chamber are the main components of an ejector. After rejecting heat at the CHX, the high-pressure refrigerant becomes saturated liquid and is passed as the motive fluid for the ejector inlet (point 14). This fluid is driven through the motive nozzle of an ejector and exits as a low-pressure refrigerant. Due to the generation of low pressure, the refrigerant which exits evaporator as saturated vapor, is drawn as suction fluid of the ejector inlet at point 20. The suction fluid is in a low temperature and pressure state and is subjected to a pressure drop of Δp in the suction nozzle. After acceleration, both fluids are homogenously mixed in the mixing chamber (point 16). Then the flow is expanded in the diffuser to recover the pressure energy and the flow exits a two-phase refrigerant (Point 17). Then the flow is separated in a flash tank, where the saturated vapor is compressed and eventually rejects heat at the CHX. The saturated liquid is expanded and passed through evaporator to remove heat from refrigerated space. The flow can be depicted from **Figure 3-5** which displays *P-h* diagram of ECAC cycle.

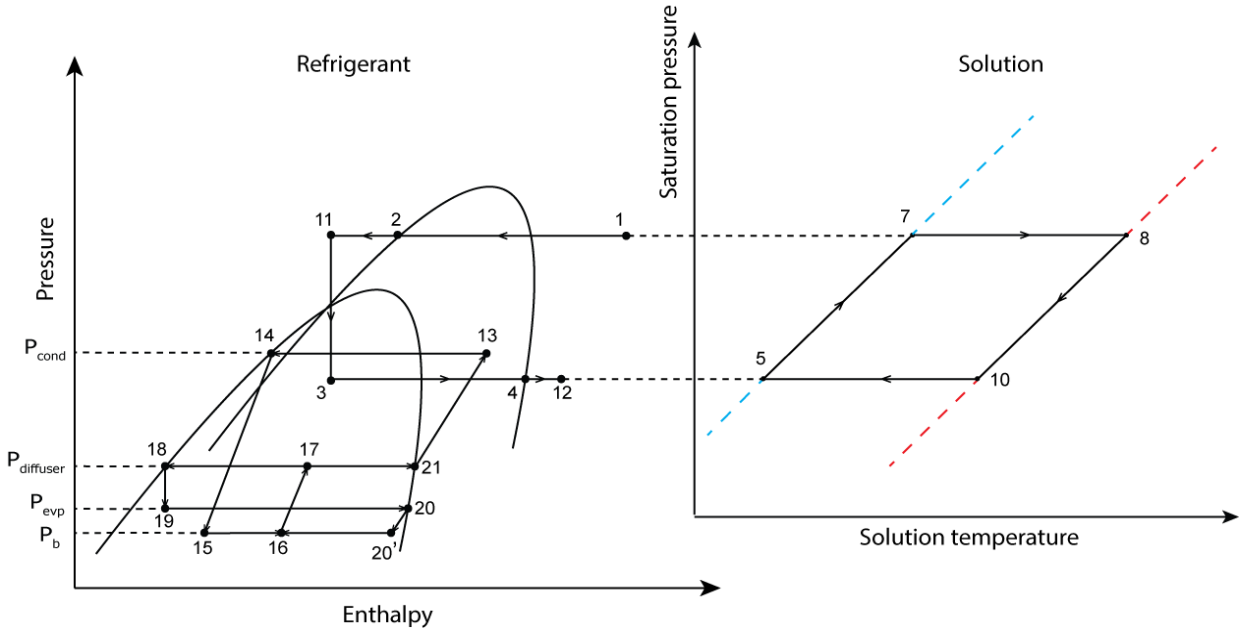

***Figure 3-5**: Pressure-enthalpy diagram of the proposed ECAC with pressure-Temperature diagram of the Solution.*

In EICAC, the Ejector integrated vapor-injection cycle is used as an alternative of simple VCR to facilitate the separation of liquid refrigerant in two stages to ensure vapor injection in a double stage compression process as shown in **Figure 3-4(b)**. At first, two-phase mixture refrigerant at the ejector exit (state 17) is separated by Flash tank-l into saturated liquid (state19) and saturated vapor (state 18); the saturated vapor is passed to the mixing chamber for high-pressure vapor injection, and saturated liquid is passed through the throttling valve-l and leaves as a two-phase mixture (state 20). Next, the flow is directed to Flash tank-II, where the refrigerant is segregated into saturated vapor (state 21) and saturated liquid (state 22). The saturated vapor is taken as the suction fluid for the ejector. The saturated liquid is expanded in throttling Valve II and transferred to evaporator (state 23) where it is evaporated completely (state 24) and further compressed in low-pressure compressor to reach the intermediate pressure (state 25). Afterward, it is mixed with the injected vapor in the mixing tank and further compressed in the high-pressure compressor to reach CHX pressure. The vapor rejects heat in CHX to become saturated liquid (state 14) and enters the ejector as motive fluid. To facilitate two stage separation, two stage compression is incorporated into the system. Double separation ensures a higher flow of refrigerant through CHX, also lower required input power due to double-stage compression. The flow can be depicted more easily from **Figure 3-6,** which displays the corresponding *P-h* diagram of EICAC cycle.

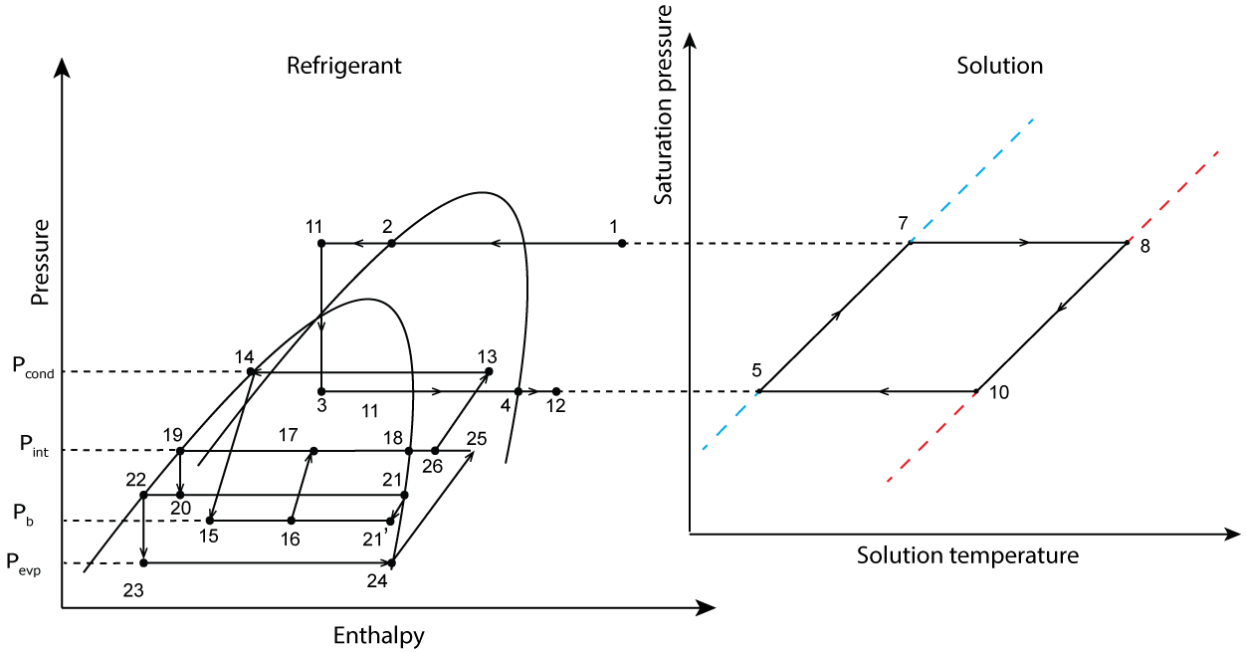

***Figure 3-6**: Pressure-enthalpy diagram of the proposed EICAC with pressure-Temperature diagram of the Solution.*

3.2.2 RAC Based Proposed Cascaded Compression Absorption Systems Equipped with Ejector.

The research further delves into the field of cascade compression absorption system by integrating an advanced Recompression Absorption Cycle (RAC) with enhanced vapor compression cycles, incorporated with an ejector to achieve enhanced energy and exergy efficiency. In a basic ARC system, a significant amount of heat is released in the condenser, presenting an opportunity for heat recovery [24]. Recompression technology has been introduced to harness the rejected heat and raise the solution temperature in the generator. As depicted in **Figure 3-7**, an auxiliary booster compressor is placed between the generator (at state 1) and the condenser (at state 2) within this recompression setup. This configuration allows for a reduced generator pressure in comparison to the conventional ARC, facilitating operation at a lower generator temperature [60]. Introducing a compact generator/compressor significantly enhances cycle efficiency and removes the necessity for a large condenser in traditional absorption cycles. Moreover, as a result of employing clean working fluid, it is more sustainable than vapor compression systems. Additionally, these systems require less electrical power compared to traditional VCR for the same working pressure ratio.

This research suggests three newly developed RAC based cascaded systems. **Figure 3-7** illustrates the proposed basic Compression Recompression Absorption Cycle (CRAC), and **Figure 3-9(a)** and **Figure 3-9(b)** represent the proposed advanced Ejector-Compression Recompression Absorption Cycle (E-CRAC) and Ejector enhanced Vapor-Injection Compression Recompression Absorption Cycle (EI-CRAC) each in order, to eliminate the constraints associated with conventional ARC based CARC system. LiBr-H_2O is utilized in RAC-HTC due to its feasibility for use in cascaded systems, alongside R41 in the low-temperature circuit (LTC) owing to its environmental viability. In LiBr/H_2O system, H_2O is the refrigerant, while in NH_3/H_2O system, NH_3 (ammonia) is used as the refrigerant.

In **Figure 3-7**, the proposed basic CRAC is depicted where a simple VCR is used as LTC to capture the heat from refrigerated space at a much lower temperature and reject it to the conventional recompression absorption cycle used as HTC through cascade heat exchanger (CHX) operating at a moderate temperature. This is why the CRAC cycle is taken as a benchmark for comparison with advanced RAC based proposed systems in the analysis section.

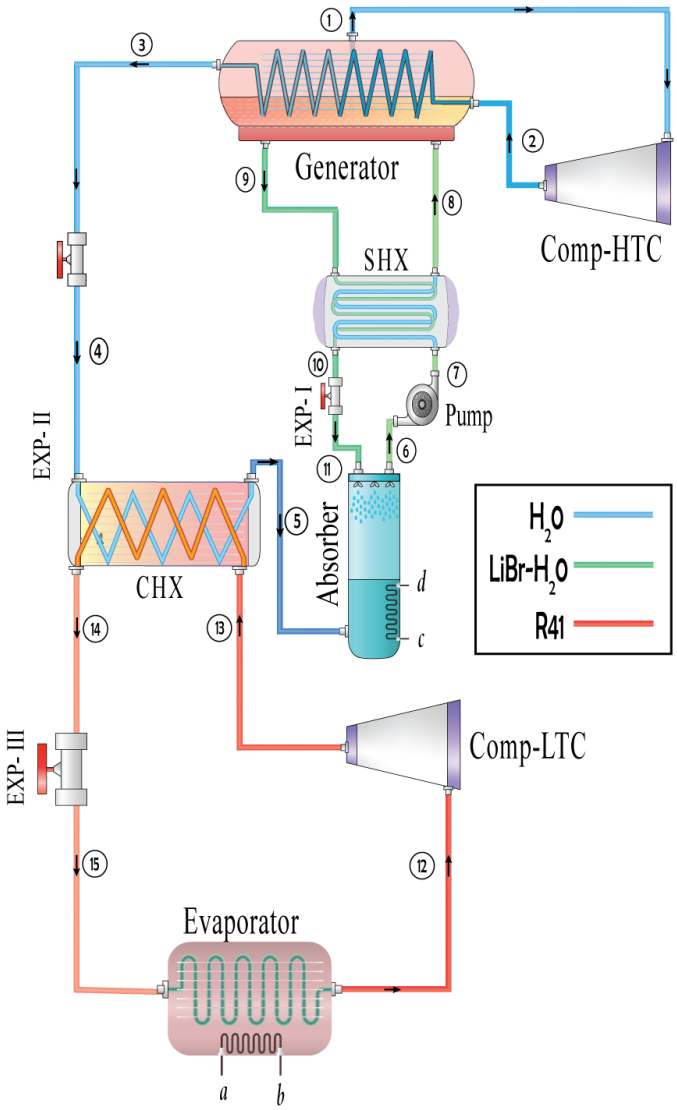

Figure 3-7: *Schematic diagram of the proposed basic Compression Recompression Absorption Cycle (CRAC).*

The Recompression Absorption Cycle (RAC) used in HTC has three pressure levels as illustrated in the system *P-h* diagram as depicted in **Figure 3-8**. Water as refrigerant, post-compression and at an elevated pressure-temperature, circulates through the generator for condensation. The heat rejected during this phase is harnessed in the generator to warm the weak LiBr-H_2O solution, enabling the extraction of pure H_2O from stream 1. Within the generator, the residual strong LiBr-H_2O solution of high temperature is discharged as stream 9 and conveys its heat to pre-warm the weak solution of stream 8. Subsequently, this solution undergoes a single valve expansion to diminish its pressure before entering the absorber (state 11). Following condensation, stream 2 transitions to a saturated liquid state as stream 3. This stream is channeled through the throttling

valve to reduce its pressure. The refrigerant-water, now at reduced pressure and temperature, traverses the CHX, drawing heat from the LTC condenser and thus transforming into a saturated vapor, identified as stream 5 and enters the absorber. Within the absorber, this H_2O vapor is combined with the expanded LiBr-H_2O strong solution, which operates at the evaporator pressure. The solution is cooled to become a weak LiBr-H_2O solution and exits as stream 6. This weak solution is then pumped to generator pressure (state 7), receives heat in SHX, and enters the generator as stream 8, and the cycle continuous.

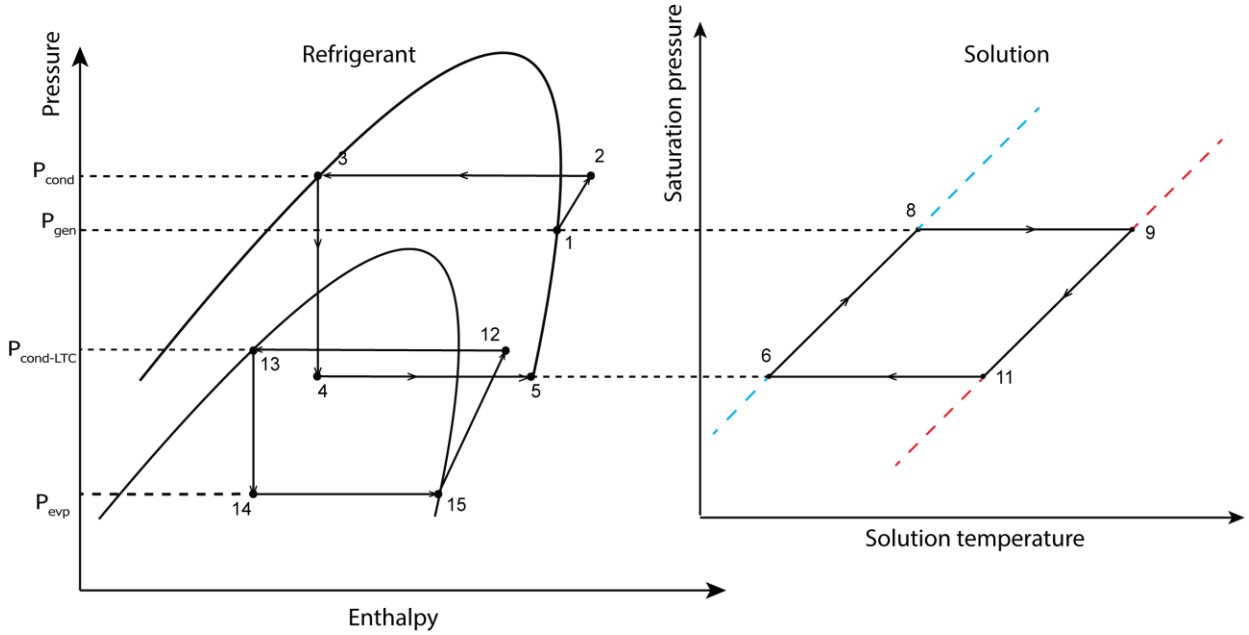

***Figure 3-8**: Pressure-enthalpy diagram of the proposed basic CRAC with pressure-Temperature diagram of the Solution.*

In **Figure 3-9(a)** and **Figure 3-9(b)**, proposed advanced configurations of E-CRAC and EI-CRAC schematic diagrams are shown where modified RAC is combined with advanced ejector-enhanced VCR cycles. RAC can be improved by introducing a RHX (refrigerant heat exchanger) at the CHX outlet. This integration allows the water vapor exiting the evaporator (at point 5) to undergo superheating (reaching point 12), facilitated by the heat transfer from the subcooled high-temperature liquid water from the condenser's outlet (point 3). As a result of the enthalpy reduction, there is an increase in the cooling capacity; consequently, COP also increases [75]. In LTC, ejector based advanced compression cycles are employed. Refrigeration systems that incorporate ejectors substantially diminish energy loss typically experienced in expansion valves by achieving a process close to isentropic throttling. Latest developments in ejector-based refrigeration

technology have introduced vapor injection into two-stage refrigeration systems, resulting in an enhanced cooling effect.

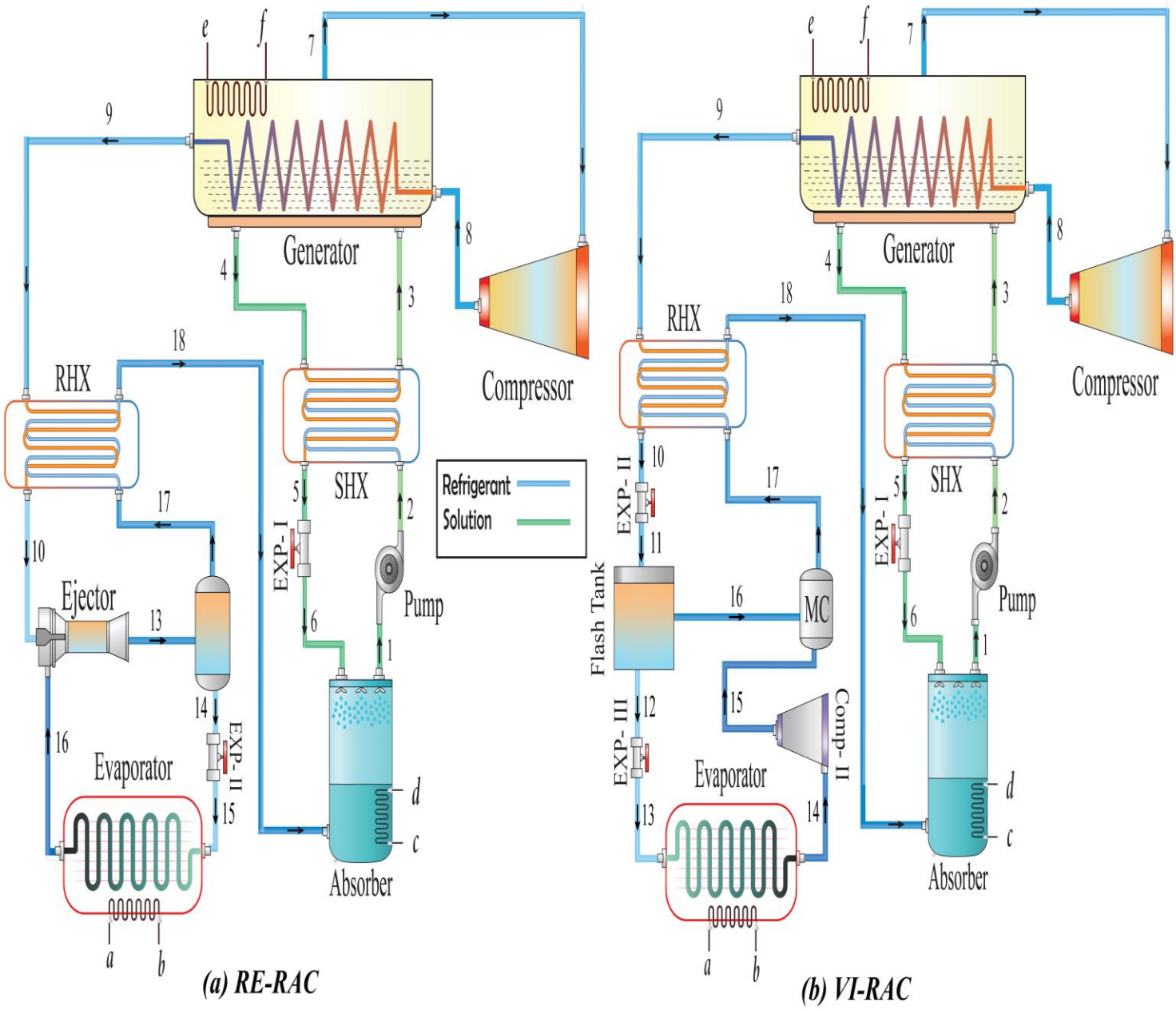

Figure 3-9: *Schematic diagram of the proposed advanced novel (a) Ejector-Compression Recompression Absorption Cycle (E-CRAC) and (b) Ejector enhanced Vapor-Injection Compression Recompression Absorption Cycle (EI-CRAC)*

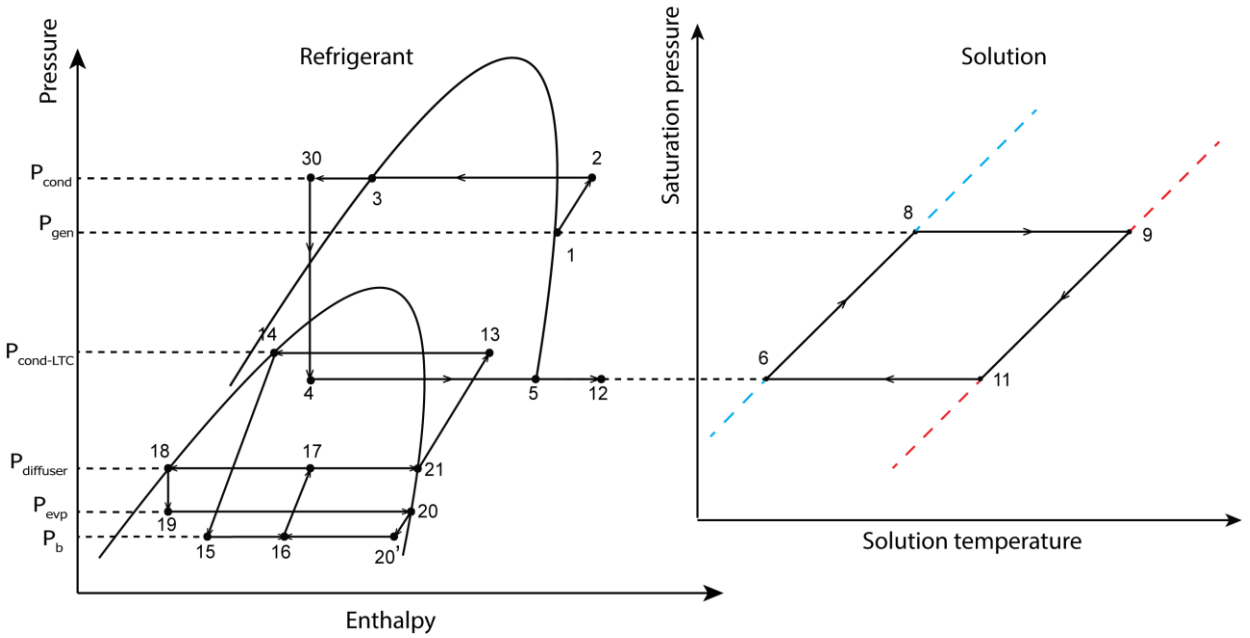

***Figure 3-10**: Pressure-enthalpy diagram of the proposed E-CRAC with pressure-Temperature diagram of the Solution.*

In the LTC, an ejector improved expansion system is integrated into the E-CRAC, as shown in the system schematic illustrated in **Figure 3-9(a).** The primary components of an ejector include the diffuser, nozzle, and mixing enclosure. Post heat rejection at the Cascade Heat Exchanger (CHX), the high-pressure refrigerant, now a saturated liquid, enters the ejector as motive fluid (state 14). This refrigerant is passed along the operating ejector nozzle and comes out at reduced pressure. This process creates a low-pressure environment that draws the refrigerant leaving the evaporator as saturated vapor into the ejector's suction inlet stated point 20. Then the suction flow experiences a pressure loss of Δp while passing through the intake nozzle. Afterward passing, the two refrigerants are uniformly combined in the mixing enclosure (point 16). Following acceleration, the fluids mix uniformly in the mixing chamber (point 16) and then expand in the diffuser, recovering pressure energy and exiting as mixture stated as point 17. The liquid vapor mixture is then split in the flash tank, during which the saturated vapor goes through compression and releases thermal energy and get condensed. And the liquid undergoes expansion and is passed along the evaporator collecting thermal energy from the cooled area. The refrigerant circulation can be visualized conveniently from **Figure 3-10**, representing the *P-h* illustration of the E-CRAC cycle.

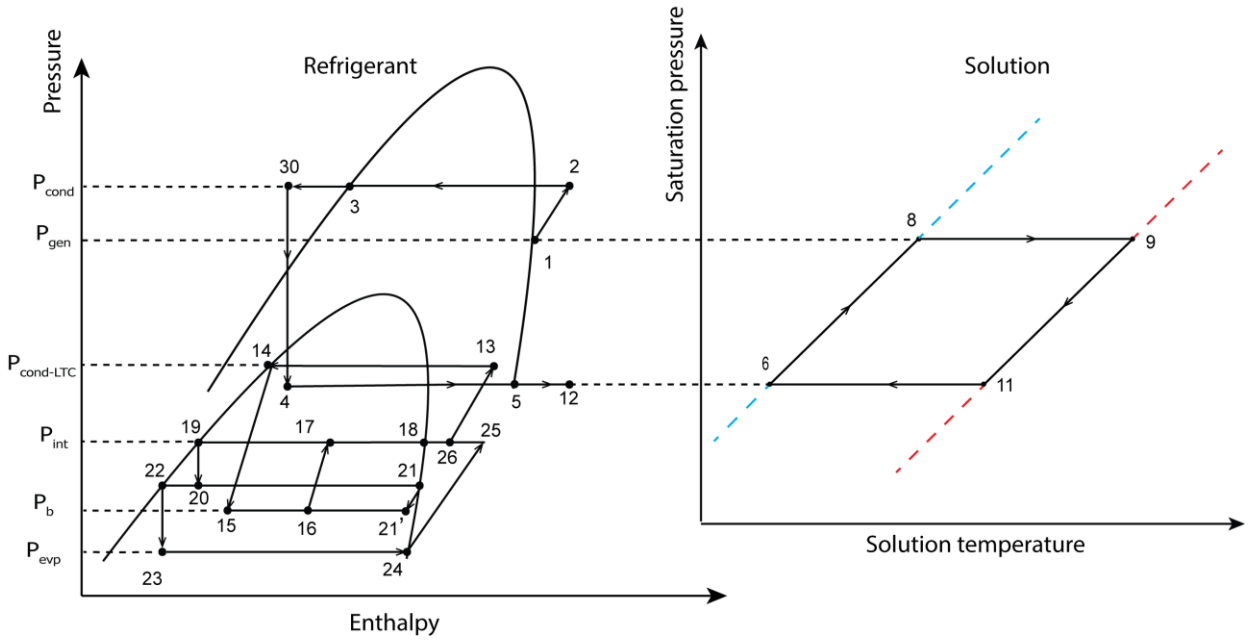

***Figure 3-11**: Pressure-enthalpy diagram of the proposed EI-CRAC with pressure-Temperature diagram of the Solution*

In the Enhanced Injection-CRAC (EI-CRAC), an Ejector enhanced vapor-injection cycle replaces the simple VCR, which is illustrated in **Figure 3-9(b)**. This system facilitates two-stage separation of liquid refrigerant, enabling injection of vapor to facilitate compression in two stages. Initially, the two-phase refrigerant mixture at the ejector outlet is split into saturated liquid (point 19) and saturated vapor (16) by Flash tank-l. Then the vapor is directed to the mixing enclosure, ensuring vapor injecting process at high pressure. At the same time, the liquid is directed along the expansion valve-l and exits as a two-phase combination (point 17). Afterward, the fluid is separated into saturated vapor (Point 21) and saturated liquid (Point 22) while passing through Flash tank-II. The ejector uses saturated vapor as its suction fluid. The saturated liquid gets expanded while passing through throttling Valve II. Then the fluid is passed through the evaporator (point 23) to be vaporized completely (point 24). Afterwards, it's compressed to reach the intermediate pressure and sent to the mixing chamber. Where, it mixes with the injected vapor (point 26) and further compressed. The refrigerant of high pressure and temperature (point 13) is then sent to CHX, rejects heat, and gets condensed. This liquid refrigerant is passed to ejector as motive fluid (point 14). Implementing double stage separation and vapor injection in the system results in an increased flow of refrigerant through the CHX, thereby reducing the amount of input power required because of the dual-phase compression. The fluid circulation can be understood conveniently from **Figure 3-11,** which shows the *P-h* illustration of EI-CRAC system.

3.2.3 Advanced Stand-Alone Recompression Absorption System Equipped with Ejector and Vapor Injection

In the recompression system, vapor refrigerant from the generator is recompressed to release heat and condense. This results in higher condensation pressure and Pressure ratio, R_p than basic ARC [25]. Directly reducing the high pressure of the condensed subcooled refrigerant through isenthalpic expansion in a single expansion valve leads to significant energy and exergy losses [26]. In conventional VCR systems, where the pressure ratio is comparably high, replacing the expansion valve and recovering lost energy have been addressed by introducing ejector and vapor injection technologies [11]. These innovations have shown promise in enhancing system efficiency.

In this regard, ejector and vapor injection technology have been incorporated in the refrigerant section of the RAC cycle to develop proposed advanced recompression absorption systems: Refrigerant Ejector enhanced Recompression Absorption Cycle (RE-RAC) and Vapor Injection enhanced Recompression Absorption Cycle (VI-RAC), respectively in this study. In these configurations, the conventional single-valve expansion is substituted, and energy is recuperated internally, facilitating the entry of refrigerant vapor into the absorber at an elevated pressure to reach higher system efficiency. Consequently, these modifications also allow the absorption system to operate at lower evaporator temperatures. Although such adaptations might not significantly boost efficiency in basic ARC systems because of the limited R_p, within the RAC framework and its 3-stage pressure setup, substantial efficiency improvements were observed because of higher R_p.

Normally LiBr-H_2O is utilized in RAC based cascaded systems for feasibility in integration. Similarly, NH_3-H_2O can also be employed in RAC systems to achieve lower evaporator temperatures, making it a preferred choice for analyzing the performance of single-effect standalone systems. This is why, in the analysis of improved single effect recompression absorption technologies, NH_3-H_2O is selected.

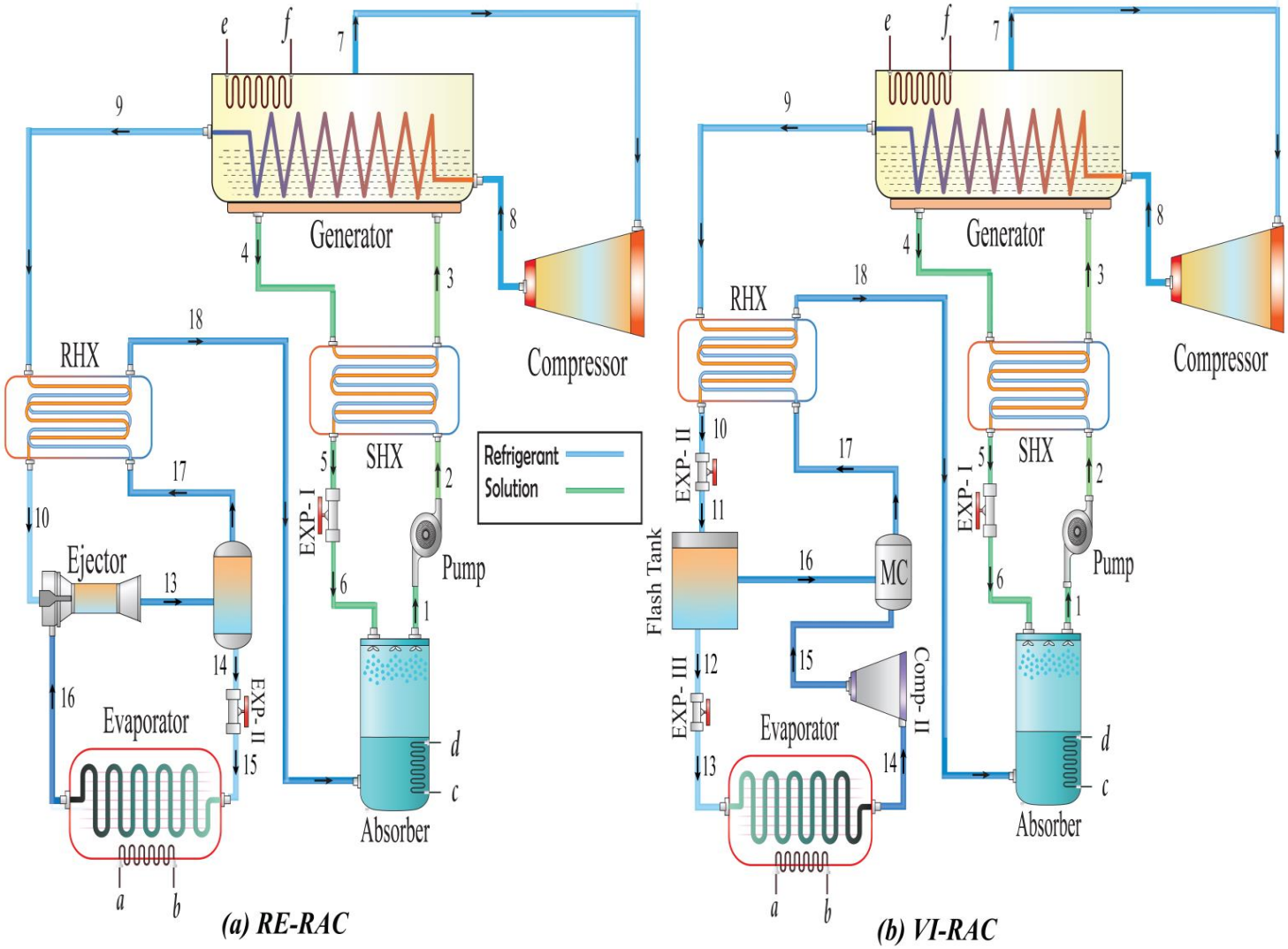

***Figure 3-12**: Schematic diagram of the proposed novel (a) Refrigeration Ejector enhanced Recompression Absorption Cycle (RE-RAC) and (b) Vapor Injection enhanced Recompression Absorption Cycle (VI-RAC)*

In RE-RAC, a gas-liquid ejector is integrated between the evaporator and condenser of the RAC cycle. The schematic of the cycle is depicted in **Figure 3-12(a)**, with the accompanying *P-h* diagram presented in **Figure 3-13**. The high-pressure liquid ammonia, after getting subcooled in the RHX, is channeled into the ejector as the motive fluid (state 10). This fluid accelerates through the nozzle until it achieves the suction pressure corresponding to stream 11. Concurrently, the low-pressure vapor exiting from the evaporator's outlet (stream 16) is introduced into the ejector as suction fluid, where it merges homogeneously with stream 11 within the mixing chamber. Subsequently, the ammonia experiences expansion within the diffuser, enabling energy and

pressure recovery, and ultimately discharges as a two-phase refrigerant labelled as stream 13. The two-phase ammonia is then separated in the flash tank. Here, the saturated liquid undergoes expansion to lower its pressure, and this reduced-pressure liquid ammonia traverses the evaporator coil, drawing heat from the refrigerated space and transforming it into a saturated vapor. Conversely, the saturated vapor from the flash tank navigates through the RHX, acquiring heat before entering the absorber, producing a high concentration solution. This arrangement allows absorber pressure to be higher than evaporator pressure, offering the possibility to decrease the evaporator temperature further if needed.

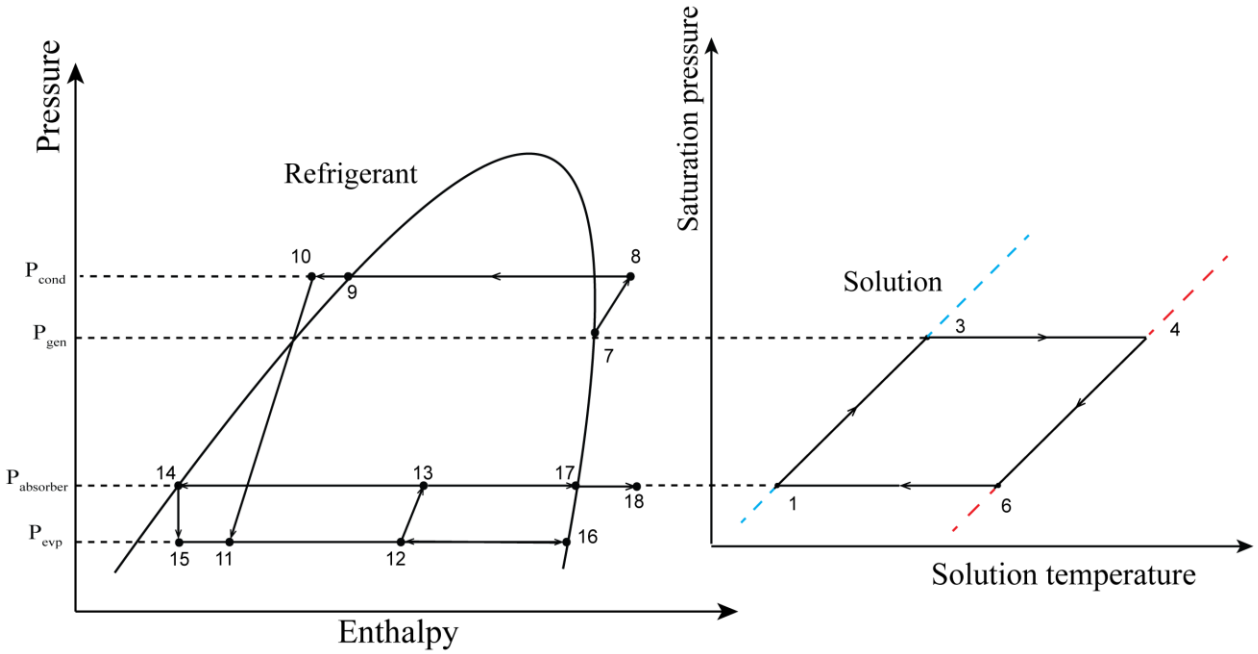

***Figure 3-13**: Pressure-enthalpy diagram of the proposed RE-RAC with pressure-Temperature diagram of the Solution.*

In VI-RAC, a flash tank is integrated between the evaporator and condenser of the RAC cycle to enable ammonia vapor to enter the absorber at an intermediate pressure. Schematic of the cycle is depicted in **Figure 3-12(b)**, with the accompanying *P-h* diagram presented in **Figure 3-14**. The high-pressure liquid ammonia, after getting subcooled in the RHX (stream 10), is throttled to an intermediate pressure (stream 11) using the EXP-II. At this state, ammonia is a mixture of vapor and liquid, which enters the flash tank and gets separated. The resulting saturated vapor (stream 16) is directed to the mixing chamber. Simultaneously, the saturated liquid (stream 12) undergoes a second throttling (EXP-III) to achieve the evaporator pressure of state 13. The low-pressure liquid ammonia is passed through the evaporator coil to extract heat from the refrigerated space to

become saturated vapor (stream 14). This vapor is sent to the compressor and mixed with the saturated vapor of intermediate pressure in the mixing tank. This mixture (stream17) goes through RHX and gains heat before entering the absorber and producing a high-concentration solution. This arrangement also allows the absorber to be at an intermediate pressure, thus increasing system efficiency and allowing the system to reach a lower evaporator temperature.

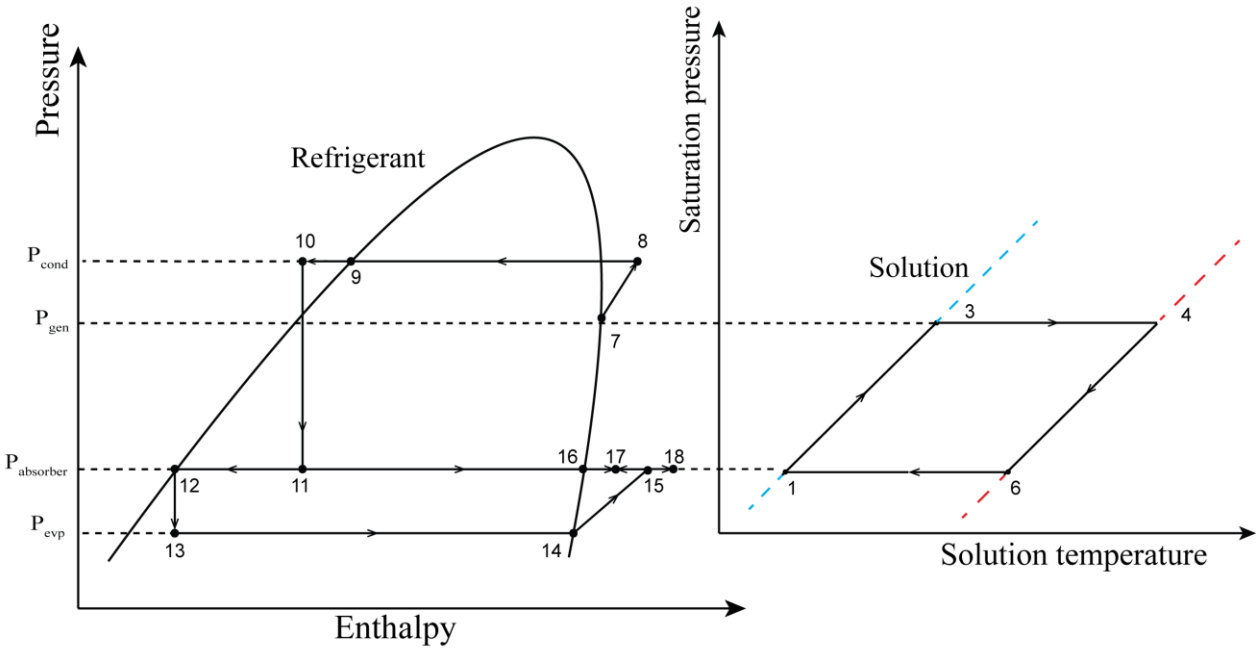

***Figure 3-14**: Pressure-enthalpy diagram of the proposed VI-CRAC with pressure-Temperature diagram of the Solution.*

Chapter 4: Research Methodology & Mathematical Modelling

4.1 Thermodynamic First Law- Energy Analysis

Mass, energy and exergy balance equations can be applied to each component of the corresponding cycle to calculate all the state properties as well as performance parameters. The equations are as follows:

Conservation of mass: Each component of the refrigeration cycle can be regarded as control volume system. Hence, employing continuity equation, conservation of mass across each component can be formulated as:

$$\sum \dot{m}_i = \sum \dot{m}_e \tag{1}$$

Solution Concentration Equilibrium Equation:

$$\sum \dot{m}_i X_i = \sum \dot{m}_e X_e \tag{2}$$

Energy conservation: 1st law of thermodynamics is applied to derive SFEE (Steady flow energy equation) to estimate the total energy flow through open systems as described: [76]

$$\sum \dot{m}_i \left(h_i + \frac{V_i^2}{2} + g z_i \right) + \dot{Q} = \sum \dot{m}_e \left(h_e + \frac{V_e^2}{2} + g z_e \right) + \dot{W} \tag{3}$$

Disregarding potential and kinetic energy, and simplifying the formulation of equation results as follows: [77]

$$\sum \dot{m}_i h_i + \dot{Q} = \sum \dot{m}_e h_e + \dot{W} \tag{4}$$

Here, ṁ represents the mass transfer rate, $\dot{Q}$ is the heat transfer rate, and $\dot{W}$ denotes the work transfer rate across the system boundary, while $\dot{X}$ signifies the solution concentration. *COP* is expressed as a quantity to assess the efficiency of the refrigeration system.

$$COP = \frac{Desirable\ output}{Cycle\ Input} \tag{5}$$

The 1st law of thermodynamics focused on the quantity of energy rather quality, and the work and heat load are considered based on only enthalpy changes inside the refrigeration cycle. So, the total input energy to operate the cycle is given as the summation of energy input to the generator and compressors separately. The desirable output of the system is the cooling effect produced at evaporator. So, the following equation to calculate the overall **system *COP*** of the **proposed cascaded compression absorption systems** can be written. Existing literature on cascade systems also follows the same convention.[12], [69], [74], [78], [79]

$$COP_{system} = \frac{\dot{Q}_{evp}}{\dot{Q}_{gen} + \dot{W}_{comp} + \dot{W}_{pump}} = \frac{\dot{Q}_{evp}}{\dot{Q}_{gen} + \dot{W}_{comp-HTC} + \dot{W}_{comp-LTC} + \dot{W}_{pump}} \quad (6)$$

To offer a comprehensive understanding of each input separately, *COP* of each **sub-cycle** of the **cascaded systems** can be calculated from the following equations. In this, COP_{LTC} is associated with the compressor load only, while COP_{HTC} is concerned exclusively with the generator load.

$$COP_{LTC} = \frac{\dot{Q}_{evp}}{\dot{W}_{comp}}, COP_{HTC} = \frac{\dot{Q}_{CHX}}{\dot{Q}_{gen} + \dot{W}_{pump}} \quad (7)$$

In the **stand-alone RAC system**, as mentioned, the required generator load ($\dot{Q}_{gen}$) is supplied from two sources [25]. Primarily, the compressed refrigerant supplies internal generator load ($\dot{Q}_{gen,int}$) and get condensed. The extra requirement of heat in the generator is taken from an external source (stream e-f) and is denoted as external generator load ($\dot{Q}_{gen,ext}$).

From conservation of energy,

$$\dot{Q}_{gen} = \dot{Q}_{gen,int} + \dot{Q}_{gen,ext} \quad (8)$$

Whereas,

$$\dot{Q}_{gen} = \dot{m}_7 \times h_7 + \dot{m}_4 \times h_4 - \dot{m}_3 \times h_3 \quad (9)$$

$$\dot{Q}_{gen,int} = \dot{m}_8 \times h_8 - \dot{m}_9 \times h_9 \quad (10)$$

So, the external heat requirements in the generator can be calculated from:

$$\dot{Q}_{gen,ext} = \dot{Q}_{gen} - \dot{Q}_{gen,int} \quad (11)$$

For the ideal RAC operation, $\dot{Q}_{gen,ext} = 0$ means all the required generator heat is provided by recompressed internal stream 8. But that would require a much higher recompression, resulting in a very high compressor load. This violates the fundamental objective of the absorption system, which is to use heat as input and decrease electricity dependency. This is why, in the RAC mechanism, the compressor load is only used to recompress the ammonia stream from the generator to a higher temperature, so that its inherent energy can be supplied to the generator to meet the requirement partially, decreasing the external load requirement significantly and enhancing performance. The internal heat exchange within the generator is defined by pinch difference ΔT_{pinch}. Thus, the saturated condensed ammonia outlet (stream 9) after internal heat release in the gen-cond is defined by,

$$T_9 = T_{gen} + \Delta \mathrm{T}_{\mathrm{pinch}} \tag{12}$$

Also, it's required to calculate the ammonia pressure after recompression (stream 8). The maximum compressor output pressure is assumed to be 0.9 times the critical NH_3 pressure for safe operation [25]. Whereas the minimum pressure is the saturated pressure corresponding to T_9 (as heat rejection occurs in constant pressure). A variable is introduced as *NPR* (normal pressure ratio) to regulate the R_P as stated in equation 10. By varying this, the recompression can be controlled; hence, the system performance also changes.

$$R_p = \frac{P_8}{P_7} = \left(\frac{P_{min}}{P_7}\right) + \left(0.9 * \frac{P_{cr}}{P_7} - \frac{P_{min}}{P_7}\right) * NPR \; ; 0 \leq NPR \leq 1 \tag{13}$$

Where,

$$P_{min} = P_{saturate}\,(NH_3\,, T = T_9 = T_{gen} + \Delta \mathrm{T}_{\mathrm{pinch}}) \tag{14}$$

The compressor's output pressure is equal to P_{min} when *NPR* =0 and 0.9 P_{cr} when *NPR* = 1. From the viewpoint of the first law of thermodynamics, the performance (***COP***) of the **proposed advanced standalone RAC systems** is assessed as:

$$COP = \frac{Desirable\ output}{Cycle\ Input} = \frac{\dot{Q}_{evp}}{\dot{Q}_{gen,ext} + \dot{W}_{comp} + \dot{W}_{pump}} \tag{15}$$

4.2 Thermodynamic Second Law- Exergy Analysis

Exergy is conceptualized as the quantity of work, equivalent to entropy-free energy, that a system can execute when it achieves thermodynamic equilibrium with its surrounding environment. In the case of an open system, exergy of a stream is defined as follows: [76]

$$\dot{\mathrm{E}}x = \dot{m}_r[(h - h_0) - T_0(s - s_0) + \frac{V^2}{2} + gz] \tag{16}$$

For simplification the influence of external mechanical energy (kinetic and potential factors) on exergy can be disregarded, so the equation becomes:

$$\dot{\mathrm{E}}x = \dot{m}_r\,[(h - h_0) - T_0(s - s_0)] \tag{17}$$

Assuming each component of the systems as control volume, exergy balance equation across each component can be formulated as: [80]

$$\sum \dot{\mathrm{E}}x_i \; + \; \dot{\mathrm{E}}_{\mathrm{Q}} \; = \sum \dot{\mathrm{E}}x_e + \; \dot{\mathrm{E}}\mathrm{x}_{\mathrm{W}} + \; \dot{\mathrm{E}}\mathrm{x}_{\mathrm{D}} \tag{18}$$

The subscript 'i' corresponds to the inbound flows for control volume element, while the 'e' subscript represents the outgoing streams. Conversely, the 'o' subscript is associated with the 'Dead state' condition. $\dot{E}x_D$, indicating the exergy destruction rate, can be expressed as:

$$\dot{\mathrm{E}}\mathrm{x}_D = \sum \dot{\mathrm{E}}x_i - \sum \dot{\mathrm{E}}x_e + \; \dot{\mathrm{E}}\mathrm{x}_W \; + \; \dot{\mathrm{E}}\mathrm{x}_{\mathrm{Q}} \tag{19}$$

Here, the terms $\dot{E}x_Q$ and $\dot{E}x_W$ represents the exergy rates corresponding to finite heat transfer and mechanical work, which are defined in the following manner [76]:

$$\dot{\mathrm{E}}\mathrm{x}_{\mathrm{Q}} = \left(1 - \frac{T_0}{T_k}\right) \dot{\mathrm{Q}}_k \tag{20}$$

$$\dot{\mathrm{E}}\mathrm{x}_W = \; \dot{\mathrm{W}}_{\mathrm{k}} \tag{21}$$

In addition, since chemical exergy has a negligible impact compared to physical exergy, it has been omitted in present study, as in most previous works in the literature [81]. It should be noted that the contributions of kinetic and potential exergies have been disregarded in the formulation[82]. The 2nd law efficiency is expressed from the definition as follows [83]:

$$\eta_{ex} = \frac{\dot{\mathrm{E}}\mathrm{x}_p}{\dot{\mathrm{E}}\mathrm{x}_f} = 1 - \frac{\dot{\mathrm{E}}\mathrm{x}_D}{\dot{\mathrm{E}}\mathrm{x}_f} \tag{22}$$

Within this context, $\dot{E}x_p$ and $\dot{E}x_f$ stand for the rate of exergy corresponding to system product and fuel, respectively. The exergy "product" of the system refers to the desirable exergy extracted from cold space (the exergy rate of net cooling effect, discarding any exergy released in the absorber). Conversely, the exergy "fuel" of the system is defined as the exergy expended by the system for its operation (exergy input that comprises the compressor load and useful external heat input in the generator).

In the context of the **cascaded compression absorption system**, the input exergy can be defined as follows:

$$\dot{\mathrm{E}}\mathrm{x}_f = \dot{E}_{x\,in,\ Generator} + \dot{E}_{x\,in,\ comp-HTC} + \dot{E}_{x\,in,\ comp-LTC} + \dot{E}_{x\,in,\ pump} \tag{23}$$

Whereas useful exergy input in the generator,

$$\dot{E}_{x\,in,\ Generator} = \dot{Q}_{gen}\left(1 - \frac{T_o}{T_{gen}}\right) = \left(\dot{\mathrm{E}}x_e - \dot{\mathrm{E}}x_f\right) \tag{24}$$

In the context of the **proposed standalone RAC systems** employed in this study, the input exergy can be defined as follows:

$$\dot{\mathrm{E}}\mathrm{x}_f = \dot{E}_{x\,in,\ gen-ext} + \dot{E}_{x\,in,\ comp} + \dot{E}_{x\,in,\ pump} \tag{25}$$

Whereas external exergy input in the generator,

$$\dot{E}_{x\,in,\ gen-ext} = \dot{Q}_{gen,ext}\left(1 - \frac{T_o}{T_{gen}}\right) = \left(\dot{\mathrm{E}}x_e - \dot{\mathrm{E}}x_f\right) \tag{26}$$

In both cases, useful exergy input in the compressor and pump,

$$\dot{E}_{x\,in,\ Compressor} = \dot{W}_{compressor}, \qquad \dot{E}_{x\,in,\ Pump} = \dot{W}_{pump} \tag{27}$$

Although a significant amount of energy is rejected in absorber and condenser, these components are operating at near ambient temperature of T_0. This is why the rate of rejection of useful energy or exergy in condenser/absorber is very negligible.

Hence the exergy product can be written as,

$$\dot{\mathrm{E}}\mathrm{x}_p = \dot{E}_{x\,in,Evaporator} = \dot{Q}_{evp} \times \left|1 - \frac{T_o}{T_{evp}}\right| \tag{28}$$

This is the reason why in many studies performed on **cascaded compression absorption systems**, the equation to find exergetic efficiency has been simplified to: [84]

$$\eta_{ex} = \frac{\dot{Q}_{evp} \times \left|1 - \frac{T_o}{T_{evp}}\right|}{\dot{Q}_{gen} \times \left[1 - \frac{T_o}{T_{gen}}\right] + \dot{W}_{comp-HTC} + +\dot{W}_{comp-LTC} + \dot{W}_{pump}} \tag{29}$$

Also, the simplified equation to determine COP of **stand-alone advanced RAC** system can be written as:

$$\eta_{ex} = \frac{\dot{Q}_{evp} \times \left|1 - \frac{T_o}{T_{evp}}\right|}{\dot{Q}_{gen,ext} \times \left[1 - \frac{T_o}{T_{gen}}\right] + \dot{W}_{comp} + \dot{W}_{pump}} \tag{30}$$

The rate of exergy destruction due to irreversibility within each component of the proposed cascade and standalone systems are stated in **Table 4-1** to **Table 4-9**. Summation of these provides the system's total loss or exergy destruction rate.

$$\begin{aligned}\dot{E}x_{D,total} = {} & \dot{E}x_{D,CHX} + \dot{E}x_{D,abs} + \dot{E}x_{D,RHX} + \dot{E}x_{D,SHX} + \dot{E}x_{D,gen} + \dot{E}x_{D,expansion\,valve} \\ & + \dot{E}x_{D,ejector} + \dot{E}x_{D,flash\,tank} + \dot{E}x_{D,evp} + \dot{E}x_{D,comp}\end{aligned} \tag{31}$$

This is an important parameter in the system analysis; pinpointing where most energy degradation occurs aids in enhancing system design, optimizing operations, and promoting sustainable practices.

4.3 Working Fluid

LiBr-H_2O and NH_3-H_2O are commonly used in traditional absorption systems. However, every refrigerant has its strengths and weaknesses. LiBr/H_2O in cascaded systems allows higher absorber pressure with non-toxic behaviors. Moreover, the generator activation temperature is lower, making them compatible for integrating with different industry heat with higher COP and exergy efficiency [25] [85] [18]. LiBr also allows for the elimination of the volatile liquid in the absorbent-refrigerant pair. This simplifies system design because the refrigerant exiting the generator is pure

water, eliminating the need for an analyzer and rectifier, making the system more compact, cost-effective, and easier to maintain [86]. However LiBr-H_2O systems face challenges with low evaporator temperatures due to crystallization and freezing [87]. Meanwhile, while NH_3 is seen as hazardous, its use within set safety guidelines allows it to perform across a diverse temperature spectrum, maintaining thermodynamic stability with flexibility. NH_3-H_2O's widespread adoption in ARC systems stems from its strong compatibility, environmental benefits, and capability to achieve lower evaporator temperatures - a key aim of this study [88]. Additionally, ejectors enhanced refrigeration systems are best suited for refrigerants with high vapor densities. This is because liquid-powered ejectors don't perform optimally with refrigerants that generate low-density vapor, as with steam in H_2O-LiBr systems [89]. Again, some research favors NH_3-$LiNO_3$ for superior *COP* over NH_3-H_2O, but real-world tests differ [90]. Also, the prime objective of this study is to enhance the performance of existing low *COP* absorption configurations using commonly used refrigerants.

As, LiBr-H_2O is utilized in cascaded compression absorption systems for simplicity and feasibility. This is why, in this research, **LiBr- H_2O** is used in the HTC absorption cycle of RAC and ARC based **proposed cascaded systems** (**ECAC, EICAC, E-CRAC, EI-CRAC**) because of feasibility in integration, alongside **R41** in the low-temperature circuit (LTC) owing to its environmental viability. Similarly, NH_3-H_2O can also be employed in absorption systems to achieve lower evaporator temperatures, making it a preferred choice for analyzing the performance of single-effect systems. This is why, in the analysis of improved **standalone recompression absorption technologies**, **NH_3-H_2O** is selected (**SE-RAC, RE-RAC, VI-RAC**). Furthermore, in the proposed standalone RAC systems, the maximum *COP* occurred at a generator pressure and temperature lower than the ARC. Thus, the proposed design could handle the high activation temperature and pressure challenges of ARCs with an NH_3-H_2O working fluid.

R41 is selected as the refrigerant for **LTC** in the **proposed cascaded systems**. This selection is motivated by the environmentally conscious and wide accessibility of this refrigerant pairing. R41 is known for its non-existent Ozone Depletion Potential (ODP), significantly low Global impact on global warming (GWP, approximately 95), and a low boiling point of -78.2 ℃ [79]. These characteristics make it a suitable choice for use in Low-Temperature Chillers (LTCs) [78][79]. For any operating condition, properties of each stream are determined using equations and integrated

library of EES. One more point to be noted, this study is mainly focused on evaluating configuration performance rather than extensive refrigerant analysis.

4.4 Ejector Modeling

The function of the ejector as a mixer of fluid streams of different pressures serves as a crucial aspect of the proposed systems' working processes. The operational fundamental of the ejector is modeled depending on the mathematical model formulated by Li et al. [91]. Numerous studies have indicated that the constant-pressure mixing ejector exhibits superior performance compared to the constant-area ejector [92], [93]. As a result, this research involves the modeling and application of a constant pressure mixing ejector. Additionally, an improved numerical model of a constant-pressure ejector, developed by Liu et.al [94], is utilized in this study, emphasizing the equations of area and area ratio of the corresponding ejector sections for analysis. Particularly, this involves the modeling of the mixing process in relation to the area variation of the mixing section, where a specific area ratio of the mixing section's entrance to exit is introduced. A schematic representation of the ejector is provided in **Figure 4-1.**

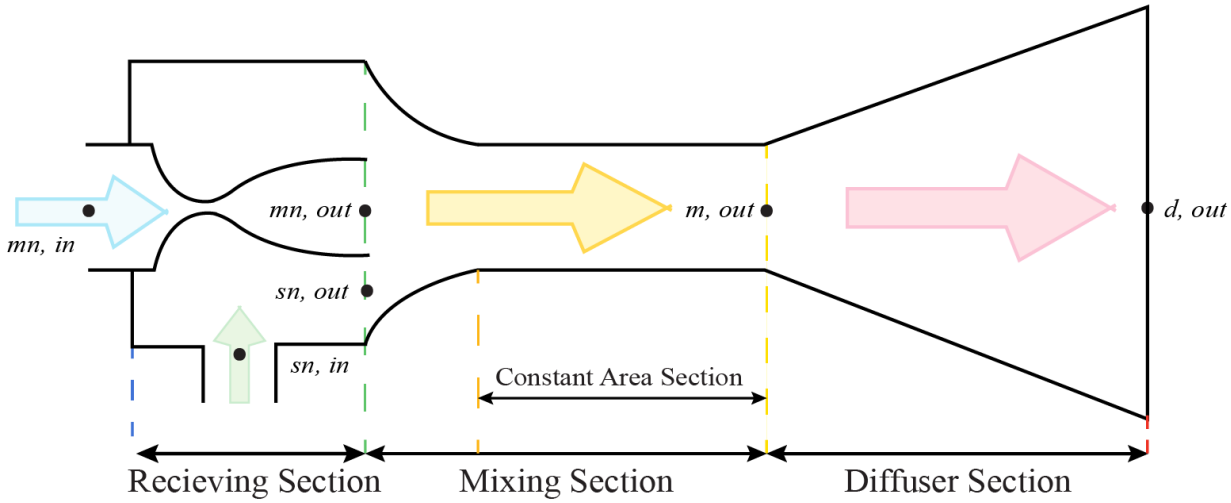

***Figure 4-1**: Illustrative Diagram of Ejector Configuration.*

The assumptions underlying the foundation of the ejector simulations include the following:

- There is no occurrence of external heat transfer.
- The ejector's flow is considered as a one-dimensional homogeneous equilibrium flow.

- It is assumed that the motive and suction streams reach equal pressure after accelerating through their respective nozzles.
- Upon exiting the mixing section, the mixed properties of refrigerants are presumed to be consistent across the cross-section.
- In the simulations, the consequences of frictional dissipation in the nozzle, mixing section and diffuser are considered. These losses are characterized by corresponding efficiency evaluations. Both the nozzle and diffuser performances are presumed to be 90%, when the mixer's performance is postulated to be about 95% [91].

In this study, the steady-state computations of the ejector model is employed based on the iterative approach of calculation suggested by Kornhauser [91]. This model, following a homogeneous equilibrium approach, takes account of the flow of refrigerants via both independent motive and suction nozzles. The design of these nozzles aims to attain equal outlet pressures, thereby promoting consistent blending in the mixing section. The discharge pressure, denoted as P_b, should maintain a value less than the suction side, regulated by the equation:

$$P_b = P_{suction} - \Delta P \tag{32}$$

In this equation, ΔP denotes the pressure drop across the suction nozzle. Additionally, fluid velocity and cross sectional area of nozzles and different sections of ejector is also calculated. In this context, the improved numerical model of a two-phase ejector by Liu et al. [94] is adopted to calculate the pertinent parameters related to the mixing chamber. In this context, a specific area ratio of the mixing section's entrance to exit, denoted as φ, is introduced.

$$\varphi = \frac{a_{mn,out} + a_{sn,out}}{a_{m,c}} \tag{33}$$

Here, $a_{mn,out}$ and $a_{sn,out}$ represents the cross-sectional area of motive and suction nozzle, respectfully. $a_{m,c}$, denotes the area of the constant section of mixing chamber, and $\varphi$is the mixing chamber area ratio. Another essential parameter in assessing the performance of the ejector is the entrainment ratio, denoted as *w*.

$$\omega = \frac{m_{suction}}{m_{motive}} \tag{34}$$

An initial guess of the entrainment ratio is assumed in the analysis and proceeded with iterations as depicted in the mathematical framework of the proposed systems. The requirement is to match the consistency of the vapor quality at the outlet of the diffuser with the system's theoretical value. For a definite working condition, ΔP is iterated to determine the optimal ΔP for maximum coefficient of performance.

At suction nozzle discharge (sn, out): The refrigerant accelerating through the suction nozzle is undergone isentropic expansion and reduction of pressure ΔP. So, the refrigerant properties can be determined as:

Pressure: $$p_{sn,out} = p_{sn,in} - \Delta p \quad (35)$$

Entropy: $$s_{sn,out} = s_{sn,in} \quad (36)$$

Applying the principal of "state postulate", the other properties can be determined as:

Idea enthalpy: $$h_{sn\,,out,is} = f\left(s_{sn\,,out,is}, P_{sn,out}\right) \quad (37)$$

Actual enthalpy: $$h_{sn\,,out} = h_{sn\,,in} - \eta_m(h_{sn\,,in} - h_{sn\,,out,is}) \quad (38)$$

Fluid Velocity: $$c_{sn,out} = \sqrt{2(h_{sn\,,in} - h_{sn\,,out})} \quad (39)$$

Density: $$\rho_{sn,out} = f\left(h_{sn\,,out}, P_{sn,out}\right) \quad (40)$$

Cross sectional Area: $$a_{sn,out} = \frac{w}{c_{sn,out}\,\rho_{sn,out}(1+\omega)} \quad (41)$$

At the discharge of the motive nozzle (mn, out): Expansion across the motive nozzle reduces the pressure of motive fluid to the outlet pressure of suction nozzle. The properties of the fluid can be determined as follows:

Pressure: $$P_{mn,out} = P_{sn,out} \quad (42)$$

Entropy: $$s_{mn,out} = s_{mn,in} \quad (43)$$

From these properties, the other properties can be found:

Idea enthalpy: $$h_{mn,out,is} = f\left(s_{mn,out,is}, P_{mn,out}\right) \quad (44)$$

Actual enthalpy: $$h_{mn,out} = h_{mn,in} - \eta_m(h_{mn,in} - h_{mn,out,is}) \quad (45)$$

Fluid velocity: $$c_{mn,out} = \sqrt{2(h_{mn,in} - h_{mn,out})} \quad (46)$$

Density: $$\rho_{mn,out} = f\left(h_{mn,out}, P_{mn,out}\right) \quad (47)$$

Cross sectional Area: $$a_{mn,out} = \frac{1}{c_{mn,out}\,\rho_{mn,out}(1+\omega)} \quad (48)$$

In the mixing section: Based on the conservation of momentum and energy during the mixing process of the primary and secondary fluids in the mixing chamber, the properties of the mixed fluid at the exit (m,out) are determined:

Pressure: $$p_m = p_{mn,out} = p_{sn,out} \quad (49)$$

Fluid velocity: $$c_{m,out} = \sqrt{\eta_{ms}}\left(\frac{1}{1+\omega}\,c_{mn,out} + \frac{\omega}{1+\omega}\,c_{sn,out}\right) \quad (50)$$

Enthalpy: $$h_{m,out} = \frac{1}{1+w}\left(h_{mn,out} + \frac{c_{mn,out}^2}{2}\right) + \frac{w}{1+w}\left(h_{sn,out} + \frac{c_{sn,out}^2}{2}\right) - \frac{c_{m,out}^2}{2} \quad (51)$$

Density: $$\rho_{m,out} = f\left(h_{m,out}, P_m\right) \quad (52)$$

Area Ratio of mixing chamber: $$\varphi = \frac{\rho_{m,out} * c_{m,out}}{\rho_{mn,out} * c_{mn,out}} * \frac{1}{1+\omega} + \frac{\rho_{m,out} * c_{m,out}}{\rho_{sn,out} * c_{sn,out}} * \frac{\omega}{1+\omega} \quad (53)$$

Area of Constant area section of mixing chamber $$a_{m,c} = \frac{a_{mn,out} + a_{sn,out}}{\varphi} \quad (54)$$

Entropy: $$s_{m,out} = s(p_m, h_{m,out}) \quad (55)$$

Considering the diffuser efficiency and utilizing the principle of energy conservation for isentropic compression within the diffuser, the pressure of the refrigerant at its outlet (d, out) and the corresponding properties can be computed as:

Enthalpy:
$$h_{d,out} = h_{m,out} + \frac{c_{m,out}^2}{2} \tag{56}$$

Ideal enthalpy:
$$h_{d,out,is} = h_{m,out} + \eta_d(h_{d,out} - h_{m,out}) \tag{57}$$

pressure at the outlet:
$$P_{d,out} = p(h_{d,out,is}, s_{m,out}) \tag{58}$$

Quality of the refrigerant:
$$x_{d,out} = f(h_{d,out,is}, P_{d,out}) \tag{59}$$

Ejector pressure lift ratio:
$$R_p = \frac{P_{d,out}}{P_{sn,in}} \tag{60}$$

To maintain energy equilibrium across the ejector, the fluid velocity at the diffuser outlet is regarded notably low [14]. Thus, the entrainment ratio is derived from the above equations as follows:

$$\omega = \sqrt{\eta_m \eta_{ms} \eta_d \frac{h_{mn,in} - h_{mn,out,is}}{h_{sn,in} - h_{sn,out,is}}} - 1 \tag{61}$$

4.5 Mathematical Modelling

When establishing mass, energy, and exergy balance equations for the relevant components of the proposed advance cascaded systems (ECAC, EICAC, E-CRAC, EI-CRAC) and standalone advanced RAC systems (RE-RAC, VI-RAC) several assumptions have been considered to facilitate model simulation as per the prior studies on refrigeration systems [68] [69] [95]. These are simplified as follows:

- A state of equilibrium, or steady state, is maintained throughout the entire system.
- Pressure fluctuations and thermal losses in the pipelines are deemed negligible.
- The throttling process in the expansion valve is considered as isenthalpic process, whereas the pump and compressor operate in an isentropic process.

- The state of refrigerant at the evaporator and condenser exit is considered as saturated conditions.
- In the generator of the ARC, the vapor refrigerant exits in pure state.
- Solutions exiting the absorber and generator are presumed to be in a saturated phase.
- A pinch temperature difference (ΔT_{pinch}) of 5°C is assumed in the *gen-cond* to enable internal heat exchange and the condensation of the recompressed ammonia [25].
- The isentropic efficiencies of the pump and compressor and the effectiveness of SHX and RHX is taken as constant.
- Power consumption in the solution pump is ignored due to negligible amount [68].

4.5.1 Modelling of ARC Based Proposed Cascaded Compression Absorption Systems

In this research, a modified ARC system as HTC is integrated with advanced VCR systems in LTC coupled with ejector and vapor injection to develop novel compression absorption cascade system ECAC (Ejector compression absorption cycle) and EICAC (Ejector injection compression absorption cycle).

The ECAC and EICAC both have a modified single-effect ARC (HTC of cycles in **Figure 3-4)** consisting of 9 components. The components are as follows: generator, condenser, absorber, solution heat exchanger, refrigerant heat exchanger, cascade heat exchanger, solution pump, and two expansion valves. Each component is modelled as a control volume, and energy-exergy balance equations are displayed in **Table 4-1**.

ECAC contains an ejector refrigeration system as LTC, whereas EICAC contains an ejector enhanced vapor injection system as LTC. Both systems contain the following components: cascade heat exchanger, ejector, flash tank, throttling valve, compressor and evaporator. As a difference between EICAC and ECAC, EICAC has an additional compressor, throttling valve, along with a mixing chamber to facilitate the vapor injection. Also, each component is regarded as control volume to formulate the mass, energy, and exergy balance equation as stated in

Table 4-2 and **Table 4-3**, for ejector expansion (LTC of ECAC illustrated in **Figure 3-4(a)**) and ejector enhanced vapor injection VCR respectively (LTC of EICAC **Figure 3-4(b)**).

***Table 4-1**. Energy and exergy balance equations of single effect modified absorption system.*

Component	Mass balance	Energy balance	Exergy destruction
Cascade heat exchanger	$\dot{m}_3=\dot{m}_4$ $\dot{m}_{13}=\dot{m}_{14}$	$\dot{Q}_{CHX} = \dot{m}_{13} \times (h_{13} - h_{14})$ $= \dot{m}_3 \times (h_4 - h_3)$	$\dot{E}_{D,CHX} = \dot{E}x_3 + \dot{E}x_{13} - \dot{E}x_4 - \dot{E}x_{14}$ $= \dot{m}_3((h_3 - h_4) - T_0(s_3 - s_4) + \dot{m}_{13}((h_{13} - h_{14}) - T_0(s_{13} - s_{14}))$
Expansion valve 2	$\dot{m}_{11}=\dot{m}_{13}$	$h_{11} = h_{13}$	$\dot{E}_{D,TV-I} = \dot{E}x_{11} - \dot{E}x_3 = \dot{m}_{11}((h_{11} - h_{13}) - T_0(s_{11} - s_{13}))$
Refrigerant heat exchanger	$\dot{m}_2=\dot{m}_{11}$ $\dot{m}_4=\dot{m}_{12}$	$\dot{Q}_{RHX} = \dot{m}_2 \times (h_2 - h_{11})$ $= \dot{m}_4 \times (h_{12} - h_4)$	$\dot{E}_{D,RHX} = \dot{E}x_2 + \dot{E}x_4 - \dot{E}x_{11} - \dot{E}x_{12}$ $= \dot{m}_2\big((h_2 - h_{11}) - T_0(s_2 - s_{11}) + \dot{m}_4((h_4 - h_{12}) - T_0(s_4 - s_{12})\big)$
Absorber	$\dot{m}_{12} + \dot{m}_{10} = \dot{m}_5$	$\dot{Q}_{abs} = \dot{m}_{12} \times h_{12} + \dot{m}_{10} \times h_{10} - \dot{m}_5 \times h_5$	$\dot{E}_{D,abs} = \dot{E}x_{12} + \dot{E}x_{10} - \dot{E}x_5 + (\dot{E}x_c - \dot{E}x_d)$ $= \dot{m}_{12}((h_{12} - h_0) - T_0(s_{12} - s_0)) + \dot{m}_{10}((h_{10} - h_0) - T_0(s_{10} - s_0)) - \dot{m}_5((h_5 - h_0) - T_0(s_5 - s_0)) + \dot{m}_c((h_c - h_d) - T_0(s_c - s_d))$
Solution Pump	$\dot{m}_5 = \dot{m}_6$	$\dot{W}_{pump} = \dot{m}_5 \times \frac{h_{6s} - h_5}{\eta_s}$	$\dot{E}_{D,Pump} = \dot{E}x_5 - \dot{E}x_6 = \dot{m}_5((h_5 - h_6) - T_0(s_5 - s_6))$
SHX	$\dot{m}_6 = \dot{m}_7$ $\dot{m}_8 = \dot{m}_9$	$\dot{Q}_{SHX} = \dot{m}_6 \times (h_7 - h_6)$ $= \dot{m}_8 \times (h_8 - h_9)$	$\dot{E}_{D,SHX} = \dot{E}x_6 + \dot{E}x_8 - \dot{E}x_7 - \dot{E}x_9$ $= \dot{m}_6((h_6 - h_7) - T_0(s_6 - s_7) + \dot{m}_7((h_8 - h_9) - T_0(s_8 - s_9))$
Generator	$\dot{m}_7$ $= \dot{m}_8 + \dot{m}_1$	$\dot{Q}_{gen} = \dot{m}_1 \times h_1$ $+\dot{m}_8 \times h_8 - \dot{m}_7 \times h_7$	$\dot{E}_{D,gen} = \dot{E}x_7 - \dot{E}x_8 - \dot{E}x_1 + \big(\dot{E}x_e - \dot{E}x_f\big)$ $= \dot{m}_7((h_7 - h_0) - T_0(s_7 - s_0)) - \dot{m}_8((h_8 - h_0) - T_0(s_8 - s_0)) - \dot{m}_1((h_1 - h_0) - T_0(s_1 - s_0)) + \dot{m}_e\big((h_e - h_f) - T_0(s_e - s_f)\big)$
Expansion valve 1	$\dot{m}_9=\dot{m}_{10}$	$h_{10} = h_9$	$\dot{E}_{D,TV-II} = \dot{E}x_{10} - \dot{E}x_9$ $= \dot{m}_{10}((h_{10} - h_9) - T_0(s_{10} - s_9))$
Condenser	$\dot{m}_1=\dot{m}_2$	$\dot{Q}_{cond} = \dot{m}_1 \times (h_1 - h_2)$	$\dot{E}_{D,con} = \dot{E}x_1 - \dot{E}x_2 + \big(\dot{E}x_g - \dot{E}x_h\big)$ $= \dot{m}_1((h_1 - h_2) - T_0(s_1 - s_2) + \dot{m}_a\big((h_g - h_h) - T_0(s_g - s_h)\big)$

***Table 4-2.** Energy and exergy balance equations of ejector expansion VCR cycle employed in ECAC.*

Component	Mass balance	Energy balance	Exergy destruction
Evaporator	$\dot{m}_{19}=\dot{m}_{20}$	$\dot{Q}_{evp} = \dot{m}_{19} \times (h_{20} - h_{19})$	$\dot{E}_{D,Evp} = \dot{E}x_{19} - \dot{E}x_{20} + (\dot{E}x_a - \dot{E}x_b)$ $= \dot{m}_{19}((h_{19} - h_{20}) - T_0(s_{19} - s_{20}) + \dot{m}_a((h_a - h_b) - T_0(s_a - s_b))$

Ejector	$\dot{m}_{14} + \dot{m}_{20} = \dot{m}_{15} = \dot{m}_{16} = \dot{m}_{17}$		$\dot{E}_{D,ejector} = \dot{E}x_{14} + \dot{E}x_{20} - \dot{E}x_{17} = \dot{m}_{14}((h_{14} - h_0) - T_0(s_{14} - s_0)) + \dot{m}_{20}((h_{20} - h_0) - T_0(s_{20} - s_0)) - \dot{m}_{17}((h_{17} - h_0) - T_0(s_{17} - s_0))$
Flash Tank	$\dot{m}_{18}=\dot{m}_{17}(1 - x_{17})$ $\dot{m}_{21}= \dot{m}_{17} x_{17}$	$\dot{m}_{17} h_{17} = \dot{m}_{18} h_{18} + \dot{m}_{21} h_{21}$	$\dot{E}_{D,FT} = \dot{E}x_{17} - \dot{E}x_{18} - \dot{E}x_{21} = \dot{m}_{17}((h_{17} - h_0) - T_0(s_{17} - s_0)) - \dot{m}_{18}((h_{18} - h_0) - T_0(s_{18} - s_0)) - \dot{m}_{21}((h_{21} - h_0) - T_0(s_{21} - s_0))$
Expansion valve 3	$\dot{m}_{18}=\dot{m}_{19}$	$h_{18} = h_{19}$	$\dot{E}_{D,TV-III} = \dot{E}x_{18} - \dot{E}x_{19} = \dot{m}_{18}((h_{18} - h_{19}) - T_0(s_{18} - s_{19})$
Compressor	$\dot{m}_5 = \dot{m}_6$	$\dot{W}_{comp} = \dot{m}_{21} \times \frac{h_{13s} - h_{21}}{\eta_s}$	$\dot{E}_{D,comp} = \dot{E}x_{21} - \dot{E}x_{13} = \dot{m}_{21}((h_{21} - h_{13}) - T_0(s_{21} - s_{13})$

***Table 4-3**. Energy and exergy balance equations of ejector-enhanced vapor injection VCR employed in EICAC.*

Component	Mass balance	Energy balance	Exergy destruction
Evaporator	$\dot{m}_{23}=\dot{m}_{24}$	$\dot{Q}_{evp} = \dot{m}_{23} \times (h_{24} - h_{23})$	$\dot{E}_{D,evp} = \dot{E}x_{23} - \dot{E}x_{24} + (\dot{E}x_a - \dot{E}x_b) = \dot{m}_{23}((h_{23} - h_{24}) - T_0(s_{23} - s_{24}) + \dot{m}_a((h_a - h_b) - T_0(s_a - s_b))$
Ejector	$\dot{m}_{14} + \dot{m}_{21} = \dot{m}_{15} = \dot{m}_{16} = \dot{m}_{17}$		$\dot{E}_{D,ejector} = \dot{E}x_{14} + \dot{E}x_{21} - \dot{E}x_{17} = \dot{m}_{14}((h_{14} - h_0) - T_0(s_{14} - s_0)) + \dot{m}_{21}((h_{21} - h_0) - T_0(s_{21} - s_0)) - \dot{m}_{17}((h_{17} - h_0) - T_0(s_{17} - s_0))$
Flash Tank 1	$\dot{m}_{19}=\dot{m}_{17}(1 - x_{17})$ $\dot{m}_{18}= \dot{m}_{17} x_{17}$	$\dot{m}_{17} h_{17} = \dot{m}_{18} h_{18} + \dot{m}_{19} h_{19}$	$\dot{E}_{D,FT-I} = \dot{E}x_{17} - \dot{E}x_{18} - \dot{E}x_{19} = \dot{m}_{17}((h_{17} - h_0) - T_0(s_{17} - s_0)) - \dot{m}_{18}((h_{18} - h_0) - T_0(s_{18} - s_0)) - \dot{m}_{19}((h_{19} - h_0) - T_0(s_{19} - s_0))$
Flash Tank 2	$\dot{m}_{22}=\dot{m}_{20}(1 - x_{20})$ $\dot{m}_{21}= \dot{m}_{20} x_{20}$	$\dot{m}_{20} h_{20} = \dot{m}_{22} h_{22} + \dot{m}_{21} h_{21}$	$\dot{E}_{D,FT-II} = \dot{E}x_{20} - \dot{E}x_{22} - \dot{E}x_{21} = \dot{m}_{20}((h_{20} - h_0) - T_0(s_{20} - s_0)) - \dot{m}_{22}((h_{22} - h_0) - T_0(s_{22} - s_0)) - \dot{m}_{21}((h_{21} - h_0) - T_0(s_{21} - s_0))$
Expansion valve 3	$\dot{m}_{19}=\dot{m}_{20}$	$h_{19} = h_{20}$	$\dot{E}_{D,TV-III} = \dot{E}x_{19} - \dot{E}x_{20} = \dot{m}_{19}((h_{19} - h_{20}) - T_0(s_{19} - s_{20})$
Expansion valve 4	$\dot{m}_{22}=\dot{m}_{23}$	$h_{22} = h_{23}$	$\dot{E}_{D,TV-IV} = \dot{E}x_{22} - \dot{E}x_{23} = \dot{m}_{22}((h_{22} - h_{23}) - T_0(s_{22} - s_{23})$
Compressor 1	$\dot{m}_{24} = \dot{m}_{25}$	$\dot{W}_{comp-I} = \dot{m}_{24} \times \frac{h_{25s} - h_{24}}{\eta_s}$	$\dot{E}_{D,comp-I} = \dot{E}x_{24} - \dot{E}x_{25} = \dot{m}_{24}((h_{24} - h_{25}) - T_0(s_{24} - s_{25})$
Compressor 2	$\dot{m}_{26} = \dot{m}_{13}$	$\dot{W}_{comp-II} = \dot{m}_{26} \times \frac{h_{13s} - h_{26}}{\eta_s}$	$\dot{E}_{D,comp-II} = \dot{E}x_{26} - \dot{E}x_{13} = \dot{m}_{26}((h_{26} - h_{13}) - T_0(s_{26} - s_{13})$

Mixing chamber	$\dot{m}_{18} + \dot{m}_{25} = \dot{m}_{26}$	$\dot{m}_{25}\, h_{25} + \dot{m}_{218}\, h_{18} = \dot{m}_{26}\, h_{26}$	$\dot{E}_{D,mixing\ chamber} = \dot{E}x_{25} + \dot{E}x_{18} - \dot{E}x_{26} = \dot{m}_{25}\big((h_{25} - h_{0)} - T_0(s_{25} - s_0)\big) + \dot{m}_{18}\big((h_{18} - h_{0)} - T_0(s_{18} - s_0)\big) - \dot{m}_{26}\big((h_{26} - h_{0)} - T_0(s_{26} - s_0)\big)$

4.5.2 Modelling of RAC Based Proposed Cascaded Compression Absorption Systems

This research further delves into the field of cascaded compression absorption system by integrating an advanced Recompression Absorption System (RAC) with an enhanced VCR equipped with ejector, resulting in the innovative proposed Ejector-Compression Recompression Absorption cycle (E-CRAC) and Ejector enhanced Vapor-Injection Compression Recompression Absorption Cycle (EI-CRAC).

In all the proposed systems within this section, recompression ARC is used in HTC. In E-CRAC and EI-CRAC, the simple recompression cycle is improved by using a RHX to recover some energy loss during the throttle process. Simple recompression Absorption cycle employed in conventional CRAC, comprises of 7 components. The components are as follows: compressor-HTC, generator-condenser, SHX, absorber, cascade heat exchanger, solution pump, and two throttling valves. Additional RHX is added to the modified recompression absorption system employed in E-CRAC and EI-CRAC (HTC of cycles in **Figure 3-12**). Across each of the controlled volume components, conservation of energy, mass and exergy balance equations can be applied as presented in **Table 4-4.**

Conventional CARC and CRAC contain VCR as LTC which consists of 4 components. Following the flow convention as depicted in **Figure 1-5**, the corresponding energy-exergy balance equation of independent components are presented in **Table 4-5.**

***Table 4-4**. Energy and exergy balance equations of Recompression Absorption Cycle (RAC).*

Elements	Mass balance	Energy balance	Exergy destruction
Cascaded Heat Exchanger	$\dot{m}_4$=$\dot{m}_5$	$\dot{Q}_{CHX} = \dot{m}_{13} \times (h_{13} - h_{14}) = \dot{m}_3 \times (h_5 - h_4)$	$\dot{E}x_{D,CHX} = \dot{E}x_4 + \dot{E}x_{13} - \dot{E}x_5 - \dot{E}x_{14} = \dot{m}_4((h_4 - h_5) - T_0(s_4 - s_5) + \dot{m}_{13}((h_{13} - h_{14}) - T_0(s_{13} - s_{14}))$
Expansion Valve 1	$\dot{m}_{10}$=$\dot{m}_{11}$	$h_{11} = h_{10}$	$\dot{E}x_{D,\exp-I} = \dot{E}x_{10} - \dot{E}x_{11} = \dot{m}_{10}((h_{10} - h_{11}) - T_0(s_{10} - s_{11}))$
Refrigerant Heat Exchanger	$\dot{m}_3 = \dot{m}_{30}$ $\dot{m}_5 = \dot{m}_{12}$	$\dot{Q}_{RHX} = \dot{m}_3 \times (h_3 - h_{30}) = \dot{m}_5 \times (h_{12} - h_5)$	$\dot{E}x_{D,RHX} = \dot{E}x_3 + \dot{E}x_5 - \dot{E}x_{30} - \dot{E}x_{12} = \dot{m}_3\big((h_3 - h_{30}) - T_0(s_3 - s_{30})\big) + \dot{m}_5((h_5 - h_{12}) - T_0(s_5 - s_{12}))$
Absorber	$\dot{m}_{12} + \dot{m}_{11} = \dot{m}_6$	$\dot{Q}_{abs} = \dot{m}_{12} \times h_{12} + \dot{m}_{11} \times h_{11} - \dot{m}_6 \times h_6$	$\dot{E}x_{D,abs} = \dot{E}x_{12} + \dot{E}x_{11} - \dot{E}x_6 + (\dot{E}x_c - \dot{E}x_d) = \dot{m}_{12}((h_{12} - h_0) - T_0(s_{12} - s_0)) + \dot{m}_{11}((h_{11} - h_0) - T_0(s_{11} - s_0)) - \dot{m}_6((h_6 - h_0) - T_0(s_6 - s_0)) + \dot{m}_c((h_c - h_d) - T_0(s_c - s_d))$
Solution Pump	$\dot{m}_6 = \dot{m}_7$	$\dot{W}_{pump} = \dot{m}_6 \times \frac{h_{7s} - h_6}{\eta_s}$	$\dot{E}x_{D,Pump} = \dot{E}x_6 - \dot{E}x_7 = \dot{m}_6((h_6 - h_7) - T_0(s_6 - s_7))$
Solution Heat Exchanger	$\dot{m}_7 = \dot{m}_8$ $\dot{m}_9 = \dot{m}_{10}$	$\dot{Q}_{SHX} = \dot{m}_7 \times (h_8 - h_7) = \dot{m}_9 \times (h_9 - h_{10})$	$\dot{E}x_{D,SHX} = \dot{E}x_7 + \dot{E}x_9 - \dot{E}x_8 - \dot{E}x_{10} = \dot{m}_7((h_7 - h_8) - T_0(s_7 - s_8) + \dot{m}_9((h_9 - h_{10}) - T_0(s_9 - s_{10}))$
Generator - Condenser	$\dot{m}_8 = \dot{m}_9 + \dot{m}_1$ $\dot{m}_1 = \dot{m}_2 = \dot{m}_3$	$\dot{Q}_{gen} = \dot{m}_1 \times h_1 + \dot{m}_9 \times h_9 - \dot{m}_8 \times h_8$ $\dot{Q}_{gen} = \dot{Q}_{cond}$ $\dot{Q}_{cond} = \dot{m}_3 \times h_3 + \dot{m}_2 \times h_2$	$\dot{E}x_{D,gen-cond} = \dot{E}x_8 - \dot{E}x_9 - \dot{E}x_1 + (\dot{E}x_2 - \dot{E}x_3) = \dot{m}_8((h_8 - h_0) - T_0(s_8 - s_0)) - \dot{m}_9((h_9 - h_0) - T_0(s_9 - s_0)) - \dot{m}_1((h_1 - h_0) - T_0(s_1 - s_0)) + \dot{m}_2((h_2 - h_0) - T_0(s_2 - s_0) - \dot{m}_3((h_3 - h_0) - T_0(s_3 - s_0))$
Comp-HTC	$\dot{m}_1 = \dot{m}_2$	$\dot{W}_{comp-HTC} = \dot{m}_1 \times \frac{h_{2s} - h_1}{\eta_s}$	$\dot{E}x_{D,HTC} = \dot{E}x_1 - \dot{E}x_2 = \dot{m}_1((h_1 - h_2) - T_0(s_1 - s_2)$
Expansion Valve 2	$\dot{m}_{30}$=$\dot{m}_4$	$h_{30} = h_4$	$\dot{E}x_{D,TV-II} = \dot{E}x_{30} - \dot{E}x_4 = \dot{m}_{30}((h_{30} - h_4) - T_0(s_{30} - s_4))$

***Table 4-5**. Energy and exergy balance equations of VCR cycle used in conventional CARC and CRAC.*

Elements	Mass balance	Energy balance	Exergy destruction
Evaporator	$\dot{m}_{15}$=$\dot{m}_{12}$	$\dot{Q}_{evp} = \dot{m}_{15} \times (h_{12} - h_{15})$	$\dot{E}x_{D,Evp} = \dot{E}x_{15} - \dot{E}x_{12} + (\dot{E}x_a - \dot{E}x_b) = \dot{m}_{15}((h_{15} - h_{12}) - T_0(s_{15} - s_{12}) + \dot{m}_a((h_a - h_b) - T_0(s_a - s_b))$
Expansion valve 3	$\dot{m}_{14}$=$\dot{m}_{15}$	$h_{14} = h_{15}$	$\dot{E}x_{D,\exp-III} = \dot{E}x_{14} - \dot{E}x_{15} = \dot{m}_{14}((h_{14} - h_{15}) - T_0(s_{14} - s_{15})$

Comp-LTC	$\dot{m}_{12} = \dot{m}_{13}$	$\dot{W}_{comp} = \dot{m}_{12} \times \frac{h_{13s} - h_{12}}{\eta_s}$	$\dot{E}x_{D,comp} = \dot{E}x_{12} - \dot{E}x_{13} = \dot{m}_{12}((h_{12} - h_{13}) - T_0(s_{12} - s_{13})$

E-CRAC contains ejector expansion VCR in LTC, whereas EI-CRAC has vapor injection facilitated ejector enhanced VCR in LTC. Both the advanced VCRs of the proposed system are comprised of the same components, such as: evaporator, compressor-LTC, expansion valve, flash tank, ejector and cascade heat exchanger.

Distinguishing between EI-CRAC and E-CRAC, the former incorporates an extra compressor, a throttling valve, and a mixing chamber to enable the process of vapor injection. Here, each component can also be assumed as control volume. Following the flow convention as depicted in **Figure 3-9(a)** and **Figure 3-9(b)** respectively, the mass, energy and exergy balance equation across each component for Ejector expansion and Ejector incorporated vapor injection VCR employed in the corresponding LTC of E-CRAC and EI-CRAC respectively is stated in **Table 4-6** and **Table 4-7**.

Table 4-6. *Energy and exergy balance equations of ejector expansion VCR cycle employed in E-CRAC.*

Elements	Mass balance	Energy balance	Exergy destruction
Comp-LTC	$\dot{m}_{21} = \dot{m}_{13}$	$\dot{W}_{comp} = \dot{m}_{21} \times \frac{h_{13s} - h_{21}}{\eta_s}$	$\dot{E}x_{D,comp} = \dot{E}x_{21} - \dot{E}x_{13} = \dot{m}_{21}((h_{21} - h_{13}) - T_0(s_{21} - s_{13})$
Evaporator	$\dot{m}_{19} = \dot{m}_{20}$	$\dot{Q}_{evp} = \dot{m}_{19} \times (h_{20} - h_{19})$	$\dot{E}x_{D,Evp} = \dot{E}x_{19} - \dot{E}x_{20} + (\dot{E}x_a - \dot{E}x_b) = \dot{m}_{19}((h_{19} - h_{20}) - T_0(s_{19} - s_{20}) + \dot{m}_a((h_a - h_b) - T_0(s_a - s_b))$
Ejector	$\dot{m}_{14} + \dot{m}_{20} = \dot{m}_{15} = \dot{m}_{16} = \dot{m}_{17}$	$\dot{m}_{14}\, h_{14} + \dot{m}_{20}\, h_{20} = \dot{m}_{17}\, h_{17}$	$\dot{E}x_{D,ejector} = \dot{E}x_{14} + \dot{E}x_{20} - \dot{E}x_{17} = \dot{m}_{14}((h_{14} - h_0) - T_0(s_{14} - s_0)) + \dot{m}_{20}((h_{20} - h_0) - T_0(s_{20} - s_0)) - \dot{m}_{17}((h_{17} - h_0) - T_0(s_{17} - s_0))$
Flash Tank	$\dot{m}_{18} = \dot{m}_{17}(1 - x_{17})$ $\dot{m}_{21} = \dot{m}_{17}\, x_{17}$	$\dot{m}_{17}\, h_{17} = \dot{m}_{18}\, h_{18} + \dot{m}_{21}\, h_{21}$	$\dot{E}x_{D,FT} = \dot{E}x_{17} - \dot{E}x_{18} - \dot{E}x_{21} = \dot{m}_{17}((h_{17} - h_0) - T_0(s_{17} - s_0)) - \dot{m}_{18}((h_{18} - h_0) - T_0(s_{18} - s_0)) - \dot{m}_{21}((h_{21} - h_0) - T_0(s_{21} - s_0))$
Expansion valve 3	$\dot{m}_{18} = \dot{m}_{19}$	$h_{18} = h_{19}$	$\dot{E}x_{D,\exp-III} = \dot{E}x_{18} - \dot{E}x_{19} = \dot{m}_{18}((h_{18} - h_{19}) - T_0(s_{18} - s_{19})$

***Table 4-7**. Energy and exergy equations of ejector enhanced vapor injection VCR employed in EI-CRAC.*

Elements	Mass balance	Energy balance	Exergy destruction
Comp-LTC I	$\dot{m}_{24} = \dot{m}_{25}$	$\dot{W}_{comp-I} = \dot{m}_{24} \times \frac{h_{25s}-h_{24}}{\eta_s}$	$\dot{E}x_{D,comp-I} = \dot{E}x_{24} - \dot{E}x_{25} = \dot{m}_{24}((h_{24} - h_{25}) - T_0(s_{24} - s_{25})$
Comp-LTC II	$\dot{m}_{26} = \dot{m}_{13}$	$\dot{W}_{comp-II} = \dot{m}_{26} \times \frac{h_{13s}-h_{26}}{\eta_s}$	$\dot{E}x_{D,comp-II} = \dot{E}x_{26} - \dot{E}x_{13} = \dot{m}_{26}((h_{26} - h_{13}) - T_0(s_{26} - s_{13})$
Evaporator	$\dot{m}_{23}$=$\dot{m}_{24}$	$\dot{Q}_{evp} = \dot{m}_{23} \times (h_{24} - h_{23})$	$\dot{E}x_{D,evp} = \dot{E}x_{23} - \dot{E}x_{24} + (\dot{E}x_a - \dot{E}x_b) = \dot{m}_{23}((h_{23} - h_{24}) - T_0(s_{23} - s_{24}) + \dot{m}_a((h_a - h_b) - T_0(s_a - s_b))$
Ejector	$\dot{m}_{14} + \dot{m}_{21} = \dot{m}_{15} = \dot{m}_{16} = \dot{m}_{17}$	$\dot{m}_{14}\, h_{14} + \dot{m}_{21}\, h_{21} = \dot{m}_{17}\, h_{17}$	$\dot{E}x_{D,ejector} = \dot{E}x_{14} + \dot{E}x_{21} - \dot{E}x_{17} = \dot{m}_{14}((h_{14} - h_0) - T_0(s_{14} - s_0)) + \dot{m}_{21}((h_{21} - h_0) - T_0(s_{21} - s_0)) - \dot{m}_{17}((h_{17} - h_0) - T_0(s_{17} - s_0))$
Flash Tank 1	$\dot{m}_{19} = \dot{m}_{17}\,(1 - x_{17})$ $\dot{m}_{18} = \dot{m}_{17}\, x_{17}$	$\dot{m}_{17}\, h_{17} = \dot{m}_{18}\, h_{18} + \dot{m}_{19}\, h_{19}$	$\dot{E}x_{D,FT-I} = \dot{E}x_{17} - \dot{E}x_{18} - \dot{E}x_{19} = \dot{m}_{17}((h_{17} - h_0) - T_0(s_{17} - s_0)) - \dot{m}_{18}((h_{18} - h_0) - T_0(s_{18} - s_0)) - \dot{m}_{19}((h_{19} - h_0) - T_0(s_{19} - s_0))$
Flash Tank 2	$\dot{m}_{22} = \dot{m}_{20}\,(1 - x_{20})$ $\dot{m}_{21} = \dot{m}_{20}\, x_{20}$	$\dot{m}_{20}\, h_{20} = \dot{m}_{22}\, h_{22} + \dot{m}_{21}\, h_{21}$	$\dot{E}x_{D,FT-II} = \dot{E}x_{20} - \dot{E}x_{22} - \dot{E}x_{21} = \dot{m}_{20}((h_{20} - h_0) - T_0(s_{20} - s_0)) - \dot{m}_{22}((h_{22} - h_0) - T_0(s_{22} - s_0)) - \dot{m}_{21}((h_{21} - h_0) - T_0(s_{21} - s_0))$
Expansion valve 3	$\dot{m}_{19} = \dot{m}_{20}$	$h_{19} = h_{20}$	$\dot{E}x_{D,TV-III} = \dot{E}x_{19} - \dot{E}x_{20} = \dot{m}_{19}((h_{19} - h_{20}) - T_0(s_{19} - s_{20})$
Expansion valve 4	$\dot{m}_{22} = \dot{m}_{23}$	$h_{22} = h_{23}$	$\dot{E}x_{D,TV-IV} = \dot{E}x_{22} - \dot{E}x_{23} = \dot{m}_{22}((h_{22} - h_{23}) - T_0(s_{22} - s_{23})$
Mixing chamber	$\dot{m}_{18} + \dot{m}_{25} = \dot{m}_{26}$	$\dot{m}_{25}\, h_{25} + \dot{m}_{18}\, h_{18} = \dot{m}_{26}\, h_{26}$	$\dot{E}x_{D,mixing\ chamber} = \dot{E}x_{25} + \dot{E}x_{18} - \dot{E}x_{26} = \dot{m}_{25}\big((h_{25} - h_{0)} - T_0(s_{25} - s_0)\big) + \dot{m}_{18}\big((h_{18} - h_{0)} - T_0(s_{18} - s_0)\big) - \dot{m}_{26}\big((h_{26} - h_{0)} - T_0(s_{26} - s_0)\big)$

4.5.3 Modelling of Advanced Stand-alone Recompression Absorption System Equipped with Ejector and Vapor Injection.

Finally, this research proposes a feasible upgrade of standalone single effect ARC by incorporating recompression technology with ejector and injection setup into the refrigerant side of the RAC cycle, resulting in the development of advanced systems: Refrigerant Ejector enhanced Recompression Absorption Cycle (RE-RAC), and Vapor Injection enhanced Recompression Absorption Cycle (VI-RAC). In these configurations, the conventional single-valve expansion of the refrigerant is substituted, and energy is recuperated internally, facilitating the entry of refrigerant into the absorber at an elevated pressure to reach higher system efficiency. Consequently, these modifications allow the absorption system to operate at lower evaporator temperature as well.

Both the advanced proposed RAC: RE-RAC and VI-RAC, have more components than the basic RAC, with RE-RAC comprising 11 and VI-RAC encompassing 13 components. The main difference is, that RE-RAC has an ejector expansion system, whereas VI-RAC has a flash tank integrated vapor injection system. Due to the mechanism of VI-RAC, an additional compressor is needed to increase the pressure of the evaporator outlet and mix it with the vapor injected from the flash tank. Meanwhile, RE-RAC directly mixes this evaporator outlet stream with the condenser outlet stream in the ejector to increase the resulting pressure and pass it to the absorber. That's why VI-RAC also requires an additional expansion valve to expand the liquid ammonia from the condenser outlet to the intermediate pressure of the flash tank. The components are as follows: solution heat exchanger, generator- condenser, solution pump, absorber, expansion valves, refrigerant heat exchanger, compressor, ejector, flash tank, and mixing chamber. Each component is modelled as a control volume, and the energy-exergy balance equations of RE-RAC (as depicted in **Figure 3-12(a)**) and VI-RAC (as depicted in **Figure 3-12(b)**) are displayed in **Table 4-8** and **Table 4-9,** respectively.

***Table 4-8**. Energy and exergy balance equations of the proposed RE-RAC system.*

Elements	Mass balance	Energy balance	Exergy destruction
Compressor	$\dot{m}_7 = \dot{m}_8$	$\dot{W}_{comp} = \dot{m}_1 \times \frac{h_{8s}-h_7}{\eta_s}$	$\dot{E}x_{D,\text{comp}} = \dot{E}x_7 - \dot{E}x_8 = \dot{m}_7((h_7 - h_8) - T_0(s_7 - s_8)$
Expansion Valve II	$\dot{m}_{14}$=$\dot{m}_{15}$	$h_{14} = h_{15}$	$\dot{E}x_{D,\text{exp}-I} = \dot{E}x_{14} - \dot{E}x_{15} = \dot{m}_{14}((h_{14} - h_{15}) - T_0(s_{14} - s_{15}))$
Refrigerant Heat Exchanger	$\dot{m}_9 = \dot{m}_{10}$ $\dot{m}_{17} = \dot{m}_{18}$	$\dot{Q}_{RHX} = \dot{m}_9 \times (h_9 - h_{10}) = \dot{m}_{17} \times (h_{18} - h_{17})$	$\dot{E}x_{D,RHX} = \dot{E}x_9 + \dot{E}x_{17} - \dot{E}x_{14} - \dot{E}x_{18} = \dot{m}_9\big((h_9 - h_{10}) - T_0(s_9 - s_{10})) + \dot{m}_{17}((h_{17} - h_{18}) - T_0(s_{17} - s_{18})\big)$
Absorber	$\dot{m}_{18} + \dot{m}_6 = \dot{m}_1$	$\dot{Q}_{abs} = \dot{m}_{18} \times h_{18} + \dot{m}_6 \times h_6 - \dot{m}_1 \times h_1$	$\dot{E}x_{D,abs} = \dot{E}x_{18} + \dot{E}x_6 - \dot{E}x_1 + (\dot{E}x_c - \dot{E}x_d) = \dot{m}_{18}((h_{18} - h_0) - T_0(s_{18} - s_0)) + \dot{m}_6((h_6 - h_0) - T_0(s_6 - s_0)) - \dot{m}_1((h_1 - h_0) - T_0(s_1 - s_0)) + \dot{m}_c((h_c - h_d) - T_0(s_c - s_d))$
Solution Pump	$\dot{m}_1 = \dot{m}_2$	$\dot{W}_{pump} = \dot{m}_1 \times \frac{h_{2s} - h_1}{\eta_s}$	$\dot{E}x_{D,Pump} = \dot{E}x_1 - \dot{E}x_2 = \dot{m}_1((h_1 - h_2) - T_0(s_1 - s_2))$
Solution Heat Exchanger	$\dot{m}_2 = \dot{m}_3$ $\dot{m}_4 = \dot{m}_5$	$\dot{Q}_{SHX} = \dot{m}_2 \times (h_3 - h_2) = \dot{m}_4 \times (h_4 - h_5)$	$\dot{E}x_{D,SHX} = \dot{E}x_2 + \dot{E}x_4 - \dot{E}x_3 - \dot{E}x_5 = \dot{m}_2((h_2 - h_3) - T_0(s_2 - s_3) + \dot{m}_4((h_4 - h_5) - T_0(s_4 - s_5))$
Generator-Condenser	$\dot{m}_3 = \dot{m}_4 + \dot{m}_7$ $\dot{m}_7 = \dot{m}_8 = \dot{m}_9$	$\dot{Q}_{gen} = \dot{m}_7 \times h_7 + \dot{m}_4 \times h_4 - \dot{m}_3 \times h_3$ $\dot{Q}_{gen} = \dot{Q}_{cond}$ $\dot{Q}_{cond} = \dot{m}_9 \times h_9 + \dot{m}_8 \times h_8$	$\dot{E}x_{D,gen-cond} = \dot{E}x_3 - \dot{E}x_4 - \dot{E}x_7 + (\dot{E}x_8 - \dot{E}x_9) = \dot{m}_3((h_3 - h_0) - T_0(s_3 - s_0)) - \dot{m}_4((h_4 - h_0) - T_0(s_4 - s_0)) - \dot{m}_7((h_7 - h_0) - T_0(s_7 - s_0)) + \dot{m}_8((h_8 - h_0) - T_0(s_8 - s_0) - \dot{m}_9((h_9 - h_0) - T_0(s_9 - s_0))$
Flash tank	$\dot{m}_{14} = \dot{m}_{13}(1 - x_{13})$ $\dot{m}_{17} = \dot{m}_{13} x_{13}$	$\dot{m}_{13} h_{13} = \dot{m}_{14} h_{14} + \dot{m}_{17} h_{17}$	$\dot{E}x_{D,FT} = \dot{E}x_{13} - \dot{E}x_{14} - \dot{E}x_{17} = \dot{m}_{13}((h_{13} - h_0) - T_0(s_{13} - s_0)) - \dot{m}_{14}((h_{14} - h_0) - T_0(s_{14} - s_0)) - \dot{m}_{17}((h_{17} - h_0) - T_0(s_{17} - s_0))$
Ejector	$\dot{m}_{10} + \dot{m}_{16} = \dot{m}_{11} = \dot{m}_{12} = \dot{m}_{13}$	$\dot{m}_{10} h_{10} + \dot{m}_{16} h_{16} = \dot{m}_{13} h_{13}$	$\dot{E}x_{D,ejector} = \dot{E}x_{10} + \dot{E}x_{16} - \dot{E}x_{13} = \dot{m}_{10}((h_{10} - h_0) - T_0(s_{10} - s_0)) + \dot{m}_{16}((h_{16} - h_0) - T_0(s_{16} - s_0)) - \dot{m}_{13}((h_{13} - h_0) - T_0(s_{13} - s_0))$
Evaporator	$\dot{m}_{15} = \dot{m}_{16}$	$\dot{Q}_{evp} = \dot{m}_{15} \times (h_{16} - h_{15})$	$\dot{E}x_{D,Evp} = \dot{E}x_{15} - \dot{E}x_{16} + (\dot{E}x_a - \dot{E}x_b) = \dot{m}_{15}((h_{15} - h_{16}) - T_0(s_{15} - s_{16}) + \dot{m}_a((h_a - h_b) - T_0(s_a - s_b))$
Expansion Valve I	$\dot{m}_5$=$\dot{m}_6$	$h_5 = h_6$	$\dot{E}x_{D,TV-II} = \dot{E}x_5 - \dot{E}x_6 = \dot{m}_5((h_5 - h_6) - T_0(s_5 - s_6))$

***Table 4-9**. Energy and exergy balance equations of the proposed VI-RAC system.*

Elements	Mass balance	Energy balance	Exergy destruction
Compressor I	$\dot{m}_7 = \dot{m}_8$	$\dot{W}_{comp} = \dot{m}_1 \times \frac{h_{8s}-h_7}{\eta_s}$	$\dot{E}x_{D,\text{comp}} = \dot{E}x_7 - \dot{E}x_8 = \dot{m}_7((h_7 - h_8) - T_0(s_7 - s_8)$
Compressor II	$\dot{m}_{14} = \dot{m}_{15}$	$\dot{W}_{comp-II} = \dot{m}_{14} \times \frac{h_{14s}-h_{15}}{\eta_s}$	$\dot{E}x_{D,\text{comp-II}} = \dot{E}x_{14} - \dot{E}x_{15} = \dot{m}_{14}((h_{14} - h_{15}) - T_0(s_{14} - s_{15})$
Expansion Valve I	$\dot{m}_5$=$\dot{m}_6$	$h_5 = h_6$	$\dot{E}x_{D,TV-I} = \dot{E}x_5 - \dot{E}x_6 = \dot{m}_5((h_5 - h_6) - T_0(s_5 - s_6))$
Refrigerant Heat Exchanger	$\dot{m}_9 = \dot{m}_{10}$ $\dot{m}_{17} = \dot{m}_{18}$	$\dot{Q}_{RHX} = \dot{m}_9 \times (h_9 - h_{10}) = \dot{m}_{17} \times (h_{18} - h_{17})$	$\dot{E}x_{D,RHX} = \dot{E}x_9 + \dot{E}x_{17} - \dot{E}x_{14} - \dot{E}x_{18} = \dot{m}_9\big((h_9 - h_{10}) - T_0(s_9 - s_{10})\big) + \dot{m}_{17}((h_{17} - h_{18}) - T_0(s_{17} - s_{18})\big)$
Absorber	$\dot{m}_{18} + \dot{m}_6 = \dot{m}_1$	$\dot{Q}_{abs} = \dot{m}_{18} \times h_{18} + \dot{m}_6 \times h_6 - \dot{m}_1 \times h_1$	$\dot{E}x_{D,abs} = \dot{E}x_{18} + \dot{E}x_6 - \dot{E}x_1 + (\dot{E}x_c - \dot{E}x_d) = \dot{m}_{18}((h_{18} - h_0) - T_0(s_{18} - s_0)) + \dot{m}_6((h_6 - h_0) - T_0(s_6 - s_0)) - \dot{m}_1((h_1 - h_0) - T_0(s_1 - s_0)) + \dot{m}_c((h_c - h_d) - T_0(s_c - s_d))$
Solution Pump	$\dot{m}_1 = \dot{m}_2$	$\dot{W}_{pump} = \dot{m}_1 \times \frac{h_{2s} - h_1}{\eta_s}$	$\dot{E}x_{D,Pump} = \dot{E}x_1 - \dot{E}x_2 = \dot{m}_1((h_1 - h_2) - T_0(s_1 - s_2))$
Solution Heat Exchanger	$\dot{m}_2 = \dot{m}_3$ $\dot{m}_4 = \dot{m}_5$	$\dot{Q}_{SHX} = \dot{m}_2 \times (h_3 - h_2) = \dot{m}_4 \times (h_4 - h_5)$	$\dot{E}x_{D,SHX} = \dot{E}x_2 + \dot{E}x_4 - \dot{E}x_3 - \dot{E}x_5 = \dot{m}_2((h_2 - h_3) - T_0(s_2 - s_3) + \dot{m}_4((h_4 - h_5) - T_0(s_4 - s_5))$
Generator - Condenser	$\dot{m}_3 = \dot{m}_4 + \dot{m}_7$ $\dot{m}_7 = \dot{m}_8 = \dot{m}_9$	$\dot{Q}_{gen} = \dot{m}_7 \times h_7 + \dot{m}_4 \times h_4 - \dot{m}_3 \times h_3$ $\dot{Q}_{gen} = \dot{Q}_{cond}$ $\dot{Q}_{cond} = \dot{m}_9 \times h_9 + \dot{m}_8 \times h_8$	$\dot{E}x_{D,gen-cond} = \dot{E}x_3 - \dot{E}x_4 - \dot{E}x_7 + (\dot{E}x_8 - \dot{E}x_9) = \dot{m}_3((h_3 - h_0) - T_0(s_3 - s_0)) - \dot{m}_4((h_4 - h_0) - T_0(s_4 - s_0)) - \dot{m}_7((h_7 - h_0) - T_0(s_7 - s_0)) + \dot{m}_8((h_8 - h_0) - T_0(s_8 - s_0) - \dot{m}_9((h_9 - h_0) - T_0(s_9 - s_0))$
Flash tank	$\dot{m}_{16} = \dot{m}_{11}(1 - x_{11})$ $\dot{m}_{12} = \dot{m}_{11} x_{11}$	$\dot{m}_{11} h_{11} = \dot{m}_{16} h_{16} + \dot{m}_{12} h_{12}$	$\dot{E}x_{D,FT} = \dot{E}x_{11} - \dot{E}x_{12} - \dot{E}x_{16} = \dot{m}_{11}((h_{11} - h_0) - T_0(s_{11} - s_0)) - \dot{m}_{12}((h_{12} - h_0) - T_0(s_{12} - s_0)) - \dot{m}_{16}((h_{16} - h_0) - T_0(s_{16} - s_0))$
Mixing Chamber	$\dot{m}_{15} + \dot{m}_{16} = \dot{m}_{17}$	$\dot{m}_{15} h_{15} + \dot{m}_{16} h_{16} = \dot{m}_{17} h_{17}$	$\dot{E}x_{D,mixing\ chamber} = \dot{E}x_{15} + \dot{E}x_{16} - \dot{E}x_{17} = \dot{m}_{15}((h_{15} - h_0) - T_0(s_{15} - s_0)) + \dot{m}_{16}\big((h_{16} - h_{0)} - T_0(s_{16} - s_0)\big) - \dot{m}_{17}\big((h_{17} - h_{0)} - T_0(s_{17} - s_0)\big)$
Evaporator	$\dot{m}_{13} = \dot{m}_{14}$	$\dot{Q}_{evp} = \dot{m}_{13} \times (h_{14} - h_{13})$	$\dot{E}x_{D,Evp} = \dot{E}x_{13} - \dot{E}x_{14} + (\dot{E}x_a - \dot{E}x_b) = \dot{m}_{13}((h_{13} - h_{14}) - T_0(s_{13} - s_{14}) + \dot{m}_a((h_a - h_b) - T_0(s_a - s_b))$
Expansion Valve II	$\dot{m}_{10}$=$\dot{m}_{11}$	$h_{10} = h_{11}$	$\dot{E}x_{D,TV-II} = \dot{E}x_{10} - \dot{E}x_{11} = \dot{m}_{10}((h_{10} - h_{11}) - T_0(s_{10} - s_{11}))$

Expansion Valve III	$\dot{m}_{12}$=$\dot{m}_{13}$	$h_{12} = h_{13}$	$\dot{E}x_{D,TV-III} = \dot{E}x_{12} - \dot{E}x_{13} = \dot{m}_{12}((h_{12} - h_{13}) - T_0(s_{12} - s_{13}))$

4.6 Multi-objective Optimization

Identifying the optimal set of operating parameters is crucial for maximizing the overall performance of the system. Multi-objective optimization (MOO) can be conducted to find the suitable combination of operating parameters that favors one or multiple aspects of system performance, i.e., 1st law efficiency or 2nd law efficiency, or both.

In this research, the modeling of the system to generate datasets and optimization is done using artificial neural networks (ANNs) and genetic algorithms (GAs), respectively. The flowchart of this multi-objective optimization is given in **Figure 4-2**. The process begins by generating an initial dataset, followed by the specification of input, output, and testing parameters. The phase involving the configuration of the neural network entails determining the appropriate number of neurons, selecting a performance function, and configuring hidden layers. Once the neural network setup is complete, the training process is initiated. Subsequently, the system evaluates whether the Mean Squared Error (MSE) has reached a predefined lower threshold. If the MSE has the desired value, the subsequent steps include preserving the trained neural network, capturing crucial data such as MSE values, regression metrics, epochs, and raw data with accompanying exporting graphs, saving the trained ANN function. This objective function is integrated with the optimization algorithm rather than the simulation code; this results in reduction of significant runtime with added flexibility. ANN, a robust mathematical framework, can effectively discern complex non-linear relationships between inputs and outputs, making it particularly useful when physical equations struggle to define process characteristics [96]. The process involves applying Genetic Algorithm (GA) optimization techniques, followed by collecting and storing optimal solutions through Pareto front analysis. While the Pareto Front indicates the set of optimal solutions for the multi-objective optimization (MOO) task, utilizing the TOPSIS decision-making method allows for the derivation of a singular solution tailored according to the user's prioritization of objectives.

In cases where the MSE fails to meet the target threshold, the current network is paused, and a new ANN architecture is devised. This initiates a loop back to the neural network configuration phase (step 4) to make necessary adjustments and continue until the desired MSE goal is attained. This

iterative approach facilitates the improvement of neural network architecture and overall performance optimization.

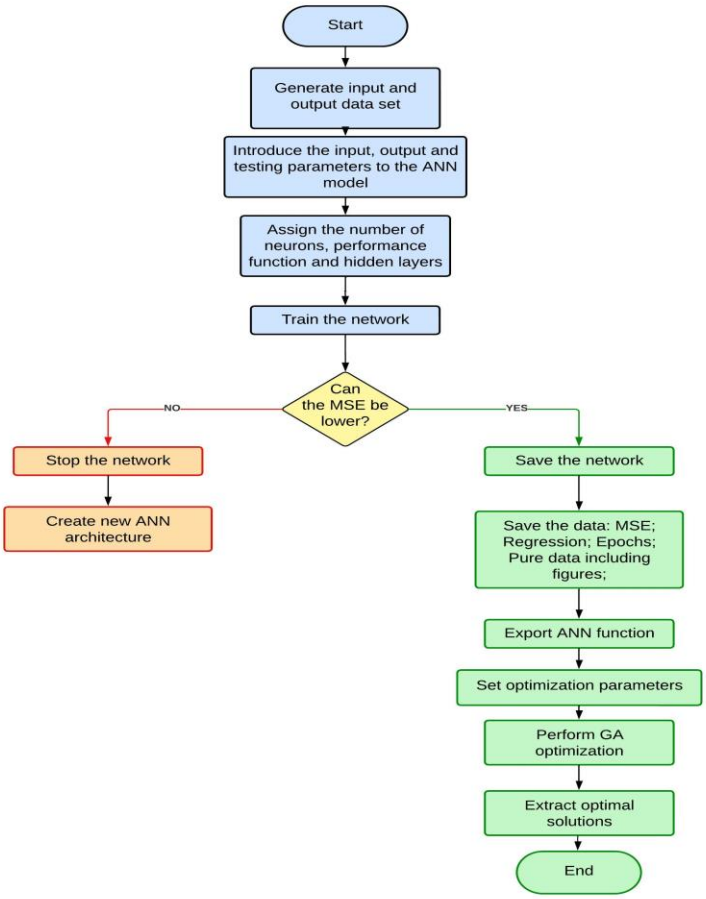

***Figure 4-2**: Mult-objective optimization flow chart of analysis.*

4.6.1 ANN based Machine Learning Model

Artificial neural networks (ANNs) are used to form a parametric model regulated by trainable parameters by using a large set of trainable data. This parametric model can be used to predict the values of unknown parameters, in between and even outside the dataset range, classify patterns, and categorize, as well as functionalize a set of data [97]. ANNs are based on the nerve cell or neuron (hence, the name Artificial *Neural* Network). Just like the biological nerve cell, a neuron of the ANN gets a multitude of inputs from other neurons, and based on the weighted total of the inputs, the output is either 0 or 1 [98]. The back-propagation learning algorithm in MATLAB 2021b (MathWorks, Massachusetts, United States) was used to acquire the objective function. With the advancement of computer technology, ANNs have diverse applications [99], [100]. An ANN comprises parallel information processing structures, encompassing an input layer of

neurons (or nodes/units), one or two hidden layers of neurons (and in some cases even three), and a final layer of output neurons [101]. A visual depiction of an ANN learning is shown in **Figure 6**. It exhibits the following characteristics:

- A mathematical model rooted in the functioning of biological neurons.
- Comprised of multiple processing elements interconnected.
- Information storage involves connection weights.
- Every processing element has the ability to react dynamically to input signals; however, the processing element's response depends solely on the local information, which includes connections and the effect of link weights on the particular processing element.
- It is able to learn, remember, and apply knowledge because of the link weights that are created during training with data.

The above characteristics make ANNs well-suited for solving complex problems.

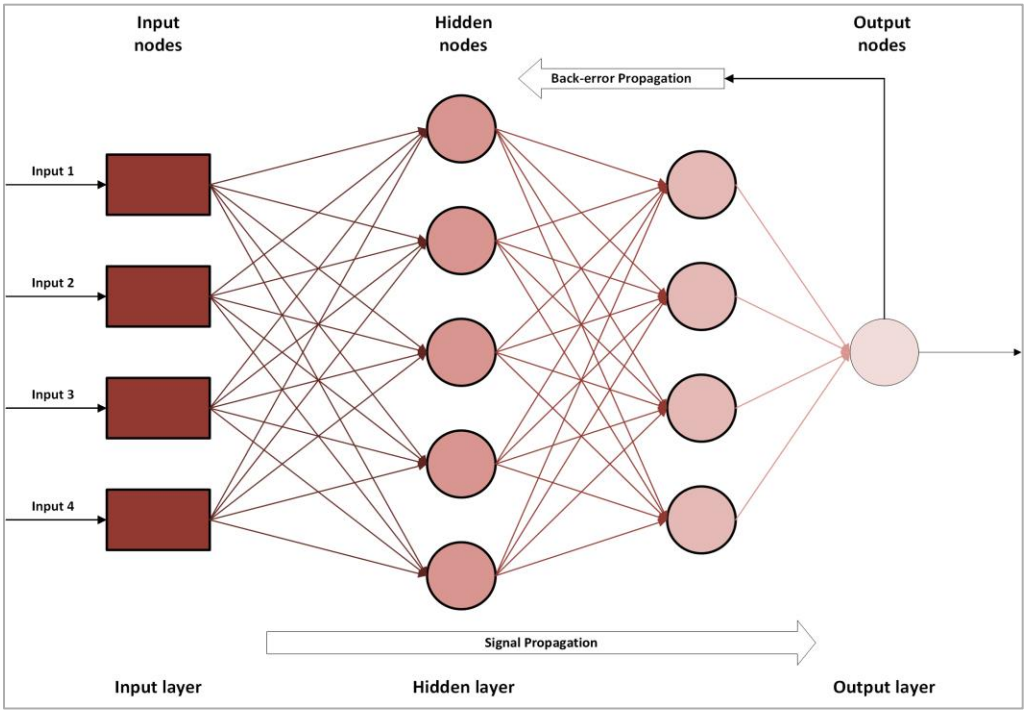

***Figure 4-3**: Illustration of an ANN model with back-propagation.*

Each connection is associated with a numeric number called weight. MSE and the correlation coefficient between the prediction value and experimental data, or R value, are the two common metrics used in this study to assess the performance of the ANN model for all pairs [102].The MSE function seeks to minimize the average squared error between the output (p_i) and goal value (t_i), which is found by using the following equation [102]:

$$MSE = \frac{\sum_i^n (t_i - p_i)^2}{N} \tag{62}$$

And the R value is found from equation (49) [102]:

$$R = \frac{(t - \overline{t})(p - \overline{p})^T}{\sqrt{(t - \overline{t})(t - \overline{t})^T}\sqrt{(p - \overline{p})(p - \overline{p})^T}} \tag{63}$$

Here, the mean values of the experiment data and the prediction data are $\bar{t}$ and $\bar{p}$, respectively. For MSE, lower value is preferable, meanwhile an ANN model is anticipated to have a higher R value. **Table 4-10** contains the process values utilized in the ANN model within this research.

***Table 4-10**. Parameters used for the ANN objective function development.*

Parameters	Value/Range
Artificial Neural Network	
Training data used in percentage	70%
Validation data used in percentage	15%
Testing data used in percentage	15%
Training method used in the optimization	Bayesian regularization
Hidden layer number	10
Simulating software used in the optimization	MATLAB

The use of artificial neural networks (ANNs) in the optimization of advanced refrigeration cycles presents numerous benefits in comparison to conventional thermodynamic models. ANNs have been shown to enhance accuracy through their ability to capture intricate, non-linear interactions. Additionally, ANNs enable adaptability in accommodating diverse situations and complexities within a given system. They have exceptional proficiency in managing complex systems, enabling quick adjustments in response to changing circumstances, leveraging data-driven analysis to inform decision-making, and speeding up software development processes by informing decision-making and, significantly, improving energy efficiency, making it extremely valuable in a variety of contexts of integrating with MOO. Nevertheless, it is imperative to utilize these tools along with thermodynamic models in order to optimally utilize their capabilities while effectively addressing their limits. To optimize design parameters, the finalized ML model is integrated with the multi-objective GA. MATLAB software is used for setting up neural network & GA- gamultiobj was set as solver for multi-obj optimization. The following subsections provide insights regarding the adopted framework for this study.

4.6.2 Optimization Using Genetic Algorithm (GA)

GA operates on a mechanism that is identical to Darwin's laws of natural selection and nowadays it has become a popular technique to optimize multiple objectives simultaneously [103]. The genetic algorithm is rooted in the concept of natural evolution, where stronger individuals have increased chances of passing on their genes (solutions) to offspring, ultimately leading to their dominance within the population. This method uses a chromosome (or individual) with a specific set of genes as a solution vector, with the population of chromosomes being initialized randomly [101]. This method is characterized as one based on the principles of natural selection, employed to tackle both unconstrained and constrained optimization problems. The algorithm involves iteratively modifying a collection of individual solutions. During each step, the algorithm randomly selects individuals to generate the subsequent iteration, continuing until an optimal solution is reached [104].

When comparing genetic algorithms to fundamental optimization tools, a notable distinction emerges; basic tools generate a single point per iteration, gradually converging to the desired optimal solution through a sequence of points. In contrast, genetic algorithms produce a "population of points" at each iteration. Eventually, the best point within the population converges to an "optimal solution." Within the framework of genetic algorithms, two functions—crossover and mutation—are utilized to create new chromosomes. Crossover involves generating new offspring (or chromosomes) by combining genetic material from parent individuals [105]. Parents are chosen from the current population based on fitness, favoring fitter individuals. Offspring inherit favorable genes from these competent parents. Through successive iterations of the crossover operator, the genes of adept individuals become more prevalent across the population, ultimately driving convergence toward the optimal solution [105]. Diversity at the genetic level is introduced through mutation, wherein the mutation rate governs changes in gene properties. This prevents the algorithm from getting stuck in local minima or maxima and aids in reaching the global solution. In each optimization step, individuals are randomly selected from the existing population to serve as parents, thus generating the subsequent generation. This ongoing evolution of the population of individual solutions persists until the optimal solution is achieved. Genetic algorithms also extend to multi-objective optimization, identifying multiple points known as Pareto optimal points, which signify optimal values for various objectives. Once these Pareto

optimal allocations are reached, enhancing one objective would invariably worsen others [101]. The Non-dominated Sorting Genetic Algorithm II (NSGA-II), a particular instantiation of GAs, is particularly noteworthy for being a highly effective multi-criteria evolutionary algorithm, commonly employed in the enhancement of energy systems [106]. It presents numerous benefits, such as its resilience and quick population distance approximation; nonetheless, its primary shortcoming is the sluggish speed of its operation [107].

In this work, the *gamultiobj* solver of the optimization toolbox in MATLAB software is used to optimize the objective functions that were generated in ANN for the considered objectives. Here, *COP* and exergy efficiency have to be maximized for four or five controllable operating conditions. Selected values for different parameters in the MATLAB optimization toolbox are listed in **Table 4-11**.

***Table 4-11**. Selected Values for different parameters of Multi-objective optimization algorithm.*

Specified Options		Selected Value
Population Size		200
Creation Function		Constraint Dependent
Tournament Size		2
Crossover	function	Intermediate
	ratio	1
Migration	fraction	0.20
	direction	forward
Mutation	probability	Constraint dependent
	function	0.10
Distance Measure Function		Distancecrowding
Population fraction of the Pareto Front		0.35
Max. Tolerance	constraint	10^{-3}
	function	10^{-4}

4.6.3 Decision Making Technique

Although all the points found in the Pareto frontier diagram after multi-objective algorithm reveal the optimal solutions. However, the optimum solution considering both the output of *COP* and Ex_{eff} should have the minimum geometric distance from the ideal point or the maximum distance from non-ideal point. Whereas the right-most and left-most point suggests optimal solutions from one output perspective only. In this analysis, TOPSIS decision-making technique is employed to find the most optimal solution considering both output perspectives.

TOPSIS (Technique for order preference by similarity to ideal solution) [108]***:***

TOPSIS is a popular multi-criteria decision-making technique that generates a ranking of alternative options based on their proximity to the ideal solution. From the Pareto front, a unique optimal solution can be extracted using this method. It offers a structured method of comparing different choices and identifying the best one. To implement TOPSIS technique for multi-objective decision making, the following steps should be followed:

Step 1: An evaluation matrix where rows (numbered as i=1….m) representing alternatives and columns (numbered as j=1….n) representing criteria should be created.

$$\begin{bmatrix} a_{11} \ldots\ldots\ldots a_{1j} \ldots\ldots a_{1n} \\ \vdots \quad\quad \vdots \quad\quad \vdots \\ a_{i1} \ldots\ldots\ldots a_{ij} \ldots\ldots a_{in} \\ \vdots \quad\quad \vdots \quad\quad \vdots \\ a_{m1} \ldots\ldots\ldots a_{mj} \ldots\ldots a_{mn} \end{bmatrix} \tag{64}$$

Step 2: Normalizing the evaluation matrix

$$a_{ij} = \frac{a_{ij}}{\sqrt{\sum_{i=1}^{m} a_{ij}^2}} \tag{65}$$

Determination of the weight of criteria using Shannon Entropy Principle [109]***:***

This theory assists in assessing the relative importance of each objective function, and this weight will be fed into TOPSIS to rank all the alternatives rather than assuming weights of the objective functions. Determination of weight for each criteria using Shannon Entropy Principle requires following steps [110]:

Considering an evaluation matrix F_{ij} which has m alternatives and n objective functions. Normalization of the evaluation matrix to get Project outcome, p_{ij}

$$p_{ij} = \frac{F_{ij}}{\sum_{i=1}^{m} F_{ij}} \tag{66}$$

Here,

i = 1,2,3,4 …, m

j = 1,2,3,4 …, n

Evaluation of the Shannon Entropy value for Project Outcome

$$SE_j = -\frac{1}{\ln(m)}\sum_{i=1}^{m} p_{ij}\ln(p_{ij}) \tag{67}$$

Evaluation of deviation degree, d_j

$$d_j = 1 - SE_j \tag{68}$$

Determination of weights of the objective functions using the following equation:

$$w_j = \frac{d_j}{\sum_{j=1}^{n} d_j} \tag{69}$$

This weight will be employed in the TOPSIS technique (step 3) to generate weighted normalized matrix and following the subsequent steps will provide the required optimum solution

Step 3: Creation of weighted normalized matrix

$$V_{ij} = w_j \times a_{ij} \tag{70}$$

$$V_{ij} = \begin{bmatrix} w_1a_{11} & w_2a_{12}\ldots\ldots w_na_{1n} \\ w_1a_{21} & w_2a_{22}\ldots\ldots w_na_{2n} \\ \vdots & \vdots \quad\quad \vdots \\ w_1a_{m1} & w_2a_{m2}\ldots\ldots w_na_{mn} \end{bmatrix} \tag{71}$$

Step 4: Evaluating both the positive and negative ideal solutions.

$$A_j^+ = \{\text{Max } V_{ij} | j \in k\}, \{\text{Min } V_{ij} | j \in k'\} \tag{72}$$

$$A_j^- = \{Min\ V_{ij} | j \in k\}, \{Max\ V_{ij} | j \in k'\} \tag{73}$$

Step 5: Determination of distances for each value in weighted matrix from positive & negative ideal solutions

$$S_i^+ = \sqrt{\sum_{j=1}^{n} (V_{ij} - A_j^+)^2} \tag{74}$$

$$S_i^- = \sqrt{\sum_{j=1}^{n} (V_{ij} - A_j^-)^2} \tag{75}$$

Step 6: Evaluating the closeness to ideal solutions for each alternative using the following equation.

$$C_i = \frac{S_j^-}{S_j^+ + S_j^-} \tag{76}$$

TOPSIS technique will finally select the alternative with largest C_i value.

4.7 Mathematical Framework

In this research, a computational model is designed for each proposed and traditional system in the Engineering Equation Solver (EES) that utilizes the conservation of energy, mass, and exergy equations of each component. The thermodynamic and physical properties of the refrigerant and solution stream states are derived using empirical equations as well as EES's integrated database. The simulation proceeds with the value of a set of predefined operational parameters that compare the suggested and traditional systems. Afterward, the parametric behavior analysis of each system is carried out with varying operational conditions within a definite range. Finally, ANN model is trained with the extracted data to integrate with the Genetic algorithm to carry out multi-objective optimization and determine the optimal condition of operation. The process flow of the simulation model of ARC based proposed cascaded systems, RAC based proposed cascaded systems and standalone improved RAC systems with ejector and vapor injection is visually represented in **Figure 4-4, Figure 4-5, and Figure 4-6,** respectively.

Engineering Equation Solver (EES) is a powerful computational tool used by engineers and scientists for solving complex mathematical equations. It is designed to handle systems of nonlinear algebraic and differential equations efficiently. EES provides a user-friendly interface that allows users to input equations in a straightforward manner, facilitating the modeling and analysis of thermodynamic problems with optimization, parametric and uncertainty analysis.

The feasible range of operation for the controllable parameters is analyzed through prior research that explored the impact of these parameters on the absorption cycle. The phenomenon of crystallization defines the limiting condition of the operational range. Along with this, the concentration of solution is dictated by the generator and absorber temperature, which also influences the viable operating range. These assumptions were corroborated by a careful review of previous works, including those by Modi et al. [111], Talbi et al. [112], and Razmi et al. [85]. Moreover, realistic circumstances are considered, leading to the decision to allow the absorber temperatures to vary from 25℃ to 35℃.

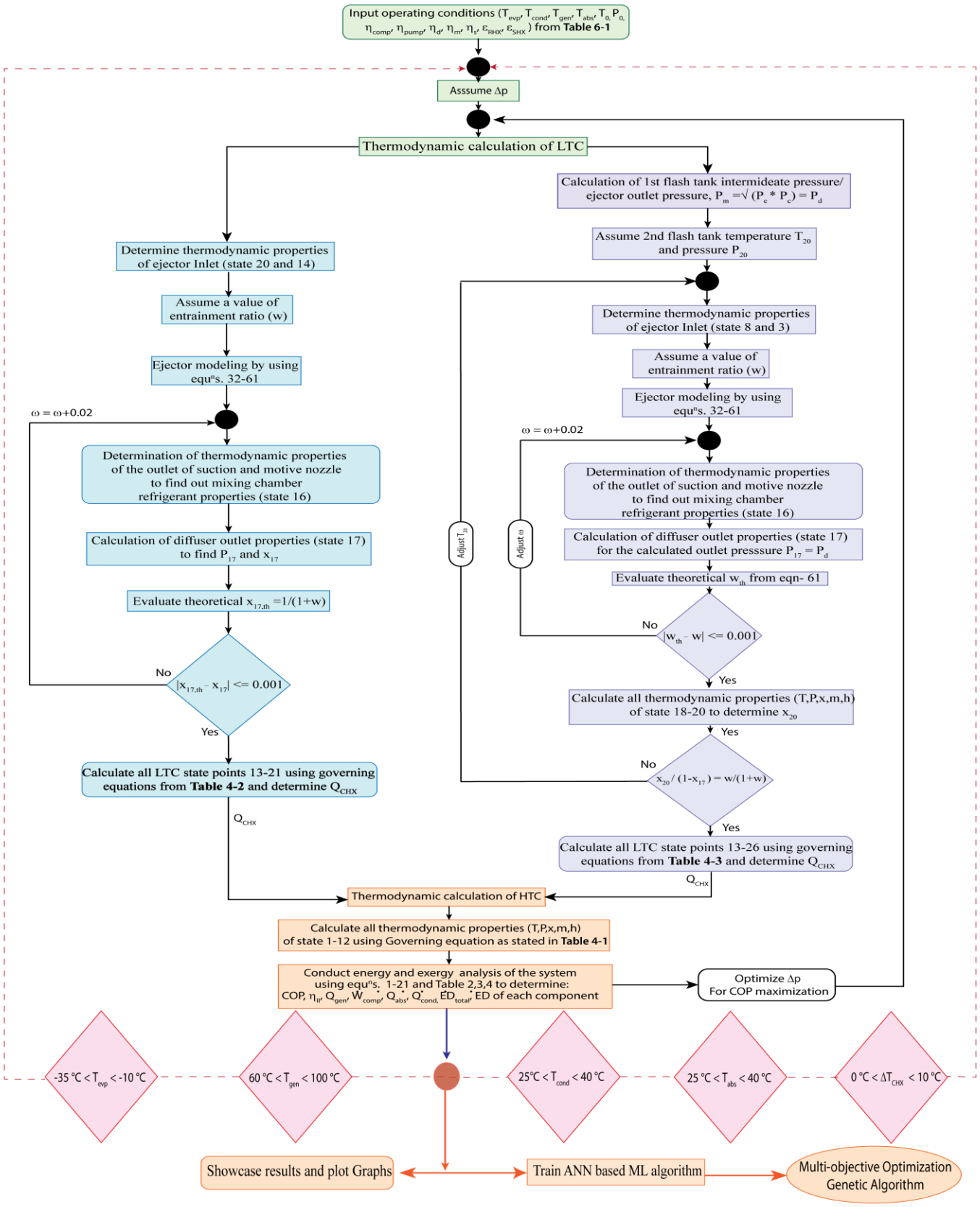

***Figure 4-4**: Flowchart of ARC based proposed cascaded compression absorption systems.*

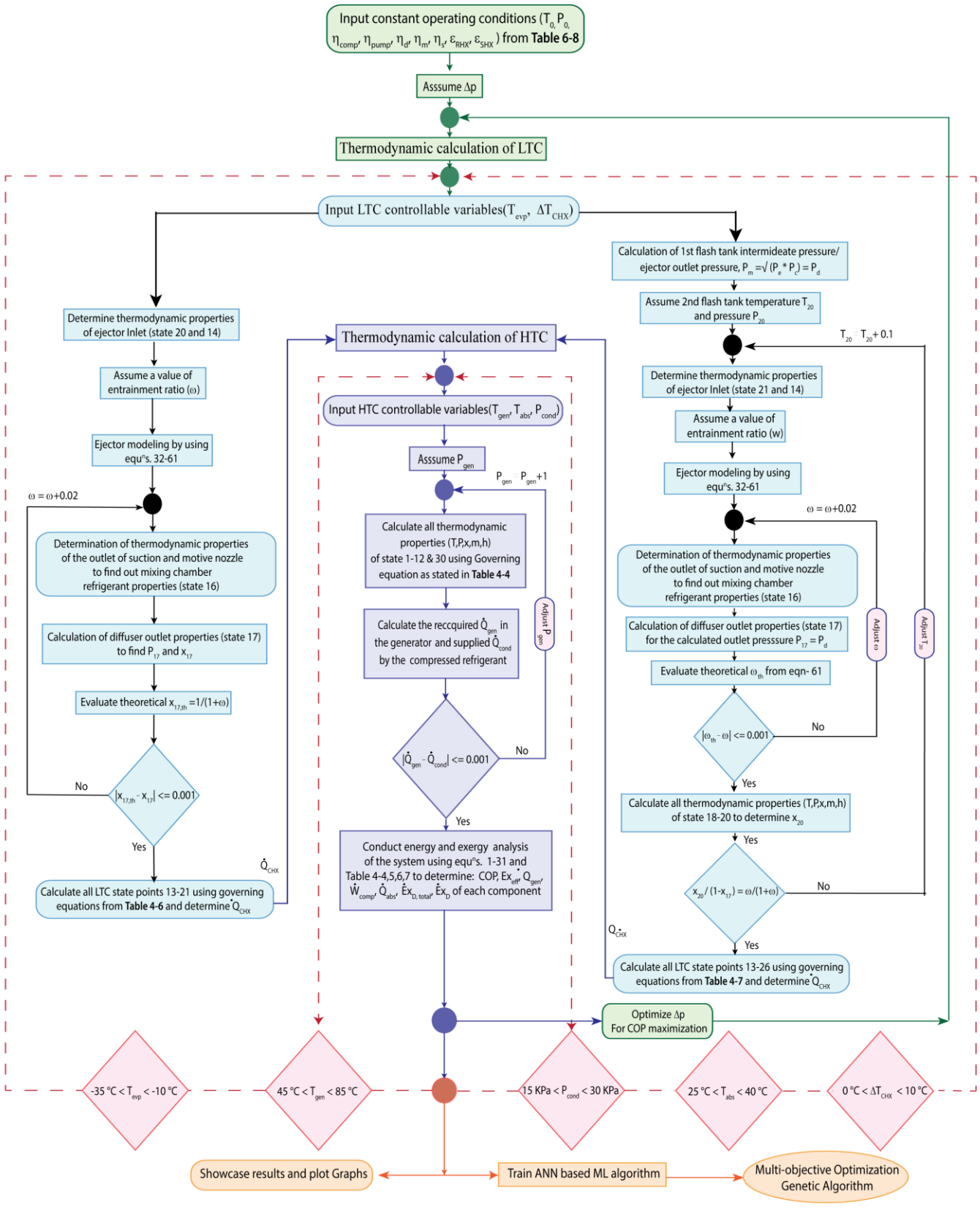

***Figure 4-5**: Flowchart of RAC based proposed cascaded compression absorption systems*

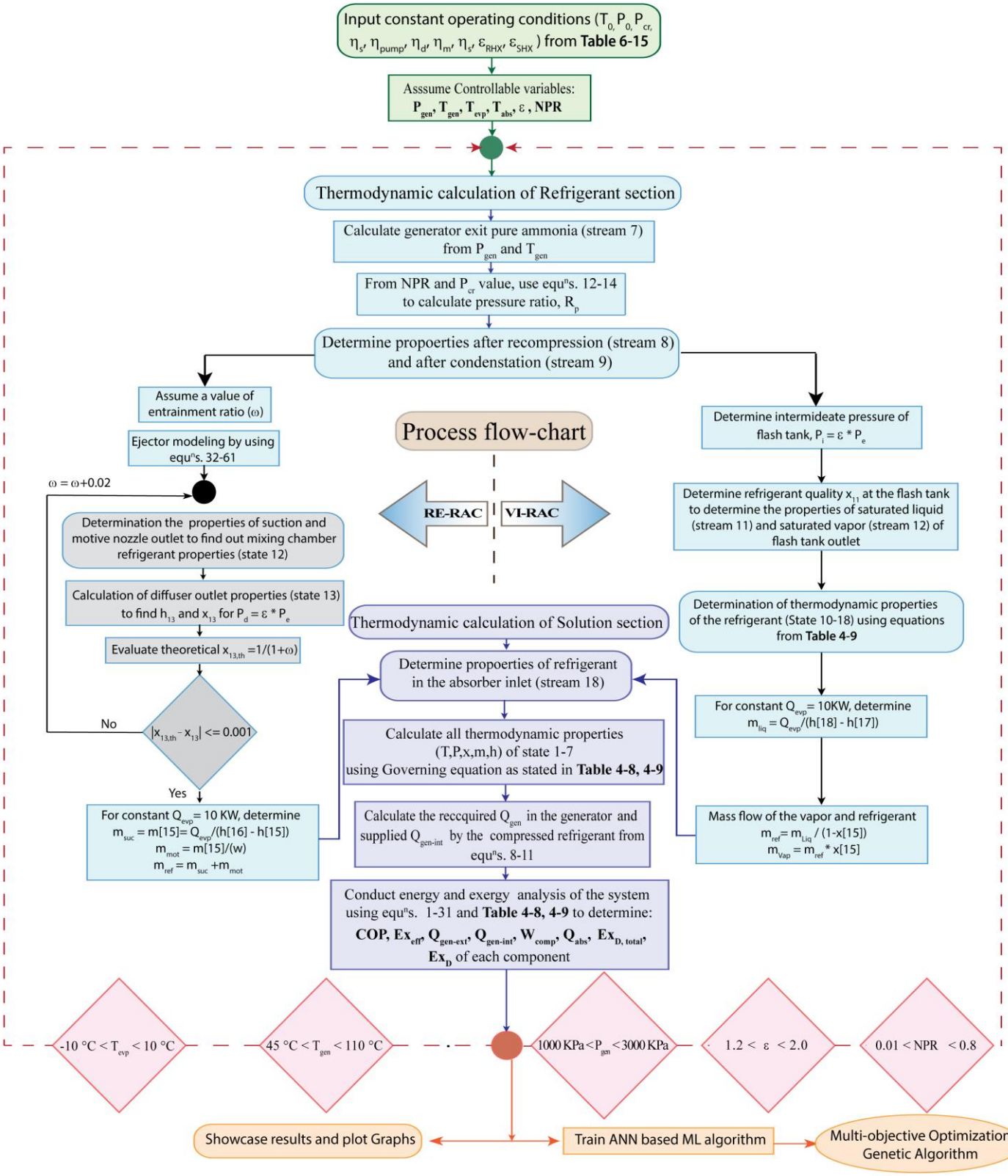

***Figure 4-6**: Flowchart of advanced stand-alone recompression absorption systems equipped with ejector and vapor injection.*

Chapter 5: System & Model Validation

Due to the innovative nature of the proposed novel systems, direct comparisons with established research for verification aren't possible. Instead, the validity and reliability of these innovative systems can be confirmed by a thorough examination and validation of the constituent sub-systems. This can be achieved by developing detailed numerical models for each sub-system in code-based platforms. These models are then validated through a meticulous review and comparison with existing numerical and experimental works. To validate, the numerical models were simulated under identical operating conditions as those numerical/experimental work documented in existing literature related to these sub-systems. The results are compared with the data from these studies, showcasing their high predictive accuracy.

These sub-systems include single-effect ARC and VCR, single-effect RAC, Solution Ejector Enhanced RAC (SE-RAC), ejector enhanced VCR, Ejector-injection enhanced VCR and Flash Tank Integrated Vapor Injection refrigeration systems. The operation of a cascaded system comprised of a vapor compression and absorption system (CARC) has also been validated with existing works to authenticate the numerical model of cascaded technology. The minimal deviation observed in these comparisons strongly suggests that the numerical models accurately replicate the behavior and trends of these refrigeration cycles under various operational conditions, both from experimental and numerical standpoints. Such a comparative validating analysis not only confirms the reliability of the individual components but also ensures the robustness and innovation of the overall configuration.

Hence, in this study, the validated models are cascaded, and the principal, mechanism, and assumptions from these validated models and technologies are used in developing the thermodynamic model of the proposed advanced ARC-based cascaded systems (EICAC and ECAC), RAC-based cascaded systems (EI-CRAC and E-CRAC) and advanced standalone RAC equipped with ejector and vapor injection (RE-RAC and VI-RAC).

5.1 Experimental Validation of Conventional VCR and ARC System

To solidate the authenticity of the proposed models, VCR simulation model is developed and compared with the experimental results of the study by Ma et al [113] under similar operating conditions. The operational parameters considered for validation have been listed in **Table 5-1.**

The COP for both the experimental and simulation models has been compared in **Table 5-2**, employing error metrics and relative deviations. The MAPE, RMSE, and relative deviations all fall well within acceptable ranges, while the R^2 value indicates a robust fit between the presented and experimental models.

Table 5-1*. Considered operational parameters for the experimental validation of VCR* [113]

Parameters	**Values**
Refrigerant	R134a
T_{evap}	-15 ℃ to -5 ℃
T_{cond}	40 ℃
Degree of sub-cooling in the condenser	2.4 ℃
Degree of superheating in the evaporator	10.6 ℃
Compressor efficiency (%)	63% at T_{evap} = -15 ℃
	54% at T_{evap} = -10 ℃
	45% at T_{evap} = -5 ℃

Table 5-2*. Comparison of the presented model and the experimental work of Ma et al.* [113]

T_{evp} (℃)	**COP**		**Deviation (%)**	**MAPE**	**RSME**	**R^2**
	Experimental Model [113]	**Presented Model**				
-15	1.61	1.63	1.24	0.00934	0.02	0.998799
-10	2.23	2.25	0.896			
-5	3.02	3.04	0.662			

To confirm the principles of the absorption system mechanism, a single-effect ARC simulation model is developed and validated against the research of Aman et al. [114] for ammonia-water and Modi et al. [111] for lithium bromide-water solution. This simulation model was built on an EES (Engineering Equation Solver) programming-oriented platform, applying conservation of energy to system components, and incorporated REFPROP libraries for calculating state point properties. The outcomes and accuracy are detailed in **Table 5-3**, including a comprehensive comparison. The results indicate that the single-effect ARC model aligns well with the findings of Modi et al. [111], thus confirming the model's precision. However, there is a minor divergence when compared to the findings of Aman et al. [114], which is because of the differing techniques taken in calculating state properties.

***Table 5-3**. Model verification of Standard Single Effect ARC Model*

Operational parameters	**ARC with LiBr/H_2O**			**ARC with NH_3/H_2O**		
Generator temperature	87.8℃			80℃		
Evaporator temperature	7.2℃			2℃		
Condenser and absorber temperature	37.8℃			30℃		
Parameters	**Validation Results**					
	Present Work (LiBr/H_2O)	**Ref.** [111] **(LiBr/H_2O)**	**Relative difference with** [111] **(%)**	**Present Work (NH_3/H_2O)**	**Ref.** [114] **(NH_3/H_2O)**	**Relative difference with** [114] **(%)**
$\dot{Q}_{Genarator}$ (kW)	3092	3092	0.00	17.07	16.75	1.78
$\dot{Q}_{Absorber}$ (kW)	2941	2942	0.03	15.64	15.34	1.88
$\dot{Q}_{Condenser}$ (kW)	2505	2505	0.00	11.46	11.44	0.18
$\dot{Q}_{Evaporator}$ (kW)	2355	2355	0.00	10.00	10.00	0.00

5.2 Validation of Conventional CARC System

The numerical model of the conventional CARC system is developed and verified against the work of Cimsit et.al [68] simulating at the same operating conditions. In this paper, the authors created an analytical model to conduct energetic and exergetic analysis. The refrigeration system models are constructed using equations obtained from numerous investigations and experimental research to compute the characteristics of the solution streams. While verifying the system, Generator temperature T_{gen} = 85℃, Evaporator temperature T_{evp} = -10.5℃, Condenser temperature T_{cond} = 35℃, Absorber temperature T_{abs} = *35℃*, Effectiveness in SHX ε_{SHX} = 0.65 are assumed. **Table 5-4** indicates a significant correlation between our numerical model and the study by Cimsit et al. [68], with minor discrepancies. These variations can be attributed to the different methodologies employed. In contrast, EES has been used to build our model due to its comprehensive collection of integrated solutions.

***Table 5-4**. Model verification for CARC system* [68]

Parameters	**LiBr-H_2O/ R134a**		**Relative difference (%)**	**NH_3-H_2O/ R134a**		**Relative difference (%)**
	Present Work	**Ref** [68]		**Present Work**	**Ref** [68]	
Generator load, $\dot{Q}_{generator}$ (kW)	75.47	75.43	0.015	116.87	119.46	0.53
Absorber load, $\dot{Q}_{absorber}$ (kW)	73.75	71.71	0.015	110.27	110.73	0.41

Condenser load, $\dot{Q}_{condenser}$ (kW)	62.07	62.03	0.015	65	66.83	0.29
Cascade heat exchanger, $\dot{Q}_{CHX}$ (kW)	56.43	58.42	0.015	56.45	55.42	0.015
COP_{system}	0.593	0.592	0.015	0.015	0.397	0.77

5.3 Validation of Recompression Absorption Cycle (RAC)

The advanced systems proposed in this study incorporate an advanced recompression absorption system where the rejected heat in the condenser is reused to enhance efficiency and disregard the use of large condensers. To establish the mathematical model of a recompression absorption system, an in-house computer code is developed in EES. The simulation model has been compared and verified with Razmi et al.'s investigation [115] to authenticate the analysis. As evidenced in **Table 5-5,** the findings of this study are in substantial alignment with the data from the literature, showcasing an impressive accuracy with an error margin of less than 1%. While verifying the model, T_{gen} = 65°C, T_{evp} = 10°C, T_{cond} = 70°C, T_{abs} = 40°C, ε_{SHX} = 0.65 and Q_{evp} = 150kW are considered as operating parameters. Additionally, to validate the corresponding behavior of the system with varying operating conditions, the generator temperature impact on the system efficiency is also validated and presented in **Figure 5-1**. The figure demonstrates that the RAC system is accurately designed, thereby enhancing the credibility of the simulation model for the suggested methods.

Table 5-5*. Model verification for Recompression-absorption refrigeration cycle (RAC)* [115]

Parameters	**Ref** [115]	**Present Work**	**Difference (%)**
Generator-Condenser load, $\dot{\boldsymbol{Q}}_{\boldsymbol{gen-cond}}$ (kW)	188	188.2	0.106
Absorber load, $\dot{\boldsymbol{Q}}_{\boldsymbol{abs}}$ (kW)	181	181.1	0.055
Compressor power, $\dot{\boldsymbol{W}}_{\boldsymbol{comp}}$ (kW)	31.05	31.31	0.830
Circulation Ratio, Cr	7.52	7.626	1.389
COP	4.83	4.791	0.814
Exergy destruction rate, $\dot{\boldsymbol{E}}\boldsymbol{x}_{\boldsymbol{D}}$ (kW)	20.23	20.49	1.269
Exergy efficiency, $\boldsymbol{\eta}_{\boldsymbol{II}}$	0.348	0.3455	0.723
Mass fraction of strong solution, $\boldsymbol{x}_{\boldsymbol{rich}}$	0.563	0.5631	0.017
Mass fraction of weak solution, $\boldsymbol{x}_{\boldsymbol{lean}}$	0.522	0.5221	0.019

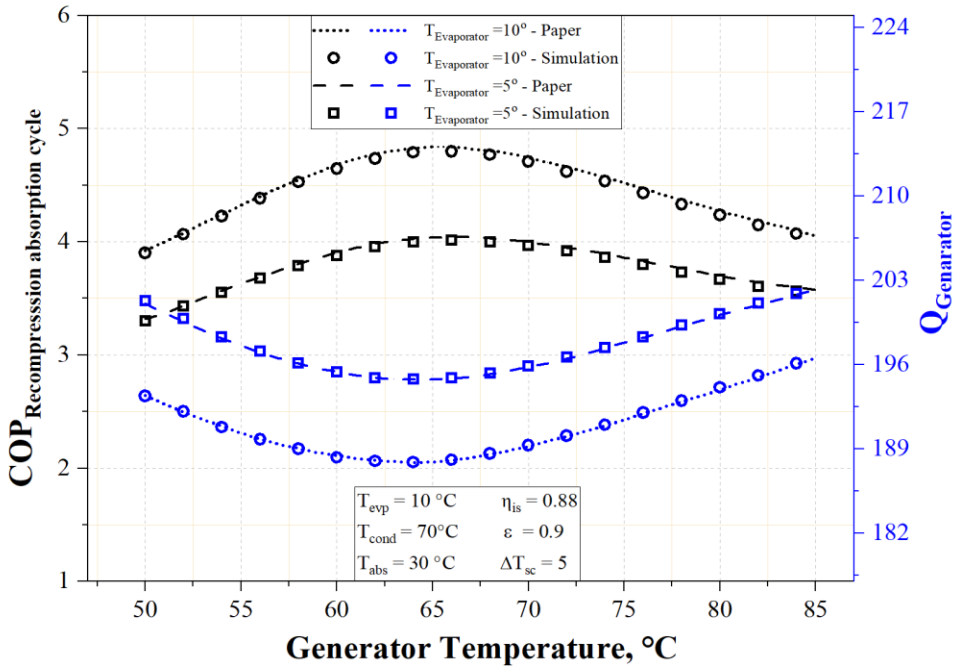

***Figure 5-1**: Validation and assessment of Recompression absorption cycle with the study of Razmi et.al* [115].

5.4 Validation of Solution Ejector Enhanced Recompression Absorption Cycle (SE-RAC)

One of the objectives of this study is to introduce advanced configurations of the standalone RAC system. To achieve this, it's imperative to comprehensively validate a model of the modified RAC and thoroughly understand its underlying principles and mechanisms for applications. To achieve this, a RAC system with a solution ejector is modeled to validate the works of Ahmad et. al [25]. In this study, recompression technology is applied to reuse the rejected heat in the condenser as generator internal load to enhance P_{abs}. Additionally, an ejector is placed in place of solution expansion valve to enhance system feasibility. The model is developed in EES according to the principles and assumptions stated in the study. Table validation between the model and the paper has been carried out for operating conditions: T_{gen} = 60.31°C, T_{evp} = 2°C, T_{abs} = 30°C, *NPR*= 0.01418, D_m= 0.01752, P_{gen}= 1288 kPa. The result of the developed validation model in comparison with the data from the paper is presented in **Table 5-6**. This validation and high accuracy of the numerical model affirms the understanding of the mechanism and working principle of a recompression system that utilizes rejected heat in the generator. Furthermore, it serves as a verification of the feasibility of incorporating an ejector into the RAC system. Based

on this principle, assumptions and mechanism, the RE-RAC system was developed, wherein the ejector is placed on the refrigerant side.

***Table 5-6**. Validation of numerical model with SE-RAC proposed by Ahmedi et.al* [25]

State	Fluid	T (C)		P (kPa)		h (kJ/ kg)		S (kJ kg-K)		m (kg/s)		X (NH_3)	
		Paper	Model	Paper	Model	Paper	Model	Paper	Model	Paper	Model	Paper	Model
1	NH_3-H_2O	30	30	587.5	587	-89.25	-89.31	0.3015	0.3015	0.01864	0.01862	0.6103	0.61
2		30.09	30.11	1288	1288	-88.25	-88.25	0.3018	0.3004	0.01864	0.01862	0.6103	0.61
3		42.32	42.31	1288	1288	-32.21	-31.97	0.483	0.4813	0.01864	0.01862	0.6103	0.61
4		60.31	60.31	1288	1288	45.75	45.73	0.7342	0.7342	0.009368	0.009367	0.5902	0.5901
5		36.14	36.06	1288	1288	-65.75	-66.14	0.3872	0.386	0.009368	0.009367	0.5902	0.5901
6		30	30	587.5	587	759	760.4	2.915	3.194	0.01864	0.01862	0.6103	0.61
7		60.31	60.31	1288	1288	1569	1569	5.481	5.481	0.009268	0.009251	1	1
8		141.5	141.6	3072	3072	1735	1735	5.541	5.118	0.009268	0.009251	1	1
9		66.75	66.76	3072	3072	527.8	527.8	2.056	2.033	0.009268	0.009251	1	1
10		41.75	40.8	3072	3072	399.5	394.8	1.664	1.648	0.009268	0.009251	1	1
11		2	2	462.6	462.6	385.4	383.4	1.674	1.648	0.009268	0.009251	1	1
12		2	2	462.6	462.6	1464	1464	5.595	5.595	0.009268	0.009251	1	1
13		53.8	55.81	462.6	462.6	1593	1597	6.023	6.014	0.009268	0.009251	1	1

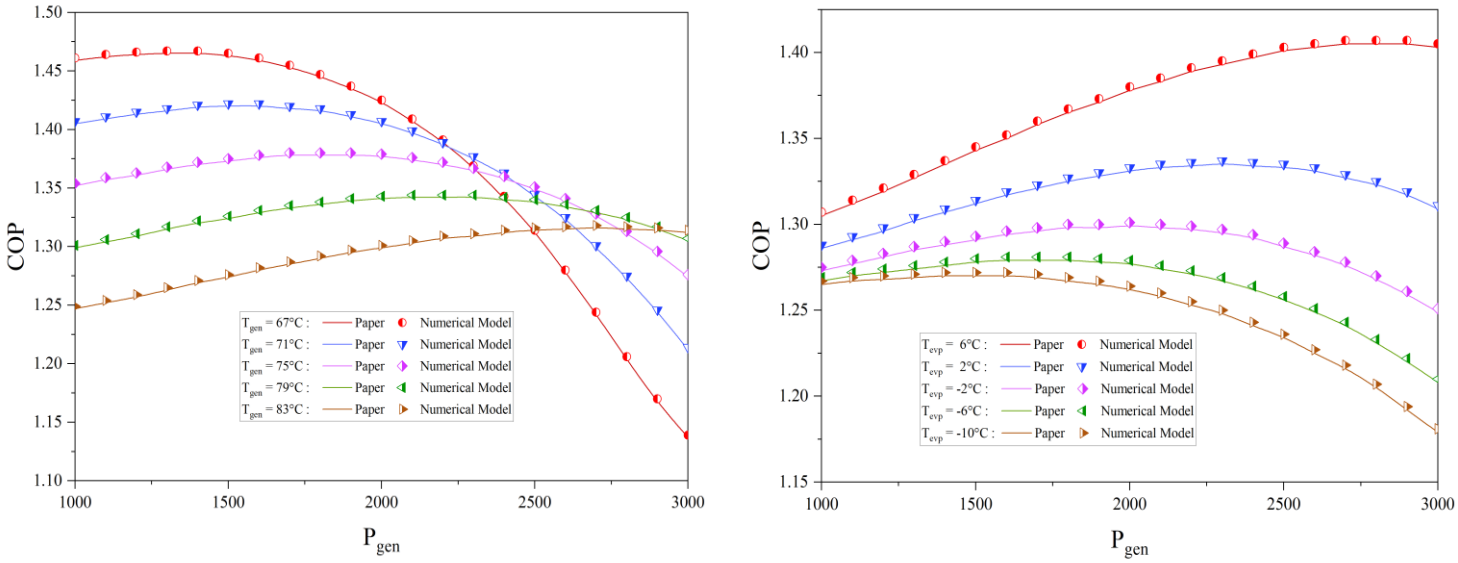

Figure 5-2: Validation and evaluation of SE-RAC cycle with the study of Ahmedi et.al [25] *for NPR = 0.1, P_{gen} = 1000 to 3000 kPa, T_{gen} = 67 to 85°C, T_{evp} = -12 to 6°C.*

Beyond state point validation, it is also essential to ascertain whether the numerically validated model aligns with the behavior of the reference system. To corroborate the system's behavior under different operating conditions, the influence of generator pressure on system efficiency is examined for varied generator and evaporator temperatures. This analysis is illustrated in **Figure 5-2**. The figure demonstrates that the SE-RAC system is accurately modeled, thereby enhancing the credibility of the simulation model of the proposed RAC systems.

5.5 Validation of Ejector and Ejector-Injection Enhanced VCR

The advanced VCRs incorporated in the LTC of the proposed cascaded compression absorption systems are also modeled and verified based on established literature. **Figure 5-3** shows the validity of the ejector enhanced VCR cycle, as demonstrated in the investigation done by Li et al. [91] using R1234yf as operating coolant. The simulation is conducted under specific operational circumstances: T_{cond} = 45 °C, T_{evp} = 0 °C, $\eta_{main\text{-}nozzle} = \eta_{secondary\text{-}nozzle} = \eta_{diffuser}$ = 0.87, and η_{ms} = 0.96.

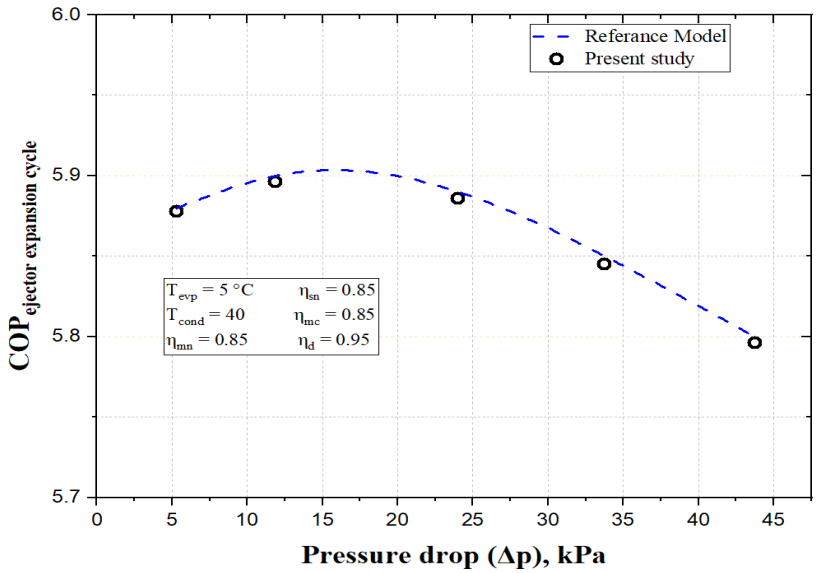

***Figure 5-3**: Verification and evaluation of ejector enhanced VCR system with the study of Li et. al.* [91].

A comprehensive analysis conducted by Wang et al. [14], introduces and verifies the Ejector improved vapor injection coolant system. A numerical model of the system is developed and simulated for validation with the reference work. **Figure 5-4** illustrates a comparative analysis of the COP between the reference data and current simulation model results for the same operating conditions. The operational conditions for this comparative analysis are: T_{cond} = 50 °C, T_{evap} = 6

to -36 ℃, $\Delta T_{sub\text{-}cool}$ = 4 ℃, loss efficiency in nozzle, mixer and diffuser respectively: 0.85, 0.84 and 0.85 and Isentropic efficiency: 0.70.

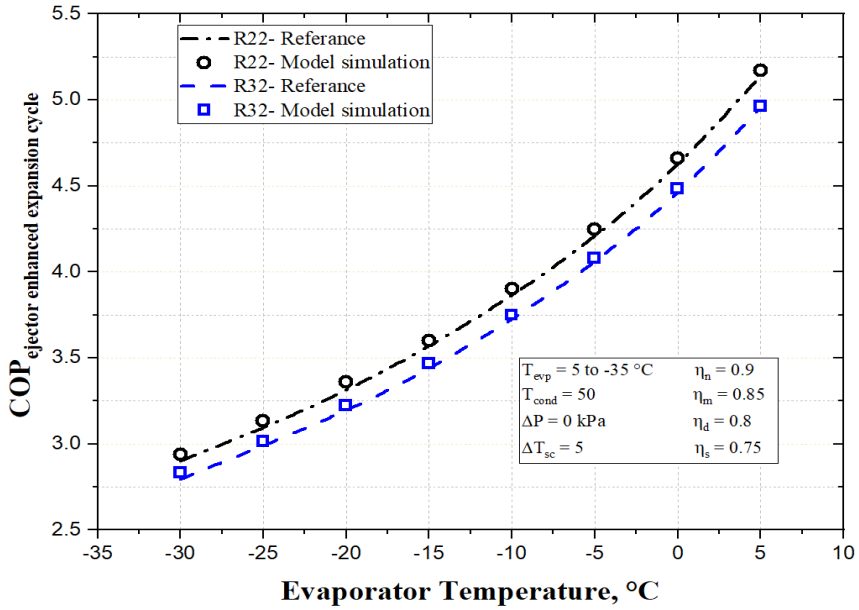

***Figure 5-4**: Verification and evaluation of ejector-injection enhanced VCR Wang et al.* [14]

5.6 Experimental Validation of Flash Tank Integrated Vapor Injection VCR

The vapor injection system with an integrated flash tank is a key mechanism in developing VI-RAC to replace refrigerant expansion valve. To solidify this system's credibility, flash tank-based vapor injection expansion refrigeration VCR is modeled and validated against the study of Babiloni et al.[116]. In their work, they designed an experimental heat pump system that operates on principles similar to the refrigeration system. **Table 5-7** compares experimental and computational results. Discrepancies are more pronounced at lower evaporator temperatures but reduce from an initial 8.99% to a minimal 3% as temperature rises. This difference arises from real-world compressor efficiency variations, referenced in [113] In the computational model, compressor efficiency is constant. As the evaporator temperature increases, the experimental and simulated data become more aligned, suggesting the numerical model offers accurate theoretical analysis.

***Table 5-7**. Model validation of Flash Tank enhanced system against the work of Babiloni et al.*[116].

	T_{cond} = 42^{0}C			T_{cond} = 45^{0}C		
T_{evap} (^{0}C)	**COP of Experimental Setup**	**COP of Simulation Model**	**Relative Deviation (%)**	**COP of Experimental Setup**	**COP of Simulation Model**	**Relative Deviation (%)**
-25	1.88	2.06	8.98	1.77	1.93	8.43
-22	2.05	2.19	6.30	1.98	2.11	7.62
-20	2.19	2.28	4.57	2.1	2.25	7.14
-15	2.54	2.65	4.32	2.41	2.54	5.82
-12	2.82	2.93	4.26	2.66	2.81	5.25
-10	3.04	3.14	3.37	2.87	3.00	4.17
-8	3.29	3.38	2.74	3.09	3.20	3.56

5.7 Experimental Validation of Ejector System

In each of the proposed configuration designs, the ejector is a key component. It recaptures energy that would otherwise be lost during the throttling process, thereby improving the efficiency of the cycle. To ensure the precision and dependability of the developed numerical model for the ejector, it is vital to validate its effectiveness by comparing it with results from established experimental studies. The standard reference for this objective is established by the experimental research performed by Elbel et al. [117], and the findings are provided in **Table 5-9**. The following **Table 5-8** provides a comprehensive review of the accuracy of the equipment utilized for obtaining the experimental measurements to establish the experiment's exactitude and credibility. The ejector expansion system is numerically modeled in EES according to the ejector operational principle stated by Li et al[91]. For different testing conditions, the calculated entrainment ratio from the numerical model is compared with the data from the experimental rig provided in the paper. The findings presented in **Table 5-9** demonstrate that the computational model provides a higher precise representation of the experimental model of the ejector, specifically when considering a diffuser angle of 5°.

***Table 5-8**. Unreliability in measurement related to apparatuses utilized for obtaining experimental results.*

Apparatus	Details/position	Precision	Range
Air-side Capacity			
T-class welded thermocouple thread	Temperatures of air	0.5% reading over 0ºC	201 ºC to 210
Differential pressure transducer	Around evaporator nozzle	0.26%	0–1247 Pa
	Around gas cooler nozzle/evaporator	0.26%	1247 Pa
	Ambient-gas cooler inlet/evaporator inlet	0.26%	0–3737 Pa
Capacitive moistness probe	Relative moisture content	2% RH absolute	0.3–100% RH
Coolant-Aspect Capability			
T-class probe of thermocouple	Coolant temperatures	More than 0.5℃ and 0.5% reading over 0℃	201℃ to 220℃
Pressure sensor	High-state pressures	0.51%	0–20.6 MPa
	Evaporator outlet/ejector diff outlet	0.11%	0–6.8 MPa
Differential pressure sensor	Ejector pressure lift	0.11%	691 kPa
	Around evaporator	0.26%	346 kPa
Transducer	Power Consumption	0.2% of the outcome	0–11 kW

***Table 5-9**. Verification of ejector design with empirical investigation* [117]

Diffuser Inclination, α_{diff}	**P_{sn}, (MPa)**	**P_{mn} (MPa)**	**$x_{sn,\ in}$**	**T_{mn}, (°C)**	**Entrainment Ratio, $w = \frac{m_{suction}}{m_{motive}}$**		**Suction pressure ratio, $\pi = \frac{P_{diffuser}}{P_{suction}}$**	
					Reference work [117]	**Present Work**	**Reference work** [117]	**Present Work**
15°	3.76	9.37	0.97	37.5	0.45	0.54	1.072	1.177
	3.74	9.73	0.97	36.2	0.55	0.63	1.022	1.48
10°	3.74	9.39	0.98	37.3	0.46	0.55	1.093	1.168
	3.64	9.51	0.94	37.2	0.51	0.56	1.077	1.155
5°	3.67	9.32	0.97	37.1	0.51	0.54	1.096	1.175
	3.56	9.65	0.94	35.3	0.55	0.58	1.071	1.154

Chapter 6: Result and Discussion

6.1 Analysis of ARC Based Proposed Advanced Cascaded Compression Absorption Systems.

The cascaded compression absorption refrigeration technology permits the system to ensure cooling at lower evaporator temperature due to the use of VCR technology at LTC and significant reduction of compressor's energy consumption due to the use of ARC system at HTC. In the traditional cascaded compression-absorption refrigeration cycle (CARC), a single-effect ARC and a simple VCR are integrated through a cascade heat exchanger. However, this system has several limitations, such as energy waste during throttling in expansion valve [16], lower heat removal in simple Vapor Absorption Refrigeration (VAR) [74], and the need for a single-stage compressor in VCR [16], which results in a relatively higher compressor power requirement.

This section of the research focuses on solving the problem by combining a modified ARC cycle with an improved VCR to achieve better energy and exergy performance. The ARC system can be improved by implementing an RHX at the evaporator outlet, which allows for more heat to be removed from heat exchanger, increasing the mass flow rate of refrigerant and solution, and leading to a higher system *COP*. In addition, the potential use of sophisticated VCR systems coupled with ejector and vapor injection in LTC is investigated to develop novel compression absorption cascade systems: **ECAC (Ejector compression absorption cycle)** and **EICAC (Ejector injection compression absorption cycle)**. The integration provides refrigeration at low evaporation temperatures with reduced energy loss during throttling.

After verification of the thermodynamic model, the comparative thermal analysis of the proposed ECAC and EICAC systems was carried out against the conventional CARC system. The assessment was based on various performance metrics, such as *COP*, generator input load ($\dot{Q}_{gen}$), compressor input load ($\dot{W}_{comp}$), exergetic efficiency (η_{II}), and total exergy destruction ($\dot{E}_{D,total}$). Four working parameters are taken as controllable variables, as such: condenser temperature (T_{cond}), generator temperature (T_{gen}), absorber temperature (T_{abs}), and evaporator temperature (T_{evp}). Furthermore, the study thoroughly examines the effects of ejector parameters to identify the

optimal operating conditions for performance enhancement while taking into account the effect and impact of each component. Lastly, multi-objective optimization is conducted to determine the optimal solution from both 1st and 2nd law perspective hence determine the feasible boundary conditions of operation. Design parameters and range of operation are provided in **Table 6-1**.

Table 6-1*. Design parameters for the analysis of ARC based conventional and proposed cascaded compression absorption systems.*

Parameters	Values
Cooling load, Q_{evp}	10 KW
Generator temperature, T_{gen}	70 ℃ to 100 ℃
Evaporator temperature, T_{evp}	-30 ℃ to -5 ℃
Condenser temperature, P_{cond}	25 ℃ to 40 ℃
Absorber temperature, T_{abs}	25 ℃ to 40 ℃
Effectiveness of RHX, $\boldsymbol{\varepsilon_{RHX}}$	0.9
Effectiveness of SHX, $\boldsymbol{\varepsilon_{SHX}}$	0.9
Cascade temperature difference, ΔT	5
Ambient temperature, T_0	25 ℃
Ambient pressure, P_0	101.325 kPa
Compressor efficiency, $\boldsymbol{\eta_s}$	0.85
Inlet external air temperature in Evaporator	T_{evp} + 8
Outlet external air temperature in Evaporator	T_{evp} + 3
Inlet cooling water temperature in Absorber	T_{abs} - 5
Outlet cooling water temperature in Absorber	T_{abs} + 5
Inlet heat source water temperature in Generator	T_{gen} + 15
Outlet heat source water temperature in Generator	T_{gen} + 10
Inlet cooling water temperature in Condenser	T_{cond} - 8
Outlet cooling water temperature in Condenser	T_{cond} – 3

6.1.1 Comparison Between Proposed and Conventional System

In this section the ARC based proposed cascaded models are simulated using an in-house EES-developed program. R41-LiBr/H_2O has been considered as the refrigerant pair for thermal performance evaluation and comparison. Availability and environmentally favorable qualities are the driving factors for the choice. R41 has a lower boiling point temperature (-78.2 °C), nil ODP, and an extremely low GWP (around 97) [79]. Because of this, it is extremely suitable for use in LTC. Also, for its superior performance in low-temperature applications, existing literature also encourages its use [78][79]. As an illustration, the thermodynamic state parameters of the proposed

novel cascade compression-adsorption refrigeration cycles are provided as an example in **Table 6-2** and **Table 6-3** for ECAC and EICAC, respectively.

***Table 6-2**. Thermodynamic state properties of ECAC for R41-LiBr/H_2O solution at T_{gen} = 75℃, T_{evp} = -30℃, T_{abs} = 30℃, T_{cond} = 30℃, and ΔT_{CHX} = 5℃*

State Point	T (℃)	P (kPa)	h (kJ kg^{-1})	s (kJ kg^{-1} K^{-1})	x (%)	$\dot{m}$ (kg s^{-1})
1	75	4.247	2641	8.714	-	0.005005
2	30	4.247	125.7	0.4368	-	0.005005
3	5	0.8725	52.51	0.1895	-	0.005005
4	5	0.8725	2510	9.025	-	0.005005
5	30	0.8725	66.62	0.1944	0.5257	0.03756
6	30	4.247	66.62	0.1944	0.5257	0.03756
7	65.1	4.247	132.8	0.4261	0.5257	0.03756
8	75	4.247	188.1	0.421	0.6066	0.03255
9	34.5	4.247	111.7	0.1875	0.6066	0.03255
10	34.5	0.8725	111.7	0.1875	0.6066	0.03255
11	12.5	4.247	52.51	0.1879	-	0.005005
12	29	0.8725	2583	9.271	-	0.005005
13	50.27	2666	606.7	2.416	-	0.0324
14	10	2666	227.1	1.093	-	0.0324
15	-31.27	783.5	218.1	1.1	-	0.0324
16	-31.27	783.5	356.3	1.671	-	0.05739
17	-26.97	907	361.2	1.674	-	0.05739
18	-26.97	907	135.1	0.7553	-	0.02499
19	-30	818.5	135.1	0.756	-	0.02499
20	-30	818.5	535.2	2.402	-	0.02499
20′	-31.27	783.5	533.3	2.403	-	0.02499
21	-26.97	907	535.7	2.383	-	0.0324

***Table 6-3**. Thermodynamic state properties of EICAC for R41-LiBr/H_2O solution at T_{gen} = 75℃, T_{evp} = -30℃, T_{abs} = 30℃, T_{cond} = 30℃, and ΔT_{CHX} = 5℃*

State Point	T (℃)	P (kPa)	h (kJ kg^{-1})	s (kJ kg^{-1} K^{-1})	x (%)	$\dot{m}$ (kg s^{-1})
1	75	4.247	2641	8.714	-	0.004845
2	30	4.247	125.7	0.4368	-	0.004845
3	5	0.8725	52.51	0.1895	-	0.004845
4	5	0.8725	2510	9.025	-	0.004845
5	30	0.8725	66.62	0.1944	0.5257	0.03636
6	30	4.247	66.62	0.1944	0.5257	0.03636
7	65.1	4.247	132.8	0.4261	0.5257	0.03636

8	75	4.247	188.1	0.421	0.6066	0.03151
9	34.5	4.247	111.7	0.1875	0.6066	0.03151
10	34.5	0.8725	111.7	0.1875	0.6066	0.03151
11	12.5	4.247	52.51	0.1879	-	0.004845
12	29	0.8725	2583	9.271	-	0.004845
13	44.76	2666	597.6	2.399	-	0.031
14	10	2666	227.1	1.093	-	0.031
15	-13.91	1345	210.2	1.098	-	0.031
16	-13.91	1345	215.8	1.568	-	0.03143
17	-11.51	1477	217.1	1.57	-	0.03143
18	-11.51	1477	536	2.289	-	0.003937
19	-11.51	1477	171.4	0.8956	-	0.02749
20	-13.91	1375	171.4	0.8962	-	0.02749
21	-13.91	1375	536.3	2.303	-	0.0006726
21′	-13.91	1345	535.2	2.307	-	0.0006726
22	-13.91	1375	165.6	0.8738	-	0.02706
23	-30	818.5	165.6	0.8818	-	0.02706
24	-30	818.5	535.2	2.402	-	0.02706
25	5.907	1477	566.7	2.413	-	0.02706
26	3.506	1477	562.8	2.387	-	0.031

Furthermore, the performance comparative analysis between the proposed systems (ECAC and EICAC) and conventional system (CARC) has been carried out at a specific working condition of T_{gen} = 75℃, T_{evp} = -30℃, T_{abs} = 30℃, T_{cond} = 30℃, and ΔT_{CHX} = 5℃. The result is displayed in **Table 6-4**. It has been discovered that ECAC improves performance by 4.6%, while EICAC improves performance by nearly 18% over traditional compression absorption systems.

Table 6-4*. Comparison of performance between ARC based conventional and proposed cascaded systems system at T_{gen} = 75℃, T_{evp} = -30℃, T_{abs} = 30℃, T_{cond} = 30℃.*

Component	**Conventional System**	**Proposed system**	
	CARC	**ECAC**	**EICAC**
Generator, $\dot{Q}_{gen}$ **(kW)**	15.13	14.85	13.89
Condenser, $\dot{Q}_{cond}$ **(kW)**	13.18	12.89	12.19
Evaporator, $\dot{Q}_{evp}$ **(kW)**	10	10	10
Absorber, $\dot{Q}_{abs}$ **(kW)**	14.56	14.36	13.62
Compressor, $\dot{W}_{comp}$ **(kW)**	2.689	2.499	1.93
Exergy destruction, $\dot{E}_{D,total}$ **(kW)**	2.45	2.09	1.716
Coefficient of performance, ***COP***	0.5688	0.595	0.6319
Exergetic efficiency, η_{II}	0.4804	0.5206	0.5687

6.1.2 Thermodynamic Parametric Sensitivity & Performance Analysis

Effect of Pressure Drop Across Ejector Nozzle on the System Performance

Performance and operation of both ARC based proposed cascaded compression absorption systems equipped with ejector is controlled by the pressure drop of the refrigerant after accelerating through motive and suction nozzle. For a definite working condition an optimal value of pressure drop can be found by continuous iteration of the model for maximum system performance. **Figure 6-1** depicts the impact of pressure drop over *COP*. For ECAC, *COP* augments with increasing pressure drop up to an optimal value obtained near 35 kPa. Increasing pressure drop further, results in a gradual decrement of *COP*. For EICAC, the gradual increment is less steep with pressure drop increase. The optimal value of *COP* can be found near 80 kPa, after which further increment of pressure drop has minimal effect on *COP*.

Furthermore, For ECAC, the *COP* changes on a scale of approximately 0.005 as pressure drop in suction nozzle increases from 0 to 120 kPa. In contrast, the *COP* changes for EICAC are on a scale of 0.001, which is five times smaller than that of ECAC. The impact of pressure drop is more prominent for ECAC with a change of *COP* 0.0001428 per kPa increase of pressure drop before reaching the maximum *COP*. Whereas for EICAC, the change is 0.0000125 per kPa pressure drop increase. Hence it is found that pressure drop has minimal impact on EICAC.

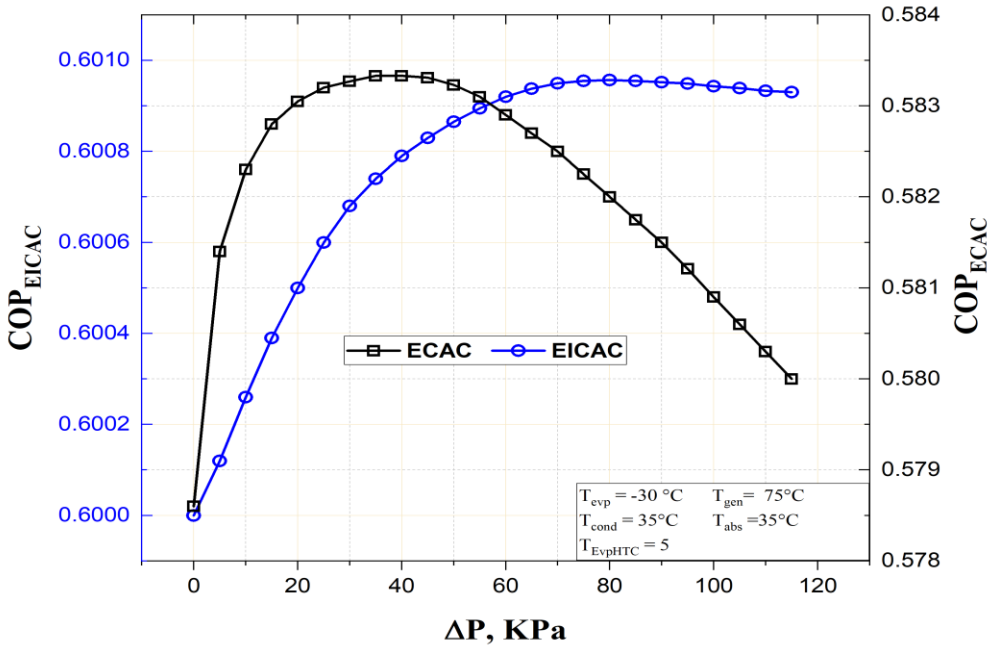

***Figure 6-1**: The impact of ΔP on COP of ARC based cascaded compression absorption systems at T_{cond} = 35 ℃, T_{abs} = 35 ℃, T_{evp} = -30 ℃, T_{gen} = 75 ℃.*

The change of *COP* can be further demonstrated by **Figure 6-2(a),** which describes the change of entrainment Ratio, ER with the pressure drop. The effect of *ER* on *COP* is due to the change of $\dot{m}_{evaporator}$ with the change of pressure drop for the same range. For ECAC, with pressure drop increasing, *ER* varies in the same manner as *COP*. Because with *ER* increasing $\dot{m}_{suction} = \dot{m}_{20} = \dot{m}_{evaporator} = \dot{m}_{19}$ increases, which results in higher cooling load as well as higher coefficient of performance. The relationship between *COP*, *ER* and $\dot{m}_{evaporator}$ is linear; for this reason their behaviour with pressure drop increasing depicts similar pattern.

But for EICAC, with pressure drop increasing, the entrainment ratio decreases until a minimum value is attained. Decrement of *ER* results in decrement of $\dot{m}_{suction} = \dot{m}_{21}$. Which in terms results in an increment of $\dot{m}_{evp} = \dot{m}_{23}$ (because $\dot{m}_{suction} = \frac{1-x_{20}}{x_{20}} m_{evap}$) as described in **Figure 6-2(b)**. The higher $\dot{m}_{evp}$ results in the enhancement of cooling load as well as *COP*. So, *COP* is proportional to $\dot{m}_{evp}$; for this reason, their behaviour with pressure drop increasing depicts a similar pattern. But both are inversely proportional to *ER*, for this reason the pattern is reversed in this case.

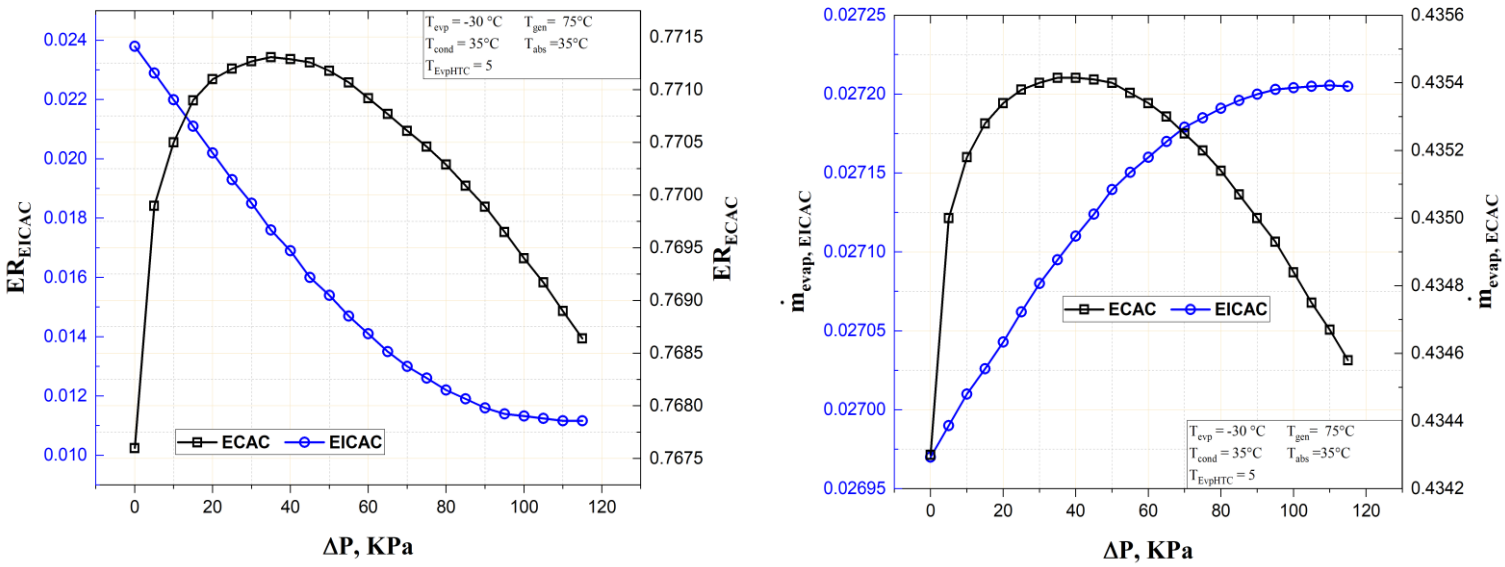

(a) (b)

***Figure 6-2**: The impact of ΔP on (a) Entrainment ratio (ER) and (b) $m_{evaporator}$ of ARC based cascaded compression absorption systems at T_{cond} = 35 °C, T_{abs} = 35 °C, T_{evp} = -30 °C, T_{gen} = 75 °C*

System Sub-cycle Performance Analysis

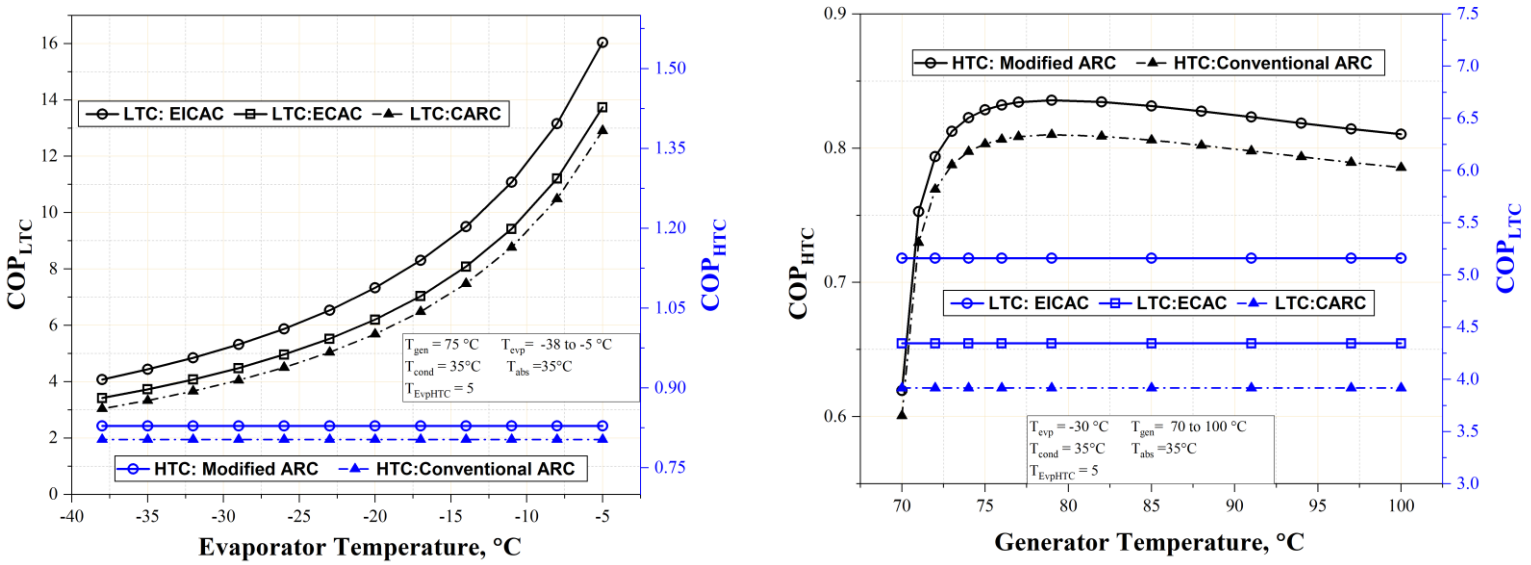

***Figure 6-3**: The effect of (a) evaporator temperature and (b) generator temperature on COP_{LTC} and COP_{HTC} of ARC based cascaded systems at T_{cond} = 35℃, T_{abs} = 35 ℃, ΔT_{CHX} = 5℃, T_{evpHTC} =5℃*

Before conducting a comprehensive analysis of the system performance, the impact of working conditions on the subsystems is evaluated first. In this context, COP_{LTC} is associated with the compressor load, while COP_{HTC} is concerned with the generator load only. In this analysis, T_{evpHTC} is fixed at 5℃ with ΔT_{CHX} = 5℃. So with increasing T_{evp}, pressure ratio in the HTC remains the same (as T_{gen} is fixed at 75℃). As a result, COP_{HTC} of the systems remains constant with T_{evp} change. But with T_{evp} increasing, pressure ratio as well as required compressor input in LTC decreases as a result COP_{LTC} increases. As illustrated in **Figure 6-3(a)**, COP_{LTC} increases significantly for higher evaporator temperatures, with the LTC of EICAC and ECAC maintaining approximately 15% and 5% higher *COP* compared to the conventional CARC.

Similarly, when T_{gen} changes, COP_{HTC} varies with the varying generator load, but COP_{LTC} remains unchanged due to the fixed pressure ratio across LTC (as T_{evp} is fixed at -30℃). COP_{LTC} of the proposed systems keeps around the same enhancement as stated before. Regarding COP_{HTC}, both HTC-ARC systems exhibit very low, nearly identical *COP* at lower T_{gen} as shown in **Figure 6-3(b)**. However, as T_{gen} increases, COP_{HTC} rises rapidly within the range of T_{gen} = 75℃. Upon reaching the optimal value, COP_{HTC} decreases, but at a slower rate. Over this range of T_{gen}, the modified ARC maintains a roughly 5% performance enhancement compared to the conventional ARC.

Impact of Operating Conditions on System Performance

To facilitate additional analysis and comparison across various working conditions, the *COP* is optimized with respect to the pressure drop of ejector during each simulation. **Figure 6-4** demonstrates that, the effective performance of the suggested ARC based cascaded compression absorption refrigeration systems is significantly influenced by T_{gen} and T_{evp}. Under similar operational circumstances, EICAC exhibits a greater *COP* than ECAC. With T_{evp} increasing, the *COP* of both ECAC and EICAC increases. However, increment rate intensifies more at lower T_{gen}. The *COP* variation relating to the T_{gen} exhibits a comparable pattern for varying constant evaporator temperatures. System *COP* experiences a rapid increase in response to increasing T_{gen}, within the lower range of approximately 70℃ to 77℃. reaching a specific optimal value, the change in *COP* with T_{gen} becomes negligible. It has been found that, EICAC reaches the optimal condition at a slightly higher evaporator temperature than ECAC and CARC.

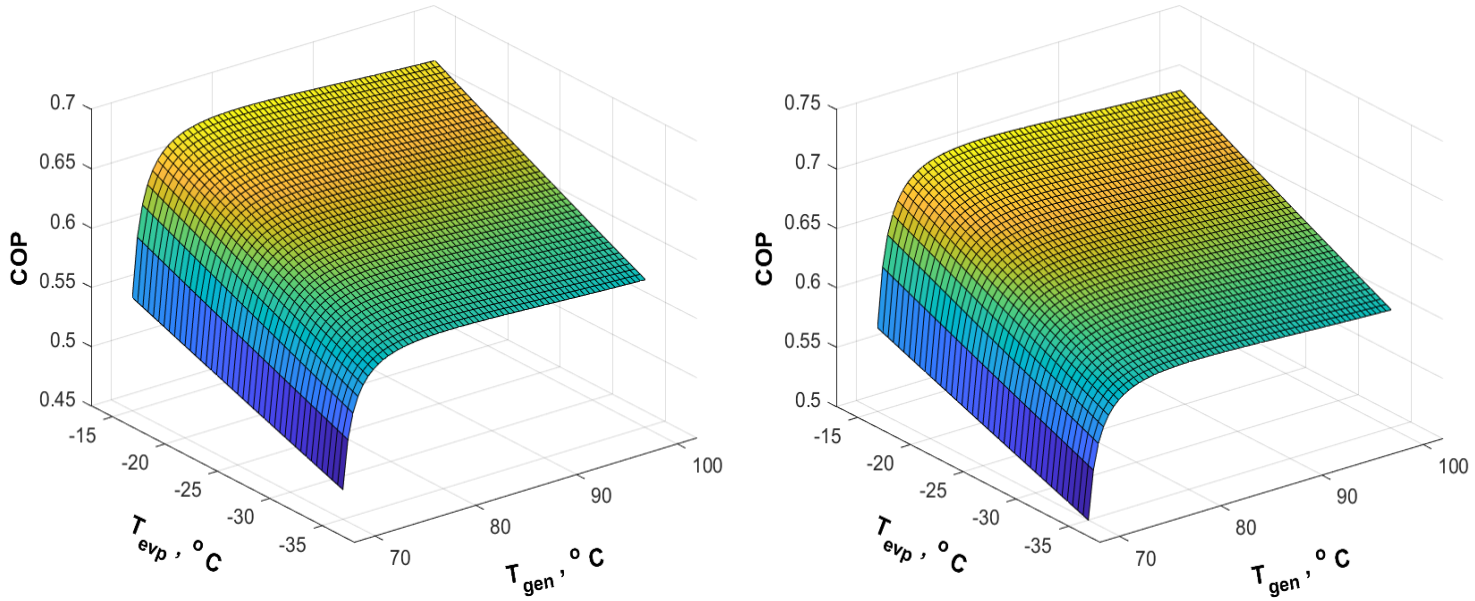

(a) ECAC **(b) EICAC**

***Figure 6-4**: The impact of T_{gen} and evaporator temperature on COP of ARC based cascaded systems compression absorption at T_{cond} = 35℃, T_{abs} = 35 ℃*

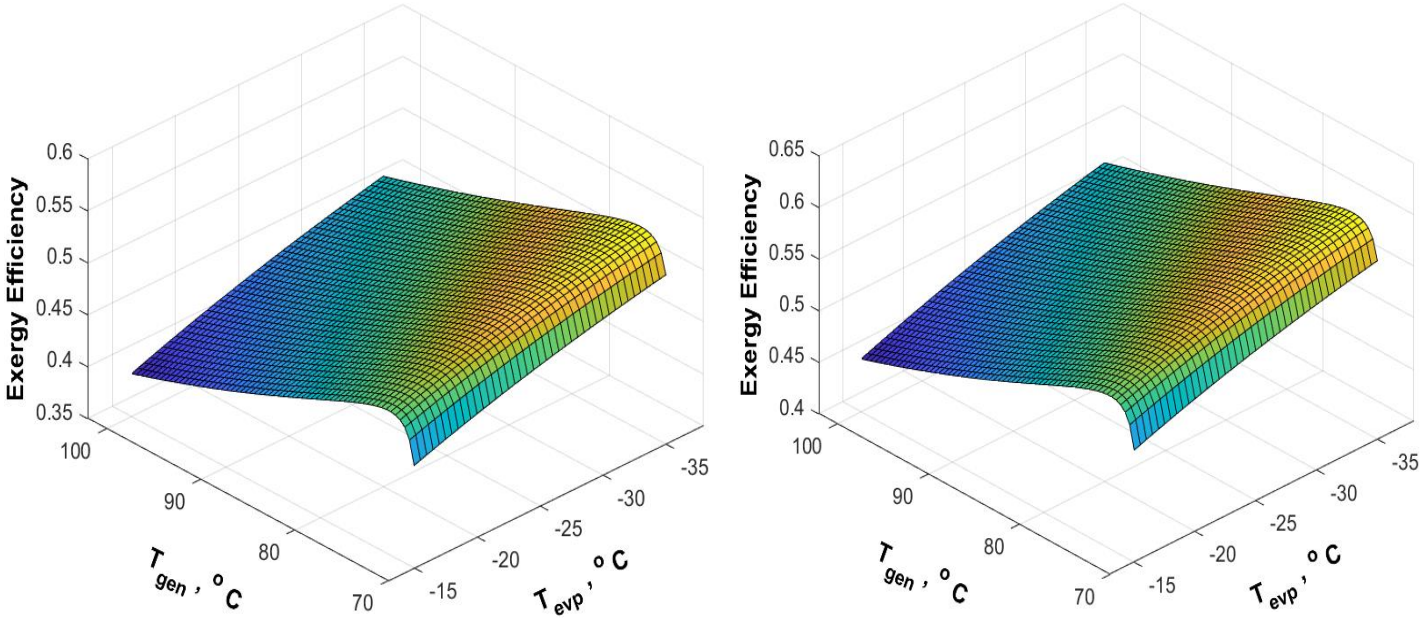

(a) ECAC (b) EICAC

***Figure 6-5**: The impact of T_{gen} and evaporator temperature on Exergy Efficiency of ARC based cascaded compression absorption systems at T_{cond} = 35 ℃, T_{abs} = 35 ℃*

Figure 6-5 illustrates the impact of operating circumstances on the 2nd law efficiency of ARC based cascaded compression absorption proposed systems. EICAC displays a significant enhancement of exergy efficiency for similar operating conditions. It can be found that with evaporator temperature increasing, exergy efficiency increases. Also, EICAC shows higher increament rate at lower evaporator temperature than ECAC. For a fixed T_{evp}, the exergy efficiency increases with the increment of T_{gen} in the range of 70℃ to 77℃. But after reaching an optimal condition, it decreases gradually with T_{gen} increasing. The figure demonstrates that optimal generator temperature increases with the T_{evp} increasing and the rate is slightly higher for EICAC system. For a detailed analysis, the effect of each operating parameter is analyzed separately while taking other variables as constant. This analysis provides an in-depth analysis with a plausible operating range and limiting factors for swift operation of the system.

Figure 6-6(a) is presented to illustrate the comparison of performance of the ARC based cascaded compression absorption refrigeration systems based upon the impact of generator temperature. As the T_{gen} rises, the system *COP* experiences a rapid increase for lower generator temperatures (approximately within the range of 70℃ to 77℃). Upon reaching a specific optimal T_{gen}, the rate of *COP* change diminishes to a minimal level. It has been found that, EICAC reaches the optimal condition slightly later (near 77℃ generator temperature) than ECAC and CARC. EICAC and

ECAC also maintain an enhancement of system *COP* of 19.83% and 5.66% respectively after reaching the optimal condition over CARC.

The above stated behavior of the *COP* curve can be clearly explained in **Figure 6-6(b).** EICAC rejects higher heat through cascade heat exchanger, resulting in lower mass flow rate of LiBr/H_2O circulating the absorption sub cycle. Which in terms decrease the generator load hence results in higher *COP* than ECAC and conventional CARC. With T_{gen} increasing from 70℃-77℃, the generator load decreases rapidly. But after reaching the minimum load (at around 77℃), the change with evaporator temperature increasing is minimal resulting in minimal change of *COP* as described in **Figure 6-6(a).** EICAC and ECAC require around 19.87 and 5.41% lesser generator load than CARC respectively for the same evaporator temperature.

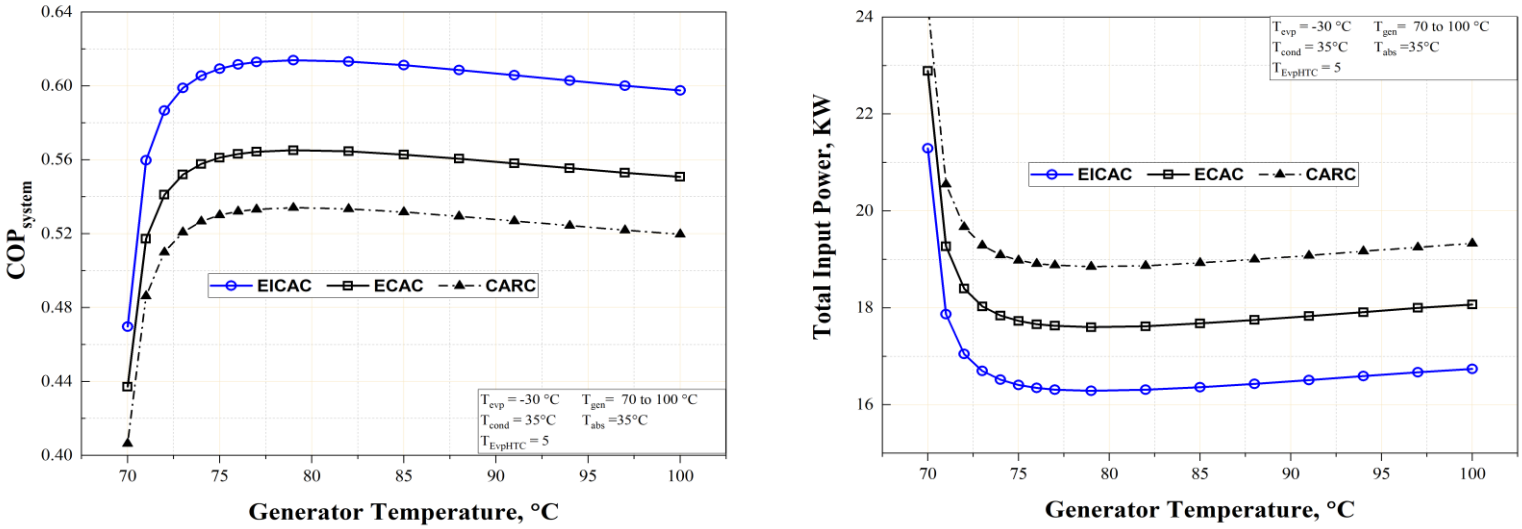

(a) **(b)**

***Figure 6-6**: The effect of T_{gen} on (a) COP and (b)Total input power of the proposed ARC based cascaded compression absorption systems at T_{cond} = 35℃, T_{abs} = 35℃, T_{evp} = -30℃*

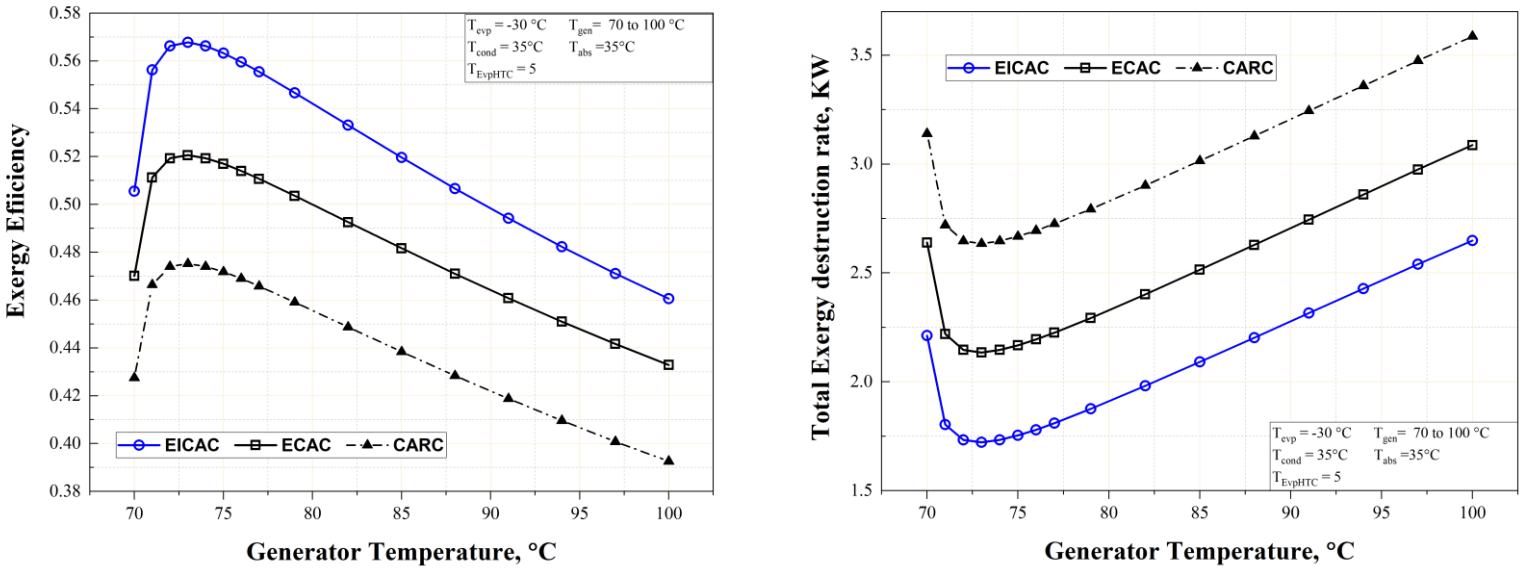

(a) **(b)**

***Figure 6-7**: The effect of T_{gen} on (a) exergetic efficiency and (b) $\dot{E}_{D,total}$ of ARC based cascaded compression absorption systems at T_{cond} = 35℃, T_{abs} = 35℃, T_{evp} = -30℃*

Figure 6-7(a) depicts the exergetic perspective of the impact of generator temperature of ARC based cascaded compression absorption systems. The optimal temperature for attaining maximum exergy efficiency is approximately 73℃. The EICAC and ECAC exhibit superior exergy efficiency of 21.47% and 10.66% respectively, in comparison to the conventional CARC. While the system's energy performance may exhibit minimal changes beyond the optimal value, the exergetic efficiency experiences a significant decrease once the optimum condition is reached. At T_{gen} below 73℃, the rate of decrease is notably steep, leading to a limiting operational state of the system. The observational evidence suggests that the exergy efficiency is more susceptible to fluctuations in generator temperature as opposed to variations in the system *COP*.

As T_{gen} increases, the refrigeration potential of the system also improves, resulting in a rapid intensification in exergy efficiency. However, when the optimal limit of the generator temperature is reached, the increase in the amount of refrigerant vapor produced at the generator significantly affects the system. This leads to higher exergy destruction rates at generator, condenser, and absorber resulting in rapid increase of total exergy destruction rate as depicted in **Figure 6-7(b)**. This leads to a significant reduction of exergy efficiency with increasing T_{gen}. To maintain optimal performance, it is crucial to keep the T_{gen} within the range of 73℃ to 75℃.

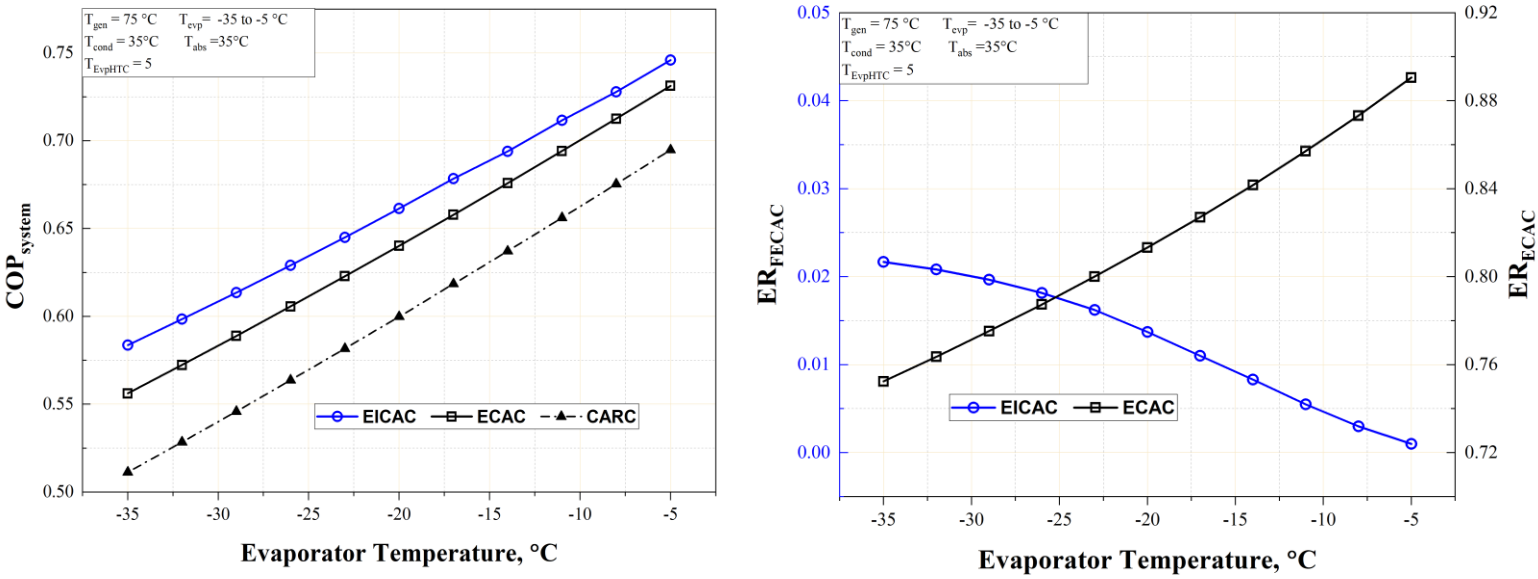

(a) **(b)**

***Figure 6-8**: The effect of T_{evp} on (a) COP and (b) Entrainment ratio (ER) of ARC based cascaded compression absorption systems at T_{cond} = 35°C, T_{abs} = 35°C, T_{gen} = 75°C*

Figure 6-8(a) illustrates the influence of T_{evp} on system *COP* of ARC based cascaded compression absorption systems. As T_{evp} increases, the required compressor load for a fixed cooling effect decreases, resulting in a linear increase in *COP*. EICAC and ECAC maintain an enhancement of system *COP* of around 13% and 8% respectively over conventional CARC for different evaporator temperatures. This phenomenon can be further explained by **Figure 6-8(b)** which shows the impact of T_{evp} on *ER*. For EICAC, with T_{evp} increasing m_{evp} increases, resulting in lower $m_{suction}$ hence lower *ER*. But for ECAC, with T_{evp} increasing $m_{evp} = m_{suction}$ increases resulting in higher *ER*.

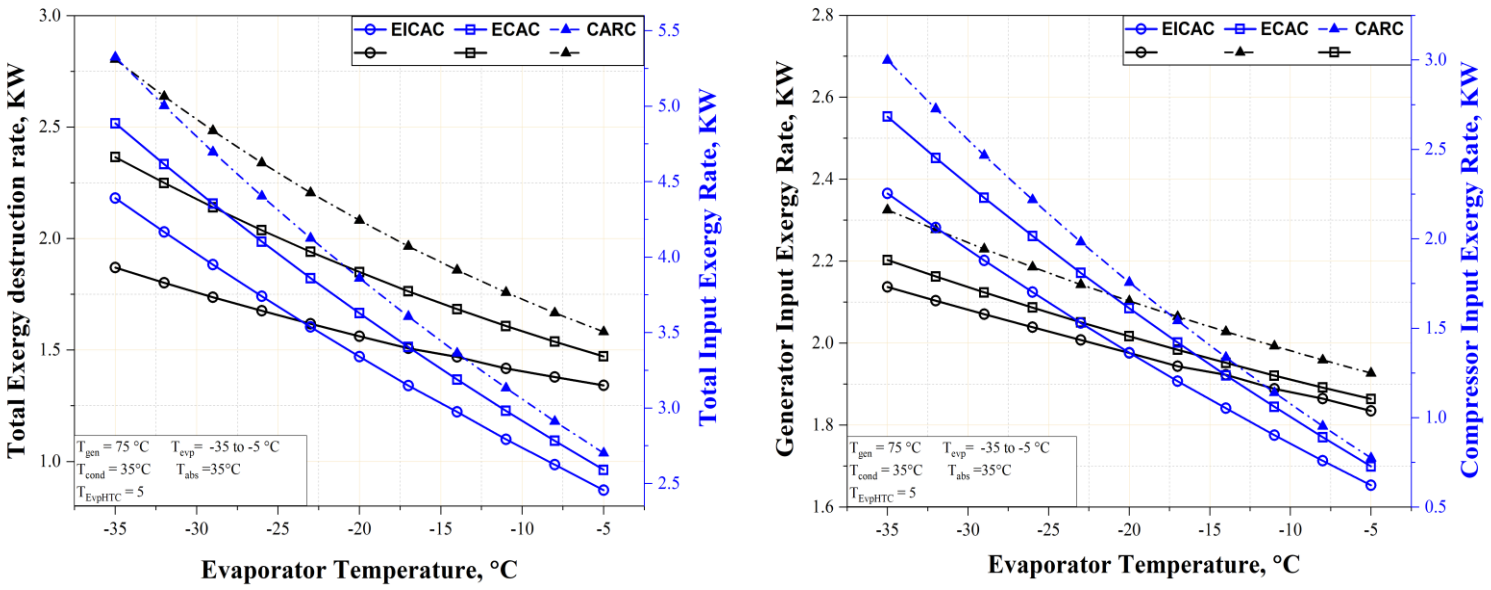

(a) (b)

***Figure 6-9**: The influence of T_{evp} on $\dot{E}_{D,total}$ and $\dot{E}_{x,in}$ of ARC based cascaded compression absorption systems at T_{cond} = 35℃, T_{abs} = 35℃, T_{gen} = 75℃*

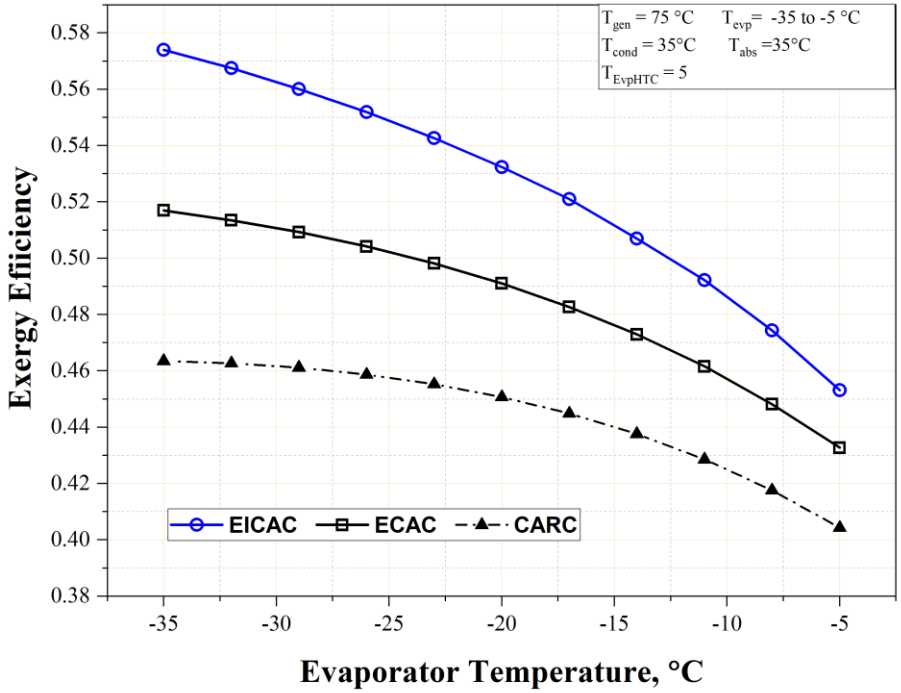

***Figure 6-10:** The influence of T_{evp} on exergetic efficiency of ARC based cascaded compression absorption systems at T_{cond} = 35℃, T_{abs} = 35℃, T_{gen} = 75℃*

However, the exergetic efficiency falls in contrast to the aforementioned patterns with T_{evp} increasing as shown in **Figure 6-10**. Total exergy destruction doesn't increase, rather it also decreases with T_{evp} increasing as shown in **Figure 6-9(a)**. With the T_{evp} increasing, the refrigerant's

heat absorbtion capacity for vaporization decreases, reducing the system's potential to extract heat. As a result, the exergy destruction across each component as well as total exergy destruction rate decreases with T_{evp} increasing as shown in **Figure 6-9(a)**.

Again, lower heat absorption capacity in evaporator, results in lower Q_{CHX}, which ultimately results in lower requirement of generator input exergy. From **Figure 6-9(b)**, it can be seen that input generator exergy decreases near linearly with T_{evp} increasing. But the required input compressor exergy rate decreases at a higher rate due to significant decrease of pressure ratio in LTC. So ultimately total input rate of exergy decreases at a higher rate than total exergy destruction. This eventually results in the reduction of exergy efficiency as depicted in **equation:**

$$\eta_{ex} = \frac{\dot{\mathrm{E}}\mathrm{x}_p}{\dot{\mathrm{E}}\mathrm{x}_f} = 1 - \frac{\dot{\mathrm{E}}\mathrm{x}_D}{\dot{\mathrm{E}}\mathrm{x}_f}$$

This phenomenon is observed in **Figure 6-10**, where it is observed that, exergy efficiency declines with evaporator temperature increasing even though total exergy destruction is decreasing. However, the decremental rate is not the same for all the systems. For T_{evp}*= -35 ℃*, EICAC and ECAC show exergy efficiency enhancement of around 23% and 11% respectively over conventional CARC, whereas for higher evaporator temperature of T_{evp}*= -5 ℃,* this increment reduces to 12.5% and 7% respectively. This can be ascribed to the fact that, at lower T_{evp}, there is a high-pressure ratio across the LTC, leading to greater differences in exergy input, exergy destruction, and exergy efficiency of the compared systems. However, at higher evaporator temperatures, the effect is insignificant due to lower pressure ratio, causing the performance of the systems to be nearly the same. So, through the analysis, it has been found that, although with increasing T_{evp}, the *COP* of all the systems increases linearly at a near similar rate but the exergy efficiency decreases at a different rate.

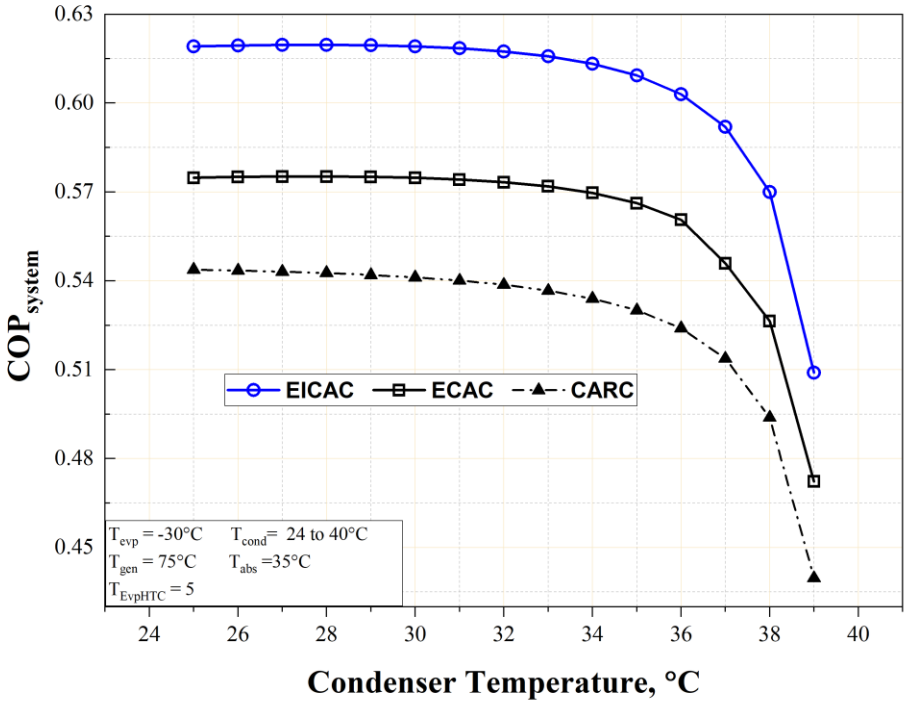

***Figure 6-11**: The effect of T_{cond} on COP of ARC based cascaded compression absorption systems at T_{evp} = -30℃, T_{abs} = 35℃, T_{gen} = 75℃*

Figure 6-11 and **Figure 6-12** demonstrate the influence of T_{cond} on system performance of ARC based cascaded compression absorption systems. As T_{cond} increases, the corresponding input loads also increases, leading to a lessening in system *COP*. The increased T_{cond} leads to a reduction in heat rejection, causing a decline in the system's utilization of potential energy. This, in turn, consequences in an increase in exergy destruction and a reduction in exergetic efficiency. The system *COP* and exergy efficiency decline linearly as the condenser temperature decreases below 34℃. However, when the T_{cond} exceeds this limit, the system's performance experiences a sharp decline, resulting in limiting operating conditions. In the safe range of condenser temperature, EICAC and ECAC maintain an enhancement of COP of around 13% and 4.6% respectively over conventional CARC at T_{evp} = -30℃, T_{abs} = 35℃, T_{gen} = 75℃.

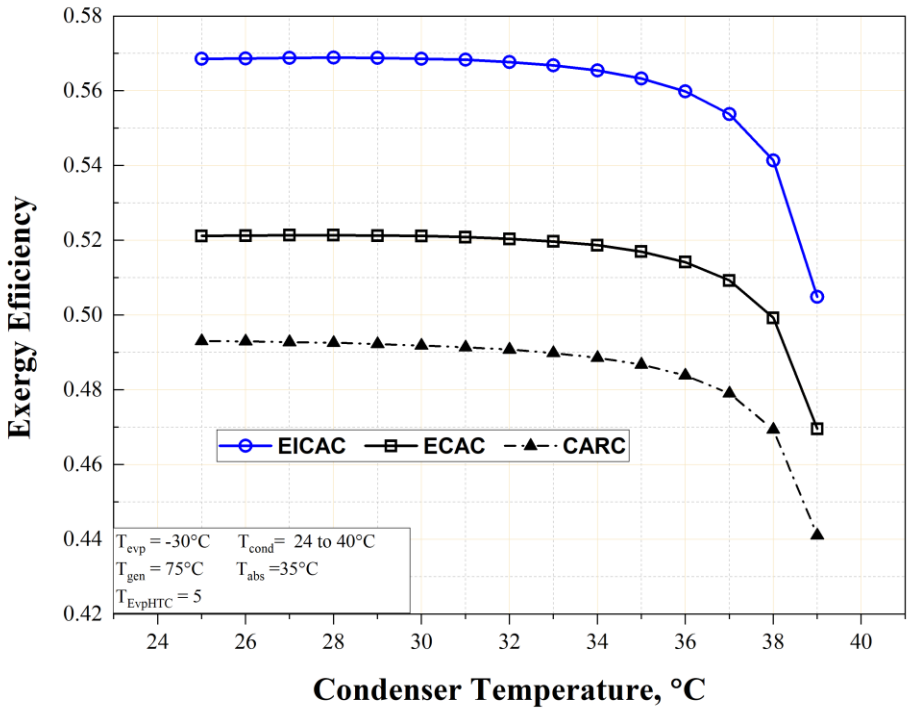

***Figure 6-12**: The effect of T_{cond} on exergy efficiency of ARC based cascaded systems at T_{evp} = -30℃, T_{abs} = 35℃, T_{gen} = 75℃, and T_{evpHTC} = 5℃.*

6.1.3 Exergy Flow and Destruction Analysis

Subsequently, an elaborate exergy analysis of the ARC based proposed cascaded compression absorption systems was performed under the following conditions: T_{gen}= 75℃, T_{evp} = -30℃, T_{abs} = 30℃, T_{cond} = 30℃, and ΔT_{CHX} = 5℃. In this context, **Figure 6-13** and **Figure 6-14** illustrates exergy flow diagram with corresponding component exergy destruction rate and percentage. The negligible amount of $\dot{E}_D$ in the flash tank, mixing chamber, and solution pump is disregarded. Evidently, the most significant exergy loss occurs at the generator, due to irreversibilities involved in high heat exchange between heat source and solution refrigerant. Whereas the least occurs at the solution heat exchanger. The EICAC exhibits a lower total exergy destruction rate than ECAC for the same output, hence has near 9% improved exergy efficiency. For both systems, the total destruction of exergy rate is nearly identical. Although due to double-stage compression, the EICAC has a relative lower loss in compressor and generator. The system has also sustained considerable exergy loss from the condenser and the absorber.

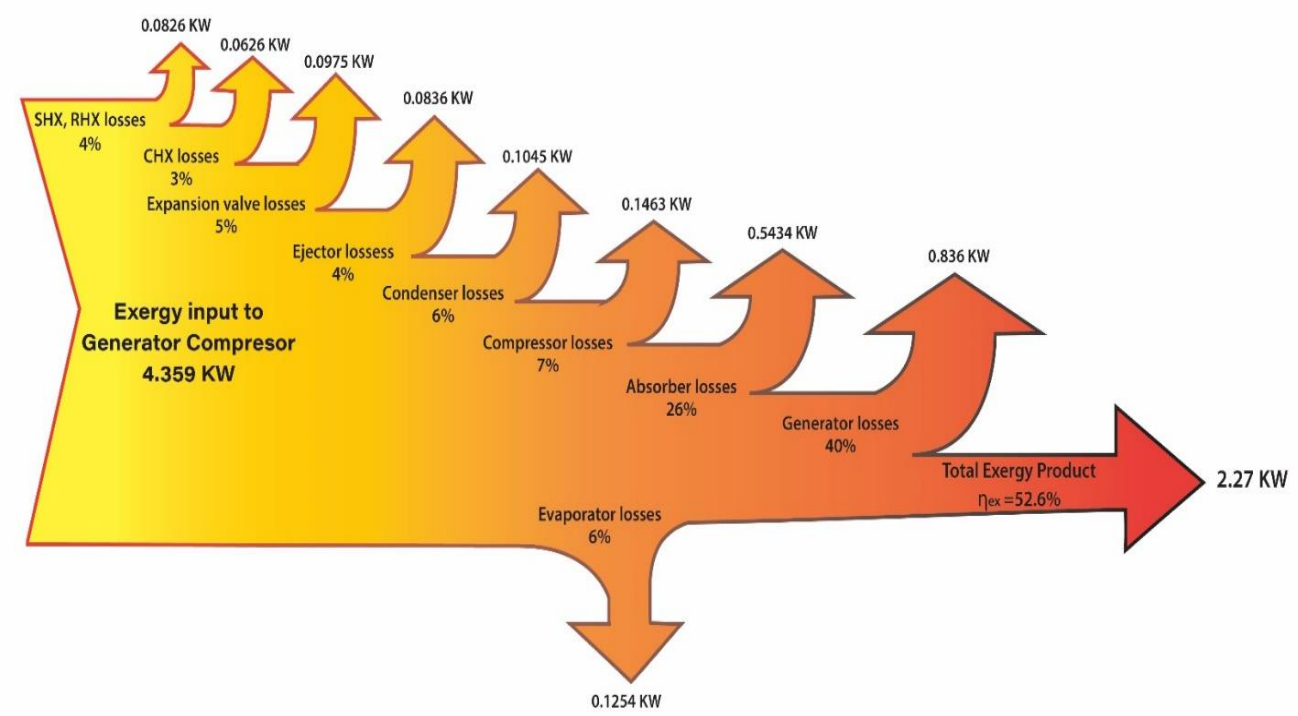

***Figure 6-13**: Exergy flow rate with associated component exergy destruction rate of the ECAC at T_{gen} = 75℃, T_{evp} = -30℃, T_{abs} = 30℃, T_{cond} = 30℃, and ΔT_{CHX} = 5℃*

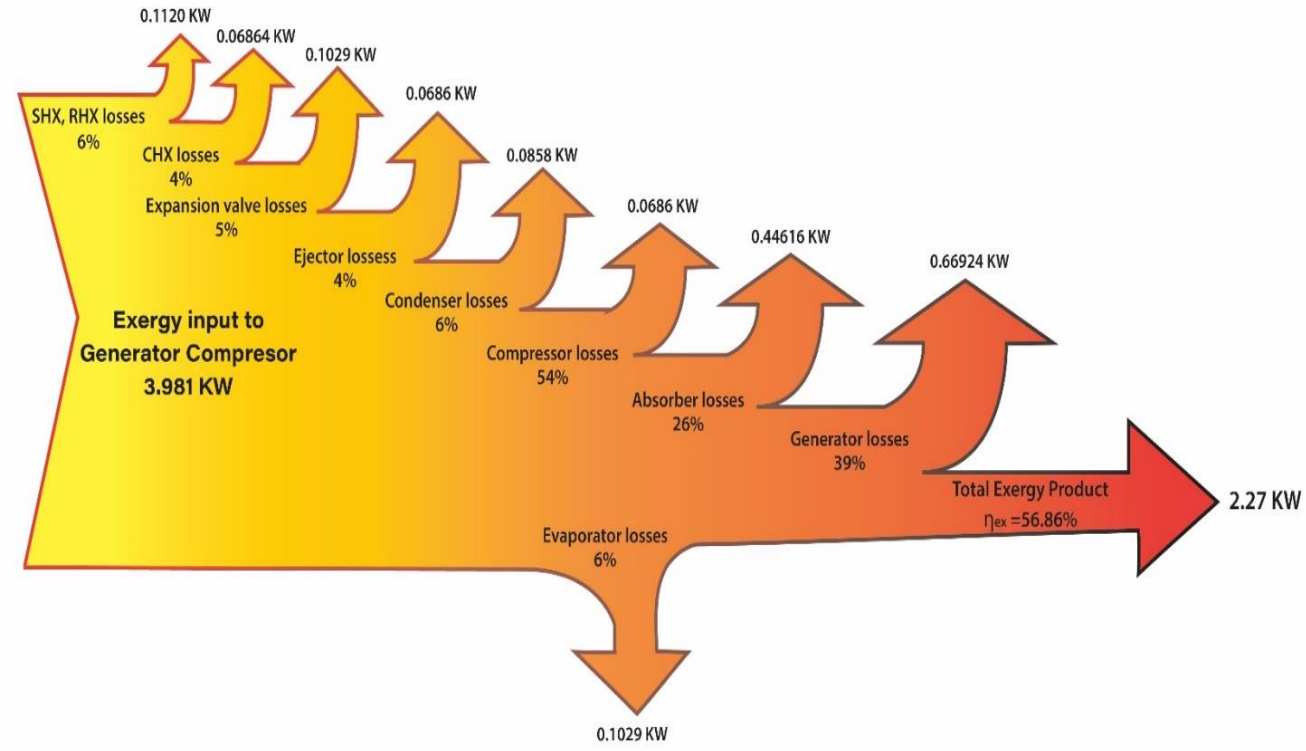

***Figure 6-14**: Exergy flow rate with associated component exergy destruction rate of the EICAC at T_{gen} = 75℃, T_{evp} = -30℃, T_{abs} = 30℃, T_{cond} = 30℃, and ΔT_{CHX} = 5℃*

6.1.4 Multi-objective Optimization

In pursuit of minimizing computational expenses and reducing simulation runtimes, a comprehensive simulation model was deployed 630 times across unique input datasets to develop objective functions based on Artificial Neural Networks (ANN) of the ARC based cascaded compression absorption systems. By integrating the objective function with the optimization algorithm, rather than directly embedding it within the simulation code, a significant decrease in runtime was achieved, enhancing the model's flexibility. ANN is recognized for their robust mathematical structure, and adept at identifying intricate non-linear relationships between variables where traditional physical equations may falter in accurately depicting process characteristics. The structure of ANN and optimization framework is presented in **Figure 6-15.**

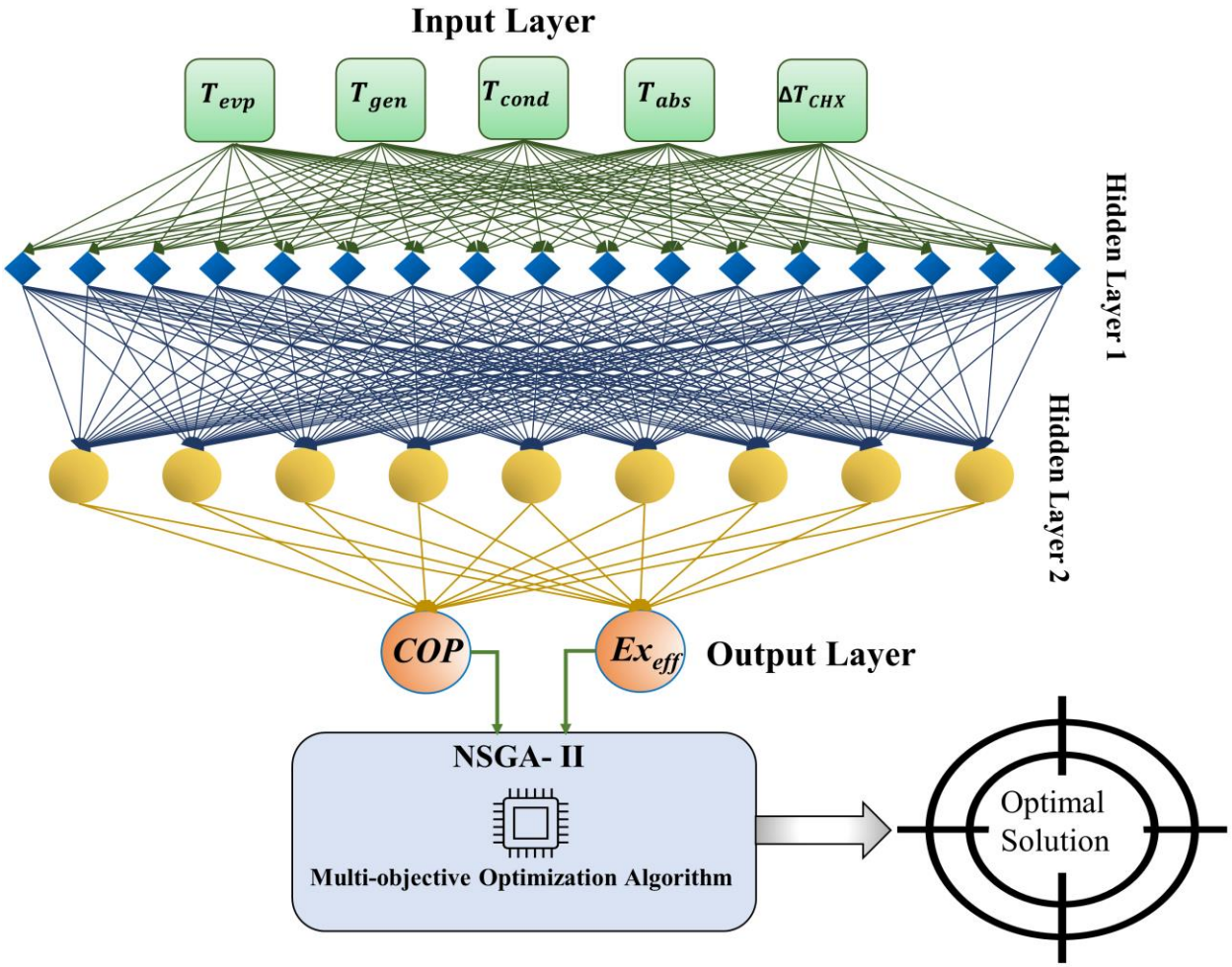

***Figure 6-15**: The outline of the optimization methodology using ANN prediction model of the ARC based cascaded compression absorption systems.*

The construction of the ANN-based predictive model's objective function of the ARC based cascaded compression absorption systems was undertaken utilizing five specific input variables (namely T_{evp}, T_{abs}, T_{gen}, P_{cond}, and ΔT_{chx}) along with two output variables (*COP* and Ex_{eff}). These variables were extracted from a comprehensive dataset encompassing 630 simulation runs. To ensure robust model training, the Bayesian regularization algorithm was employed on a substantial portion of the dataset, consisting of 567 rows (representing approximately 80% of the total data). The remaining 63 rows (about 20%) were reserved for testing purposes, thereby ensuring a comprehensive evaluation of the model's predictive capabilities. The architecture of the chosen ANN model is characterized by a two-layer feedforward network, which is equipped with 100 sigmoid hidden neurons and linear output neurons, showcasing the model's complexity and design rationale. The model summary is presented in **Figure 6-16**.

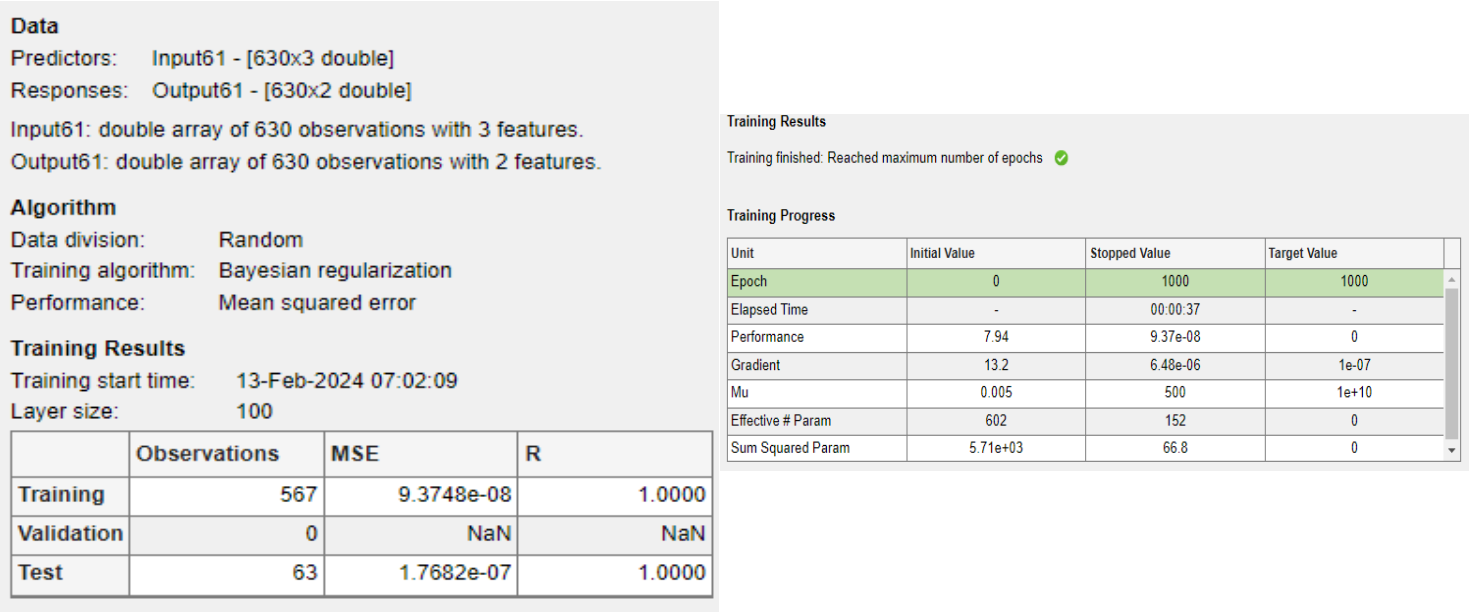

Data

Predictors: Input61 - [630x3 double]
Responses: Output61 - [630x2 double]

Input61: double array of 630 observations with 3 features.
Output61: double array of 630 observations with 2 features.

Algorithm

Data division: Random
Training algorithm: Bayesian regularization
Performance: Mean squared error

Training Results

Training start time: 13-Feb-2024 07:02:09
Layer size: 100

	Observations	MSE	R
Training	567	9.3748e-08	1.0000
Validation	0	NaN	NaN
Test	63	1.7682e-07	1.0000

Training Results

Training finished: Reached maximum number of epochs

Training Progress

Unit	Initial Value	Stopped Value	Target Value
Epoch	0	1000	1000
Elapsed Time	-	00:00:37	-
Performance	7.94	9.37e-08	0
Gradient	13.2	6.48e-06	1e-07
Mu	0.005	500	1e+10
Effective # Param	602	152	0
Sum Squared Param	5.71e+03	66.8	0

***Figure 6-16**: ANN model summary of training and testing Data of ARC based proposed cascaded compression absorption systems.*

This strategic configuration underscores the model's capacity for processing and analyzing the intricate relationships between the defined input and output variables, thus reinforcing the reliability and accuracy of the predictive model developed through this rigorous approach. Integration of ANN-based objective functions into the optimization framework not only signifies a leap towards computational efficiency but also enhances the flexibility and applicability of the simulation model in addressing complex engineering problems.

ML Model Accuracy Check and Error Evaluation

Accuracy checks and error evaluation are crucial for assessing machine learning model performance. While accuracy measures how well a model predicts or classifies data, it may not always provide a complete picture, especially with imbalanced datasets. Metrics like Precision, Recall, F1 Score, and Mean Squared Error (MSE) offer deeper insights into model effectiveness, addressing the balance between different types of errors and the precision of predictions. These metrics are essential for refining models, optimizing their performance, and ensuring their reliability and applicability to various datasets.

The model's performance was quantitatively assessed through the measure of determination (R^2) and mean squared errors (MSE), which serve as indicators of efficacy. The R^2 value, a metric for variance in response data, approached unity, indicating a high level of model reliability. The MSE for the training and testing datasets were recorded at $9.37* 10^{-8}$ and $1.76* 10^{-7}$, respectively, with an R^2 value of 0.998, demonstrating a commendable fit for the proposed model.

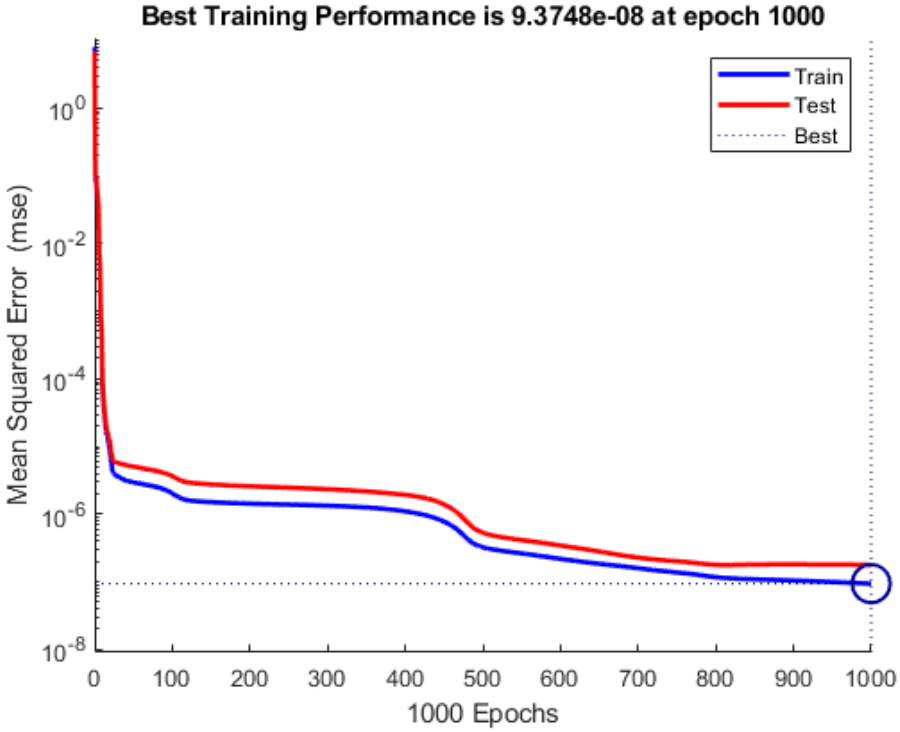

***Figure 6-17**: Performance test analysis of the ANN objective function of ARC based proposed cascaded compression absorption systems.*

In **Figure 6-17**, it is evident that both the trained and test datasets exhibited a close match, with an initial deviation from the optimal value line eventually narrowing, indicating convergence and alignment. This observation, coupled with the exceptionally low MSE values and an R^2 value equal to 1 as shown in **Figure 6-18,** underscores the model's suitability for optimization studies.

The alignment of data points around the unity line corroborates the successful and reliable application of the ANN in this context, marking a significant milestone in optimization study methodologies.

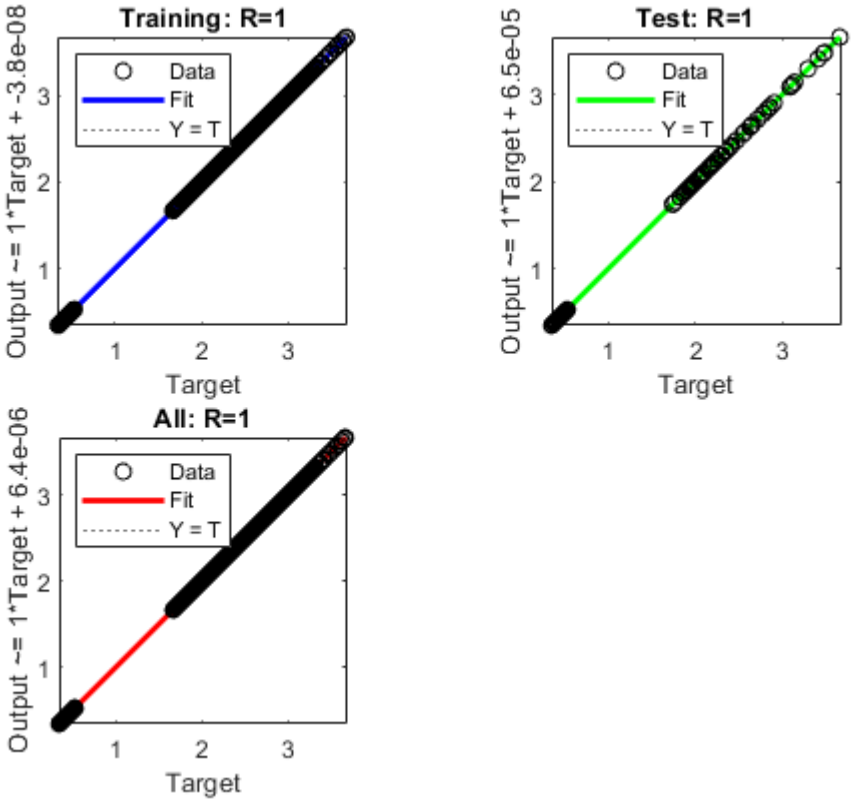

***Figure 6-18**: Accuracy levels of test and training data as well as their verification of ARC based proposed cascaded compression absorption systems.*

Optimization Strategy and Variables

One of the common optimization methods for the proposed cycles is the genetic algorithm (GA), which can explore multiple solutions at the same time by using a population of solutions. A specific type of GA is the Non-dominated Sorting Genetic Algorithm II (NSGA-II), which is a powerful multi-criteria evolutionary algorithm that is often used to improve energy systems. It has some

advantages, such as its robustness and fast population distance estimation, but it also has a drawback of being slow in its operation.

This work uses the optimization toolbox in MATLAB software to optimize the objective functions developed in ANN to maximize COP and exergy efficiency for 5 controllable variables of the ARC based cascaded compression absorption systems. The chosen values for different parameters in MATLAB optimization toolbox and the range of input controllable variables are given in **Table 6-5.**

Table 6-5*. Selected Values for different parameters of Multi objective optimization algorithm of ARC based proposed cascaded compression absorption systems.*

Specified Options		**Selected Value**
Population Size		200
Creation Function		Constraint Dependent
Crossover	function	Intermediate
	ratio	1
Migration	fraction	0.20
	direction	forward
Mutation	probability	Constraint dependent
	function	0.10
Population fraction of the Pareto Front		0.35
Max. Tolerance	constraint	10^{-3}
	function	10^{-4}
Generator temperature,	T_{gen}, ℃	65 to 100
Evaporator temperature	T_{evp}, ℃	-35 to -10
Absorber temperature	T_{abs}, ℃	20 to 35
Condenser temperature	T_{cond}, ℃	20 to 35
Pinch difference at CHX	ΔT_{chx}	2 to 5

Decision Making and Optimization Result

In multi-objective optimization, the Pareto frontier is a curve that showcases an array of optimal solutions. Each point on this frontier stands as a testament to an optimal trade-off between competing objectives. On this frontier, the point farthest to the left indicates the scenario with the highest exergy efficiency (point A), while the point farthest to the right (point C) shows the scenario with the best Coefficient of Performance (COP). To determine the most balanced optimal

solution that takes both COP and exergy efficiency (Exeff) into account, one can look for the point that is closest to the ideal scenario by measuring geometric distance, or furthest from the least desirable scenario. In this analysis, TOPSIS decision making technique is employed to find the most optimal solution (point B) considering both output perspective. This balanced approach ensures a comprehensive consideration of the multiple facets of energy optimization, leading to a more informed and holistic decision-making process.

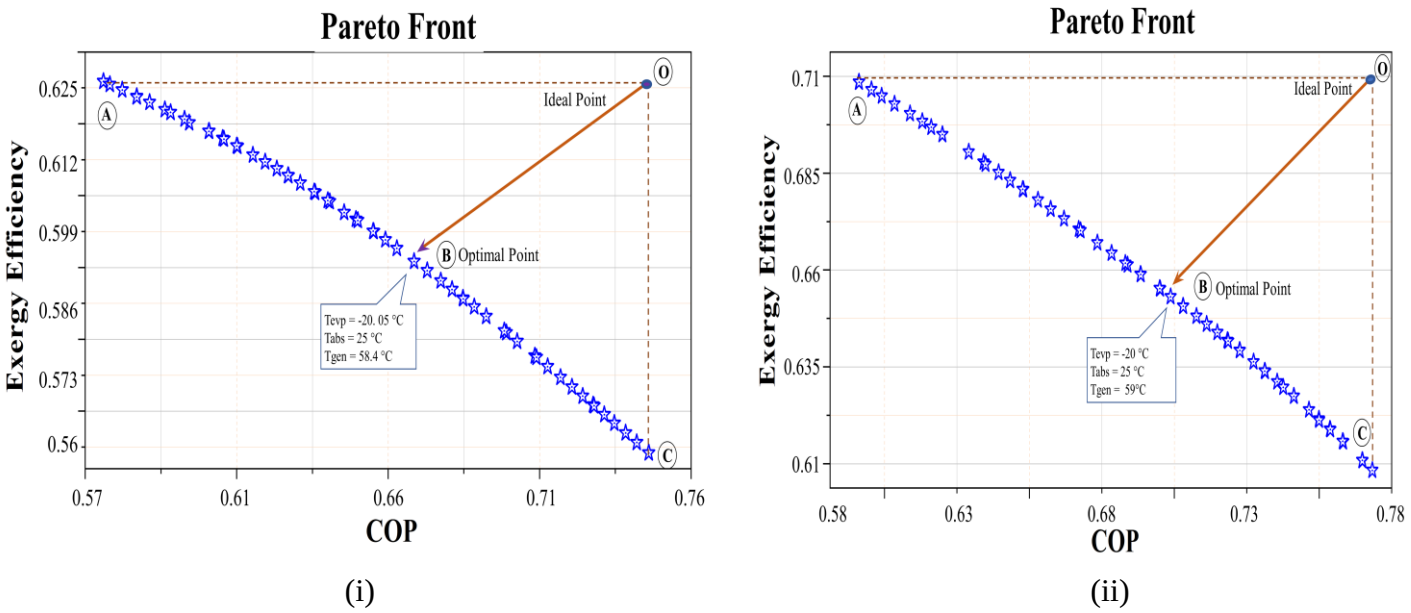

(i) (ii)

***Figure 6-19**: Pareto front of Ga-multi objective optimization of the proposed systems, (i) ECAC and (ii) EICAC to find the optimal solution using TOPSIS at T_{cond} = 30 ℃.*

The illustration in **Figure 6-19** presents the Pareto front of optimization solutions for two proposed models at a condensation temperature (T_{cond}) of 30°C. This Pareto front highlights all the points that represent optimal solutions, with particular emphasis on point A and B which denote the optimal solutions from the perspectives of maximizing the Coefficient of Performance (*COP*) and exergy efficiency, respectively. For a maximum value of ΔT_{CHX} = 5℃, the optimal points for both COP and exergy efficiency (Ex_{eff}) maximization occur.

Moreover, with T_{evp} and T_{abs} increasing exergy efficiency decreases linearly for both the systems. However, while the COP decreases with an increase in T_{abs}, it increases with an increase in T_{evp}, indicating the existence of an optimal T_{evp} value for optimal performance from both COP and exergy efficiency perspectives. Additionally, both *COP* and Ex_{eff} achieve their maximum at a specific generator temperature, although this optimum generator temperature for performance

maximization varies by 3-4℃ between the *COP* and exergy efficiency perspectives. From a specific perspective, the operating condition for optimal performance varies slightly between the proposed systems.

This is why, maximum *COP* condition of point A, is obtained at T_{evp} = -10℃, T_{abs} = 25℃ and T_{gen} = 62℃ around, and the values of max COP are 0.7464 and 0.76 for ECAC and EICAC respectively. Whereas, maximum Ex_{eff} condition of point B, is obtained at T_{evp} = -35℃, T_{abs} = 25℃ and T_{gen} = 56℃ around, and the values of max Ex_{eff} are 0.6259 and 0.7059 for ECAC and EICAC respectively. The optimal condition is determined by TOPSIS technique, and the optimum value of *COP*: 0.6788 and 0.6983, Ex_{eff} = 0.5993 and 0.6592 for ECAC and EICAC respectively at T_{evp} = -20℃, T_{abs} = 25℃ and T_{gen} = 58℃ around. The comparison of performance metrics along with optimal parameters of performance from different scenarios is provided in **Table 6-6** in details.

***Table 6-6**. Optimization Results for* ECAC and EICAC *configuration*s at T_{cond} = 30℃.

Input Parameters	**Units**	**Multi-Objective Optimization Scenarios**					
		(a) Max. *COP*		**(b) Optimal**		**(c) Max. Ex_{eff}**	
		ECAC	**EICAC**	**ECAC**	**EICAC**	**ECAC**	**EICAC**
Evaporator Temperature, T_{evp}	℃	-10	-10	-20.05	-20	-35	-35
Generator Temperature, T_{gen}	℃	61.8	62.2	58.4	59	55.6	56
Absorber Temperature, T_{abs}	℃	25	25	25	25	25	25
Pinch Temp. Diff. at CHX, ΔT_{chx}	℃	5	5	5	5	5	5
Output Parameters							
Generator Load, $\dot{Q}_{gen}$	kW	12.39	12.3	12.98	12.86	14.72	14.44
Condenser Rejection, $\dot{Q}_{cond}$	kW	11.17	11.09	11.61	11.51	12.8	12.56
Evaporator Extraction, $\dot{Q}_{evp}$	kW	10	10	10	10	10	10
Absorber Rejection, $\dot{Q}_{abs}$	kW	12.25	12.15	12.86	12.75	14.61	14.33
Compressor Load, $\dot{W}_{comp}$	kW	2.361	2.204	2.771	2.538	4.045	3.596
Exergy destruction, $\dot{E}_{D,total}$	kW	1.024	0.8676	1.079	0.8461	1.518	1.068
Coefficient of performance, *COP*		0.7464	0.76	0.6788	0.6983	0.5748	0.5989
Exergetic efficiency, η_{II}		0.5561	0.6074	0.5993	0.6592	0.6259	0.7059

Table 6-7 is presented to show the determined optimal parameters and performance comparison of the proposed systems for different T_{cond} conditions. As found earlier, from a specific perspective, the operating condition for optimal performance varies slightly between the proposed systems. This is why, in a specific scenario, a set of optimal parameters is selected to showcase the

performance comparison between the systems. ΔT_{CHX} is not included because, from all the perspective the optimal condition is found at its maximum value. The resulted *COP* and Ex_{eff} along with the optimal input parameters after optimization are presented for understanding the effect of each parameters individually. Additionally, with T_{cond} increases, this optimal value of the optimal T_{gen} also increases from all the perspectives. But the optimal T_{gen} for maximization of Ex_{eff}, increases at a slightly higher rate compared to the rate observed for *COP*. Again, regardless of change of T_{cond}, the optimal T_{evp} and T_{abs} value remain nearly unchanged. Moreover, with T_{cond} increasing, both *COP* and Ex_{eff} decrease, but Ex_{eff} increases at a much higher rate compared to *COP*. In all the conditions EICAC portraits significant higher value of *COP* and Ex_{eff} compared to ECAC. But this difference is much found significantly higher at max Ex_{eff} perspective compared to other scenarios.

Table 6-7. *Multi-objective optimization solution of ARC based proposed cascaded systems with result for different condenser temperatures.*

T_{cond}(℃)	Scenario	Operating Condition			
		T_{evp} (℃)	T_{abs} (℃)	T_{gen} (℃)	
25	Maximum COP	-10	25	54.6	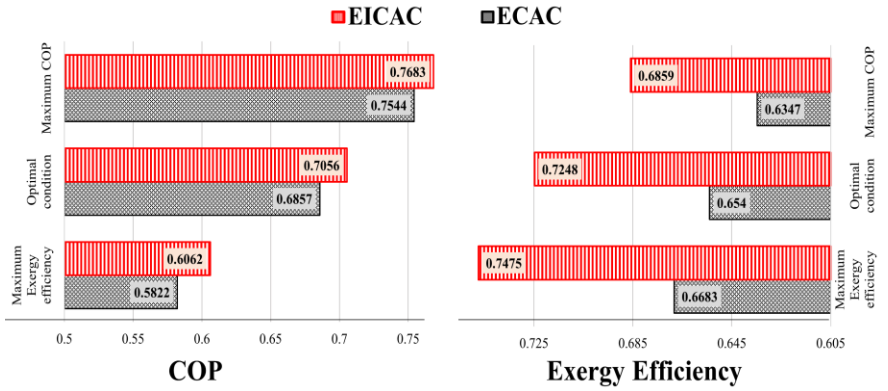
	Optimal Condition	-20	25	52.1	
	Max Exergy Efficiency	-35	25	49.1	
30	Maximum COP	-10	25	61.8	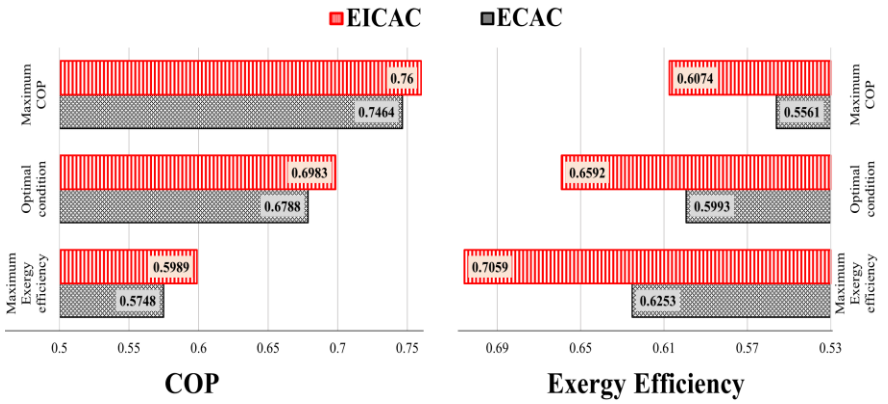
	Optimal Condition	-20.05	25	58.4	
	Max Exergy Efficiency	-35	25	55.6	

35	Maximum COP	-10	25	67.5
	Optimal Condition	-19.95	25	64
	Max Exergy Efficiency	-35	25	62.3

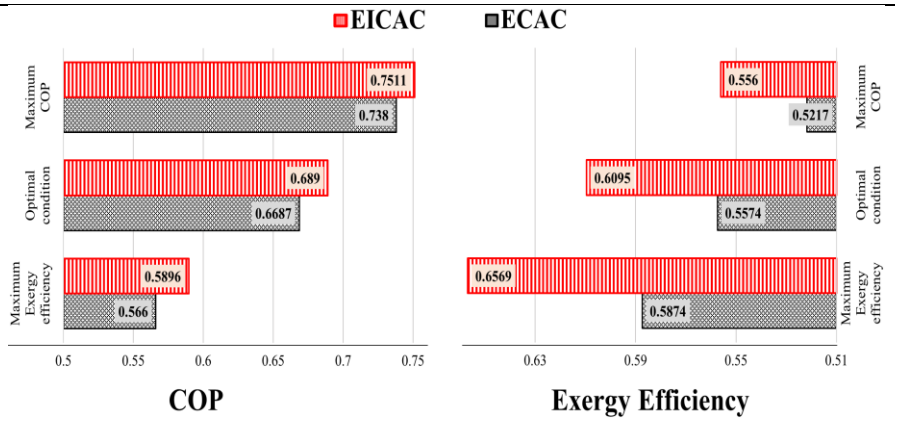

6.1.5 Section Summery

This research section addresses the limitations of traditional cascade absorption technology by integrating a modified Absorption Refrigeration Cycle (ARC) with an enhanced Vapor Compression Refrigeration (VCR) system equipped with ejector setup, aiming to thoroughly investigate the performance of the proposed systems. The analysis within this section demonstrates the superior energy and exergy performance achieved at lower cooling temperatures by these innovative systems.

To fulfill and implement the first objective of the study, a modified Absorption Refrigeration Cycle (ARC) is combined with an improved Vapor Compression Refrigeration (VCR) system, leading to the development of advanced systems like ECAC and EICAC. Following the verification of the thermodynamic model, a comparative thermal analysis of the proposed ECAC and EICAC systems versus the conventional CARC system is conducted along with corresponding parametric sensitivity analysis, utilizing various performance metrics for assessment. The research further delves into the effects of ejector parameters to pinpoint the optimal operating conditions that enhance performance, while also considering the impact of each component. Conclusively, multi-objective optimization is employed to identify the optimal solutions from both the 1st and 2nd law thermodynamics perspectives, thereby determining the feasible operational boundary conditions. The conclusion of the comprehensive theoretical thermodynamic analysis presented in this section as follows:

- The results indicate that both ECAC and EICAC systems can achieve near 15% and 6% higher *COP*, respectively, compared to the traditional system when exploiting the R41-LiBr/H2O refrigerant pair under different working conditions.

- The peak exergetic performance can be accomplished at approximately 77℃, with the EICAC and ECAC demonstrating an exergy efficiency increase of around 20% and 10%, respectively, in comparison with CARC system. While the system's energy performance may exhibit only minimal changes beyond the optimal value, the exergetic perspective reveals a significant decrease in exergy efficiency once the optimum condition has been reached. At temperatures below 73℃, the rate of decrease is notably steep, leading to a constraining operational state. This suggests that generator temperature has a more significant impact on exergetic efficiency than on *COP*.

- Although system *COP* of all systems increases linearly with increasing T_{evp} at a near similar rate, the exergy efficiency decreases at different rates. Hence, from an exergetic perspective, the absorption cycle demonstrates greater effectiveness in low-temperature applications. The EICAC system exhibits a lower total exergy destruction rate than the ECAC system, leading to a near 9% improved exergy efficiency.

- The study further identifies that the optimal generator temperature increases with $T_{cond.}$ Also, this optimum value varies 5-6℃ from energy and exergy perspective, whereas the optimal performance is gained at an evaporator temperature of -21℃.

6.2 Analysis of RAC Based Proposed Advanced Cascaded Compression Absorption Systems

This section advances the study of compression absorption technology by incorporating sophisticated and advanced systems to address the challenges inherent in conventional systems, thereby proposing more viable solutions. Specifically, it introduces and analyzes the integration of an advanced Recompression Absorption System (RAC) with an enhanced Vapor Compression Refrigeration (VCR) systems incorporated with an ejector. This leads to the development of advanced proposed cycles: the **Ejector-Compression Recompression Absorption Cycle (E-CRAC)** and the **Ejector-enhanced vapor-Injection Compression Recompression Absorption Cycle (EI-CRAC)**. In this advanced systems, the RAC working in the HTC enables the system to utilize the released heat from the condenser to warm the solution in the generator, thus lessening the required generator load and increasing system performance by removing the need for bulky condenser. Moreover, this configuration allows for a reduced generator pressure in comparison to the conventional ARC, facilitating operation at a lower generator temperature [60]. Thus, increasing its prospect in industrial applicability. Additionally, the advanced ejector-based VCRs in LTC of the proposed system also enable the extraction of heat from the refrigerated space more efficiently, thus assisting these proposed system to be more industry compatible. These integrations aim to overcome the limitations of existing technologies by offering improved efficiency and performance, highlighting the potential for significant advancements in the field of refrigeration and air conditioning technologies.

A detailed comparative and parametric analysis have been carried out for varying controllable operating conditions in order to gain insight about the effect of each parameter and performance enhancement of the proposed systems over conventional systems. Output parameters selected for system performance analysis are: 1st law efficiency (COP), 2nd law efficiency (Ex_{eff}), exergy destruction rate of system and across each component and overall exergy destruction ($\dot{E}x_D, \dot{E}x_{D,tot}$), HTC and LTC compressor load ($\dot{W}_{comp}$). In this section, an extensive analysis from multiple viewpoints has been carried out to ensure a comprehensive and thorough understanding. Finally, ANN model is trained with the extracted data to integrate with Genetic algorithm to carry out multi-objective optimization and determine the optimal conditions of operation to ascertain the operational feasibility and limitations to pave the way for further research and innovation.

Design parameters and range of operation are provided in **Table 6-8.**

Table 6-8*. Design parameters for the analysis of RAC based conventional and proposed cascaded compression absorption systems.*

Parameters	Values
Cooling load, Q_{evp}	150 KW
Generator temperature, T_{gen}	45 ℃ to 65 ℃
Evaporator temperature, T_{evp}	-30 ℃ to -5 ℃
Condenser Pressure, P_{cond}	15 kPa to 30 kPa
Absorber temperature, T_{abs}	25 ℃ to 30 ℃
Effectiveness of RHX, $\boldsymbol{\varepsilon_{RHX}}$	0.9
Effectiveness of SHX, $\boldsymbol{\varepsilon_{SHX}}$	0.9
Cascade temperature difference, ΔT	5
Ambient temperature, T_0	25 ℃
Ambient pressure, P_0	101.325 kPa
Compressor efficiency, $\boldsymbol{\eta_s}$	150 KW
Inlet external air temperature in Evaporator	T_{evp} + 8
Outlet external air temperature in Evaporator	T_{evp} + 3
Inlet cooling water temperature in Absorber	T_{abs} - 5
Outlet cooling water temperature in Absorber	T_{abs} + 5
Inlet heat source water temperature in Generator	T_{gen} + 15
Outlet heat source water temperature in Generator	T_{gen} + 10

6.2.1 Comparison Between Proposed and Conventional System

In this section, the RAC based proposed cascaded compression absorption models are evaluated using a simulation conducted with an EES-developed program. LiBr/H2O and R41 are chosen as the refrigerant pair for their distinct advantages. LiBr/H2O, utilized in the High-Temperature Cycle (HTC), enhances absorber pressure and exhibits non-toxic properties, facilitating the use of low-grade industrial heat due to its lower generator activation temperature. This contributes to a higher Coefficient of Performance (COP) and exergy efficiency. The use of LiBr also simplifies the system design by eliminating volatile liquids in the absorbent-refrigerant pair, thereby negating the need for an analyzer and rectifier and enabling a more compact, cost-effective system that can easily integrate with other technologies. For the Low-Temperature Cycle (LTC), R41 is selected for its environmental benefits, including a negligible Ozone Depletion Potential (ODP) and a low Global Warming Potential (GWP of approximately 95), alongside its low boiling point of -78.2 ℃, making it an ideal choice for Low-Temperature Chillers (LTCs). As an illustration, the thermodynamic state parameters of the proposed novel cascade compression-recompression

absorption cycles are provided as an example in **Table 6-9**, **Table 6-10** and **Table 6-11** for CARC, E-CRAC and EI-CRAC configuration respectively.

***Table 6-9**. Thermodynamic property of each flow stream of CRAC system at T_{gen} = 60℃, T_{evp} = -20℃, T_{abs} = 35℃, Pr = 7.13(P_{cond} = 25 kPa) and ΔT_{CHX} = 5℃.*

State Point	P (kPa)	T (℃)	s (kJ kg^{-1} K^{-1})	h (kJ kg^{-1})	$\dot{m}$ (kg s^{-1})	x (%)
1	3.49	60	8.721	2612	0.08101	-
2	24.88	287.6	8.817	3051	0.08101	-
3	24.88	65	0.8918	271.5	0.08101	-
4	1.216	10	0.9619	271.5	0.08101	-
5	1.216	10	8.903	2519	0.08101	-
6	1.216	35	0.2301	75.84	1.436	0.5221
7	3.49	35	0.2301	75.84	1.436	0.5221
8	3.49	56.2	0.3716	119	1.436	0.5221
9	3.49	60	0.369	136	1.355	0.5533
10	3.49	37.5	0.2264	90.22	1.355	0.5533
11	1.216	37.5	0.2264	90.22	1.355	0.5533
12	1133	-20	2.341	536.4	0.5075	-
13	3009	50.8	2.371	599.6	0.5075	-
14	3009	15	1.14	240.8	0.5075	-
15	1133	-20	1.173	240.8	0.5075	-

***Table 6-10**. Thermodynamic property of each flow stream of E-CRAC cycle at T_{gen} = 60℃, T_{evp} = -20℃, T_{abs} = 35℃, Pr = 7.13(P_{cond} = 25 kPa) and ΔT_{CHX} = 5℃.*

State Point	P (kPa)	T (℃)	s (kJ kg^{-1} K^{-1})	h (kJ kg^{-1})	m (kg s^{-1})	x (%)
1	3.488	60	8.722	2612	0.07304	-
2	24.88	287.7	8.818	3052	0.07304	-
3	24.88	65	0.8918	271.5	0.07304	-
4	1.216	10	0.2304	64.47	0.07304	-
5	1.216	10	8.903	2519	0.07304	-
6	1.216	35	0.2301	75.84	1.292	0.5221
7	3.488	35	0.2301	75.84	1.292	0.5221
8	3.488	56.2	0.3716	119	1.292	0.5221
9	3.488	60	0.369	136	1.219	0.5534
10	3.488	37.5	0.2264	90.24	1.219	0.5534
11	1.216	37.5	0.2264	90.24	1.219	0.5534
12	1.216	54	9.521	2726	0.07304	-
13	3009	47.2	2.351	593.4	0.5086	-
14	3009	15	1.14	240.8	0.5086	-
15	1103	-20.8	1.145	233.4	0.5086	-

16	1103	-20.8	1.672	366.4	0.9042	-
17	1235	-17.3	1.674	370.2	0.9042	-
18	1235	-17.3	0.8422	157.3	0.3957	-
19	1133	-20	0.8429	157.3	0.3957	-
20	1133	-20	2.341	536.4	0.3957	-
21	1235	-17.3	2.325	536.5	0.5086	-
22	1103	-20.8	2.342	535.3	0.3957	-
30	24.88	15.5	0.2295	64.47	0.07304	-

Table 6-11*. Thermodynamic property of each flow stream of EI-CRAC cycle at T_{gen} = 60℃, T_{evp} = -20℃, T_{abs} = 35℃, Pr = 7.13(P_{cond} = 25 kPa) and ΔT_{CHX} = 5℃.*

State Point	P (kPa)	T (℃)	s (kJ kg-1 K-1)	h (kJ kg-1)	$\dot{m}$ (kg s-1)	x (%)
1	3.488	60	8.722	2612	0.07212	-
2	24.88	287.7	8.818	3052	0.07212	-
3	24.88	65	0.8918	271.5	0.07212	-
4	1.216	10	0.2304	64.47	0.07212	-
5	1.216	10	8.903	2519	0.07212	-
6	1.216	35	0.2301	75.84	1.275	0.5221
7	3.488	35	0.2301	75.84	1.275	0.5221
8	3.488	56.2	0.3716	119	1.275	0.5221
9	3.488	60	0.369	136	1.203	0.5534
10	3.488	37.5	0.2264	90.24	1.203	0.5534
11	1.216	37.5	0.2264	90.24	1.203	0.5534
12	1.216	54	9.521	2726	0.07212	-
13	3009	46.6	2.348	592.3	0.4841	-
14	2656	10	1.092	226.6	0.4841	-
15	1710	-6.1	1.092	224		-
16	1710	-6.1	1.115	230.1	0.4918	-
17	1846	-3.6	1.116	231.2	0.4918	-
18	1846	-3.6	2.241	534.3	0.05805	-
19	1846	-3.6	0.9658	190.6	0.4338	-
20	1720	-6.1	0.9665	190.6	0.4338	-
21	1720	-6.1	2.256	535	0.01142	-
22	1720	-6.1	0.943	184.3	0.426	-
23	1133	-20	0.9497	184.3	0.426	-
24	1133	-20	2.341	536.4	0.426	-
25	1846	12.3	2.351	564.9	0.426	-
26	1846	10.2	2.338	561.2	0.4841	-
27	1710	-6.1	2.256	534.7		-
30	24.88	15.5	0.2295	64.47	0.07212	-

Based on the properties of fluid streams, the output parameters are calculated to conduct a thorough comparison analysis between the proposed recompression cascaded compression absorption systems along with their comparison with traditional CARC and is presented in **Table 6-12**. For the same operating conditions, it has been found that, *COP* of the RAC based proposed cascaded systems is nearly three times higher than the conventional CARC system. Among the proposed systems, EI-CRC and E-CRAC show near 10% and 20% increase of *COP* compared to basic CRAC. From exergetic point of view, the proposed basic CRAC displays deterioration of performance over conventional system whereas the other proposed systems, EI-CRAC and E-CRAC shows near 15% and 25% exergetic performance increase over CRAC.

***Table 6-12**. Comparison among the RAC based proposed cascaded systems and traditional cascaded system at T_{gen} = 60℃, T_{evp} = -20℃, T_{abs} = T_{cond} = 35℃, Pr = 7.13(P_{cond} = 25 kPa) and ΔT_{CHX} = 5℃.*

Components	Traditional Cycle	Proposed Cycles		
	CARC	**CRAC**	**ECRAC**	**EICRAC**
Generator, $\dot{Q}_{gen}$ **(kW)**	215.6	225	202.8	200.3
Condenser, $\dot{Q}_{cond}$ **(kW)**	189.8	225	202.8	200.3
Evaporator, $\dot{Q}_{evp}$ **(kW)**	150	150	150	150
Absorber, $\dot{Q}_{abs}$ **(kW)**	207.9	217.4	211.1	208.5
Compressor, $\dot{W}_{comp}$ **(kW)**	32.07	67.63	61.02	56.14
Exergy destruction, $\dot{E}x_{D,total}$ **(kW)**	36.04	40.95	34.02	29.3
Coefficient of performance, ***COP***	0.6056	2.218	2.458	2.672
Exergetic efficiency, η_{II}	0.421	0.3945	0.4373	0.4752

6.2.2 Thermodynamic Parametric Sensitivity & Performance Analysis

Impact of Fluid Expansion and Pressure Drop Across Ejector Nozzles

The functioning and efficiency of the proposed ejector-equipped advanced RAC based cascaded compression absorption systems are dictated by the expansion of refrigerants after its acceleration via the motive and suction nozzle. The outcome exhibits a significant pressure drop (ΔP) of the corresponding streams. For a set of operational parameters, an optimal value of ΔP is present for COP maximization, which can be calculated through continuous iterations.

The influence of ΔP on the *COP* of the RAC based cascaded compression absorption systems is illustrated in **Figure 6-20**. In the case of the E-CRAC system, an increase in ΔP up to an optimum

value of around 35 kPa leads to a rise in *COP*. However, any further increase in pressure drop gradually reduces the *COP*. For the EI-CRAC system, the *COP*'s incremental rise is less steep with the increase in ΔP, with the optimal *COP* value observed near 80 kPa. Beyond this point, additional increases in pressure drop have a negligible effect on *COP*. Additionally, for the E-CRAC system, the *COP* experiences a change on a scale of roughly 0.02. In contrast, the EI-CRAC system's *COP* changes on a scale of 0.004, fivefold less than the E-CRAC system. The E-CRAC system shows a more pronounced impact of pressure drop, with a *COP* change of 0.0005 per kPa increase of ΔP before it reaches its peak. Thus, it is deduced that the EI-CRAC system is minimally affected by ΔP.

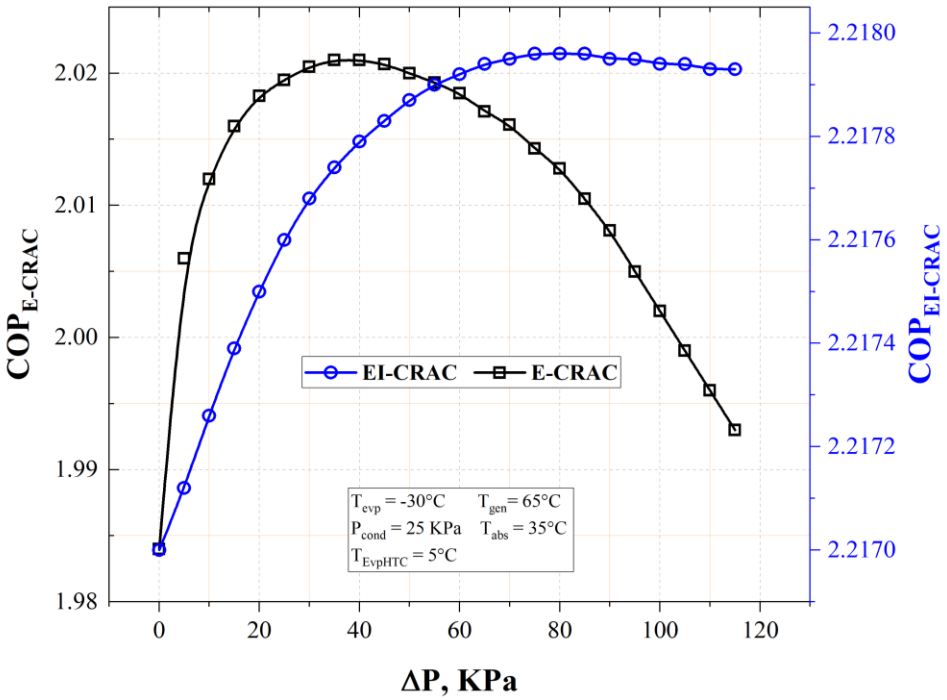

***Figure 6-20**: Influence of ΔP on 1st law efficiency of the RAC based proposed cascaded compression absorption systems at P_{cond} = 25kPa, T_{abs} = 35 ℃, T_{evp} = -30 ℃, T_{gen} = 65 ℃.*

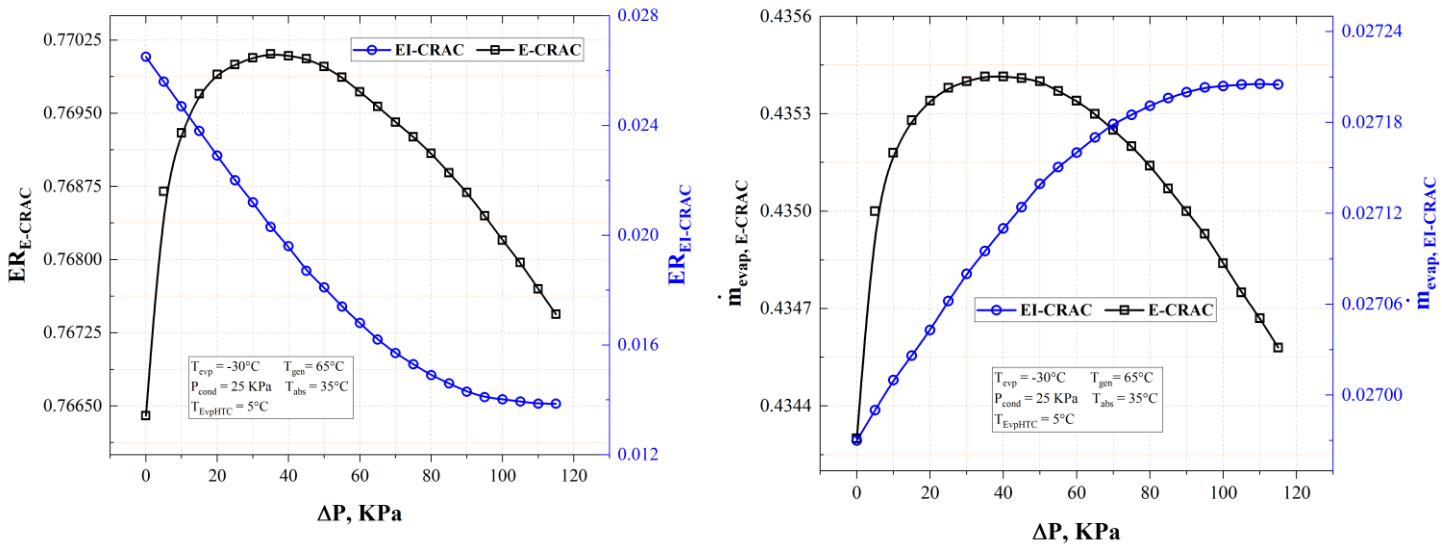

(a) **(b)**

Figure 6-21*: Influence of ΔP on (a) Entrainment ratio (ER) and (b) $m_{evaporator}$ of the RAC based proposed cascaded compression absorption systems at P_{cond} = 25kPa, T_{abs} = 35 ℃, T_{evp} = -30 ℃, T_{gen} = 65 ℃.*

Figure 6-21 effectively illustrates the relationship between the Entrainment Ratio (ER) and variations in pressure drop, highlighting its direct influence on the *COP* of the RAC based proposed cascaded compression absorption systems. In the case of the E-CRAC system, as the pressure drop increases, the *ER* follows a similar upward trend. This increase in *ER* results in a rise in the $\dot{m}_{suction}$. From the refrigerant flow, $\dot{m}_{suction} = \dot{m}_{20} = \dot{m}_{evp} = \dot{m}_{19}$. So, increase of $\dot{m}_{suction}$, subsequently leads to a larger cooling capacity and an enhanced *COP*. The interrelation among *COP*, *ER*, and $\dot{m}_{evp}$ is linear, which explains the similar pattern they exhibit with an increasing Δ*P*. On the other hand, the EI-CRAC system behaves differently. As Δ*P* increases in this system, the *ER* decreases until it reaches a minimum value. This reduction results in a decrease of $\dot{m}_{suction} = \dot{m}_{21}$. However, this decrease leads to an increase of $\dot{m}_{evp} = \dot{m}_{23}$ (as $\dot{m}_{suction} = \frac{1-x_{20}}{x_{20}} m_{evap}$). So $\dot{m}_{suction}$ and $\dot{m}_{evp}$ are inversely related. The increase in $\dot{m}_{evp}$ results in an enhanced cooling load and, leading to an improved *COP*. Therefore, both COP and $\dot{m}_{evp}$, inversely proportional to the *ER*, exhibit similar patterns of increase with a rising Δ*P*, while the *ER* displays a reverse trend.

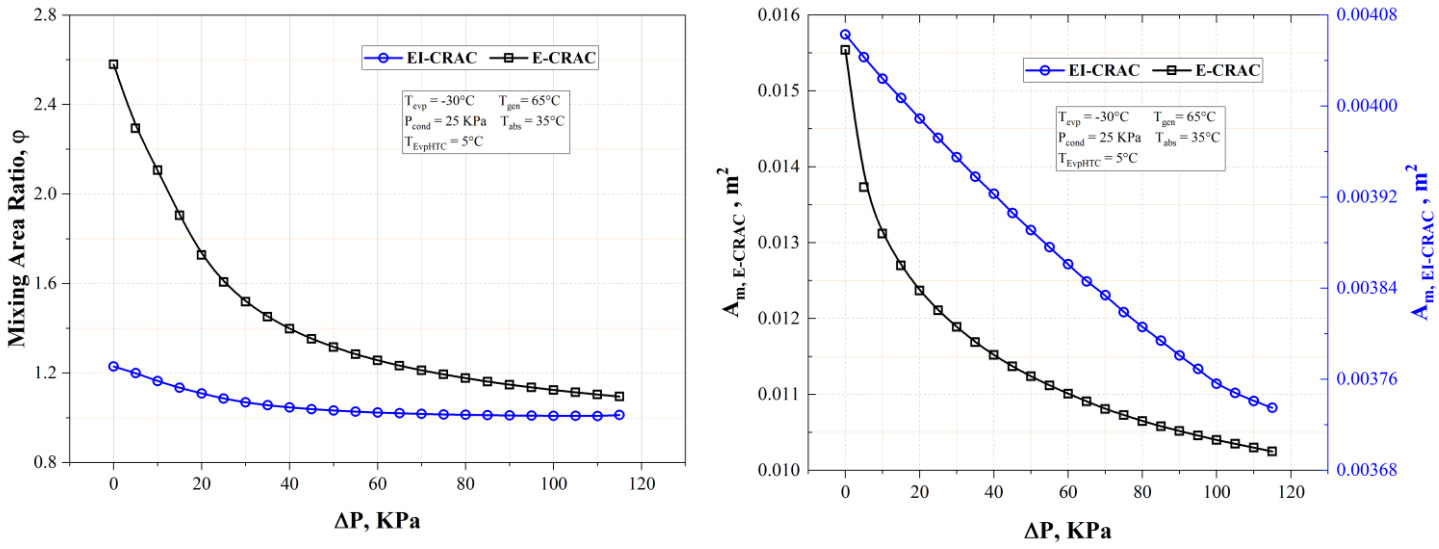

(a) **(b)**

***Figure 6-22**: Influence of ΔP on (a) Mixing area ratio (φ) and (b) Area of constant area section of ejector's mixing chamber of RAC based proposed cascaded systems at P_{cond} = 25kPa, T_{abs} = 35 ℃, T_{evp} = -30 ℃, T_{gen} = 65 ℃.*

The area ratio of the mixing section, represented by the symbol φ, plays a vital role in determining the design and size of an ejector of the RAC based proposed cascaded compression absorption systems. This ratio is directly related to the pressure drop (Δp) across the nozzle. **Figure 6-22** clearly illustrates this effect. As seen from **Figure 6-22(a)**, with Δp increasing, ejector area ratio φ of both systems experiences a decline. Consequently, the constant area of mixing, denoted as A_m, also decreases, as observed in **Figure 6-22 (b)**. Notably, the ejector used in the E-CRAC system demonstrates a higher value of φ, leading to a larger A_m compared to EI-CRAC system's ejector. E-CRAC also shows a more pronounced decrease in φ and A_m, as the pressure drop Δp increases. Initially, as Δp increases, φ decreases rapidly, but this rate of decrease slows down with further increase in Δp. In contrast, the ejector system used in the LTC of EI-CRAC demonstrates a lower φ value. With an increase in Δp, φ approaches close to 1, indicating the use of a Constant Area Mixing (CAM) type ejector. Consequently, the mixing area A_m of this configuration's ejector is also near 4 times lower compared to E-CRAC's and this area decreases almost linearly with changes in Δp.

Effect of Ejector Integration on LTC Performance

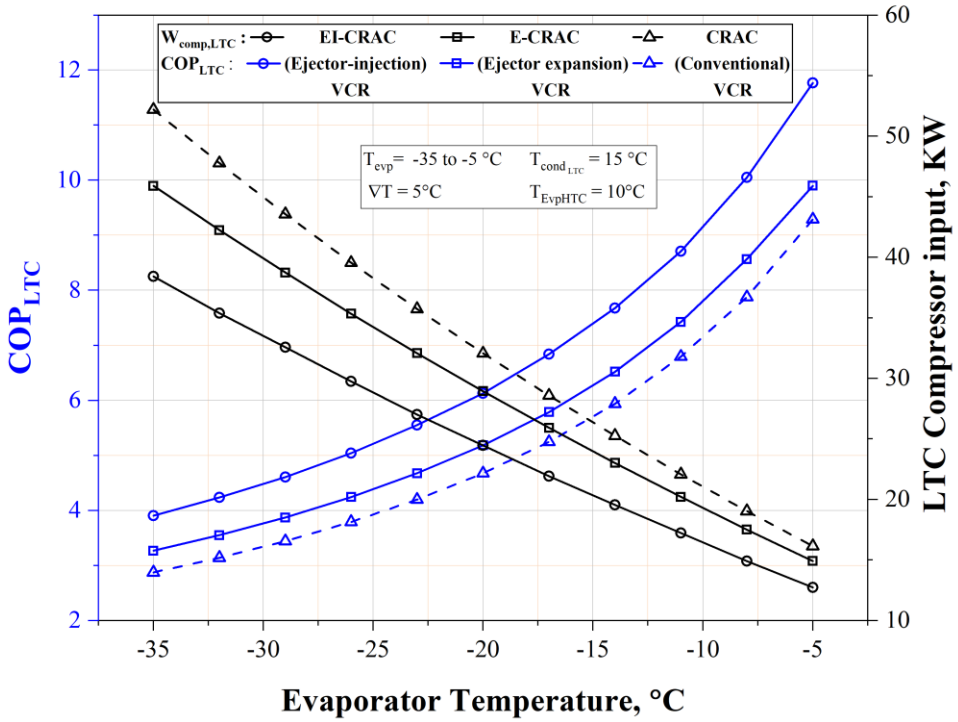

***Figure 6-23**: Influence of ejector on performance improvement of LTC-VCR of the RAC based proposed cascaded systems.*

Figure 6-23 highlights the advantages of incorporating an ejector in the LTC system, particularly in enhancing the COP and reducing the compressor's workload of the RAC based cascaded compression absorption systems. At an evaporator temperature of -20 ℃, the incorporation of ejector significantly reduces the LTC compressor's load requirement from 32 KW (for VCR) to 28 KW (Ejector expansion LTC employed in E-CRAC) and 24 KW (ejector injection LTC employed in EI-CRAC). It's also observed that as the evaporator temperature increases, the impact of the ejector on enhancing pressure lift lessens. This results in a narrowing gap in the load requirements between the systems. Consequently, the COP improvement offered by the ejector expansion and injection systems compared to traditional VCR systems reduces from 7% and 33% to 6% and 28%, respectively, as the evaporator temperature increases from -35°C to -5°C.

Impact of Operating Conditions on System Performance

The investigation into the performance of the proposed Recompression Absorption Cycle (RAC) based cascaded compression-absorption systems has been conducted with a thorough parametric sensitivity analysis. This analysis examines the impact of various operating conditions on system performance. The investigation identifies a suitable range of operating conditions and delineates the different limiting conditions for operation, providing a comprehensive understanding of the system's behavior under diverse scenarios.

Effect of Generator- Condenser Temperature

As illustrated in **Figure 6-24**, both the proposed models exhibit a similar trend with changing operational parameters. However, it is worth noting that the EI-CRAC model demonstrates around 10% higher *COP* compared to the E-CRAC model. The increase in P_{cond} is observed to have a negative impact on the system *COP*, resulting in a decrease. But the decremental rate increases with T_{gen} increasing. Furthermore, as T_{gen} increases, the *COP* initially increases until it reaches an optimal point, after which it decreases at a faster rate with further increases in T_{gen}. For a specific condenser pressure, this value of T_{gen} represents the optimal condition for maximizing system performance. Additionally, it has been found, as P_{cond} increases, the heat rejected in the gen-cond decreases, leading to a decrease in the pressure ratio and an increase in generator pressure (P_{gen}).

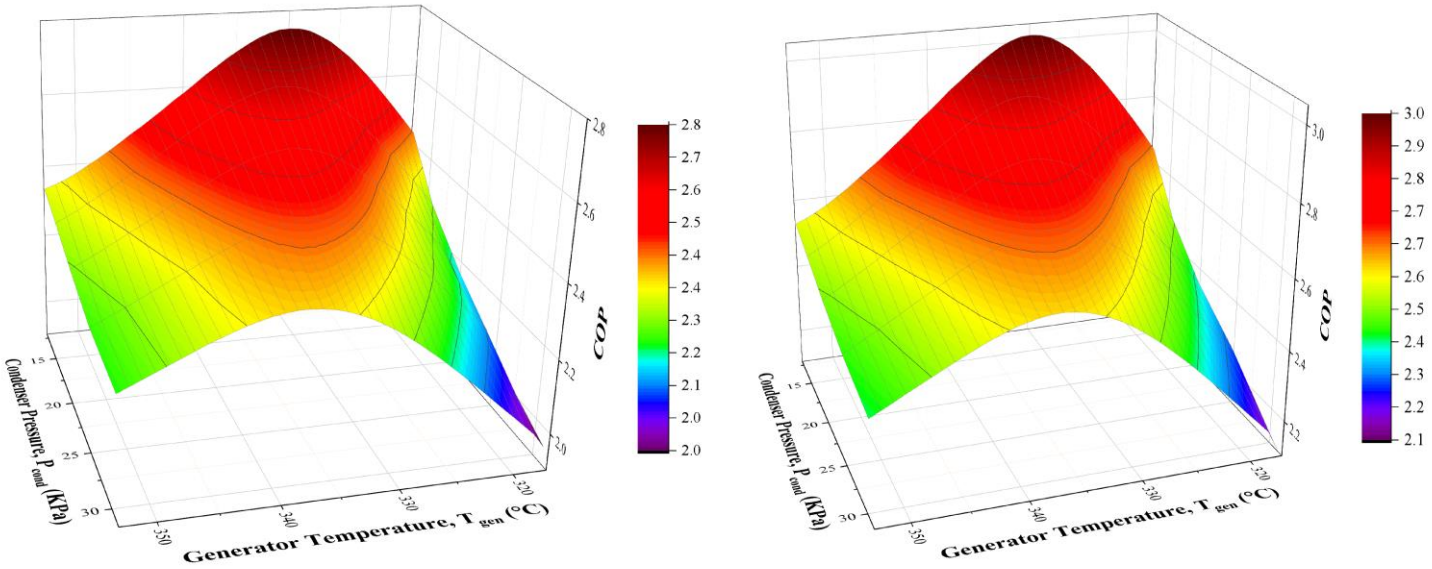

(a) E-CRAC ***(b)EI-CRAC***

Figure 6-24*: The influence of T_{gen} and P_{cond} on 1st law efficiency of the RAC based proposed cascaded systems at at T_{abs} = 35 ℃, T_{evp} = -20 ℃, T_{evpHTC} = 10 ℃.*

Figure 6-25 illustrates the consequences of T_{gen} and P_{cond} on exergy efficiency (Ex_{eff}) of the RAC based proposed cascaded compression absorption systems. The effect mirrors the same trend as *COP*, but with a notable difference: as P_{cond} increases, Ex_{eff} decreases at a more accelerated rate. Moreover, the optimal T_{gen} value, which corresponds to the peak Ex_{eff}, also increases at a higher rate compared to the rate observed for *COP* in **Figure 6-24**. For the same range of operating conditions, the difference between the maximum and minimum value of *COP* is 32% whereas, for Ex_{eff} the difference is nearly 42%. Therefore, it can be inferred that T_{gen} and P_{cond} have a more pronounced effect on Ex_{eff}.

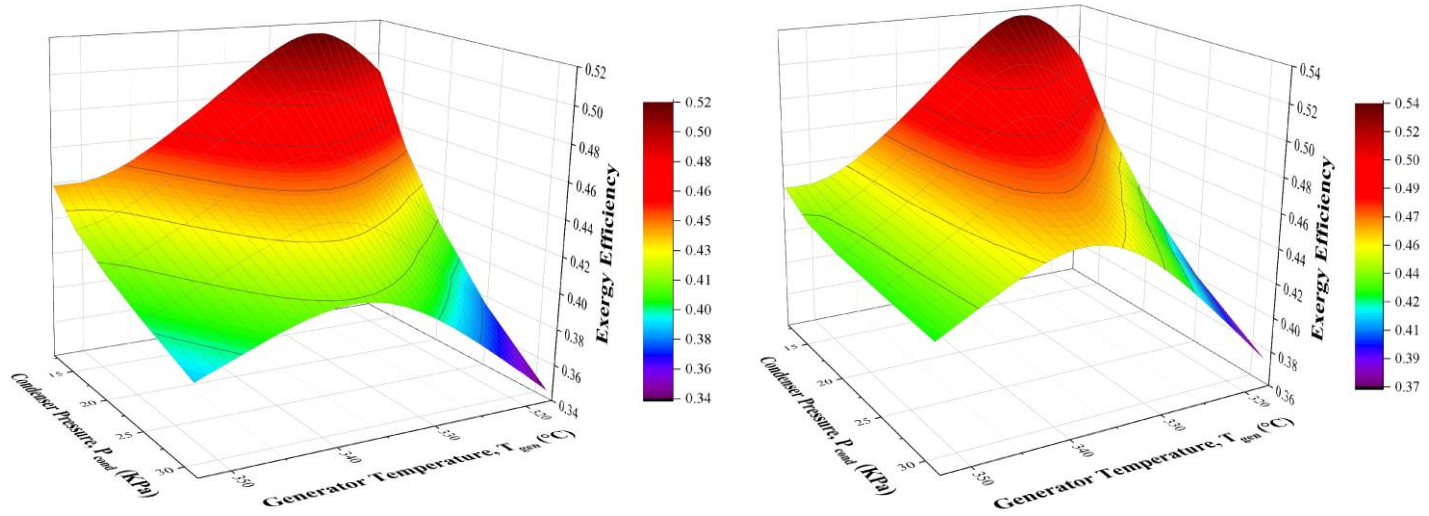

(a) E-CRAC *(b)EI-CRAC*

***Figure 6-25**: The influence of T_{gen} and P_{cond} on 2nd law efficiency of the RAC based proposed cascaded systems at at T_{abs} = 35 ℃, T_{evp} = -20 ℃, T_{evpHTC} = 10 ℃.*

Impact of Generator temperature

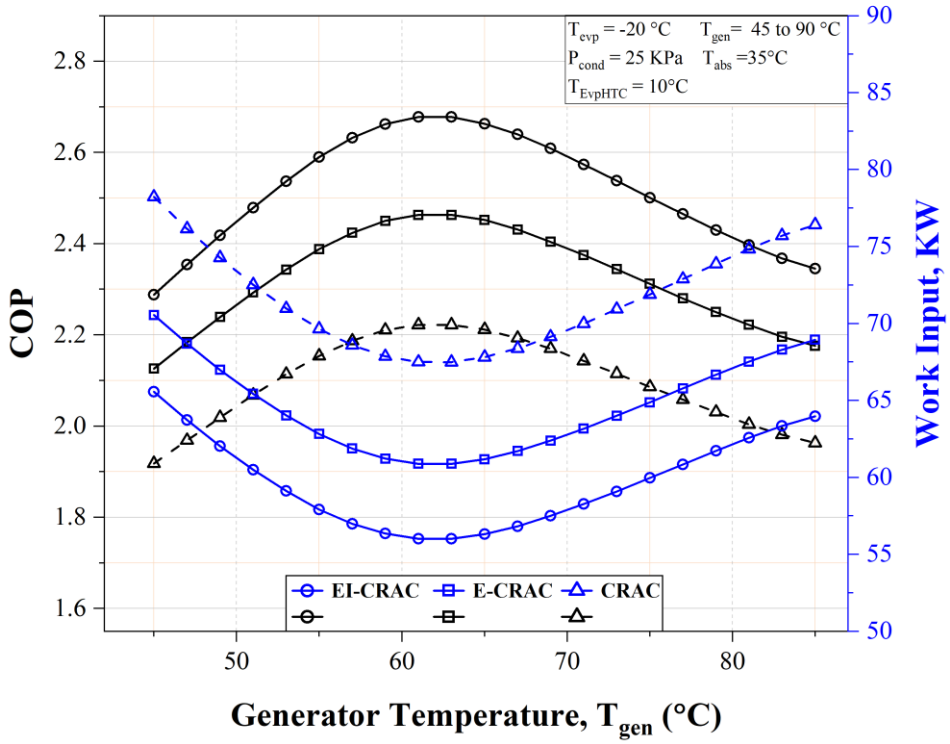

***Figure 6-26**: Impact of T_{gen} on COP and Total input power of the RAC based cascaded compression absorption systems P_{cond} = 25kPa, T_{abs} = 35 ℃, T_{evp} = -20 ℃.*

Figure 6-26 shows the influence of T_{gen} on system performance of the RAC based proposed cascaded compression absorption systems from the 1st law perspective. For a specific condenser pressure, an optimal value of T_{gen} exists where the required heat in the generator is minimum. Since the vapor compressor increase the enthalpy of the stream to provide this required heat, the optimal T_{gen} corresponds to lowest pressure ratio P_r, hence lowest power consumption of the system. As, cooling effect is kept constant, this lowest $\dot{W}_{comp\text{-}HTC}$ results in Maximum *COP*. All the systems follow the same trend for a specific P_{cond}. However, ejector expansion LTC enables E-CRAC to operate at lower electricity consumption than VCR. In EI-CRAC due to dual stage compression, the required power consumption is lesser which also results in lower $\dot{Q}_{CHX}$ and lower $\dot{Q}_{gen}$. Hence EI-CRAC shows an improved *COP* of near 20% over conventional compression recompression cycle, whereas E-CRAC shows enhancement of near 9% throughout the varying T_{gen}.

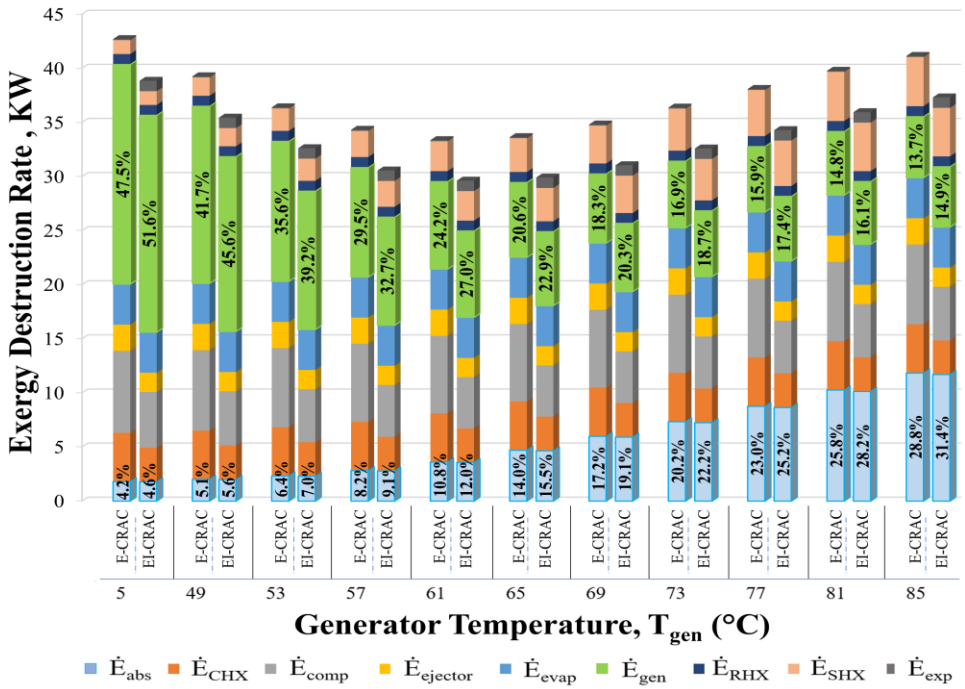

***Figure 6-27**: Impact of T_{gen} on total exergy destruction of the of the RAC based proposed cascaded systems at P_{cond} = 25 kPa, T_{abs} = 35 ℃, T_{evp} = -20 ℃, T_{evpHTC} = 10 ℃.*

The impact of T_{gen} from exergetic perspective is shown in **Figure 6-27**. As T_{gen} increases, the exergy destruction rate in most components increases in near linear ratio, apart from the generator and absorber. With an increase in T_{gen}, more useful energy becomes available for use in the generator, leading to a decrease in exergy destruction rate across the generator, $\dot{E}x_{D,gen}$. However, a higher T_{gen} results in an increased concentration of the strong solution (x_{ss}). Given that the concentration of the weak solution remains constant for a fixed absorber temperature (T_{abs}), an increase in x_{ss} leads to a higher rate of exergy release and destruction rate, $\dot{E}x_{D,abs}$. But at lower T_{gen}, the decrement rate of $\dot{E}x_{D,gen}$ dominates over the increment rate of $\dot{E}x_{D,abs}$, hence total exergy destruction rate decrease. However, this trend reverses at higher T_{gen}, indicating the existence of an optimal temperature where the system experiences minimal total exergy destruction rate and, consequently, maximum exergy efficiency. The EI-CRAC system, requiring less heat in the generator, also results in lower exergy destruction compared to the E-CRAC system. Furthermore, the use of a double compressor in the low-temperature circuit (LTC) allows the system to operate with reduced energy consumption. As a result, the EI-CRAC system exhibits approximately 23% higher exergy efficiency than the conventional CRAC system, while the E-CRAC system shows a near 15% improvement.

Impact of Evaporator Temperature

Figure 6-28 demonstrates the effect of T_{evp} on 1st law efficiency of the RAC based proposed cascaded compression absorption systems. As T_{evp} increases, for the same cooling load, corresponding mass flow rate decreases as $\dot{m}_{evp} = \dot{Q}_{evp}/\Delta h$. Additionally, pressure ratio decreases due to increase of T_{evp}, as a result *COP* increases near linearly. Due to lower power consumption, for varying T_{evp}, EI-CRAC maintains 17% and 9% performance enhancement over CRAC and E-CRAC respectively.

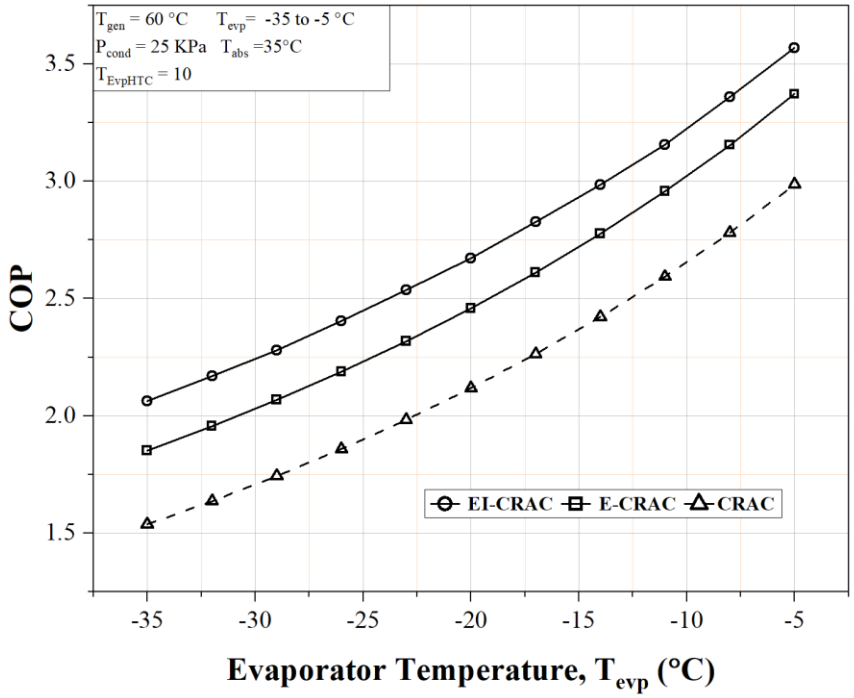

***Figure 6-28**: Impact of T_{evp} on COP of the RAC based proposed cascaded compression absorption systems at P_{cond} = 25kPa, T_{abs} = 35 °C, T_{gen} = 60 °C.*

This effect on COP can be further illustrated in **Figure 6-29** which shows how T_{evp} affects ejector entrainment ratio, *ER* of the RAC based proposed cascaded compression absorption systems. The E-CRAC system not only demonstrates a higher ER in comparison to the EI-CRAC system, but it is also more sensitive to changes in parameters. For EI-CRAC, with the increase of T_{evp}, the mass flow in evaporator increases, resulting in lower $m_{suction}$. As a result, ER decreases. Whereas, for E-CRAC the reverse behavior can be seen. With the increase of T_{evp}, the mass flow in evaporator increases. But, in this configuration $m_{suction}$ = m_{evp}. So, $m_{suction}$ also increases, consequently increasing the value of *ER*. Notably, when T_{evp} is raised from -35°C to -5°C, the ER for the ejector in the E-CRAC system increases by 0.13, while in the EI-CRAC system, it experiences a marginal

decrease of 0.015. **Figure 6-29** also presents how different ejector systems respond in terms of their pressure lift ratio, R_p, a key measure of sensitivity. The ejector employed in the EI-CRAC system achieves a higher-pressure lift owing to its vapor injection technique, resulting in a superior COP compared to the E-CRAC system. Furthermore, an increase in evaporator temperature results in a reduced pressure ratio, leading to a corresponding decrease in the ejector lift ratio. However, this rate of decrease is more pronounced in the EI-CRAC system than in the E-CRAC system.

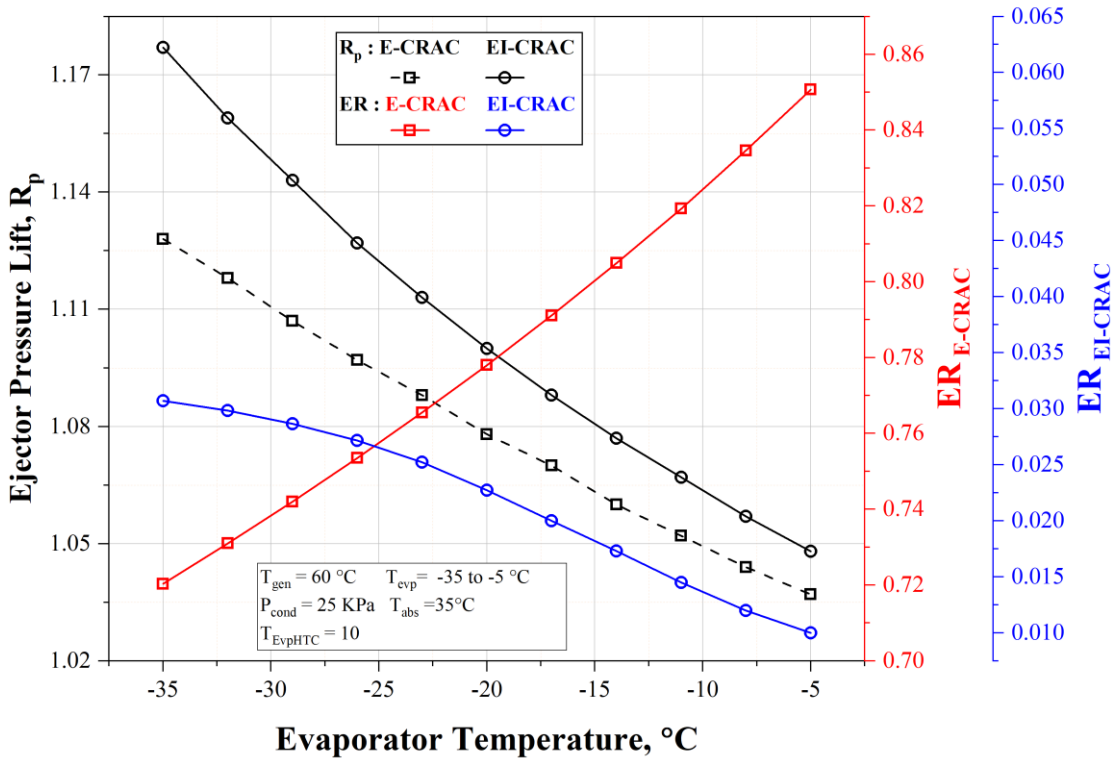

***Figure 6-29**: Impact of T_{evp} on ejector pressure lift ratio and entrainment ratio of the RAC based proposed cascaded compression absorption systems at P_{cond} = 25kPa, T_{abs} = 35 ℃, T_{gen} = 60 ℃.*

.

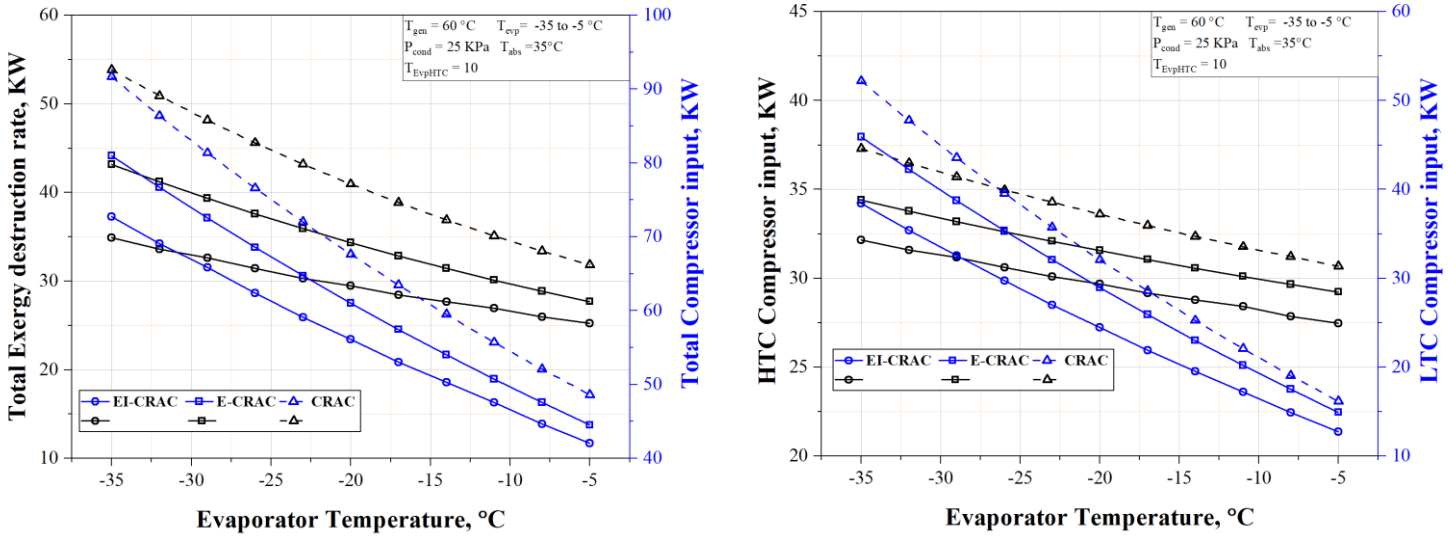

***Figure 6-30**: Impact of T_{evp} on total exergy destruction and input appended exergy rate of the RAC based proposed cascaded compression absorption systems at P_{cond} = 25kPa, T_{abs} = 35 ℃, T_{gen} = 60 ℃.*

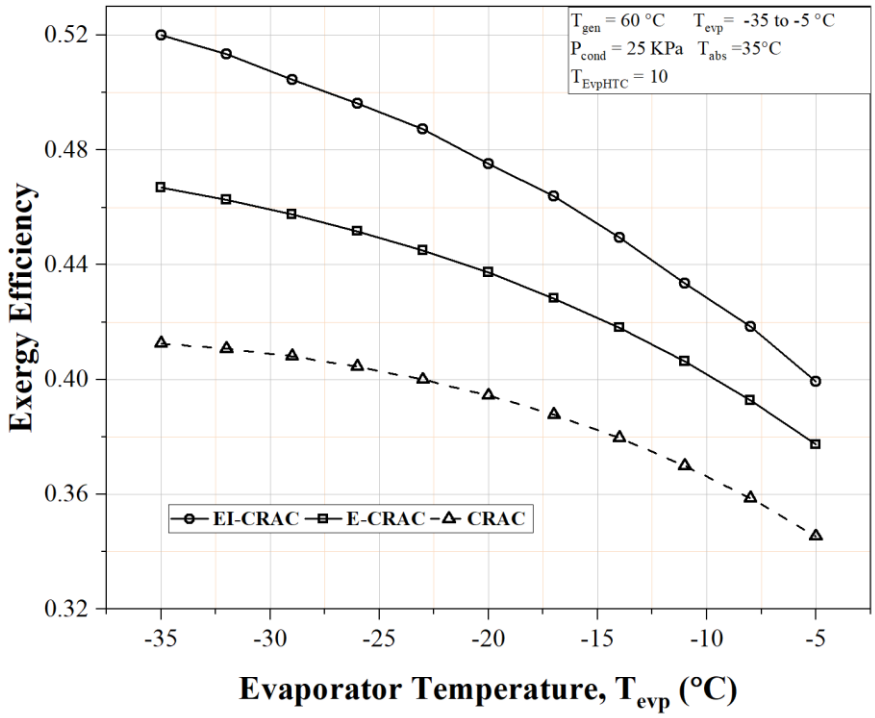

***Figure 6-31**: Impact of T_{evp} on 2nd law efficiency of the RAC based proposed cascaded compression absorption systems at P_{cond} = 25kPa, T_{abs} = 35 ℃, T_{gen} = 60 ℃.*

.

Contrary to the patterns previously discussed, the exergetic efficiency declines as T_{evp} rises, as depicted in **Figure 6-31**. However, instead of increasing, the total $\dot{E}x_{D,total}$ actually decreases as T_{evp} rises, as seen in **Figure 6-30(a)**. As T_{evp} increases, the refrigerant's ability to absorb heat for vaporization lessens, thereby reducing the system's heat extraction capacity. Consequently, the rate of $\dot{E}x_D$ within each component, as well as the overall rate of exergy destruction, decreases with the rise in T_{evp}. The evaporator's decreased ability to absorb heat leads to a reduction in $\dot{Q}_{CHX}$, which subsequently results in a lesser heat demand in the generator and therefore a lower power consumption in the HTC compressor. As illustrated in **Figure 6-30 (b)**, the exergy input to the comp-HTC decreases almost linearly as T_{evp} rises. However, the exergy input required for the comp-LTC reduces at a faster rate because of a significant reduction in the pressure ratio in the LTC. As a result, the total rate of exergy input decreases more rapidly than $\dot{E}x_{D,total}$. This ultimately leads to a decrease in exergy efficiency, as expressed in the following equation:

$$Ex_{eff} = \frac{\dot{\mathrm{E}}\mathrm{x}_p}{\dot{\mathrm{E}}\mathrm{x}_f} = 1 - \frac{\dot{\mathrm{E}}\mathrm{x}_D}{\dot{\mathrm{E}}\mathrm{x}_f}$$

This occurrence is depicted in **Figure 6-31**, where the exergy efficiency decreases as the evaporation temperature rises, despite a decrease in total exergy destruction. However, it's important to note that the rate of decrease is not uniform across all systems. At an evaporation temperature (T_{evp}) of -35℃, both EI-CRAC and E-CRAC demonstrate an improvement in Ex_{eff} of approximately 23% and 11% each in order, compared to the basic CRAC. However, when the evaporator temperature rises to T_{evp}= -5 ℃, this increase diminishes to 12.5% and 7% respectively. This phenomenon can be attributed to the high-pressure ratio across the LTC at lower T_{evp} values, which results in significant disparities in $\dot{E}x_{input}$, $\dot{E}x_{D,total}$, and exergy efficiency among the systems being compared. Nevertheless, at an increased T_{evp} values the impact becomes negligible due to a reduced pressure ratio, leading to nearly identical performance across the systems. Therefore, the analysis reveals that while 1st law efficiency of increases linearly at a nearly identical rate with rising T_{evp}, the 2nd law efficiency declines at a varying rate for all the systems.

Impact of Condenser Pressure

The influence of condenser pressure on system performance of the RAC based proposed cascaded compression absorption systems is illustrated in **Figure 6-32**. At 5 kPa, the EI-CRAC and E-CRAC display nearly 17% and 8% improvement over CRAC. This ratio of improvement increases slightly up to a certain P_{cond}, after system *COP* decreases at a significant rate. With P_{cond} increasing, the rate of latent heat of condensation of the refrigerant decreases. But the required generator load is fixed with a certain generator temperature. As a result, to account for the extra condensation, the refrigerant needs to be compressed to a higher temperature. As a result, required $\dot{W}_{comp}$ increases and *COP* decreases rapidly. Among the systems, EI-CRAC displays a slightly lower decremental rate of *COP* whereas for CRAC this decrement increases further for higher P_{cond}. At P_{cond} of 55 kPa, the enhancement of *COP* of EI-CRAC and E-CRAC increases to 22% and 12% over conventional CRAC system.

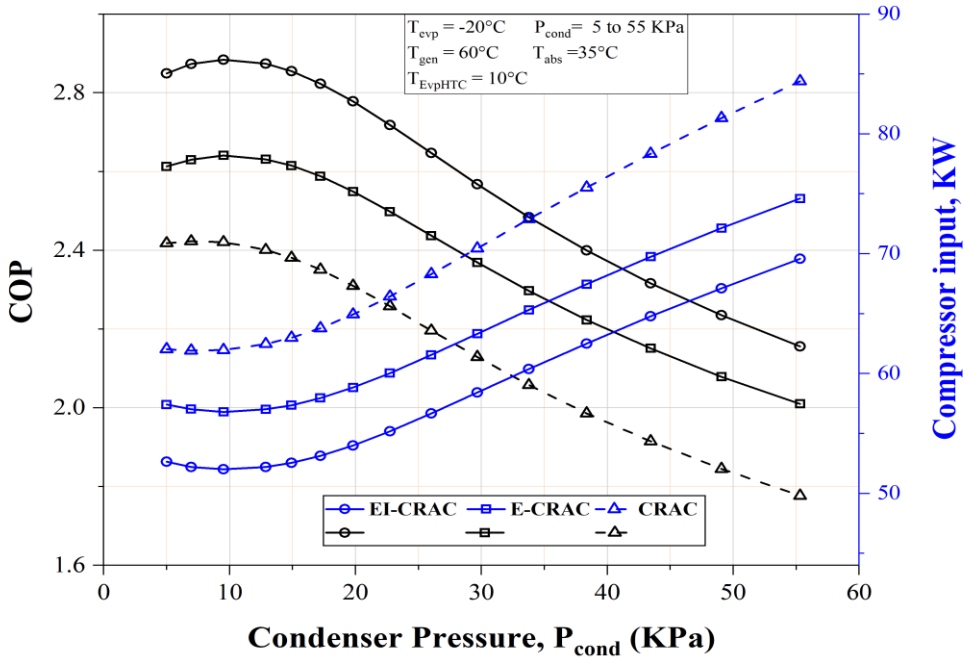

***Figure 6-32**: Impact of T_{cond} on COP and compressor load of the RAC based proposed cascaded compression absorption systems at T_{abs} = 35 ℃, T_{evp} = -20 ℃, T_{gen} = 60 ℃.*

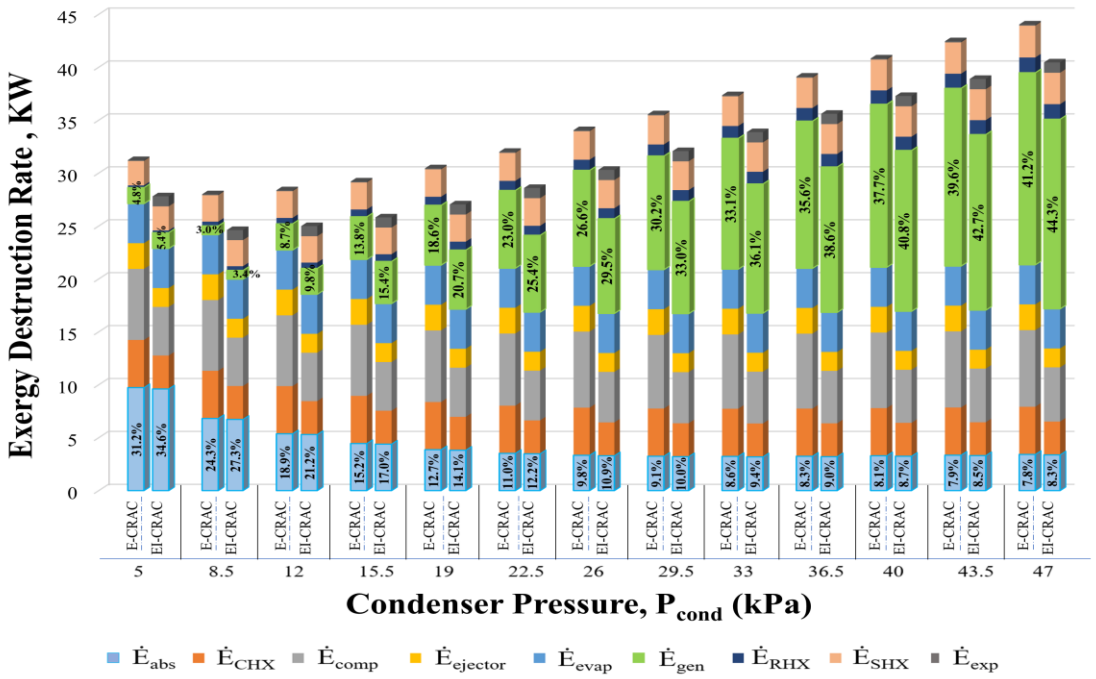

***Figure 6-33**: Impact of condenser pressure on total exergy destruction rate of the RAC based proposed cascaded systems at T_{gen} = 60 ℃, T_{evp} = -20 ℃, T_{abs} = 35 ℃, T_{evp} = -20 ℃, T_{evpHTC} = 10 ℃.*

With increasing P_{cond}, the impact on exergy efficiency also follows the same trend as *COP*. As exergy efficiency is proportionally reverse to total exergy destruction rate, similarly total ĖD decreases slightly up to an optimal point of maximum Ex_{eff}, then it increases rapidly with increasing P_{cond} as illustrated in **Figure 6-33**. With P_{cond} increasing, refrigerant with higher potential (temperature and pressure) provides required heat in the generator, hence irreversibility increase, as a result $\dot{E}x_{Dgen}$ also increase. But $\dot{E}x_{D,abs}$ decreases in a reverse manner. But at lower P_{cond} the decrement rate of $\dot{E}x_{D,abs}$ dominates over the increment rate of $\dot{E}x_{D,gen}$, hence total exergy destruction rate decrease. However, this trend reverses at higher P_{cond}, indicating the existence of an optimal temperature where the system experiences minimal total exergy destruction rate and, consequently, maximum exergy efficiency.

Impact of Absorber Temperature

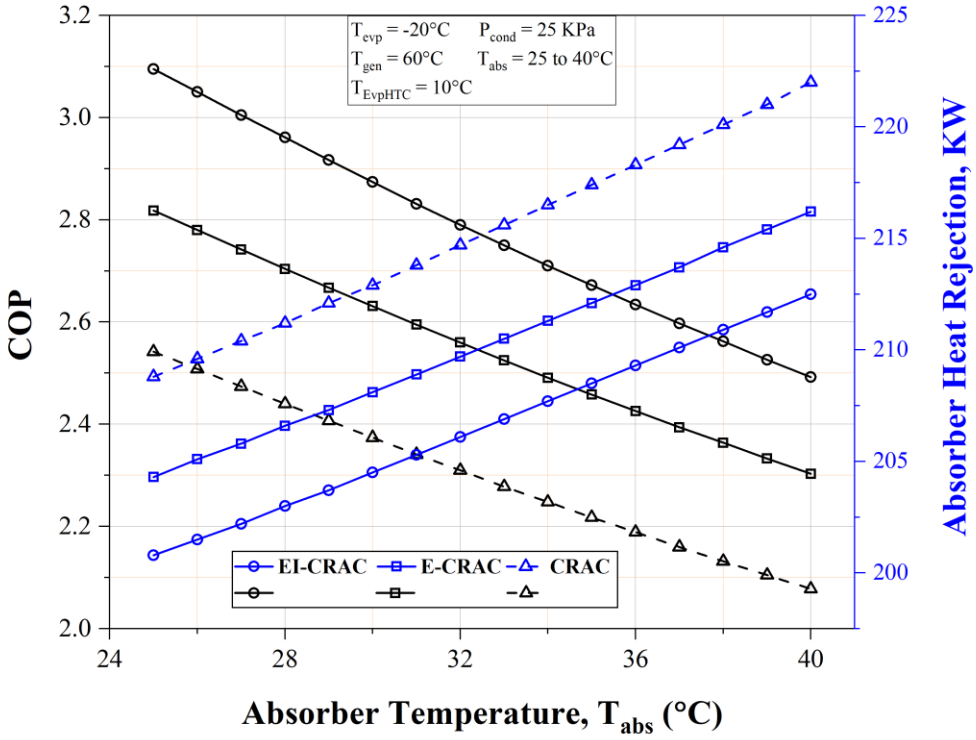

***Figure 6-34**: Impact of T_{abs} on COP and absorber rejected heat of the RAC based proposed cascaded compression absorption systems at P_{cond} = 25kPa, T_{evp} = -20 ℃, T_{gen} = 60 ℃.*

Figure 6-34 and **Figure 6-35** illustrate the impact of T_{abs} on 1st and 2nd law parameters of the RAC based proposed cascaded compression absorption systems for assessment. An increase in the absorber temperature T_{abs}, results in a proportional rise in the corresponding input loads, which subsequently results in a drop in 1st law efficiency (*COP*) of the systems. The higher T_{abs} leads to an increased irreversibility in the heat rejection due to deviation of the heat sink temperature from ambient temperature. This results in increase of $\dot{E}x_{D,total}$ and decrease of Ex_{eff}. A linear and swift decline in both the system *COP* and exergetic efficiency (Ex_{eff}) is observed as T_{abs} increases. The decrease of *COP* is near 0.18 per 4℃ absorber temperature increase, whereas Ex_{eff} decreases by 0.03 for the same increase of T_{abs}. Moreover EI-CRAC and E-CRAC maintain an improvement of *COP* of around 21% and 10% and improvement of Ex_{eff} of around 22% and 11% respectively over conventional CRAC.

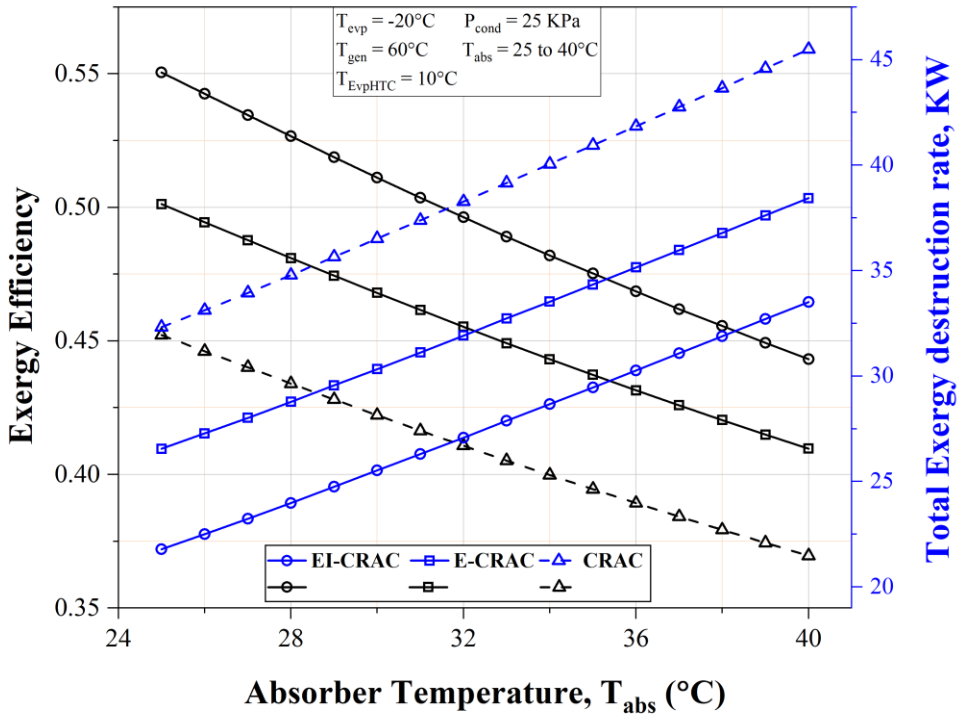

***Figure 6-35**: Impact of T_{abs} on 2nd law efficiency of the RAC based proposed cascaded compression absorption systems at P_{cond} = 25kPa, T_{evp} = -20 ℃, T_{gen} = 60 ℃.*

6.2.3 Exergy Flow and Destruction Analysis

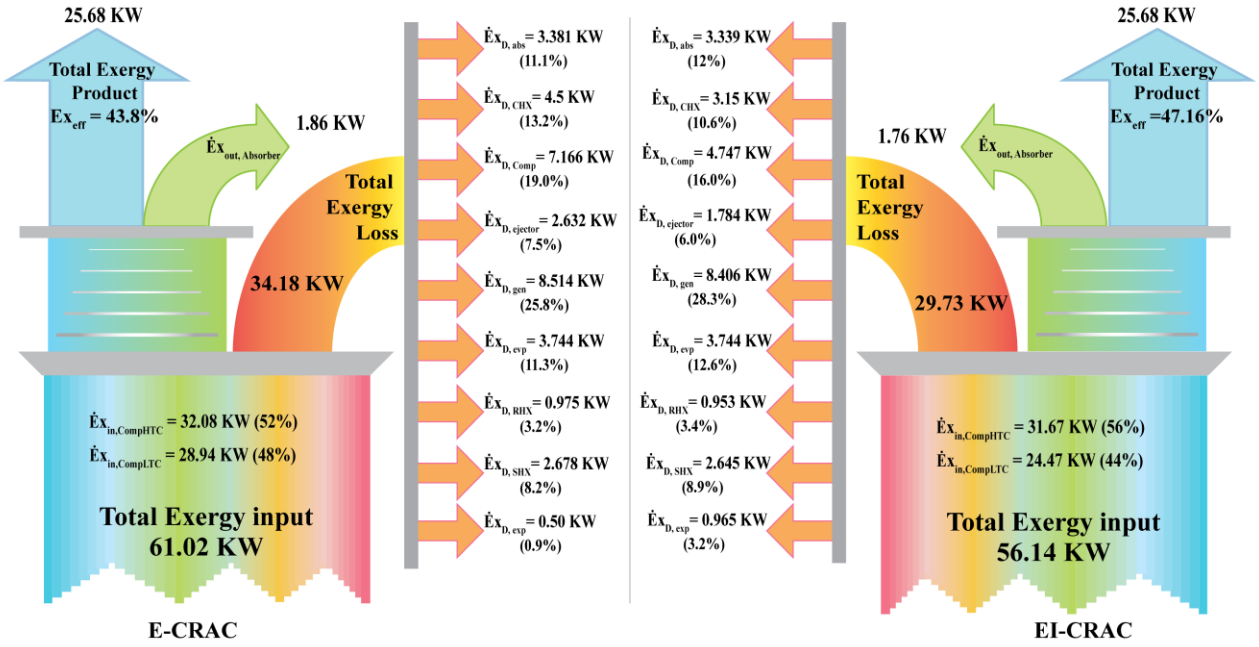

***Figure 6-36**: The exergy flow diagram with associated component exergy destruction rate of the proposed E-CRAC and EI-CRAC at T_{gen} = 60 ℃, P_{cond} = 25 kPa, T_{abs} = 35 ℃, T_{evp} = -20 ℃, $T_{evp}HTC$ = 10 ℃.*

An exhaustive exergy analysis has been subsequently performed on the proposed systems under a set of predefined conditions. **Figure 6-36** effectively visualizes the exergy flow chart, showcasing exergy destruction rates and associated percentages for each component. $\dot{E}x_D$ across the flash tank, the mixing chamber, or the solution pump is deemed negligible and hence ignored. The most substantial exergy loss is observed in the generator, primarily attributable to the irreversible nature of the intensive heat transfer between the solution refrigerant and compressed condensing refrigerant. Conversely, the solution heat exchanger registers the lowest exergy loss, owing to the high effectiveness assumption. Compared to the E-CRAC, the EI-CRAC demonstrates a reduced overall $\dot{E}x_D$ for the same output, resulting in approximately 10% enhancement in exergy efficiency. For both proposed models, there's a close match in the percentage of $\dot{E}x_D$ across the individual components. But EI-CRAC displays relatively lower exergy losses in the compressor and generator due to its double-stage compression and lower required $\dot{Q}_{gen}$.

6.2.4 Multi-objective Optimization

In an effort to minimize run time and curtail additional computational expenses, the elaborated simulation model has been simulated 756 times on corresponding sets of unique input data to formulate the ANN based objective functions of the RAC based proposed cascaded compression absorption systems. This objective function is integrated with the optimization algorithm rather than the simulation code, this results in reduction of significant runtime with added flexibility. ANN, a robust mathematical framework, can effectively discern complex non-linear relationships between inputs and outputs, making it particularly useful when physical equations struggle to define process characteristics [96]. The structure of ANN and optimization framework is presented in **Figure 6-37**.

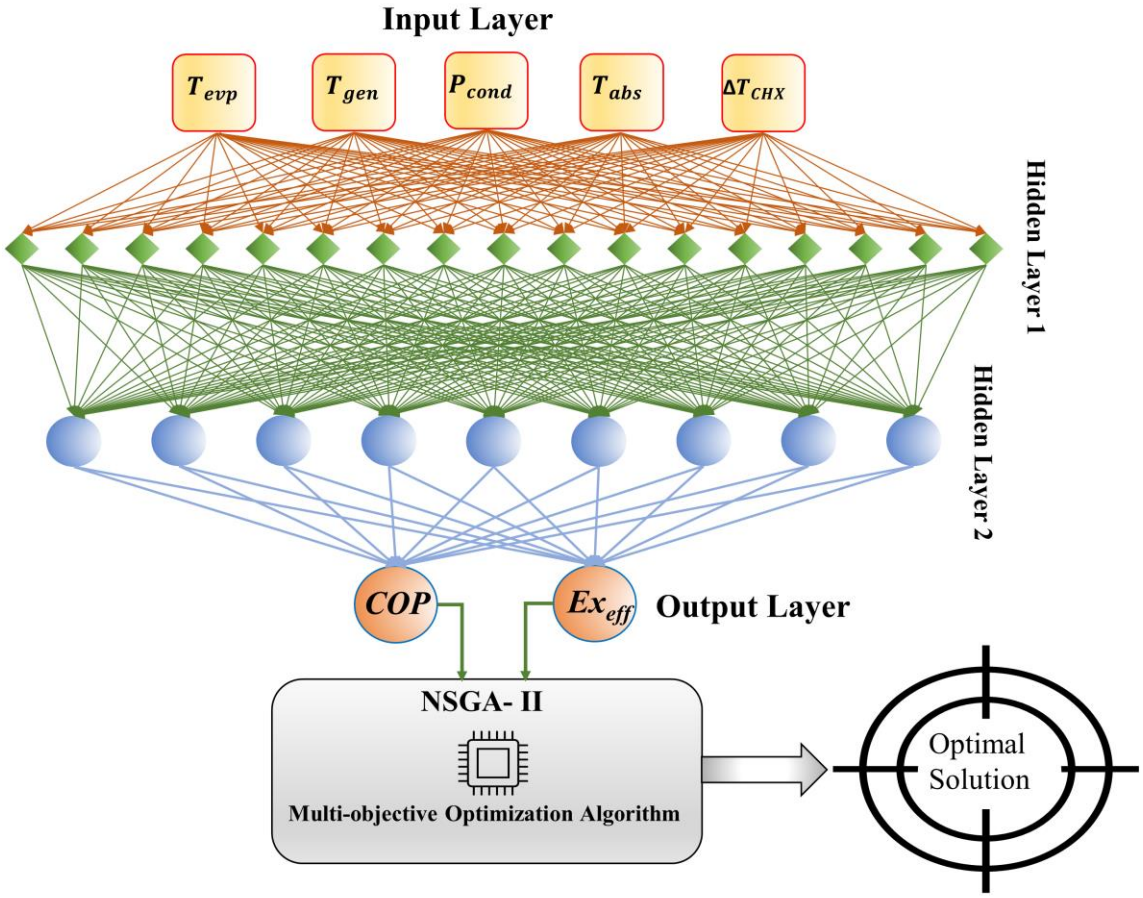

***Figure 6-37**: The outline of the optimization methodology using ANN prediction model of the RAC based cascaded compression absorption systems.*

Five distinct input variables (T_{evp}, T_{abs}, T_{gen}, $P_{cond,}$, ΔT_{chx}) and two output variables (*COP*, Ex_{eff}) from the 756 rows of simulation data have been employed to establish the ANN-based prediction model objective function of each proposed model (E-CRAC and EI-CRAC). The training is implemented using the Bayesian regularization algorithm on a dataset consisting of 680 rows (approximately 80%), while a testing set comprised the remaining 76 rows (approximately 20%). The selected ANN model was a two-layer feedforward network featuring 100 sigmoid hidden neurons and linear output neurons. The model summary is presented in **Figure 6-38**.

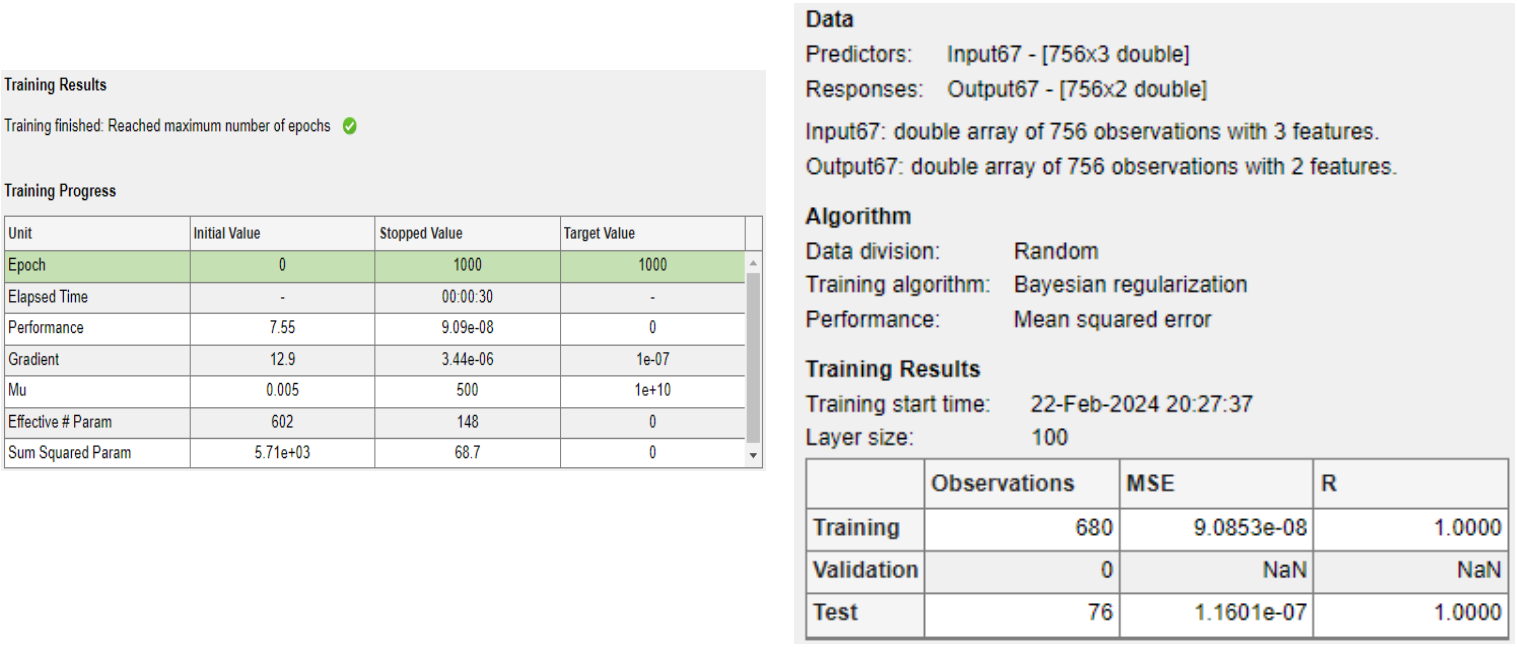

Training Results

Training finished: Reached maximum number of epochs

Training Progress

Unit	Initial Value	Stopped Value	Target Value
Epoch	0	1000	1000
Elapsed Time	-	00:00:30	-
Performance	7.55	9.09e-08	0
Gradient	12.9	3.44e-06	1e-07
Mu	0.005	500	1e+10
Effective # Param	602	148	0
Sum Squared Param	5.71e+03	68.7	0

Data

Predictors: Input67 - [756x3 double]

Responses: Output67 - [756x2 double]

Input67: double array of 756 observations with 3 features.

Output67: double array of 756 observations with 2 features.

Algorithm

Data division: Random

Training algorithm: Bayesian regularization

Performance: Mean squared error

Training Results

Training start time: 22-Feb-2024 20:27:37

Layer size: 100

	Observations	MSE	R
Training	680	9.0853e-08	1.0000
Validation	0	NaN	NaN
Test	76	1.1601e-07	1.0000

***Figure 6-38**: ANN Model summary of training and testing data of RAC based proposed cascaded compression absorption systems.*

This strategic configuration underscores the model's capacity for processing and analyzing the intricate relationships between the defined input and output variables, thus reinforcing the reliability and accuracy of the predictive model developed through this rigorous approach. Integration of ANN-based objective functions into the optimization framework not only signifies a leap towards computational efficiency but also enhances the flexibility and applicability of the simulation model in addressing complex engineering problems.

ML Model Accuracy Check and Error Evaluation

Accuracy checks and error evaluation are crucial for assessing machine learning model performance. Metrics like Precision, Recall, F1 Score, and Mean Squared Error (MSE) offer deeper insights into model effectiveness, addressing the balance between different types of errors

and the precision of predictions. The measure of determination (R^2) and mean squared errors (MSE) serves as an efficacy gauge for the ANN model. R^2 assesses the variance of the response data; proximity to unity signifies a high degree of reliability for the ANN model. The corresponding MSE for the training and testing datasets were $9.108* 10^{-8}$ and $1.601* 10^{-7}$ respectively, along with R^2 values of 0.995, indicating a good fit for the proposed model. The verification of accuracy for predicted data compared to the actual simulation data is demonstrated in **Figure 6-39**.

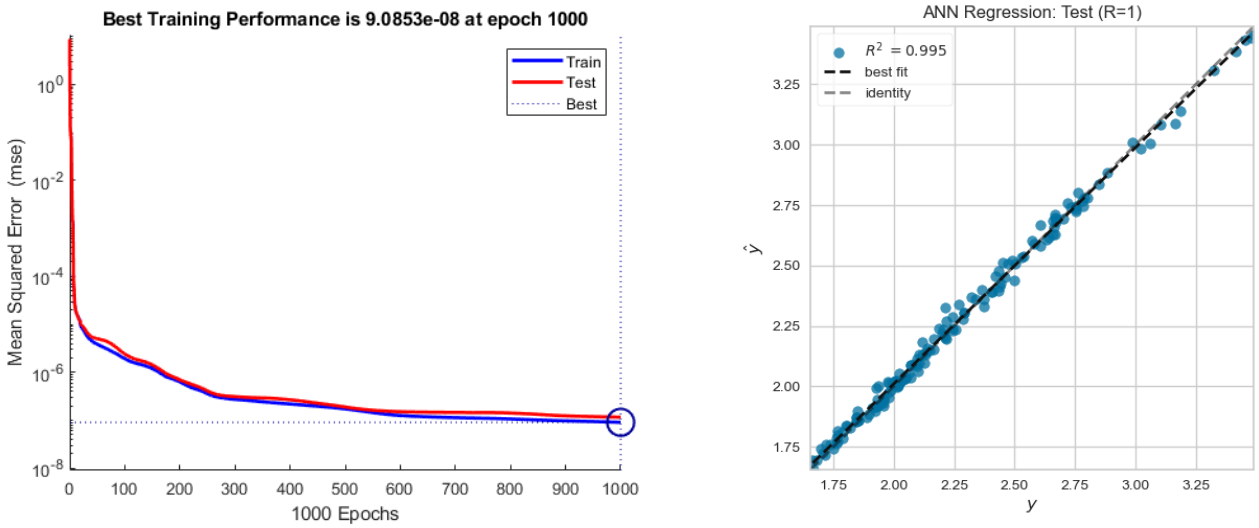

***Figure 6-39**: Performance test analysis of the ANN objective function of RAC based proposed cascaded compression absorption systems.*

In **Figure 6-39**, it is evident that both the trained and test datasets exhibited a close match, showing an initial departure from the ideal line of values which gradually diminishes, signaling a convergence towards alignment. This pattern, in conjunction with remarkably low Mean Squared Error (MSE) values and a coefficient of determination (R^2) of one, as depicted in **Figure 6-40**, highlights the model's efficacy for optimization research.

The convergence of data points towards the line of unity further validates the effective and dependable utilization of the Artificial Neural Network (ANN) within this domain, establishing a noteworthy advancement in the methodologies employed for optimization studies.

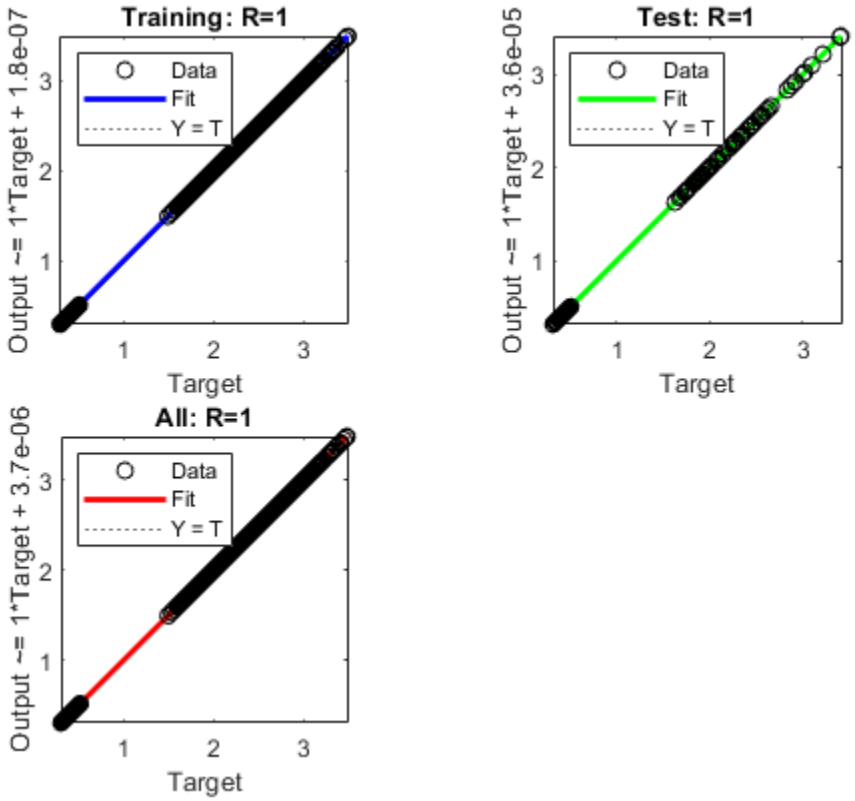

***Figure 6-40**: Accuracy levels of test and training data as well as their verification of RAC based proposed cascaded compression absorption systems.*

Optimization Strategy and Variables

The genetic algorithm (GA) is a prominent method for optimizing cycles, leveraging a solutions population for parallel exploration and showing superior adaptability and efficacy in diverse optimization scenarios, including those with mixed variables. The Non-dominated Sorting Genetic Algorithm II (NSGA-II) exemplifies GAs' efficiency in multi-criteria optimization, particularly in energy system enhancements, offering robustness and fast population evaluation, albeit with slower execution speed as its main drawback.

In the present study, the optimization toolbox provided within the MATLAB software suite serves as the primary computational tool for the optimization of objective functions of the RAC based proposed cascaded models. These objective functions have been meticulously crafted through the application of Artificial Neural Networks (ANN) with the aim of achieving maximal values for the Coefficient of Performance (*COP*) and exergy efficiency. This optimization process focuses on five key controllable variables, namely the evaporator temperature (T_{evp}), the absorber

temperature (T_{abs}), the generator temperature (T_{gen}), the condenser pressure (P_{cond}), and the temperature difference across the cascade heat exchanger (ΔT_{chx}).

To facilitate a rigorous and comprehensive optimization exercise, specific values for a range of parameters within the MATLAB optimization toolbox have been carefully selected. Moreover, the input ranges for these controllable variables have been comprehensively defined to ensure an extensive exploration of the solution space. The detailed configuration of these parameters, along with the prescribed ranges for the controllable variables, are given in **Table 6-13**. This setup not only underscores the methodological precision employed in the optimization task but also highlights the sophisticated integration of ANN-derived objective functions with MATLAB's optimization capabilities, paving the way for enhanced COP and exergy efficiency in the system under study.

***Table 6-13**: Selected Values for different parameters of Multi objective optimization algorithm of RAC based proposed cascaded systems.*

Specified Options		Selected Value
Population Size		200
Creation Function		Constraint Dependent
Crossover	function	Intermediate
	ratio	1
Migration	fraction	0.20
	direction	forward
Mutation	probability	Constraint dependent
	function	0.10
Population fraction of the Pareto Front		0.35
Max. Tolerance	constraint	10^{-3}
	function	10^{-4}
Generator-Condenser temperature,	T_{gen}, ℃	45 to 85
Evaporator temperature	T_{evp}, ℃	-35 to -10
Absorber temperature	T_{abs}, ℃	20 to 35
Condenser pressure	P_{cond}, kPa	20 to 30
Pinch difference at CHX	ΔT_{chx}	2 to 10

Decision Making and Optimization Result

In multi-objective optimization, the Pareto frontier is a curve that showcases an array of optimal solutions. Each point on this frontier stands as a testament to an optimal trade-off between competing objectives. At one extremity of this frontier, the leftmost point (designated as point A) embodies the scenario with maximal exergy efficiency, whereas the opposite extremity, the rightmost point (point C), signifies the condition with the optimal Coefficient of Performance (*COP*). The quest for a solution that harmoniously balances both COP and exergy efficiency (Ex_{eff}) involves identifying a point that either minimizes the geometric distance to an idealized scenario or maximizes the distance from the least favorable condition. Within this context, the Technique for Order of Preference by Similarity to Ideal Solution (TOPSIS) serves as a strategic decision-making tool, facilitating the identification of the most advantageous solution (point B) from both perspectives. This methodical approach affords a holistic evaluation of the diverse aspects of energy optimization, fostering a nuanced and comprehensive decision-making process. To implement TOPSIS technique for multi-objective decision making, the following steps should be followed [118]:

- Forming the Decision Matrix
- Normalizing the Matrix
- Assigning Weights
- Identifying Ideal and Negative-Ideal Solutions
- Estimating Closeness to the Ideal Solution
- Ranking Options

Figure 6-41 illustrates the pareto front of optimization solution for both proposed models for P_{cond} = 25 kPa. Although all the points are optimal solutions, point A and B refer to the optimum solution for maximum COP and maximum exergy efficiency individually. For the maximum value of ΔT_{CHX} = 5, all the optimal points of *COP* and Ex_{eff} maximization occurs.

With T_{evp} and T_{cond} increasing *COP* increases linearly for both the systems. But exergy efficiency increases with T_{cond} and decreases with T_{evp}, indicating the existence of an optimal T_{evp} value for optimal performance from both COP and exergy efficiency perspectives. Again, both *COP* and Ex_{eff} are found to be maximum at a specific generator temperature. This is why, maximum *COP* condition of point A, is obtained at T_{evp} = -10°C, T_{abs} = 35°C and T_{gen} = 60°C, and the values are

3.50 and 3.75 for E-CRAC and EI-CRAC respectively. Whereas, maximum Ex_{eff} condition of point B, is obtained at T_{evp} = -35℃, T_{abs} = 35℃ and T_{gen} = 60℃, and the values are 0.515 and 0.58 for E-CRAC and EI-CRAC respectively. The optimal condition is determined by TOPSIS technique, and the optimum value of *COP*: 3 and 3.3, Ex_{eff} = 0.585 and 0.53 for E-CRAC and EI-CRAC respectively.

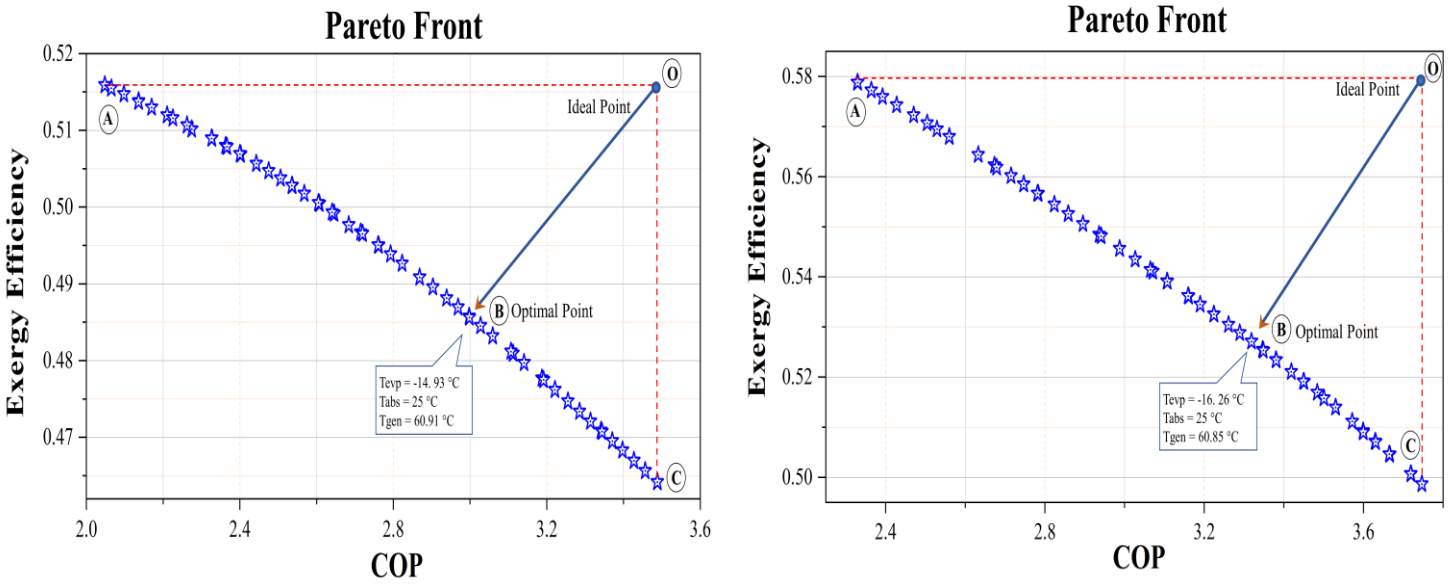

(i) **(ii)**

Figure 6-41*: Pareto front of Ga-multi objective optimization of the proposed systems, (i) E-CRAC and (ii) EI-CRAC to find the optimal solution using TOPSIS at P_{cond} = 25 kPa*

Table 20 is presented to show the determined optimal parameters for different P_{cond} conditions. ΔT_{CHX} is not included because, from all the perspective the optimal condition is found at its maximum value. The resulted *COP* and Ex_{eff} along with the optimal input parameters after optimization are presented for understanding the effect of each parameters individually. Additionally, with P_{cond} increases, this optimal value of the optimal T_{gen} also increases. But the optimal T_{gen} for maximization of Ex_{eff}, increases at a slightly higher rate compared to the rate observed for *COP*. This why for max Ex_{eff} condition the optimal T_{gen} is found slightly higher than that for max *COP* condition. Moreover, with P_{cond} increasing, both COP and Ex_{eff} increases, but *COP* increases at a slightly higher rate compared to Ex_{eff}. Again, regardless of change of P_{cond}, the optimal T_{evp} and T_{abs} value remain nearly unchanged. In all the conditions EI-CRAC portraits significant higher value of *COP* and Ex_{eff} compared to E-CRAC, and this difference remains near consistent.

***Table 6-14**. Multi-objective optimization solution of RAC based proposed cascaded systems with result for different condenser pressure.*

$P_{cond}(kPa)$	Scenarios	E-CRAC/ EI-CRAC		
		T_{evp} (K)	T_{abs} (K)	T_{gen} (K)
27.19	Maximum COP	262.985/ 263	298.008/ 298.01	333.891/ 334.8792
	Max Exergy Efficiency	238/ 238.095	298/ 298.02	334.095/ 334.84
	Optimal Condition	258.069/ 256.74	298/ 298.01	333.918/ 334.85
23.78	Maximum COP	262.998/ 262.99	298.003/ 298.00	332.021/ 332.95
	Max Exergy Efficiency	238.055/ 238.01	298.003/ 298.00	332.072 /332.9
	Optimal Condition	258.659/ 257.65	298.003/ 298.002	331.963/ 332.92
20.75	Maximum COP	262.999/ 263	298.009/ 298	330.083/ 331.05
	Max Exergy Efficiency	238.032/ 238.045	298.002/ 298	330.020/ 331.059
	Optimal Condition	258.500/ 257.85	298.002/ 298	330.083/ 331.048

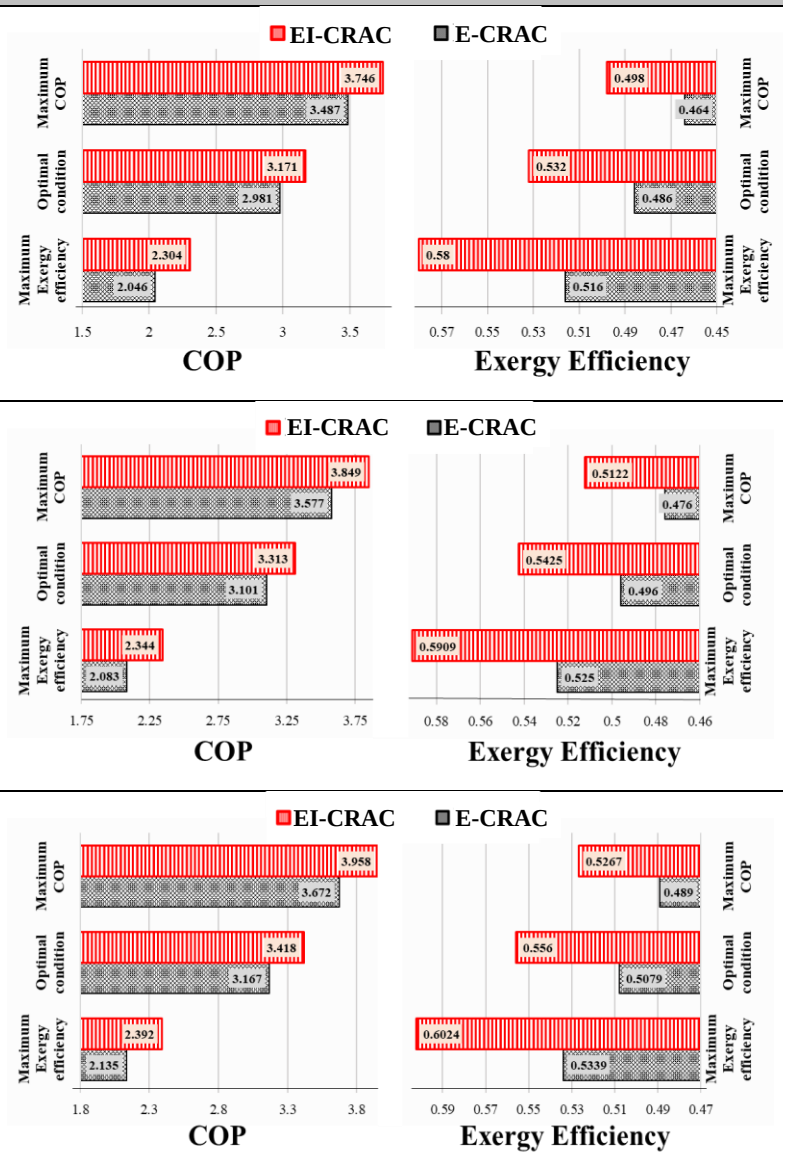

6.2.5 Section Summery

This section of this study addresses the crucial challenge of high energy consumption in the refrigeration sector by delving further into the unexplored territory of cascaded compression absorption systems. Specifically, it introduces and analyzes the integration of an advanced Recompression Absorption System (RAC) with an enhanced Vapor Compression Refrigeration (VCR) systems incorporated with an ejector.

Recognizing the inherent limitations of conventional Compression Absorption Refrigeration Cycle (CARC), this investigation proposes and critically examines three novel configurations: one basic Compression Recompression Absorption Cycle (CRAC) and two advanced configurations as: the Ejector-Compression Recompression Absorption Cycle (E-CRAC) and the Ejector enhanced Vapor-Injection Compression Recompression Absorption Cycle (EI-CRAC). These innovative systems seamlessly integrate advanced Recompression Absorption Cycle (RAC) and ejector-based Vapor Compression Refrigeration (VCRs) to effectively overcome critical limitations like energy wastage, inadequate thermal absorption, and excessive compressor power requirements. Notably, by strategically utilizing waste heat to improve generator performance and optimize compressor operation, the proposed systems hold immense promise for paving the way towards efficient and sustainable cooling solutions at a lower temperature with broader industrial applicability.

A computational model developed in Engineering Equation Solver (EES) is used to simulate the thermodynamic and parametric behavior of both proposed and traditional systems. A detailed comparative and parametric analysis is carried out for varying controllable operating conditions in order to gain insight about the effect of each parameter and performance enhancement of the proposed systems over conventional systems. Finally, ANN model is trained with the extracted data to integrate with Genetic algorithm to carry out multi-objective optimization and determine the optimal conditions of operation to ascertain the operational feasibility and limitations to pave the way for further research and innovation. The results of the thorough theoretical investigation based on 1st and 2nd law of thermodynamics and the multi-objective optimization are as follows:

- The *COP* of the proposed systems (CRAC, EI-CRC and E-CRAC) is nearly three times higher than the traditional CARC system, showing an improved efficiency in cooling operations. Whereas EI-CRAC and E-CRAC demonstrate near 10% and 20% *COP* enhancement, as well as 15% and 25% increase of Ex_{eff} over CRAC respectively.

- An optimal ΔP value exists for each proposed system, beyond which the *COP* begins to decrease, demonstrating the importance of maintaining proper pressure conditions for optimal performance. Compared to E-CRAC, the EI-CRAC system displays a fivefold smaller COP variation (0.004 vs. 0.02) and minimal sensitivity to pressure drop. While E-CRAC's COP noticeably drops by 0.0005 per kPa ΔP rise, EI-CRAC barely changes. This highlights EI-CRAC's superior stability under varying operating conditions.

- T_{gen} increases, the *COP* and Ex_{eff} initially increases until it reaches an optimal point, after which it decreases at a faster rate with further increases in T_{gen}. EI-CRAC outperforms basic CRAC by nearly 20% in COP and 23% in Ex_{eff}, while E-CRAC's improvement over T_{gen} variations maintains about 9% and 15% respectively. Additionally, with P_{cond} increases, this optimal value of the optimal T_{gen} also increases. But the optimal T_{gen} for maximization of Ex_{eff}, increases at a slightly higher rate compared to the rate observed for *COP*.

- For increasing T_{gen} and T_{evp}, *COP* of the proposed E-CRAC and EI-CRAC system maintains near consistent improvement over CRAC. But the enhancement of Ex_{eff} does not remain the same with changing T_{evp}. Although EI-CRAC exhibits higher Ex_{eff}, but its decremental rate with T_{evp} increasing is also higher. At an evaporator temperature (T_{evp}) of -35°C, both EI-CRAC and E-CRAC demonstrate an improvement in Ex_{eff} of approximately 23% and 11% respectively, compared to the traditional CRAC. However, when the evaporator temperature rises to T_{evp} = -5 °C, this increase diminishes to 12.5% and 7% respectively.

- The impact of P_{cond} on system performance is minimal below a specific threshold, but beyond this threshold, the performance declines significantly. For T_{gen} at 60°C, this limiting value of P_{cond} is 15 kPa, and this value increases with a rise in T_{gen}. But, as for T_{abs} increasing, the rate of decline in system performance is nearly linear.

- At a fixed operating condition the generator attributed to maximum exergy destruction rate (25.8% for E-CRAC and 28.3% for EI-CRAC) while the solution heat exchanger registers the minimum. Compared to E-CRAC, the EI-CRAC demonstrates a reduced overall $\dot{E}x_D$ (34.18 KW for E-CRAC and 29.73 KW for EI-CRAC) for the same output, resulting in approximately 10% enhancement in exergy efficiency.

- An optimal value of T_{gen} and T_{evp} exists for a specific operating condition, at which the systems provide the optimal solution of operation. Whereas at lowest T_{abs}, T_{evp} and P_{cond} but highest ΔT_{chx}, maximum *COP* condition can be achieved. And at highest T_{evp} and ΔT_{chx} but lowest T_{abs}, P_{cond} the maximum exergy efficiency condition can be achieved.

6.3 Analysis of Advanced Stand-alone Recompression Absorption System Equipped with Ejector and Vapor Injection.

In this section, the primary aim of the research, which **is "to enable the absorption system to operate at reduced evaporator temperatures with higher efficiency"** is further investigated. To achieve this, this section introduces the adaptation of a novel single-effect stand-alone absorption framework, incorporated with ejector-injection and recompression technologies directly within as opposed to employing a cascading approach as discussed in **Sections 6.1** and **6.2**. This innovation permits the single-effect system to operate at lower evaporator temperatures due to ejector-injection incorporation at the refrigerant side while simultaneously achieving a higher COP due to recompression technology employed in the generator. Thus, contributing to the broader objectives of energy optimization and system effectiveness within the study's scope.

ARC offers a more sustainable solution compared to VCR systems, but it faces challenges due to its reduced working pressure and *COP*. By integrating Recompression technology into ARC, an efficient generator-condenser heat exchanger setup can be established. This approach harnesses the rejected heat in condensation, reducing the external generator load and enhancing system performance. In this system, the refrigerant released from the generator is recompressed to a higher pressure and temperature, so that it may release heat to the generator and get condensed. So, the condensation pressure as well as the pressure ratio between the evaporator and condensed stream is much higher than basic ARC. Directly reducing the high pressure of the condensed subcooled ammonia through isenthalpic expansion in a single expansion valve leads to significant energy and exergy losses.

To address these inefficiencies, in this study, ejector and vapor injection techniques are incorporated into the refrigerant side of the RAC cycle, replacing the expansion valve and recovering lost energy to increase system efficiency [11]. This results in the development of advanced systems: **Refrigerant Ejector enhanced Recompression Absorption Cycle (RE-RAC)** and **Vapor Injection enhanced Recompression Absorption Cycle (VI-RAC)**. In these configurations, the conventional single-valve expansion of the refrigerant is substituted, and energy is recuperated internally, facilitating the entry of refrigerant into the absorber at an elevated pressure to reach higher system efficiency. Consequently, these modifications allow the absorption system to operate at lower evaporator temperature as well.

A detailed comparative and parametric analysis have been carried out for varying controllable operating conditions in order to gain insight about the effect of each parameter and performance enhancement of the proposed recompression absorption systems over conventional systems. For this sensitivity analysis, output parameters selected for system performance metrics are: 1st law efficiency (*COP*), 2nd law efficiency (Ex_{eff}), exergy destruction rate of system and across each component ($\dot{E}x_D$, compressor load ($\dot{W}_{comp}$), external heat requirement in generator ($\dot{Q}_{gen,ext}$) and generator internal heat use ($\dot{Q}_{gen,int}$). In this section, an extensive analysis from multiple viewpoints has been carried out to ensure a comprehensive and thorough understanding of the advanced single effect RAC systems. Finally, ANN model is trained with the extracted data to integrate with Genetic algorithm to carry out multi-objective optimization and determine the optimal conditions of operation to ascertain the operational feasibility and limitations to pave the way for further research and innovation. Design parameters and range of operation are provided in **Table 6-15.** Both constant and variable parameters are detailed, and the influence of these variable parameters on the system will be explored.

Table 6-15*. Design parameters for the analysis of proposed advanced stand-alone recompression absorption systems.*

Parameters	Values	Remark
Cooling load, Q_{evp}	*10 KW*	Constant
Generator-Condenser temperature, T_{gen}	*45 ℃ to 110 ℃*	Variable
Generator-Condenser pressure, P_{gen}	*1000 to 3000 kPa*	Variable
Evaporator temperature, T_{evp}	*-12 ℃ to 10 ℃*	Variable
Absorber temperature, T_{abs}	*25 ℃ to 30 ℃*	Variable
Normal pressure ratio in compressor (*NPR*)	*0.1 to 0.8*	Variable
Evaporator recovery pressure, ε	*1.2 to 2.0*	Variable
Effectiveness of RHX, $\boldsymbol{\varepsilon_{RHX}}$	*0.7*	Constant
Effectiveness of SHX, $\boldsymbol{\varepsilon_{SHX}}$	*0.9*	Constant
Ejector nozzle efficiency, $\boldsymbol{\eta_n}$	*0.9*	Constant
Ejector mixing efficiency, $\boldsymbol{\eta_m}$	*0.85*	Constant
Ejector diffuser efficiency, $\boldsymbol{\eta_d}$	*0.8*	Constant
Ambient temperature, T_0	*25 ℃*	Constant
Ambient pressure, P_0	*101.325 kPa*	Constant
Compressor efficiency, $\boldsymbol{\eta_s}$	*0.85*	Constant
Absorber's inlet cooling water temperature	T_{abs} *- 5*	Constant
Absorber's outlet cooling water temperature	T_{abs} *+ 5*	Constant
Evaporator's inlet cooling air temperature	T_{evp} *+ 8*	Constant
Evaporator's outlet cooling air temperature	T_{evp} *+ 3*	Constant
Generator's inlet water temperature of external source	T_{Gen} *+ 15*	Constant
Generator's outlet water temperature of external source	T_{Gen} *+ 10*	Constant

6.3.1 Comparison Between Proposed and Conventional System

The methodology of the validated models has been implied to model the proposed RAC systems: RE-RAC and VI-RAC. A detailed comparative analysis between the conventional and proposed stand-alone RAC system has been carried out.

In this analysis, NH_3-H_2O has been selected as the refrigerant of choice. Despite the potential hazards associated with ammonia (NH_3), adhering to established safety protocols enables its application across a wide temperature range, ensuring thermodynamic stability and operational flexibility. The preference for NH_3-H_2O in Absorption Refrigeration Cycle (ARC) systems is attributable to its excellent compatibility, environmental advantages, and its proficiency in reaching lower evaporator temperatures, aligning with the primary objectives of this research. Moreover, refrigeration systems integrated with ejectors are particularly well-suited for refrigerants exhibiting high vapor densities. This specificity arises because liquid-powered ejectors are less efficient with refrigerants that produce low-density vapor, such as the steam in LiBr-H_2O systems. Furthermore, in the RAC based stand-alone proposed absorption systems, the maximum *COP* occurred at a generator pressure and temperature lower than the conventional ARC. Thus, the proposed design could handle the high activation temperature and pressure challenges of ARCs with an NH_3-H_2O working fluid.

For any operating condition, properties of each stream are determined using equations and integrated library of EES. For a specific boundary condition, state point tables of the proposed RE-RAC, and VI-RAC configuration are stated in **Table 6-16** and **Table 6-17** respectively.

Table 6-16*. Thermodynamic property of each flow stream of RE-RAC cycle at T_{gen} = 70℃, P_{gen} = 1100kPa, T_{evp} = 2℃, T_{abs} = 30℃, ε = 1.75 and NPR = 0.1.*

State Point	P (kPa)	T (℃)	h (kJ/kg)	h (kJ/kg-K)	x (%)	m (kg/s)	Ex (kJ/Kg)
1	809.6	30	-45.75	0.3488	0.72	0.0201	5.456
2	1100	30	-45.55	0.3482	0.72	0.0201	5.464
3	1100	47.44	33.4	1.387	0.72	0.0201	0.8277
4	1100	70	75.8	0.8526	0.4862	0.01096	2.661
5	1100	38	-69.07	0.4095	0.4862	0.01096	2.52
6	809.6	30	-105.1	0.2934	0.4862	0.01096	2.504
7	1100	70	1604	5.655	-	0.009147	3.109
8	4361	208.4	1897	5.748	-	0.009147	5.534
9	4361	82.4	614.2	2.297	-	0.009147	3.208

10	4361	24.13	314.9	1.381	-	0.009147	2.968
11	457.6	2	304.7	1.381	-	0.009147	2.875
12	457.6	2	865.2	3.42	-	0.01763	4.709
13	809.6	18.21	903.3	3.421	-	0.01763	5.375
14	809.6	18.21	285.1	1.299	-	0.00848	2.705
15	462.6	2	285.1	1.309	-	0.00848	2.681
16	462.6	2	1464	5.595	-	0.00848	1.851
17	809.6	18.21	1479	5.396	-	0.009147	2.669
18	809.6	161.5	1838	6.404	-	0.009147	3.206

Table 6-17*. Thermodynamic property of each flow stream of VI-RAC cycle at T_{gen} = 70℃, P_{gen} = 1100kPa, T_{evp} = 2℃, T_{abs} = 30℃, ε = 1.75 and NPR = 0.1.*

State Point	P (kPa)	T (℃)	h (kJ/kg)	h (kJ/kg-K)	x (%)	m (kg/s)	Ex (kJ/kg)
1	809.6	30	-45.75	0.3488	0.72	0.01902	5.162
2	1100	30	-45.55	0.3482	0.72	0.01902	5.169
3	1100	47.44	33.4	1.387	0.72	0.01902	0.783
4	1100	70	75.8	0.8526	0.4862	0.01036	2.517
5	1100	38	-69.07	0.4095	0.4862	0.01036	2.384
6	809.6	30	-105.1	0.2934	0.4862	0.01036	2.369
7	1100	70	1604	5.655	-	0.008653	2.941
8	4361	208.4	1897	5.748	-	0.008653	5.236
9	4361	82.4	614.2	2.297	-	0.008653	3.034
10	4361	24.63	317.3	1.389	-	0.008653	2.808
11	809.6	18.21	317.3	1.41	-	0.008653	2.754
12	809.6	18.21	285.1	1.299	-	0.008419	2.686
13	462.6	2	285.1	1.309	-	0.008419	2.661
14	462.6	2	1464	5.595	-	0.008419	1.837
15	809.6	44.52	1552	5.636	-	0.008419	2.469
16	809.6	18.21	1479	5.396	-	0.000234	0.06819
17	809.6	43.76	1550	5.63	-	0.008653	2.537
18	809.6	165.1	1847	6.425	-	0.008653	3.057

Based on the properties of fluid streams, the output parameters are calculated to conduct a thorough comparative analysis between the proposed recompression stand-alone systems along with their comparison with traditional RAC and ARC. The result is presented in **Table 6-18**. For the same operating conditions, it has been found that, *COP* of the RE-RAC and VI-RAC is nearly 76% and 63% times higher than the RAC system. These systems also show 28% and 19% *COP*

enhancement over conventional SE-RAC. Moreover, RE-RAC shows an 8% and 4.8% enhancement of *COP* and Ex_{eff} over VI-RAC.

***Table 6-18**. Comparison among the proposed systems and traditional system at at T_{gen} = 70℃, T_{evp} = 2℃, T_{abs}= 30℃, P_{gen}= 1100 kPa, T_{cond}= 30℃, ε = 1.75 and NPR = 0.1*

Parameters	Traditional Cycle		Proposed Cycles	
	RAC	SE-RAC	RE-RAC	VI-RAC
$\dot{Q}_{gen,ext}$ (kW)	5.878	4.402	3.092	2.931
$\dot{Q}_{gen,int}$ (kW)	16.57	13.06	11.73	11.1
$\dot{Q}_{evp}$ (kW)	10	10	10	10
$\dot{Q}_{abs}$ (kW)	19.92	17.6	16.58	15.76
$\dot{W}_{comp}$ (kW)	4.2	2.981	2.678	3.27
$\dot{E}x_{D,total}$ (kW)	4.213	3.704	2.873	3.012
COP	0.9846	1.352	1.74	1.612
Ex_{eff}	0.161	0.2341	0.2708	0.2586

Figure 6-42 illustrates the performance comparison of the conventional and proposed advanced stand-alone RAC systems for varying generator temperatures.

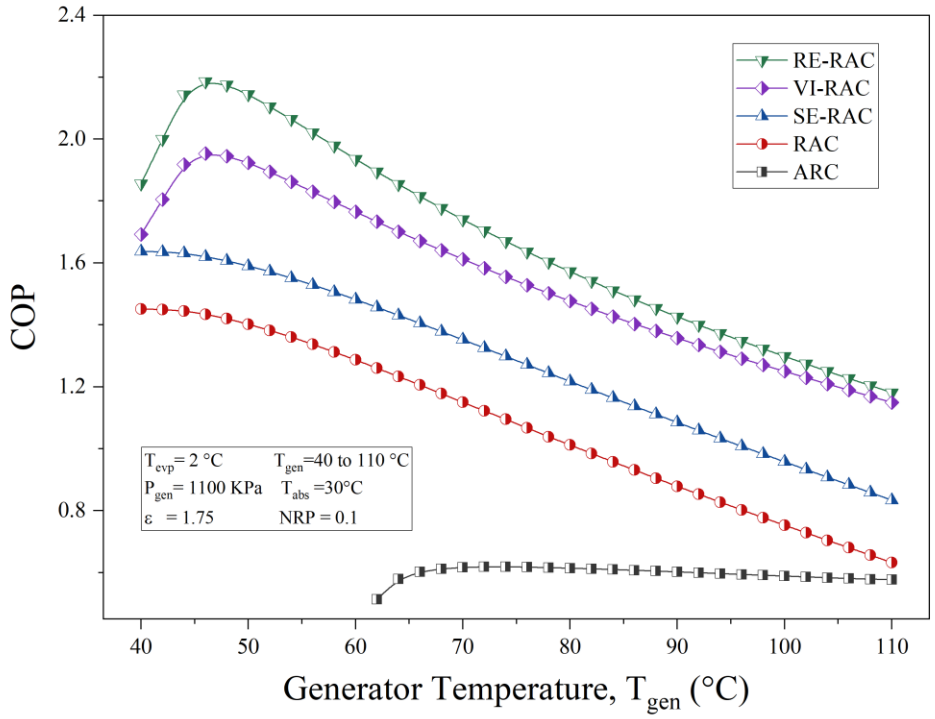

***Figure 6-42**: Impact of T_{gen} on the 1st law efficiency of conventional and proposed stand-alone RAC (recompression absorption cycle) and basic ARC(absorption refrigeration cycle) systems.*

The Basic ARC shows the lowest *COP*, which remains near constant with increasing T_{gen} after around 70°C. This cycle cannot function beyond 60°C as P_{gen} is constrained by the condenser's T_{cond} ($P_{cond} = P_{gen}$). All RAC systems have a superior *COP* to ARC and can function at reduced generator temperatures due to the flexibility in lowering P_{gen}. In this analysis, P_{gen} is set at 1100 kPa. However, distinct performance trends and values are observed among systems, attributed to variations in the energy load for the generator and compressor, as shown in **Figure 6-43**.

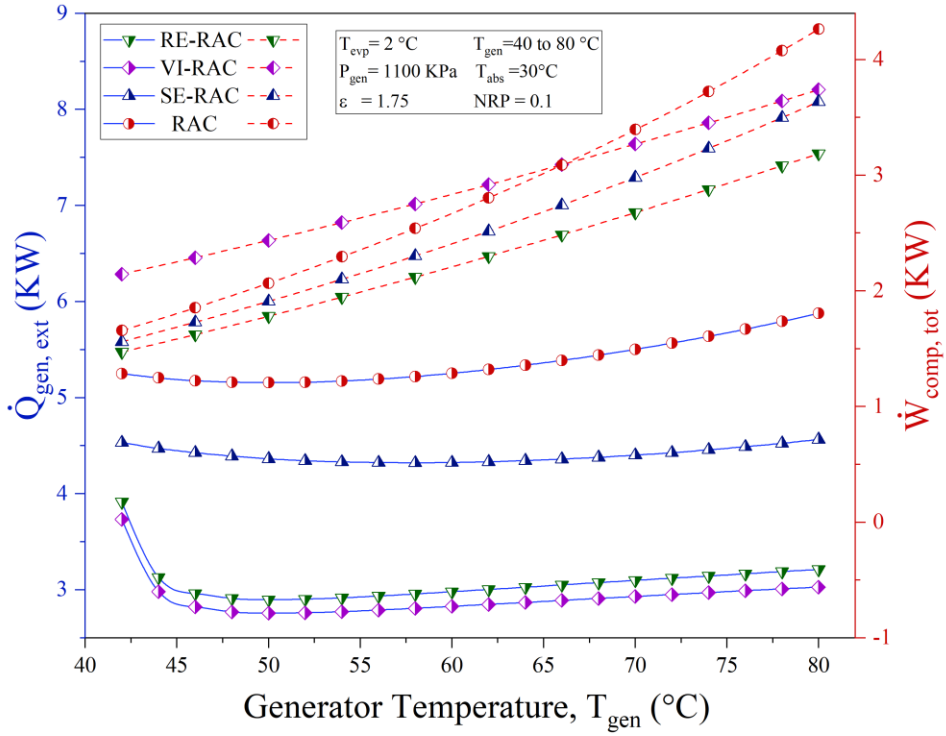

***Figure 6-43**: Impact of T_{gen} on external generator load and total required compressor load of conventional and proposed stand-alone recompression absorption systems*

Proposed RE-RAC and VI-RAC show higher *COP* than conventional RAC. With T_{gen} increasing, *COP* increases rapidly at lower T_{gen}. The peak *COP* is obtained at around 50°C, after which increasing T_{gen} results in decrement of *COP* at a much slower rate. The trend can be explained by **Figure 6-43**. With T_{gen} increasing, the required external heat in the generator decreases rapidly and reaches a minimal value. Beyond 50°C, this generator requirement becomes near constant with T_{gen} increase. But the compressor load keeps increasing with T_{gen} at a constant pace. Due to this, the resulting *COP* decreases for T_{gen} beyond 50°C. But the required $\dot{W}_{comp}$ of VI-RAC increases at slower rate than RE-RAC. As a result, *COP* of RE-RAC decreases at a higher pace and the difference of *COP* between RE-RAC and VI-RAC keeps decreasing with T_{gen} increasing after

optimal T_{gen}. For the conventional RAC and SE-RAC, *COP* keeps decreasing with increasing T_{gen} with similar trend as shown in **Figure 6-42**. But with increasing T_{gen}, the required $\dot{Q}_{gen,ext}$ and $\dot{W}_{comp}$ of basic RAC increases at a much higher manner than SE-RAC, VI-RAC and RE-RAC as shown in **Figure 6-43**. Consequently, *COP* decreases at a higher rate for RAC.

At the optimal point of around 50°C, RE-RAC shows around 25% *COP* enhancement over VI-RAC. But due to slower increment of required $\dot{W}_{comp}$ of VI-RAC. At 100°C this enhancement decreases to around 5% only. Again, at 50°C RE-RAC shows around 35% and 53% enhancement of *COP* over conventional SE-RAC and RAC respectively. Whereas at 100°C this enhancement of RE-RAC over SE-RAC remains same 35%. But as *COP* of RAC drops significantly, and enhancement of RE-RAC over RAC increases to 70%.

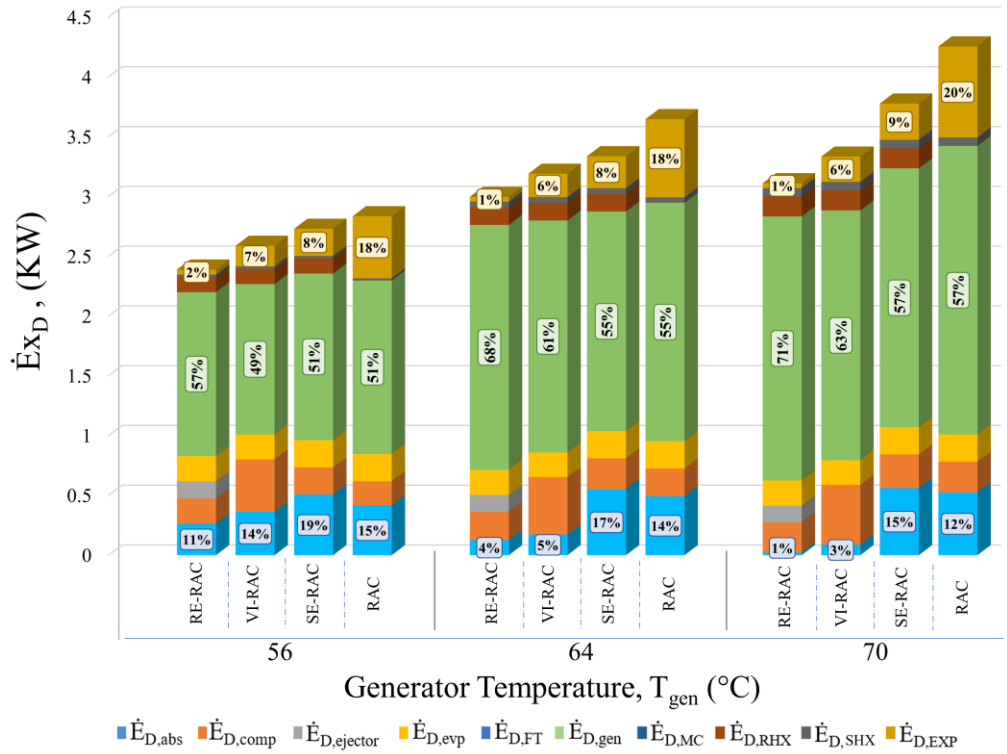

***Figure 6-44**: Impact of T_{gen} on rate of total exergy destruction of conventional and proposed* stand-alone *recompression absorption systems.*

Figure 6-44 depicts the impact of T_{gen} on both the total and component-specific exergy destruction rates of conventional and advanced stand-alone RAC systems. The conventional RAC exhibits the highest exergy destruction, primarily due to significant exergy losses during the throttling process in both the refrigerant and solution sections. With T_{gen} increasing, $\dot{E}x_{D,exp}$ also increases, resulting

in higher increase of $\dot{E}x_D$. SE-RAC also shows a significant and increasing $\dot{E}x_D$ in expansion valve, because of conventional refrigerant throttling. In contrast, the proposed systems show reduced overall exergy destruction, attributed to the substitution of refrigerant expansion with the ejector and injection systems. Also, as absorber pressure is increased $\dot{E}x_{D,abs}$ decreases significantly. While RE-RAC requires more external $\dot{Q}_{gen,ext}$ compared to VI-RAC and SE-RAC, but its fewer components result in lower $\dot{E}x_{D,tot}$. Again, RE-RAC exhibits higher $\dot{E}x_{D,gen}$ but a relatively smaller $\dot{E}x_{D,abs}$ compared to VI-RAC. SE-RAC posessess the highest $\dot{E}x_{D,abs}$ because of mixing of solution just before the absorber. With increasing T_{gen}, the $\dot{E}x_D$ difference between the systems also increase.

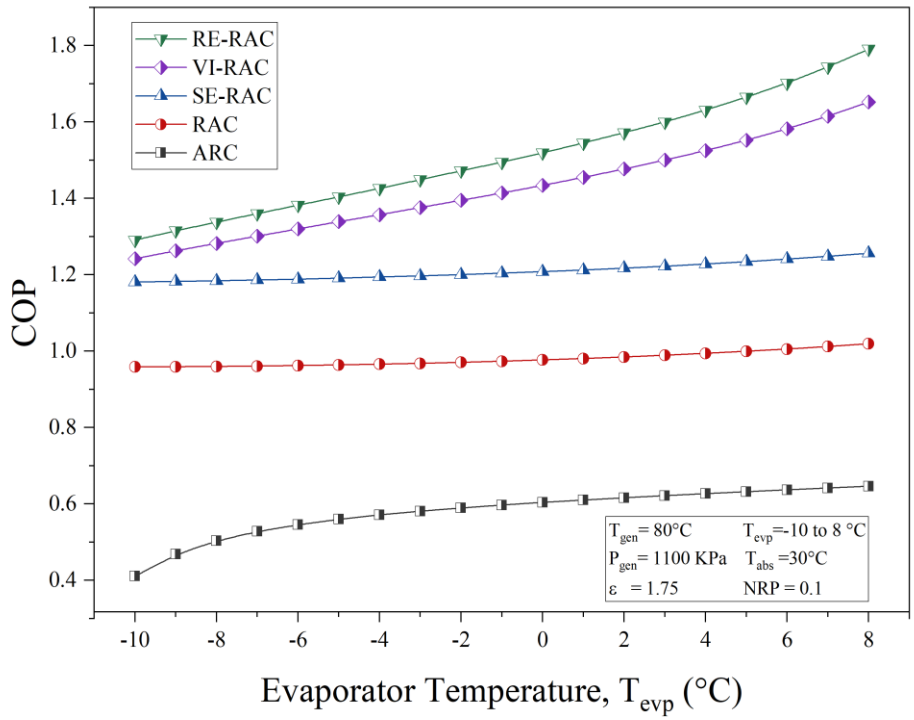

***Figure 6-45**: Impact of T_{evp} on the 1st law efficiency of conventional and proposed stand-alone RAC(recompression absorption cycle) and basic ARC(absorption refrigeration cycle) systems.*

Figure 6-45 depicts how *COP* varies with T_{evp}. Different systems demonstrate distinct behavioral trends. ARC has the lowest *COP*, rising sharply at lower T_{evp} levels but showing only slight increases at higher T_{evp} levels. The *COP* for both conventional RAC and SE-RAC increases at a very subtle rate, consistent across the entire T_{evp} range. On the other hand, for the proposed RE-RAC and VI-RAC, *COP* keeps increasing with T_{evp} increasing. Consequently, this rate of increment also keeps increasing but for RE-RAC this incremental rate is higher than VI-RAC over

T_{evp} increasing. At -10°C, RE-RAC shows around 35%, 9% and 4% improvement over RAC, SE-RAC, and VI-RAC. But at 8°C, this improvement increases to around 75%, 42% and 8.5% respectively. **Figure 6-46** displays the change of Ex_{eff} with T_{evp}. With T_{evp} increasing, the mass flow rate within the system increases, that results in an increase of $\dot{E}x_D$ at a consistent significant manner. As a result, Ex_{eff} decreases in a similar rate for all the recompression systems. But the proposed systems show a higher decremental rate. As a result, the difference of Ex_{eff} between the system decreases with increasing T_{evp}.

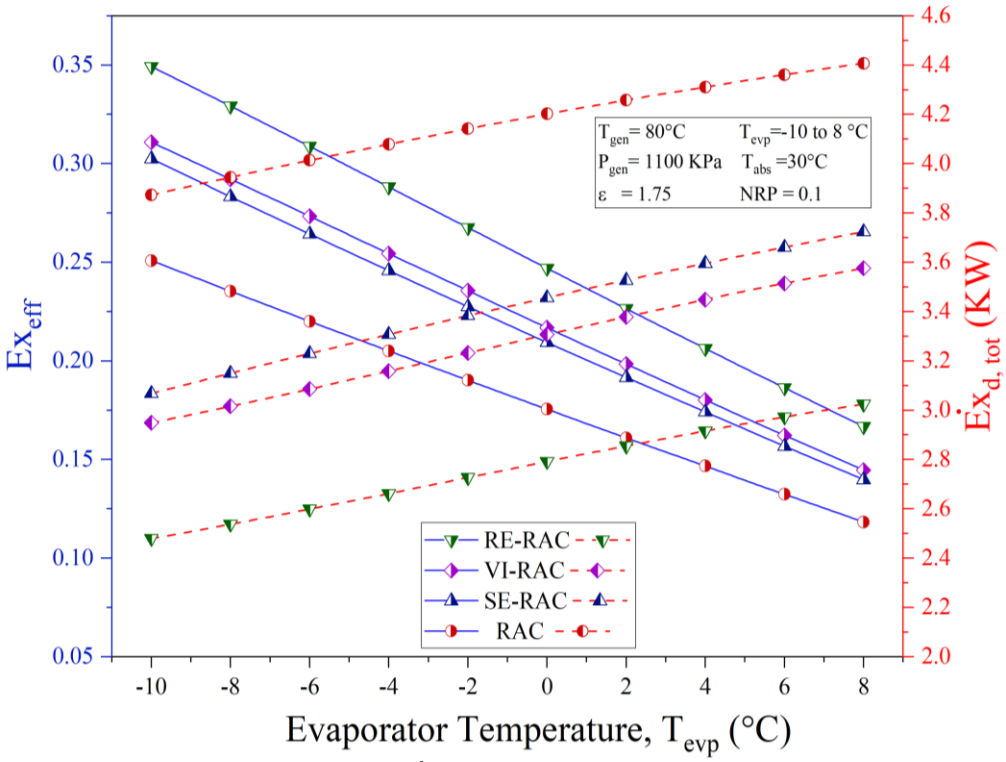

***Figure 6-46**: Impact of T_{evp} on the 2nd law efficiency and total exergy destruction rate of conventional and proposed stand-alone recompression absorption systems.*

6.3.2 Energy Analysis of the Advanced Stand-alone RAC Systems

The proposed advanced RE-RAC and VI-RAC has been proved to be significantly better than basic RAC and modified SE-RAC from both energy and exergy perspective. Hence, it's necessary to carry out comprehensive parametric analysis to figure out the effect and sensitivity of controlled variables to determine the optimal range of operations.

Impact of T_{gen} – T_{evp} - P_{gen}

Higher the generator temperature is, the lower x_{NH_3} of the weak solution is. In the same way, higher the absorber pressure is, the higher x_{NH_3} of the strong solution is. **Figure 6-47** depicts the influence of T_{gen} on system *COP* across varying evaporator temperatures.

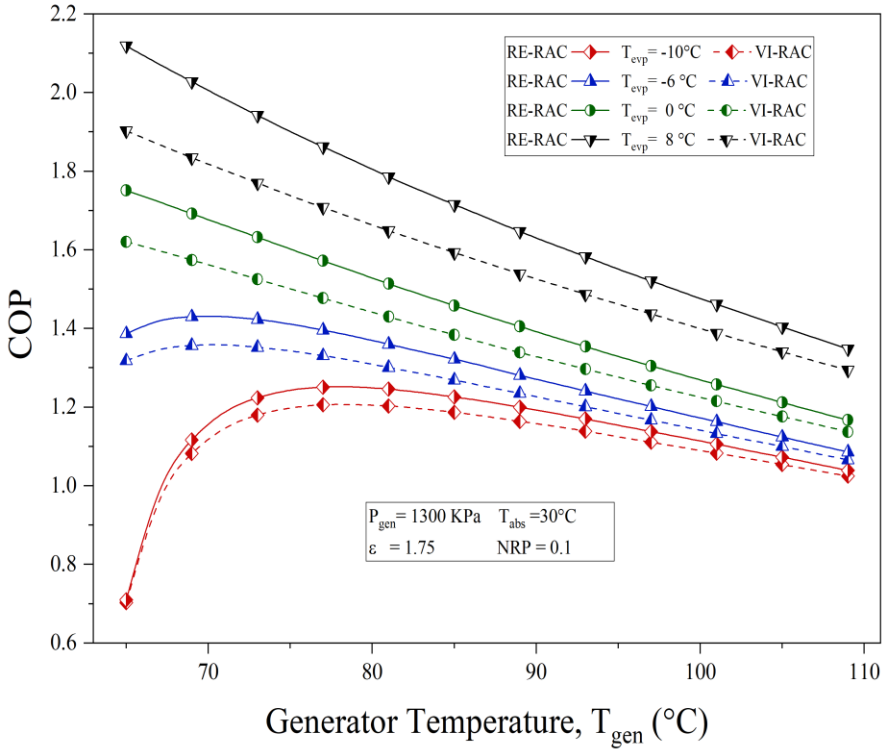

***Figure 6-47**: Impact of T_{gen} on COP of the proposed stand-alone recompression absorption systems at P_{gen} = 1300 kPa, T_{abs}= 30°C, ε = 1.75 and NPR = 0.1 for different T_{evp}*

Higher T_{evp} lines have higher *COP* for both the proposed systems. Because, as shown in **Figure 6-48,** with T_{evp} increasing, $\dot{W}_{comp}$ increases (increase of $\Delta\dot{W}_{comp}$ between T_{evp} : -10°C and 8°C of either system is around 0.5 kW for T_{gen} = 80°C) but required $\dot{Q}_{gen,ext}$ decreases rapidly ($\Delta\dot{Q}_{gen,ext}$ decrease between -10°C and 8 °C T_{evp} is around 2 kW), hence higher T_{evp} system has higher *COP*. With T_{gen} increasing, input temperature to the compressor (state 9) increases, leading to a linear increase in compressor power. Meanwhile, the required $\dot{Q}_{gen,ext}$ initially drops rapidly until reaching a minimal value, causing a sharp increase in *COP*. After reaching this optimal T_{gen}, the change in $\dot{Q}_{gen,ext}$ is marginal. However, due to the steady rise in $\dot{W}_{comp}$, the *COP* consistently declines. As evident from the figure, for T_{evp}= -10°C, the optimal T_{gen} is around at 75°C for P_{gen}=

1300 kPa. But with T_{evp} increasing, the optimal value of T_{gen} decreases. for T_{evp}= 0℃, the optimal T_{gen} is reduced to around 60℃.

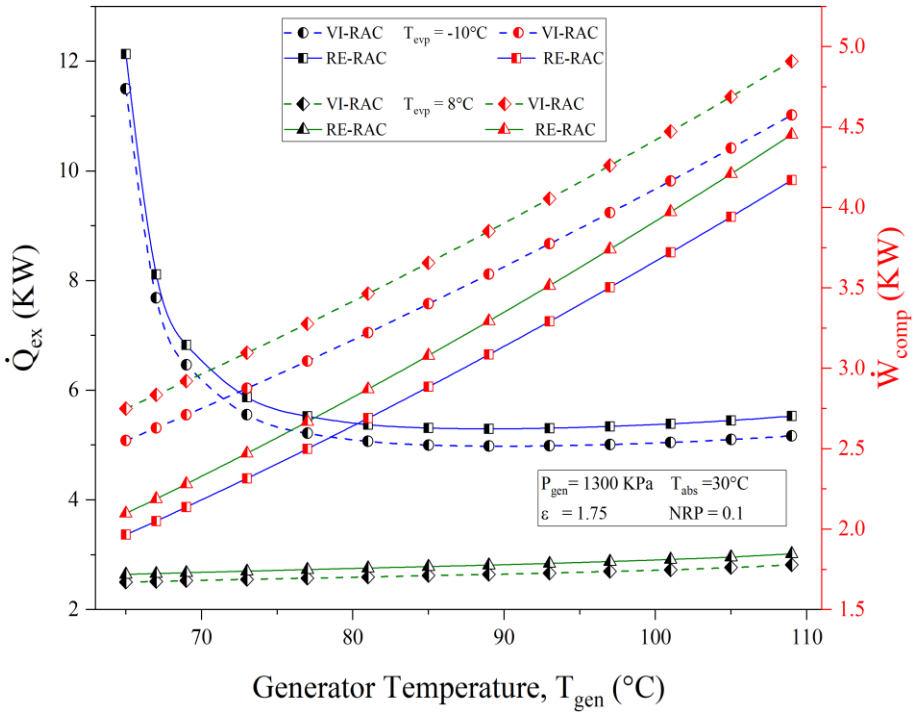

***Figure 6-48**: Impact of T_{gen} on compressor and generator external load of the proposed stand-alone recompression absorption systems at P_{gen} = 1300 kPa, T_{abs}= 30°C, ε = 1.75 and NPR = 0.1 for different Tevp*

Moreover, from **Figure 6-48**, it can be seen that, RE-RAC requires more $\dot{Q}_{gen,ext}$ than VI-RAC to operate, but VI-RAC has an additional compressor and requires much higher $\dot{W}_{comp}$. The difference in required $\dot{W}_{comp}$ is higher than $\dot{Q}_{gen,ext}$. Hence, RE-RAC has higher *COP*. With decreasing T_{evp}, the requirement of $\Delta\dot{Q}_{gen,ext}$ for RE-RAC increases at higher manner than VI-RAC, but $\Delta\dot{W}_{comp}$ doesn't increases at such rate, resulting in decrease $\Delta Total\ Power$ between the systems and *COP* difference decreases. This enhancement of *COP* and ΔTP of RE-RAC is maximum at the optimal T_{gen} and this difference decreases with increasing T_{gen} beyond this value.

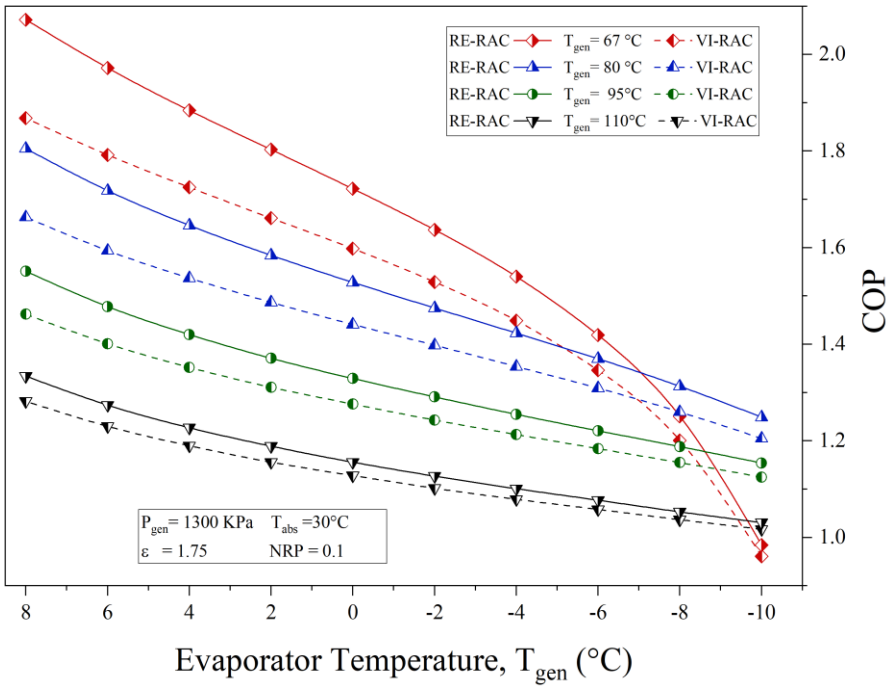

***Figure 6-49**: Impact of T_{evp} on COP of the proposed stand-alone recompression absorption systems at P_{gen} = 1300 kPa, T_{abs}= 30°C, ε = 1.75 and NPR = 0.1 for different T_{gen}*

Figure 6-49 illustrates the impact of T_{evp} on *COP* of the proposed stand-alone RAC systems for different T_{gen}. For same T_{gen} and P_{gen}, the x_{weak} remains constant. But with T_{evp} decreasing P_{abs} as well as x_{strong} decreases as a result Δx_{NH_3} decreases and required $\dot{Q}_{gen}$ increases. Again, with T_{evp} decreasing, mass flow of the system also decreases. As a result, for constant *NPR*, the required compressor load also decreases. But $\dot{Q}_{gen}$ increases at a much higher rate compared to the decrement rate of $\dot{W}_{comp}$ as depicted in **Figure 6-50**. As a result, *COP* also decreases with T_{evp}.

But different T_{gen} lines of either system show different behavior. Lower T_{gen} results in higher x_{NH_3} of the weak solution. Hence, they have lower $\dot{Q}_{gen}$ and higher *COP*. And Higher T_{gen} results in higher $\dot{Q}_{gen}$ and lower *COP*. For lower T_{gen}, the decline in *COP* is more pronounced, and below T_{evp} = -4°C, the required $\dot{Q}_{gen}$ surges rapidly, causing a significant drop in *COP*. However, with higher T_{gen}, the *COP* decrease remains consistent across the T_{evp} range, and the limiting condition emerges at a considerably lower T_{evp}. Consequently, it's inferred that while lower T_{gen} results in a superior *COP* at moderate T_{evp}, reducing the evaporator temperature further poses challenges for low T_{gen} systems. For systems with low T_{evp}, it's essential to raise the T_{gen} for either of the proposed systems.

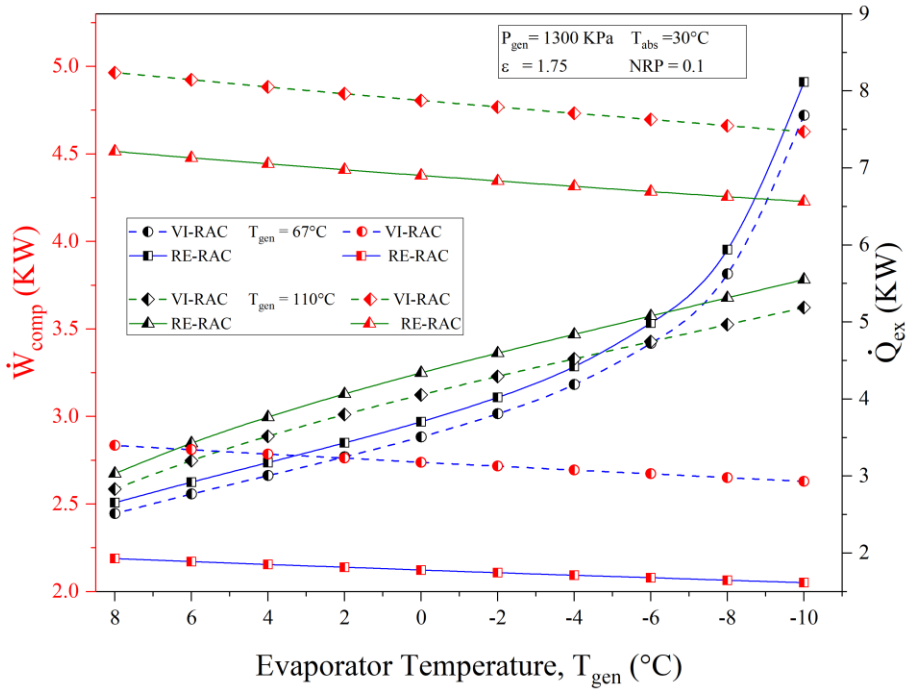

***Figure 6-50**: Impact of T_{evp} on compressor and generator external load of the proposed stand-alone recompression absorption systems at P_{gen} = 1300 kPa, T_{abs}= 30°C, ε = 1.75 and NPR = 0.1 for different T_{gen}*

Again, as depicted in **Figure 6-49**, RE-RAC shows much enhancement of *COP* over VI-RAC at higher T_{evp}. For same T_{gen} = 67°C, at T_{evp} = 8°C, the RE-RAC required only 0.10 kW more $\dot{Q}_{gen,ext}$ and 0.65 kW less $\dot{W}_{comp}$ than VI-RAC. The difference is higher; hence RE-RAC shows 35% higher *COP* over VI-RAC. but at -10°C the requirement in $\dot{Q}_{gen,ext}$ increases to 0.46 kW and $\dot{W}_{comp}$ decreases to 0.58 kW of RE-RAC over VI-RAC. The difference decreases, hence, the *COP* enhancement is reduced to 5%. Also, for same T_{evp}, for lower T_{gen}, the enhancement of RE-RAC is also higher.

Figure 6-51 and **Figure 6-52** discuss the effect of P_{gen} on the system performance for different T_{gen} values with T_{evp} set at 6°C for the analysis. This setting is chosen because a substantial decrease in T_{evp} would introduce a limiting condition for lower T_{gen}, as depicted in **Figure 6-49**, making it challenging to elucidate the relationship between P_{gen} and T_{gen} adequately.

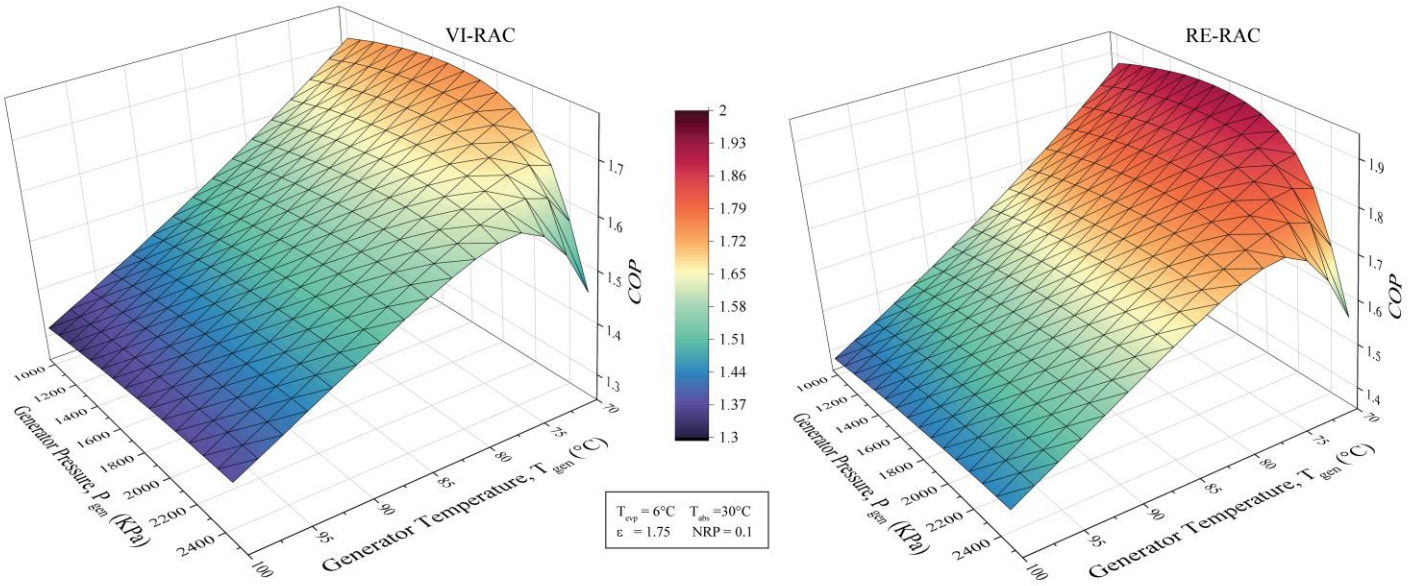

***Figure 6-51**: Impact of T_{gen} and P_{gen} on the 1st law efficiency of the proposed stand-alone recompression absorption systems at T_{evp} = 6°C, T_{abs}= 30°C, ε = 1.75 and NPR = 0.1*

As seen from the **Figure 6-52**, Lower T_{gen} results in lower required $\dot{Q}_{gen,ext}$ and lower $\dot{W}_{comp}$ for either of the stand-alone RAC systems. Hence resulting in a higher *COP* compared to higher T_{gen} as illustrated in **Figure 6-52 (a)**. For a fixed *NPR*, the pressure after recompression (P_8) remains constant. Hence with increasing P_{gen}, the pressure ratio R_p decreases. As a result, required $\dot{W}_{comp}$ decreases with P_{gen} increasing as shown in **Figure 6-52 (b)**. On the other hand, increasing P_{gen} results in higher CR, hence required $\dot{Q}_{gen,ext}$ increases with P_{gen}. The interaction of these two factors maximizes *COP* with increasing P_{gen}. In lower P_{gen}, the decremental rate of $\dot{W}_{comp}$ is slightly higher than incremental rate of required $\dot{Q}_{gen,ext}$. As a result, with P_{gen} increasing, *COP* increases in a minimal rate before reaching an optimal point. After which $\dot{Q}_{gen,ext}$ increases suddenly and *COP* drops.

For higher T_{gen}, with increasing P_{gen}, the change of $\dot{W}_{comp}$ and $\dot{Q}_{gen,ext}$ is consistent, hence *COP* increases in a near linear trend for either system. So, *COP* maximization happens at much higher P_{gen}. But for lower T_{gen}, if P_{gen} is increased beyond an optimal value around 1600-2000 kPa, the required $\dot{Q}_{gen,ext}$ increases suddenly, consequently *COP* drops in a rapid manner. So, it can be concluded that, although lower T_{gen} system has higher *COP*, but it's optimal P_{gen} is also lower.

Beyond the optimal point, performance of lower T_{gen} system becomes even lower than higher T_{gen} system creating a limiting condition of operation as shown in **Figure 6-51.**

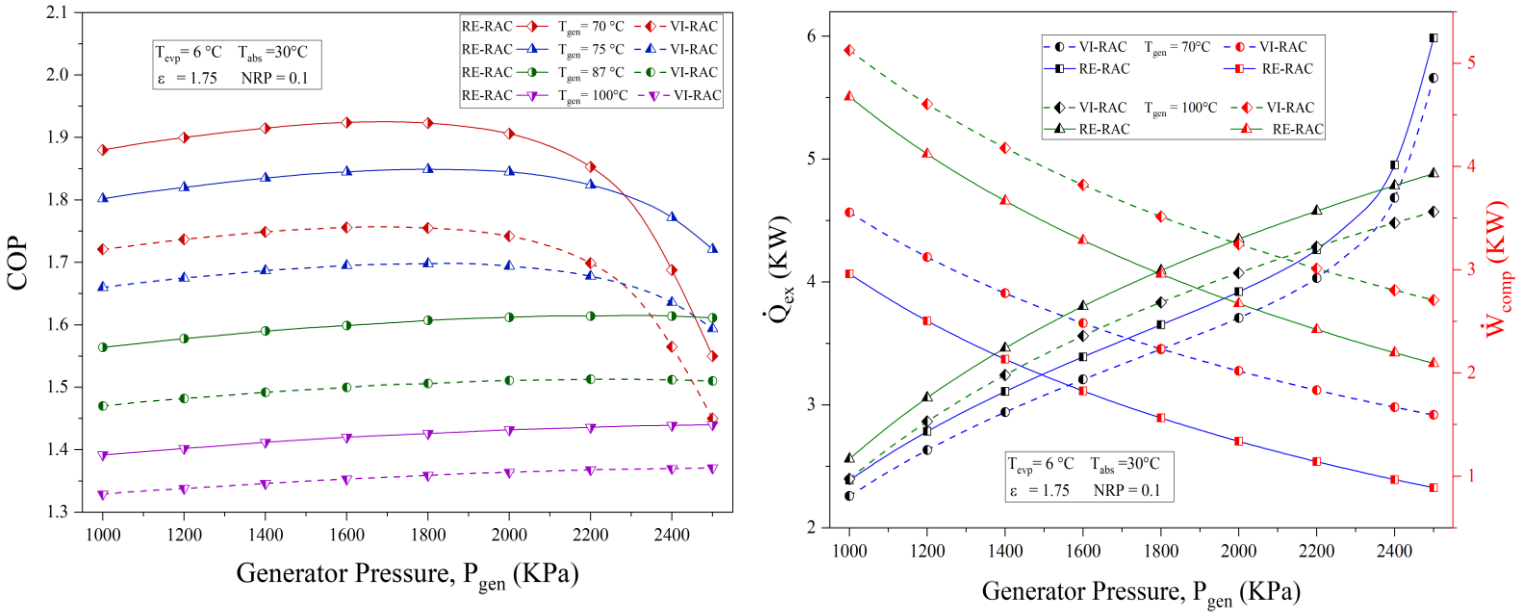

(a) *(b)*

***Figure 6-52**: Impact of P_{gen} on the performance of the proposed stand-alone recompression absorption systems at T_{evp} = 6°C, T_{abs}= 30°C, ε = 1.75 and NPR = 0.1 for different T_{gen}*

Additionally, RE-RAC demonstrates a notable improvement over VI-RAC at lower generator temperatures. For P_{gen}= 1400, RE-RAC exhibits about a 10% enhancement over VI-RAC at T_{gen} = 70°C. However, at T_{gen} = 100°C, this enhancement reduces to nearly 4%. Furthermore, as P_{gen} increases, the pressure ratio of the refrigerant compressor (comp-II) in VI-RAC also rises. Consequently, with an increasing P_{gen}, the required $\dot{W}_{comp}$ for VI-RAC decreases at a slower rate than RE-RAC. Thus, the difference in *COP* between the advanced systems narrows as P_{gen} increases, as illustrated in **Figure 6-52**

Figure 6-53 and **Figure 6-54** discuss the effect of P_{gen} on the system performance for different T_{evp} values. T_{gen} is fixed at 100℃ for the analysis. Because if T_{gen} is lowered significantly, that'll cause a limiting condition for lower T_{evp} as shown in **Figure 6-47**, and the relation between P_{gen} and T_{evp} can't be explored properly.

Lower T_{evp} results in lower $\dot{W}_{comp}$. But, with associated lower P_{abs} results in a much higher $\dot{Q}_{gen,ext}$ as shown in **Figure 6-54(b)**. Hence, lower T_{evp} systems have lower *COP* as seen in **Figure 6-54 (a)**. Again, with P_{gen} increasing, the required $\dot{W}_{comp}$ decreases and $\dot{Q}_{gen,ext}$ increases. Their

interaction determines the optimal P_{gen}. With P_{gen} increasing, *COP* increases in a minimal rate before reaching an optimal point. After which $\dot{Q}_{gen,ext}$ increases suddenly and *COP* drops.

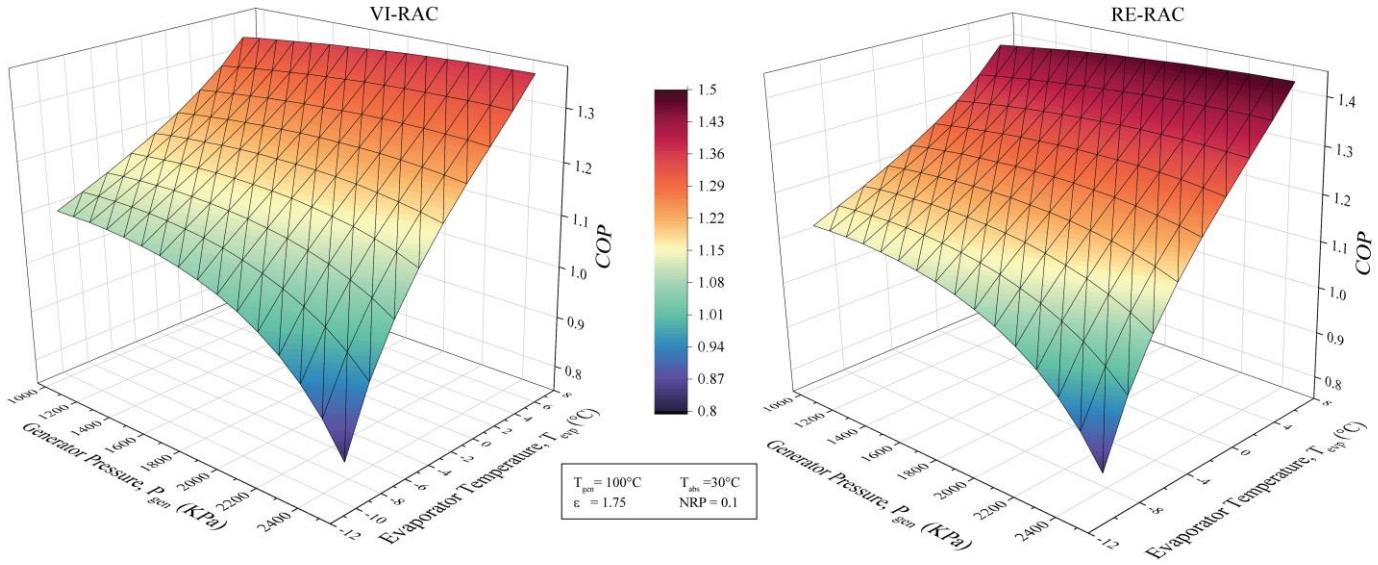

***Figure 6-53**: Impact of T_{evp} and P_{gen} on the 1st law efficiency of the proposed stand-alone recompression absorption systems at T_{gen} = 100°C, T_{abs}= 30°C, ε = 1.75 and NPR = 0.1.*

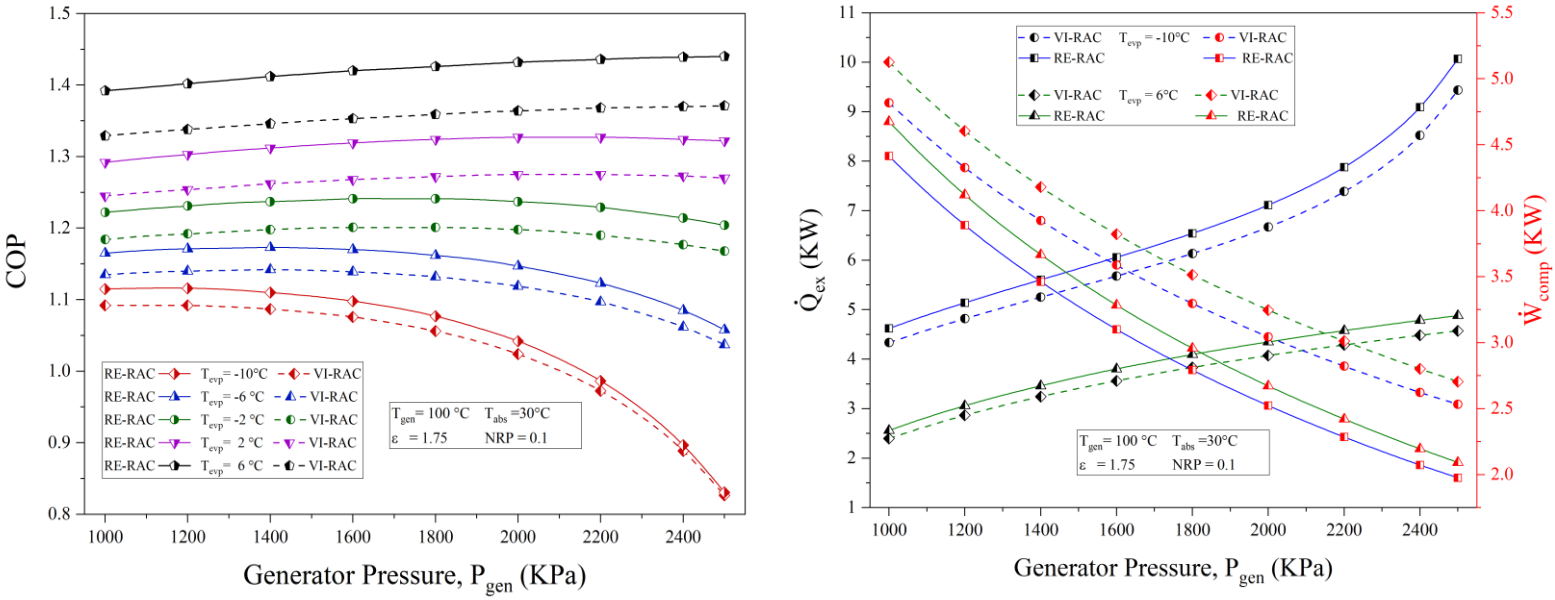

(a) ***(b)***

***Figure 6-54**: Impact of P_{gen} on the performance of the proposed standalone recompression absorption systems at T_{gen} = 100°C, T_{abs}= 30°C, ε = 1.75 and NPR = 0.1 for different T_{evp}*

At a lower T_{evp}, there's a sharp rise in $\dot{Q}_{gen,ext}$ at a relatively low P_{gen}, leading to a rapid decline in *COP* as illustrated in **Figure 6-54**. However, for a higher T_{evp}, the peak *COP* is achieved at a

greater P_{gen} value. For instance, at T_{evp} = -6°C, the optimal P_{gen} is roughly 1200 kPa. Beyond this point, a significant increase in $\dot{Q}_{gen,ext}$ results in a steep *COP* drop. Conversely, at T_{evp} = 6°C, the ideal P_{gen} is closer to 2400 kPa. In this scenario, the rise in $\dot{Q}_{gen,ext}$ is more gradual compared to the reduction in $\dot{W}_{comp}$, allowing the *COP* to consistently rise until reaching the optimal P_{gen}. Then $\dot{Q}_{gen,ext}$ increases rapidly, and *COP* drops. So, the evaporator temperature is found to affect the optimal generator pressure to maximize *COP* significantly, i.e., a rise in the evaporator temperature raised the optimal generator pressure to maximize *COP* for the fixed T_{gen} system of 100°C. Again, as discussed before, RE-RAC system shows higher enhancement of *COP* over VI-RAC system at higher evaporator. With increasing P_{gen}, the performance enhancement of RE-RAC over VI-RAC decreases.

Impact of $T_{gen} - T_{evp} - \varepsilon$

The influence of T_{gen} and the recovery pressure ratio (ε) is depicted in **Figure 6-55** and **Figure 6-56**. T_{evp} is maintained at a moderate value of 3°C. Because, for a higher value of ε at a higher T_{evp}, P_{abs} approaches P_{gen}, risking the failure of the absorption system.

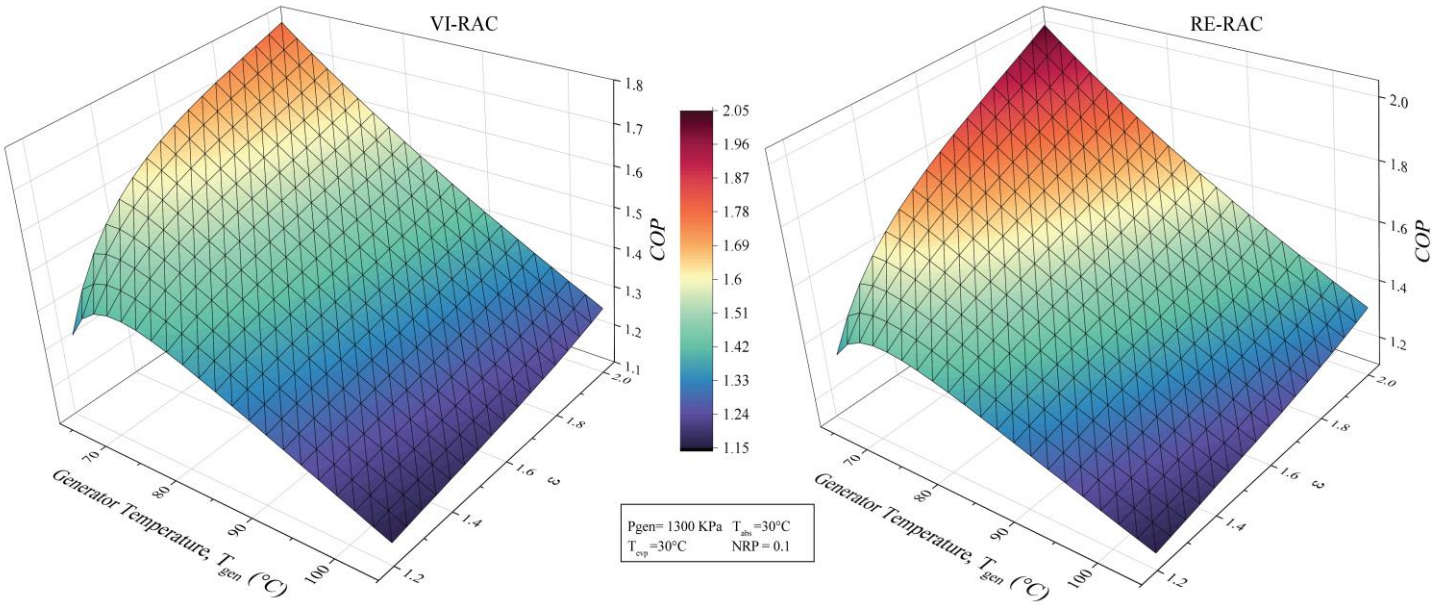

***Figure 6-55**: Impact of T_{gen} and ε on the 1st law efficiency of the proposed stand-alone recompression absorption systems at P_{gen} = 1300 kPa, T_{abs}= 30°C, T_{evp} = 3 °C and NPR = 0.1.*

The effect of ε is very similar to T_{evp}. An increase in ε leads to a rise in P_{abs}. Consequently, both CR and x_{strong} experience an increment, which in turn results in a reduction of $\dot{Q}_{gen}$ and an enhancement in *COP*, as illustrated in **Figure 6-56.**

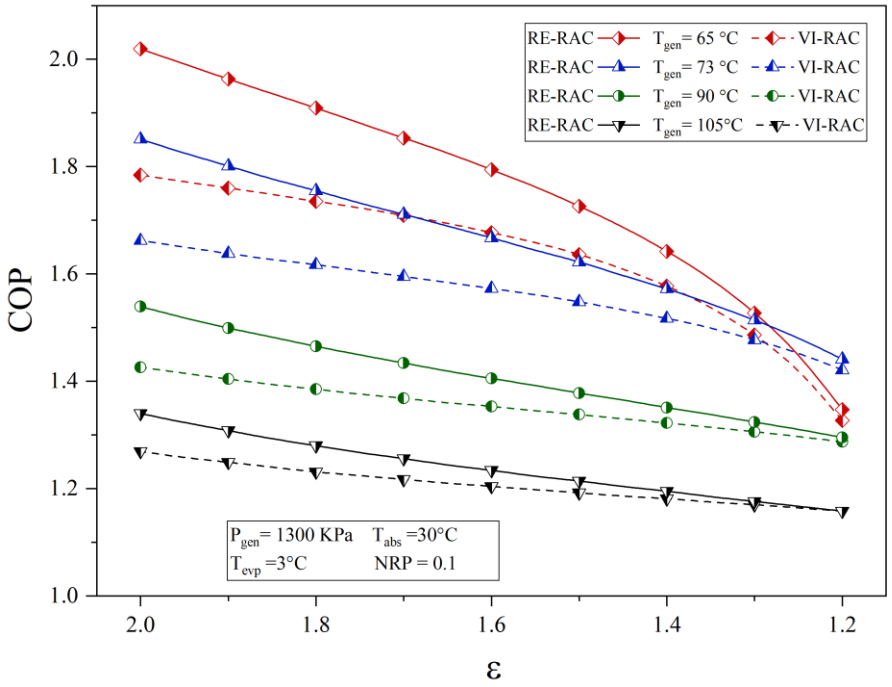

***Figure 6-56**: Impact of ε on COP of the proposed stand-alone recompression absorption systems at P_{gen} = 1300 kPa, T_{abs}= 30°C, T_{evp} = 3 °C and NPR = 0.1 for different T_{gen}.*

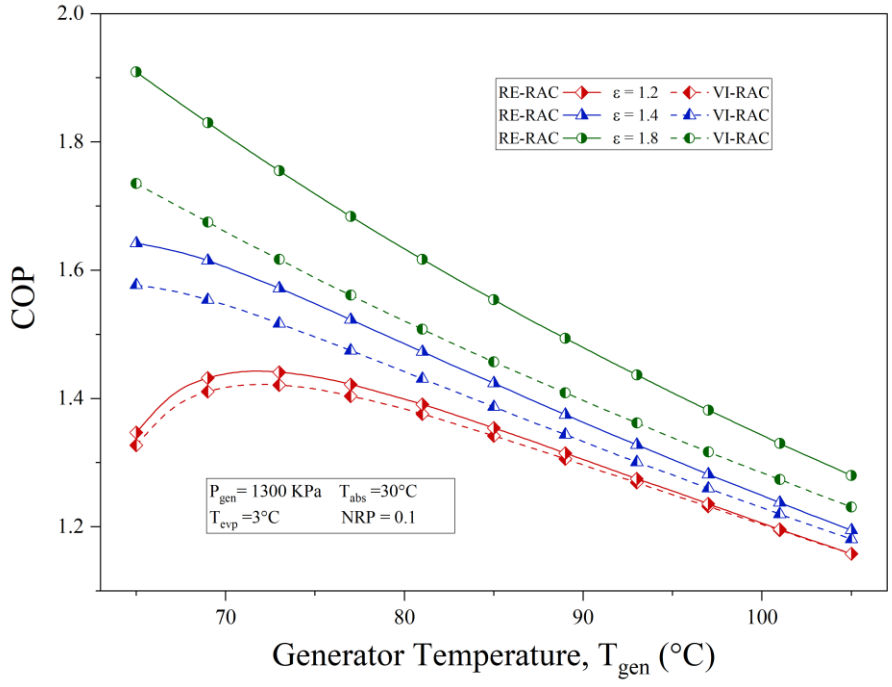

***Figure 6-57**: Impact of T_{gen} on COP of the proposed stand-alone recompression absorption systems at P_{gen} = 1300 kPa, T_{abs}= 30°C, T_{evp} = 3 °C and NPR = 0.1 for different ε.*

Systems with a lower T_{gen} exhibit a higher *COP* at elevated ε values as illustrated in **Figure 6-56**. But their declination rate with decreasing ε is also higher and if ε lowered beyond a limiting value, $\dot{Q}_{gen,ext}$ increases suddenly and causes rapid reduction of *COP*. For a T_{gen} of 67℃, this threshold is determined to be at ε= 1.5. In systems with a higher T_{gen}, while the *COP* might be lower, the threshold value of ε is also higher. **Figure 6-57** further demonstrates that systems with a higher ε value tend to have a superior *COP*. As T_{gen} increases, the *COP* escalates swiftly until it reaches an optimal point. Beyond this T_{gen}, $\dot{Q}_{gen}$ decreases at a minimal rate. And *COP* decreases at a consistent rate with increasing $\dot{W}_{comp}$. For smaller ε values, the optimal T_{gen} is on the higher end. However, as ε increases, this optimal T_{gen} value decreases.

Again, RE-RAC shows a significant enhancement over VI-RAC. This improvement is more pronounced for systems with elevated ε values, as depicted in **Figure 6-57**. As ε reduces, the disparity in *COP* between these two systems narrows, as illustrated in **Figure 6-56**. Moreover, for equivalent ε values, the difference is more significant in lower T_{gen} lines, as highlighted in **Figure 6-56**. As the T_{gen} value ascends, the relative superiority of RE-RAC over VI-RAC diminishes, as evidenced in **Figure 6-57**.

The combined effect of T_{evp} and recovery pressure ratio (ε) is illustrated in **Figure 6-58**. Both parameters exhibit analogous impacts on P_{abs}.

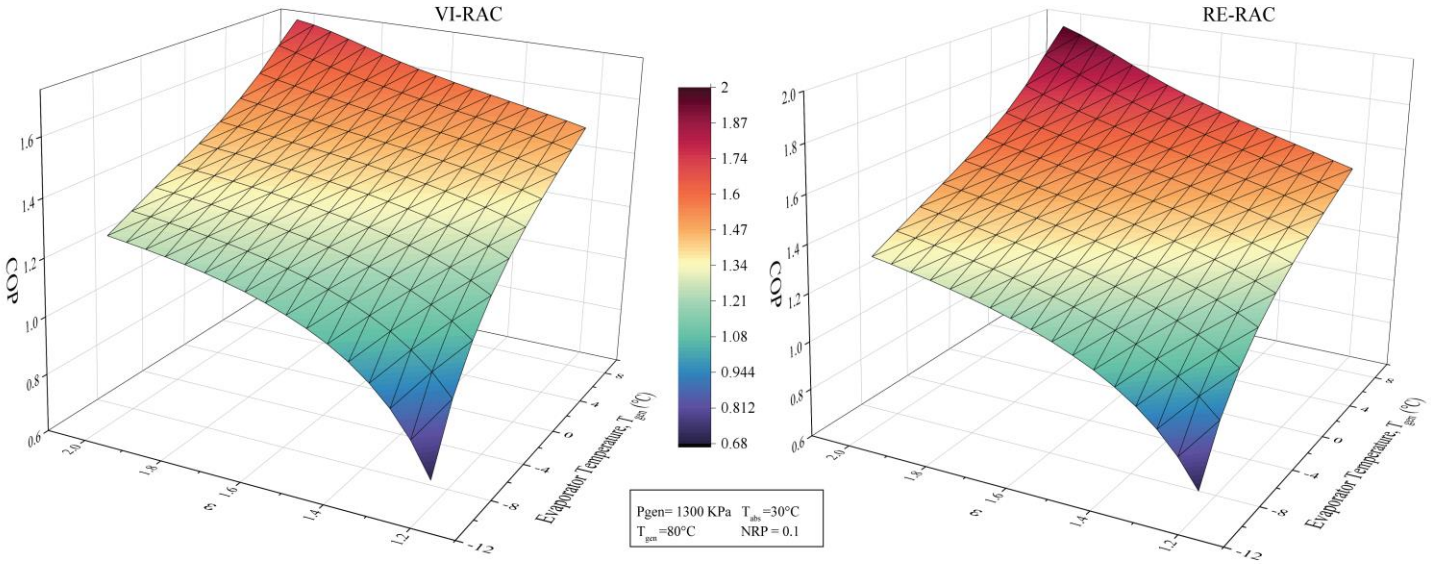

***Figure 6-58**: Impact of T_{evp} and ε on the 1st law efficiency of the proposed stand-alone recompression absorption systems at P_{gen} = 1300 kPa, T_{abs}= 30°C, T_{gen} = 80 °C and NPR = 0.1.*

Elevating either T_{evp} or ε, while holding the other variable constant, leads to an increase in P_{abs}, subsequently resulting in an enhancement of *COP*. However, the rate of increment with T_{evp} is more pronounced, exerting a more substantial influence on *COP* compared to ε, as observed in the 3D plot representing the T_{evp} – ε – *COP* relationship in **Figure 6-58.**

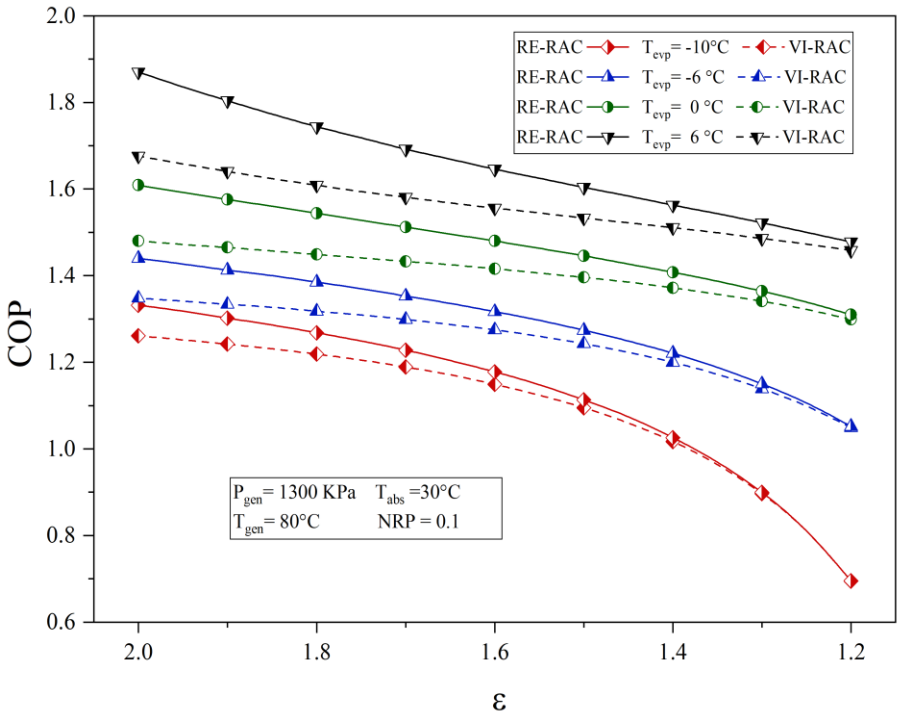

***Figure 6-59**: Impact of ε on COP of the proposed stand-alone recompression absorption systems at P_{gen} = 1300 kPa, T_{abs}= 30°C, T_{gen} = 80 °C and NPR = 0.1 for different T_{evp}.*

The results indicate that, if T_{evp} is to be lowered, in that case a higher value of ε has to be maintained otherwise *COP* will drop drastically, producing a limiting condition of operation. The relation is clarified in **Figure 6-59** and **Figure 6-60**. With a constant ε value of 1.8, elevating the T_{evp} from -10℃ to 6℃ in either system results in a near 1 kW increment in $\dot{W}_{comp}$. However, the required $\dot{Q}_{gen,ext}$ diminishes by approximately 2 kW, as depicted in **Figure 6-60**. Consequently, systems with a lower T_{evp} exhibit a reduced *COP*, as portrayed in **Figure 6-59.** Again, for T_{evp} = -10 ℃, $\dot{Q}_{gen,ext}$ increases in rapid manner with increasing ε compared to T_{evp} =6 ℃. This is why systems with lower T_{evp} exhibit a more rapid decline in *COP* compared to those with higher T_{evp} values.

RE-RAC demonstrates a notable improvement in *COP* over VI-RAC when operating at elevated values of ε and T_{evp}. As these parameters decrease, the magnitude of this enhancement diminishes swiftly. Specifically, at ε = 2 and T_{evp} = 6℃, the improvement stands at approximately 12%, while

at T_{evp} = -10°C, the enhancement is about 5%. However, when ε is reduced to 1.5, the enhancement for T_{evp} values of 6°C and -10°C decreases to roughly 5% and 1.5%, respectively. Thus, to fully capitalize on the benefits offered by RE-RAC, it is advisable for the system to operate at higher levels of ε and T_{evp}.

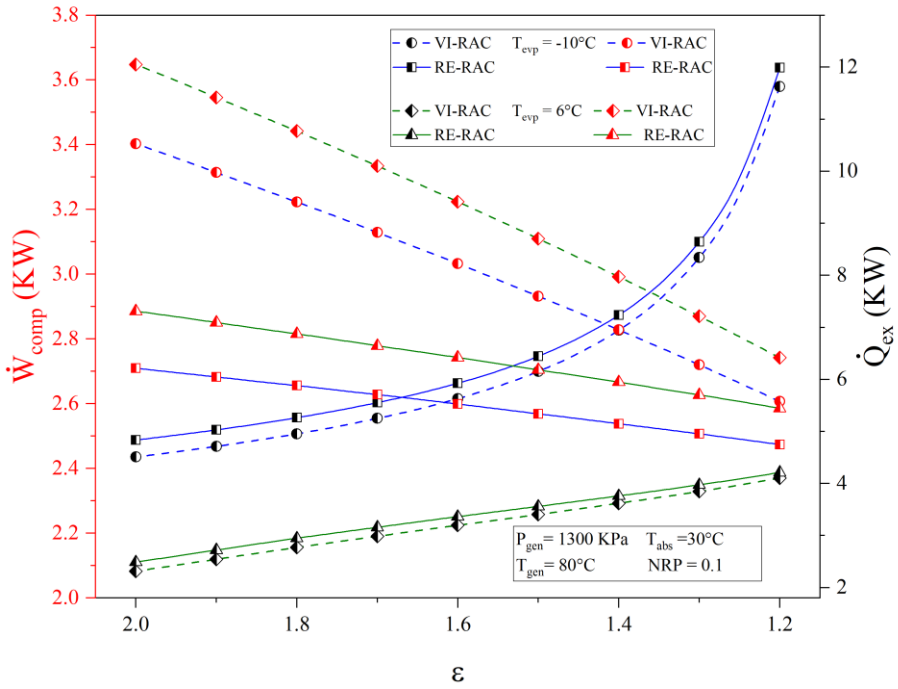

***Figure 6-60**: Impact of ε on compressor and generator external load of the proposed stand-alone recompression absorption systems at P_{gen} = 1300 kPa, T_{abs}= 30°C, T_{gen} = 80 °C and NPR = 0.1 for different T_{evp}.*

Impact of NPR and T_{abs}

The dynamic effect of *NPR* is illustrated in **Figure 6-61** and **Figure 6-63** for varying T_{gen} and T_{evp} respectively. As illustrated in **Figure 6-62** and **Figure 6-63(b)**, a higher *NPR* leads to an increase in the required $\dot{Q}_{gen,ext}$ and $\dot{W}_{comp}$, which consequently results in a decreased *COP*, as depicted in **Figure 6-61** and **Figure 6-63(a)**.

For systems operating at lower *NPR*, the maximum enhancement in *COP* over those with higher *NPR* is observed at the optimal T_{gen} as illustrated in **Figure 6-61**. Beyond this optimal T_{gen}, for lower *NPR*, $\dot{Q}_{gen,ext}$ and $\dot{W}_{comp}$ increases at a much higher rate than higher *NPR* systems as depicted in **Figure 6-62**. Hence beyond optimal T_{gen}, lower *NPR* systems have higher *COP* declination rate than higher *NPR* lines.

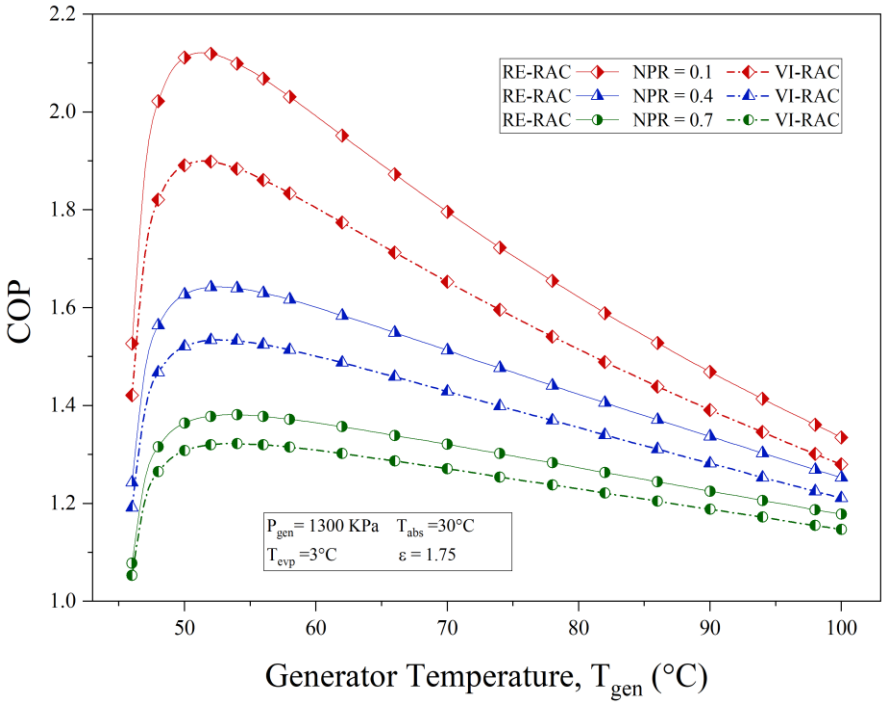

***Figure 6-61**: Impact of NPR on COP of the proposed stand-alone recompression absorption systems at P_{gen} = 1300 kPa, T_{abs}= 30°C, T_{evp} = 3°C and ε = 1.75 for varying T_{gen}.*

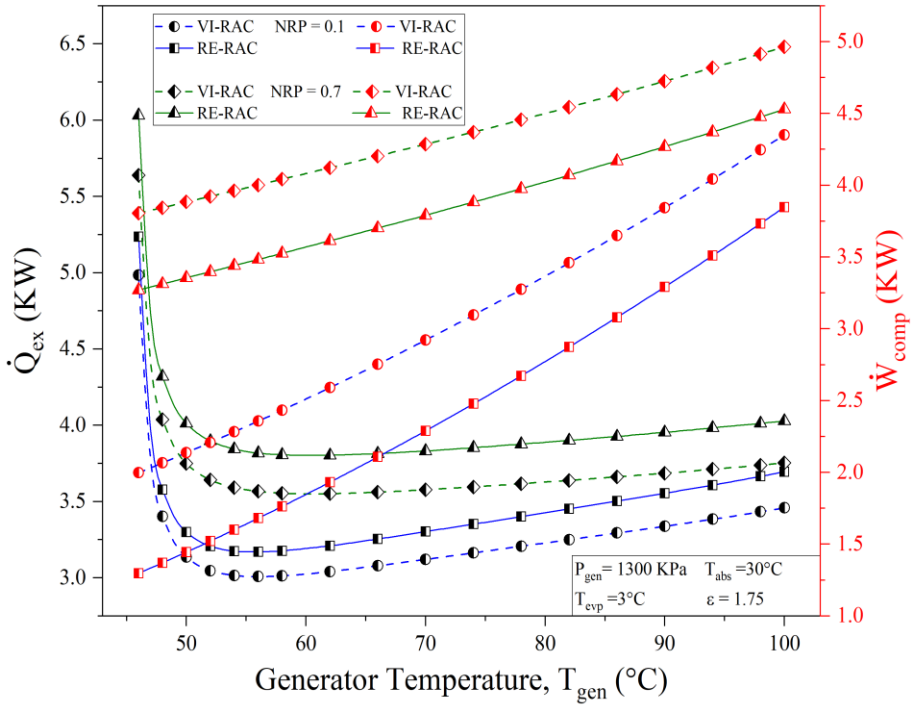

***Figure 6-62**: Impact of NPR on compressor and generator external load of the proposed stand-alone recompression absorption systems at P_{gen} = 1300 kPa, T_{abs}= 30°C, T_{evp} = 3°C and ε = 1.75 for varying T_{gen}.*

At this optimal T_{gen}, not only do the lower *NPR* systems display the highest *COP* enhancement over the higher *NPR* systems, but the RE-RAC also demonstrates a peak enhancement, approaching 35% over VI-RAC at lower *NPR* of 0.1 and optimal T_{gen} of 53 °C. With both *NPR* and T_{gen} increasing, this enhancement between the systems decreases. Furthermore, *NPR* influences the optimal T_{gen} as well; an increase in *NPR* from 0.1 to 0.7 results in a slight elevation of the optimal T_{gen} by approximately 3-4°C, attributable to the dynamic interaction of $\dot{Q}_{gen,ext}$ and $\dot{W}_{comp}$.

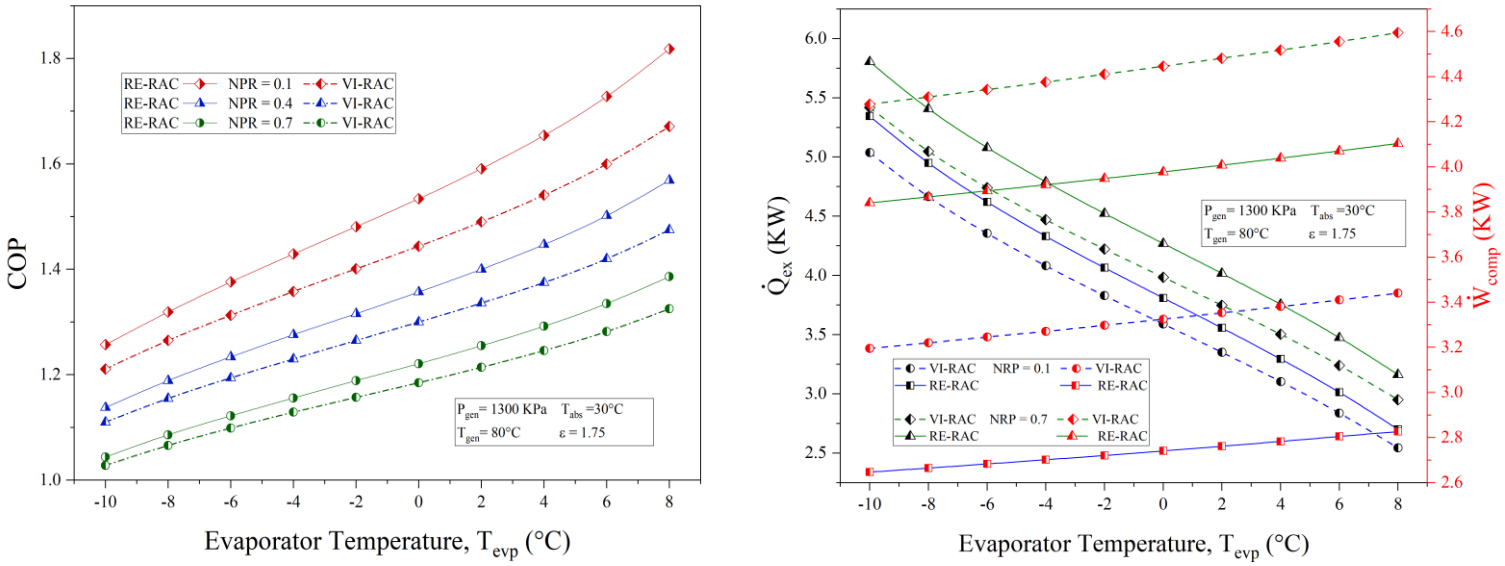

***Figure 6-63**: Impact of NPR on the performance of proposed stand-alone recompression absorption systems at P_{gen} = 1300 kPa, T_{abs}= 30°C, T_{gen} = 80 °C and ε = 1.75 for varying T_{evp}.*

The sensitivity of *NPR* with T_{evp} of the proposed stand-alone RAC systems is discussed in **Figure 6-63.** Lower *NPR* systems have higher *COP*. With T_{evp} increasing, $\dot{Q}_{gen,ext}$ decreases at higher rate than $\dot{W}_{comp}$ increasing. Leading to an elevation in *COP*. But, for lower *NPR*, the rate of decreasing $\dot{Q}_{gen,ext}$ is higher, hence the incremental rate of lower *NPR* systems is higher compared to higher *NPR* lines. Additionally, RE-RAC also shows significantly higher *COP* compared to VI-RAC for lower *NPR*. At a set T_{evp} of 0°C, for *NPR* of 0.7, RE-RAC shows about a 5% improvement. But at a lower *NPR* of 0.1, this improvement jumps to 20%. This improvement becomes more noticeable as T_{evp} increases. As T_{evp} rises from -10°C to 8°C for an *NPR* of 0.1, the improvement range expands from 5% to 35%.

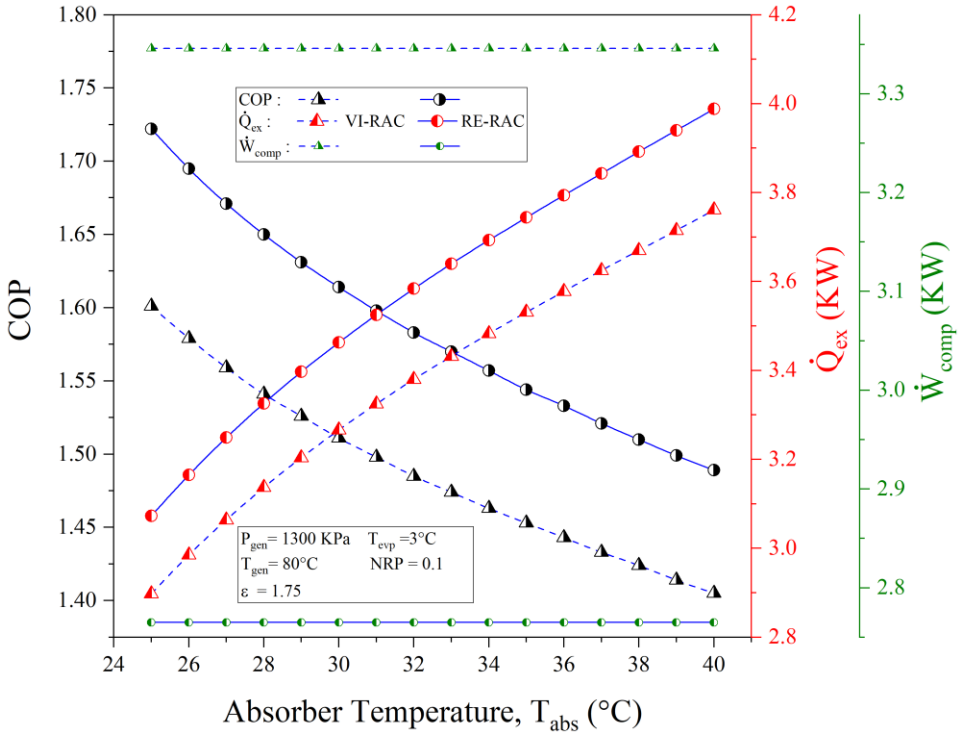

***Figure 6-64**: Impact of T_{abs} on COP, compressor and generator external load of the proposed stand-alone recompression absorption systems at P_{gen} = 1300 kPa, T_{abs}= 30°C, T_{evp} = 3 °C, T_{gen} = 80 °C and ε = 1.75.*

The effect of T_{abs} on system performance of the proposed advanced RAC is shown in **Figure 6-64** As shown in the figure, although RE-RAC has near 0.5KW higher $\dot{Q}_{gen,ext}$ over VI-RAC, but it has near 1.4 kW less $\dot{W}_{comp}$. Consequently, across the range of T_{abs}, RE-RAC consistently demonstrates a superior *COP* compared to VI-RAC. As T_{abs} increases, the required $\dot{W}_{comp}$ remains unchanged due to the constant P_{gen} and *NPR* values. However, with an increase in T_{abs}, x_{strong} diminishes, leading to a decrease in Δx_{NH_3}. This results in an escalation of both required $\dot{Q}_{gen}$ and $\dot{Q}_{abs}$, causing a subsequent reduction in *COP*. Increasing T_{abs} from 25℃ to 40 ℃, results in near 16% decrease of *COP*. Again, with T_{abs} increasing, the $\dot{Q}_{gen,ext}$ increasing rate of RE-RAC is slightly higher than VI-RAC, hence the *COP* difference between these systems also decreases slightly with increasing T_{abs}.

6.3.3 Exergy Analysis of the Advanced Stand-alone RAC Systems

Similar to energy, exergy is also highly affected by the boundary parameters of T_{gen}, P_{gen}, T_{evp}, ε and T_{evp}. The dynamic interaction between them allows exergy destruction in different components to increase and decrease. Ultimately an optimal lowest value of total exergy destruction rate can be found because of this change in component exergy destruction.

Impact of P_{gen} and T_{gen}

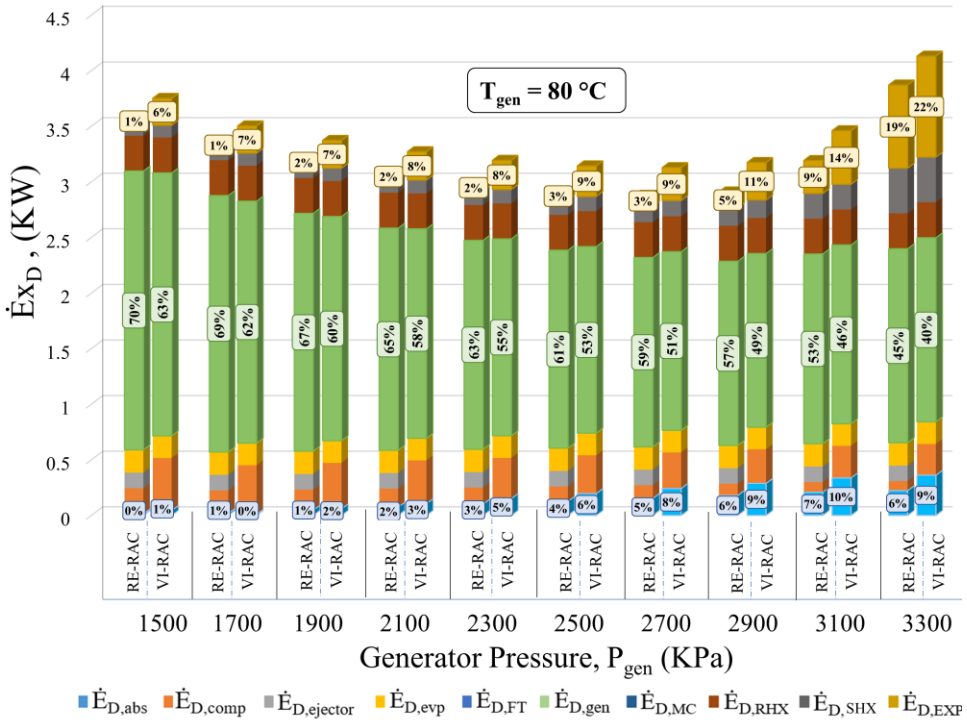

***Figure 6-65**: Impact of P_{gen} on the exergy destruction rate of the proposed stand-alone recompression absorption systems at T_{evp}= 6°C, T_{abs} = 30 °C, ε = 1.75 and NPR = 0.1 for T_{gen} = 80°C.*

As **Figure 6-65** shows, With P_{gen} increasing, the exergy destruction rate in most components increases in near linear ratio, apart from the generator and absorber. With an increase in P_{gen}, more useful energy becomes available for use in the generator, leading to a decrease in exergy destruction rate across the generator, $\dot{E}x_{D,gen}$.

However, a higher P_{gen} results in an increased concentration of x_{weak}. Given that the x_{strong} remains constant for a fixed absorber temperature (T_{abs}), an increase in x_{weak} leads to a higher rate of exergy release and destruction rate in absorber, labelled $\dot{E}x_{D,abs}$. At lower P_{gen} values, the rate of decrease in $\dot{E}x_{D,gen}$ is predominant over the rate of increase in $\dot{E}x_{D,abs}$, resulting in an overall decline

in the total exergy destruction rate. However, this trend reverses at higher P_{gen}, indicating the existence of an optimal P_{gen} where the system experiences minimal total exergy destruction rate and, consequently, maximum exergy efficiency.

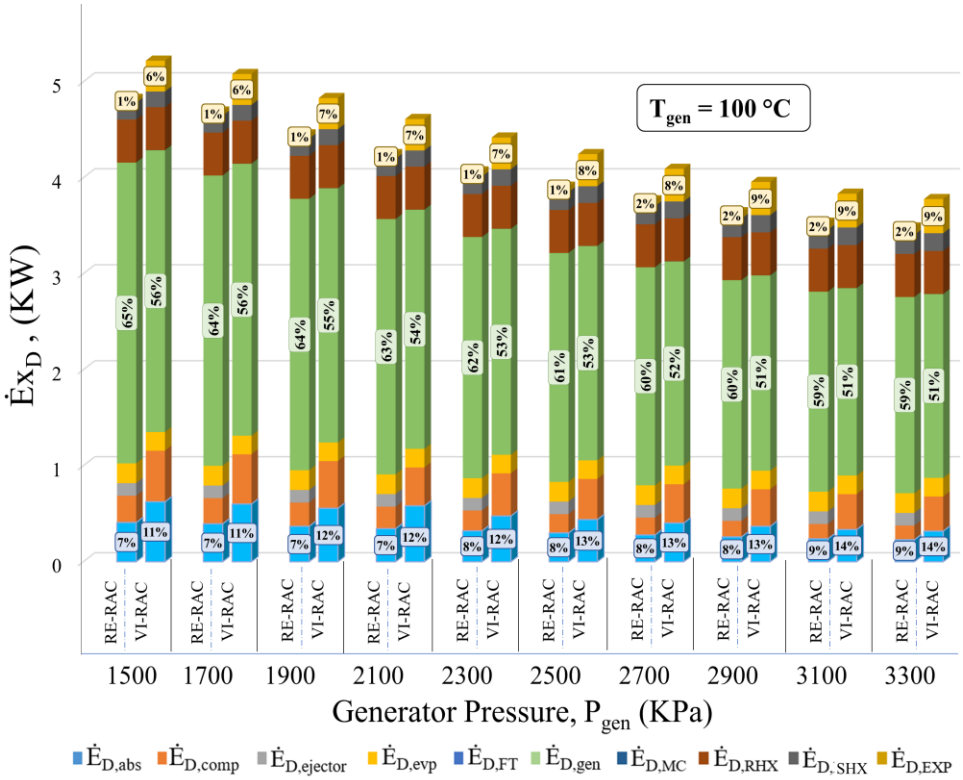

***Figure 6-66**: Impact of P_{gen} on the exergy destruction rate of the proposed stand-alone recompression absorption systems at T_{evp}= 6°C, T_{abs} = 30 °C, ε = 1.75 and NPR = 0.1 for T_{gen} = 100°C.*

As seen from **Figure 6-65,** for T_{gen}= 80°C, the lowest $\dot{E}x_{D,tot}$ of the systems is identified at 2500 kPa, whereas for T_{gen}= 80°C, the optimum P_{gen} for lowest $\dot{E}x_{D,tot}$ increases to near 3500 kPa as shown in **Figure 6-66**. Additionally, it is also noted that higher T_{gen} results in higher $\dot{E}x_{D,tot}$ for the same range of P_{gen}.

Moreover, a significant difference between $\dot{E}x_D$ of different components can be noticed for RE-RAC and VI-RAC. Although, RE-RAC has higher $\dot{E}x_{D,gen}$ compared to VI-RAC because of higher $\dot{Q}_{gen}$. But, VI-RAC has an additional compressor, hence a much larger value of $\dot{E}x_{D,comp}$. Both $\dot{E}x_{D,abs}$ and $\dot{E}x_{D,exp}$ for VI-RAC is also higher. Consequently, RE-RAC displays a reduced $\dot{E}x_{D,tot}$ in comparison to VI-RAC. This reduction of the $\dot{E}x_{D,tot}$ of RE-RAC over VI-RAC also changes with P_{gen} and T_{gen}. As P_{gen} rises, the disparity narrows until an optimal P_{gen} is attained. Beyond this point, a further increase in generator pressure primarily affects $\dot{E}x_{D,exp}$, widening the gap in $\Delta\dot{E}x_{D,tot}$

between the systems. Notably, as illustrated in **Figure 6-66,** at a higher generator temperature of 100℃ and within the same P_{gen} range, the reduction in $\dot{E}x_{D,tot}$ for RE-RAC relative to VI-RAC is more significant than at T_{gen} = 80℃ as illustrated in **Figure 6-65** .

Impact of T_{evp} and T_{gen}

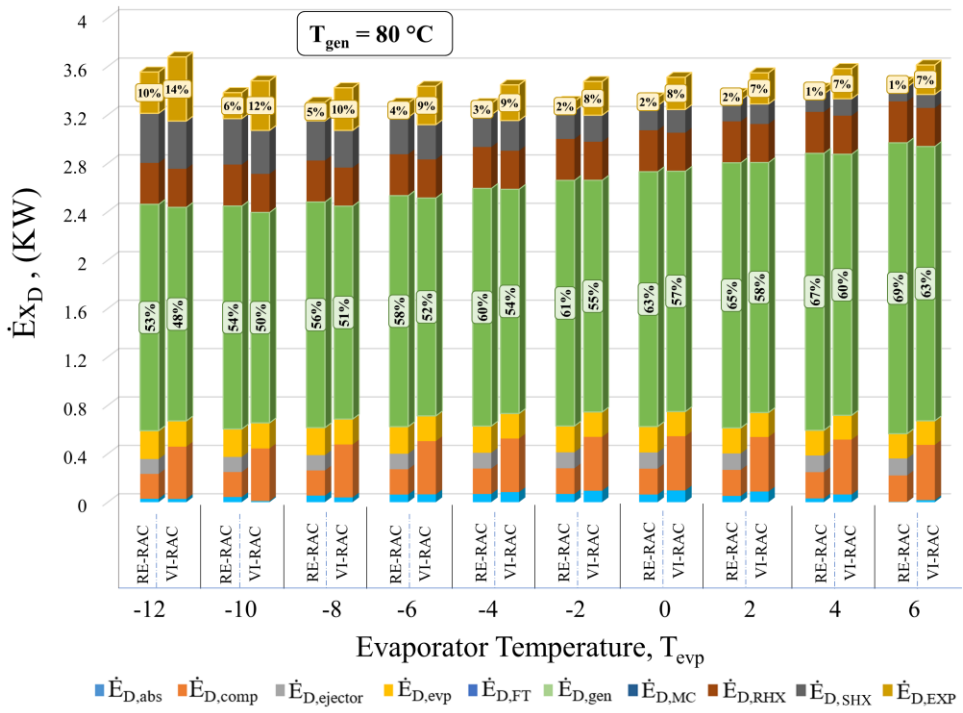

***Figure 6-67**: Impact of T_{evp} on the exergy destruction rate of the proposed* stand-alone *recompression absorption systems at P_{gen}= 1600 kPa, T_{abs} = 30 °C, ε = 1.75 and NPR = 0.1 for T_{gen} = 80°C.*

Figure 6-67 explains the effect of T_{evp} on total as well as component wise exergy destruction rate. With T_{evp} increasing, the total $\dot{m}$ increases, hence required $\dot{Q}_{gen}$ increases for either system. As a result, $\dot{E}x_{D,gen}$ also increases. But as with T_{evp} increasing, pressure ratio across generator and evaporator also decreases. Hence, associated exergy loss in expansion valve, SHX and RHX also decreases with T_{evp} increasing. So, there exists an optimal T_{evp} where the system experiences minimal total exergy destruction rate and, consequently, maximum exergy efficiency.

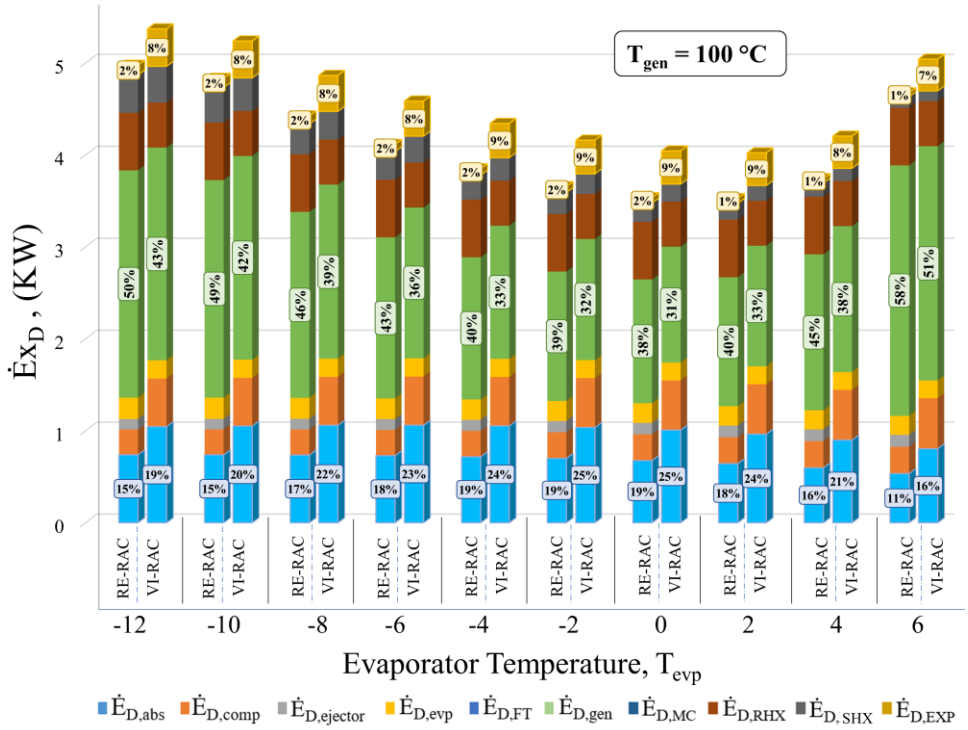

***Figure 6-68**: Impact of T_{evp} on the exergy destruction rate of the proposed* stand-alone *recompression absorption systems at P_{gen}= 1600 kPa, T_{abs} = 30 °C, ε = 1.75 and NPR = 0.1 for T_{gen} = 100°C.*

As seen from **Figure 6-67**, for T_{gen} = 80°C, the optimal T_{evp} for lowest $\dot{E}x_{D,tot}$ is around -6°C. Whereas, for for T_{gen}=100°C, the optimal T_{evp} is around 0°C as shown in **Figure 6-68**. So, with T_{gen} increasing, the optimal value for T_{evp} also increases. Additionally, with T_{evp} increasing, the $\Delta\dot{E}x_{D,tot}$ between RE-RAC and VI-RAC remains near consistent in **Figure 6-67**. But with T_{gen} increasing from 80 to 100 °C, the reduction in $\dot{E}x_{D,tot}$ for RE-RAC relative to VI-RAC is more significant similar to **Figure 6-66** as illustrated in **Figure 6-68**. And maximum $\Delta\dot{E}x_{D,tot}$ of near 8% is observed at the optimal T_{evp}. Beyond this T_{evp}, the gap widens.

Impact of ε and NPR

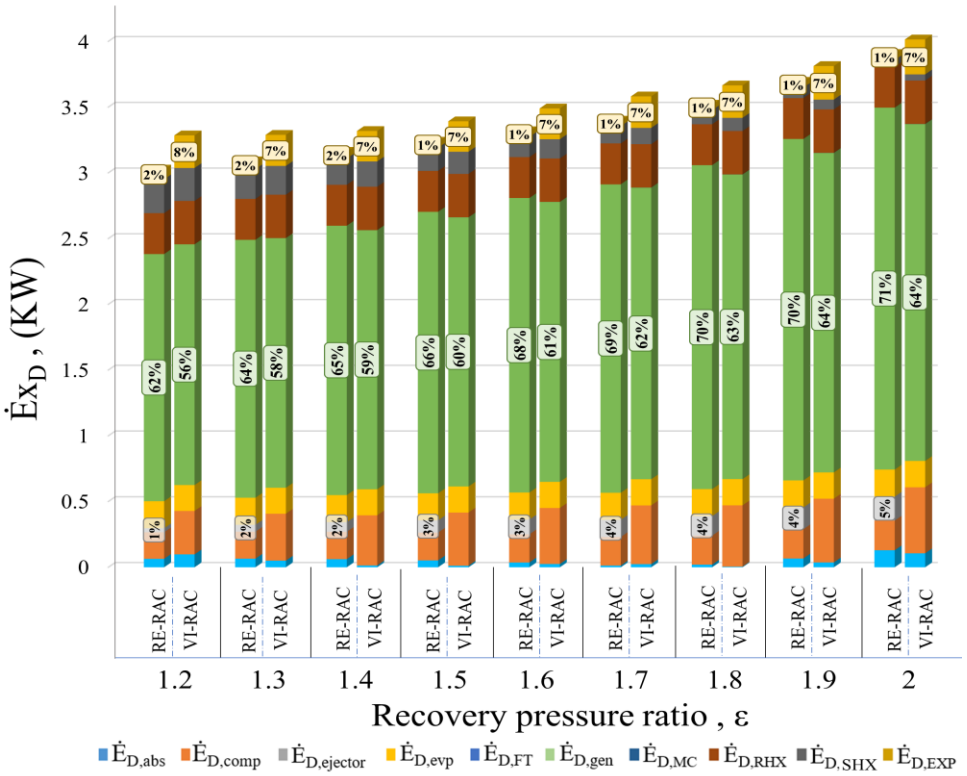

***Figure 6-69**: Impact of ε on the exergy destruction rate of the proposed stand-alone recompression absorption systems at P_{gen}= 1600 kPa, T_{abs} = 30 °C, T_{gen} = 80 °C and NPR=0.1*

Figure 6-69 illustrates the influence of ε on $\dot{E}x_{D,tot}$. Its effect closely mirrors that of T_{evp}. However, when T_{evp} is held constant, an increase in ε impacts only the solution stream side. As a result, $\dot{E}x_{D,tot}$ rises sharply beyond a specific ε value. With an increase in ε, the corresponding x_{strong} also escalates, leading to a rise in $\dot{E}x_{D,gen}$. At lower ε, the increase rate of $\dot{E}x_{D,tot}$ is small, but at higher value of ε, $\dot{E}x_{D,tot}$ increases at a higher rate. Again for RE-RAC, $\dot{E}x_{D,ejector}$ increases with increasing ε for the same T_{evp}. This ultimately results in decrease of $\Delta\dot{E}x_{D,tot}$ between RE-RAC and VI-RAC with increasing ε.

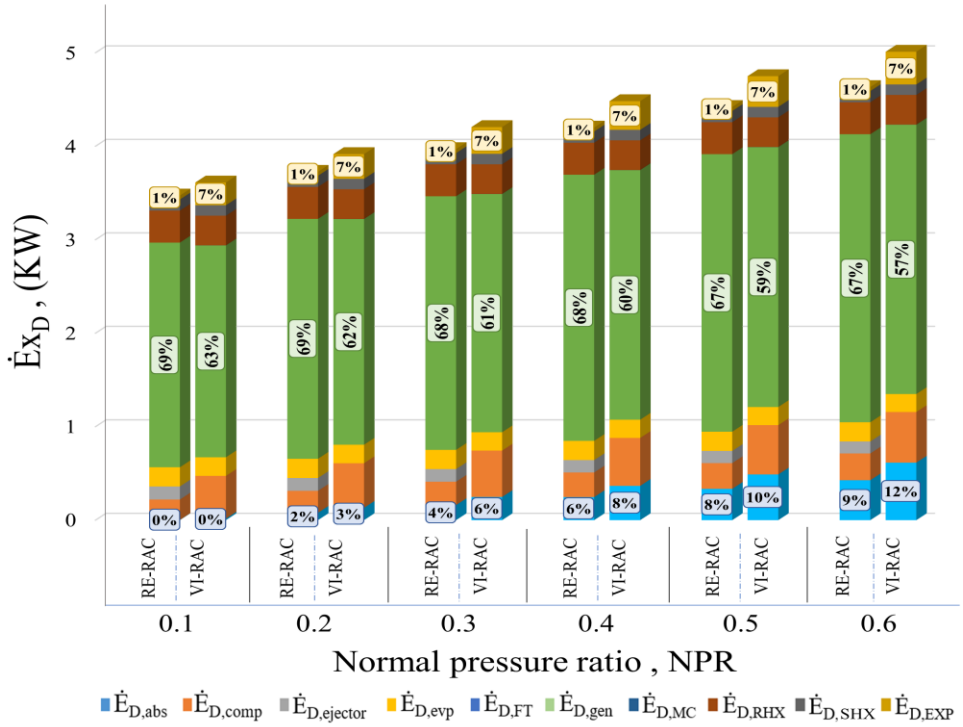

Figure 6-70 *Impact of NPR on the exergy destruction rate of the proposed recompression absorption systems at P_{gen}= 1600 kPa, T_{abs} = 30 °C, T_{gen} = 80 °C and ε=1.75*

Figure 6-70 displays the effect of *NPR* on $\dot{E}x_{D,tot}$. With *NPR* increasing, the pressure ratio across the recompression increases, hence the quality of vapor after recompression increases. As a result, the relative useful energy loss across gen-cond $\dot{E}x_{D,gen}$ decreases. But, associated $\dot{E}x_{D,comp}$ also increases. Due to *NPR* increasing, $\dot{E}x_{D,abs}$ also increases at higher rate than the decrease of $\dot{E}x_{D,gen}$. As result, with *NPR* increasing the total $\dot{E}x_{D,tot}$ increases at linear increment. The $\Delta\dot{E}x_{D,tot}$ between RE-RAC and VI-RAC also increases in a linear manner with *NPR*.

6.3.4 Multi-objective Optimization

In an effort to minimize run time and curtail additional computational expenses, the elaborated simulation model of the advanced stand-alone recompression absorption systems (RE-RAC and VI-RAC) has been simulated 756 times on corresponding sets of unique input data to formulate the ANN based objective functions of the corresponding refrigeration system. This objective function is integrated with the optimization algorithm rather than the simulation code, this results in reduction of significant runtime with added flexibility. The structure of ANN and optimization framework is presented in **Figure 6-71**.

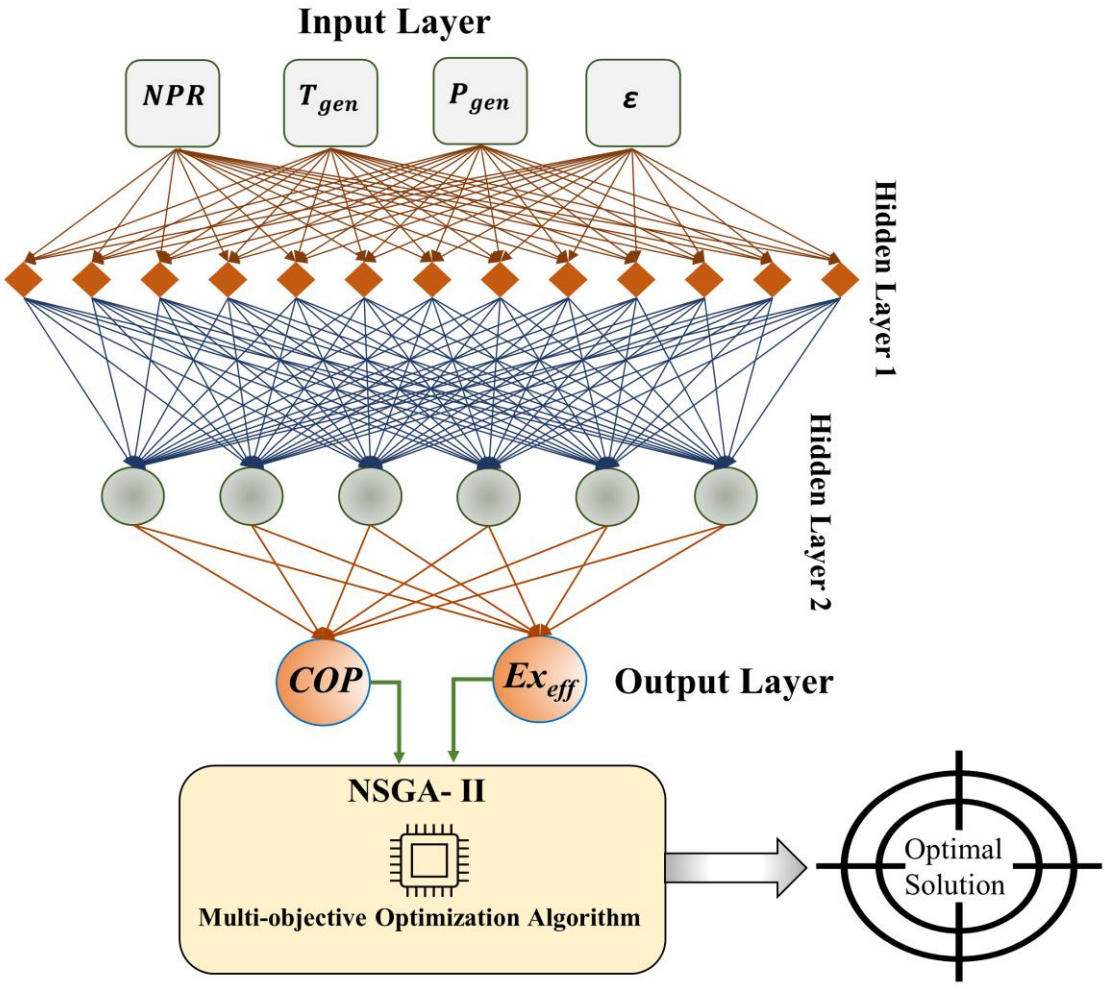

***Figure 6-71**: The outline of the optimization methodology using ANN prediction model of the proposed advanced stand-alone RAC systems.*

Four distinct input variables (T_{gen}, P_{gen}, NPR, ε) and two output variables (COP, Ex_{eff}) from the 756 rows of simulation data have been employed to establish the ANN-based prediction model objective function of each proposed stand-alone systems (VI-RAC and RE-RAC). The training is

implemented using the Bayesian regularization algorithm on a dataset consisting of approximately 80% of data, while a testing set comprised the remaining (approximately 20%). The selected ANN model was a two-layer feedforward network featuring 100 sigmoid hidden neurons and linear output neurons. This strategic configuration underscores the model's capacity for processing and analyzing the intricate relationships between the defined input and output variables, thus reinforcing the reliability and accuracy of the predictive model developed through this rigorous approach.

Optimization Strategy and Variables

One of the common optimization methods for the proposed cycles is the genetic algorithm (GA), which can explore multiple solutions at the same time by using a population of solutions. A specific type of GA is the Non-dominated Sorting Genetic Algorithm II (NSGA-II), which is a powerful multi-criteria evolutionary algorithm that is often used to improve energy systems. It has some advantages, such as its robustness and fast population distance estimation, but it also has a drawback of being slow in its operation.

This work uses the optimization toolbox in MATLAB software to optimize the objective functions developed in ANN to maximize *COP* and exergy efficiency for 4 controllable variables of the advanced stand-alone RAC systems (RE-RAC and VI-RAC). The chosen values for different parameters in MATLAB optimization toolbox and the range of input controllable variables are given in **Table 6-19.**

Table 6-19. *Selected Values for different parameters of Multi objective optimization algorithm of proposed stand-alone recompression absorption systems.*

Specified Options		Selected Value
Population Size		200
Creation Function		Constraint Dependent
Crossover	function	Intermediate
	ratio	1
Migration	fraction	0.20
	direction	forward
Mutation	probability	Constraint dependent
	function	0.10
Population fraction of the Pareto Front		0.35
	constraint	10^{-3}

Max. Tolerance	function	10^{-4}
Generator-Condenser temperature,	T_{gen}	*45 ℃ to 110 ℃*
Generator-Condenser pressure	P_{gen}	*1000 to 3000 kPa*
Normal pressure ratio in compressor	***NPR***	*0 to 0.8*
Evaporator recovery pressure	ε	*1.2 to 1.8*

Decision Making and Optimization Result

In multi-objective optimization, the Pareto frontier is a curve that showcases an array of optimal solutions. Each point on this frontier stands as a testament to an optimal trade-off between competing objectives. On this frontier, the point farthest to the left indicates the scenario with the highest COP (point A), while the point farthest to the right (point C) shows the scenario with the best Exergy Efficiency (*COP*). To determine the most balanced optimal solution that takes both *COP* and exergy efficiency (Ex_{eff}) into account, one can look for the point that is closest to the ideal scenario by measuring geometric distance, or furthest from the least desirable scenario. In this analysis, TOPSIS decision making technique is employed to find the most optimal solution (point B) considering both output perspective. This balanced approach ensures a comprehensive consideration of the multiple facets of energy optimization, leading to a more informed and holistic decision-making process.

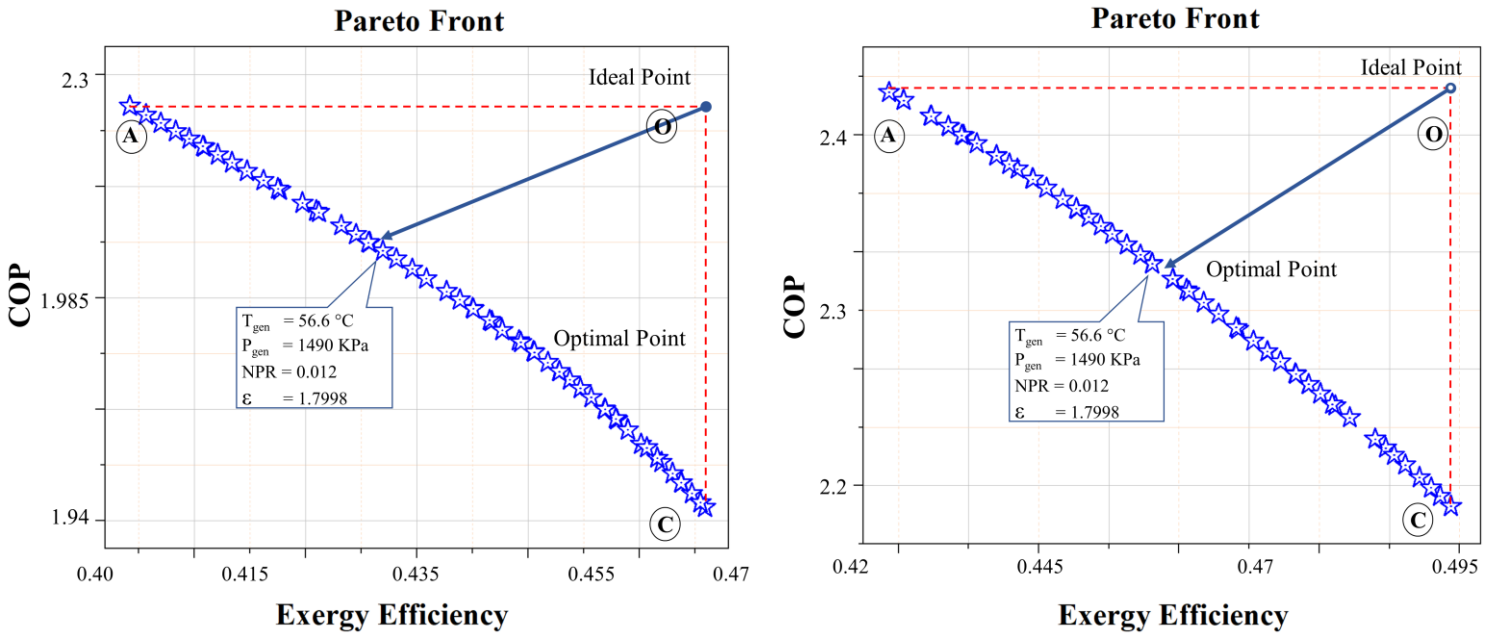

***Figure 6-72**: Pareto front of Ga-multi objective optimization of the proposed systems, (a) VI-RAC and (b) RE-RAC to find the optimal solution using TOPSIS at T_{evp} = 4℃ and T_{abs} = 30℃.*

The illustration in **Figure 6-72** presents the Pareto front of optimization solutions for two proposed models at an evaporator temperature (T_{evp}) and absorber temperature (T_{abs}) of 4°C and 30°C respectively. This Pareto front highlights all the points that represent optimal solutions, with particular emphasis on point A and B which denote the optimal solutions from the perspectives of maximizing the Coefficient of Performance (*COP*) and exergy efficiency, respectively. For a maximum value of ε = 1.8 and minimum value of *NPR* = 0.01 the optimal points for both COP and exergy efficiency (Ex_{eff}) maximization occur.

From both the *COP* and Ex_{eff} perspectives, an optimal value for generator temperature (T_{gen}) and pressure (P_{gen}) exists to maximize performance. However, this optimal boundary condition varies between energy and exergy perspectives. Hence, an optimal value of performance is obtained with a tradeoff at a mid-operating conditions compared to previous cases. Furthermore, RE-RAC shows significant performance improvement over VI-RAC, although the optimal operating conditions between these systems do not significantly differ across all scenarios. This is why, maximum *COP* condition of point A, is obtained at T_{gen} = 55℃, P_{gen} = 1333 kPa, ε=1.79 and *NPR* = 0.017 around, and the values of max COP are 2.25 and 2.429 for VI-CRAC and RE-CRAC respectively. Whereas, maximum Ex_{eff} condition of point B, is obtained at T_{gen} = 58℃, P_{gen} = 1667 kPa, ε=1.79 and *NPR* = 0.013 around, and the values of max Ex_{eff} are 0.4687 and 0.4894 for VI-RAC and RE-RAC respectively. The optimal condition is determined by TOPSIS technique, and the optimum value of *COP*: 2.051 and 2.339, Ex_{eff} = 0.4313 and 0.449 for VI-RAC and RE-RAC respectively at T_{gen} = 56.5℃, P_{gen} = 1490 kPa, ε=1.7998 and *NPR* = 0.012 around. The comparison of performance metrics along with optimal parameters of performance from different scenarios is provided in **Table 6-20** in details.

***Table 6-20**: Optimization Results for VI-RAC* and RE-RAC *configuration*s at T_{evp} *= 4℃ and* T_{abs} *= 30℃.*

Input Parameters	**Units**	**Multi-Objective Optimization Scenarios**					
		(a) Max. *COP*		**(b) Optimal**		**(c) Max. Ex_{eff}**	
		RE-RAC	**VI-RAC**	**RE-RAC**	**VI-RAC**	**RE-RAC**	**VI-RAC**
Generator Temperature, T_{gen}	°C	55		56.6		58	
Generator Pressure, P_{gen}	°C	1333		1490		1667	
Normal pressure ratio, NPR		0.017		0.012		0.01	
Evaporator recovery pressure ratio, ε		1.7995		1.7998		1.7997	
Output Parameters							
Evaporator Load, $\dot{Q}_{evp}$	kW	10	10	10	10	10	10
Generator Load, $\dot{Q}_{gen}$	kW	13.81	13.14	13.86	13.18	14.05	13.35
Generator External Load, $\dot{Q}_{cond}$	kW	2.951	2.808	3.25	3.09	3.694	3.511
Generator Internal Load, $\dot{Q}_{evp}$	kW	10.86	10.33	10.61	10.09	10.35	9.84
Absorber Rejection, $\dot{Q}_{abs}$	kW	14.77	14.39	14.8	14.39	14.83	14.4
Compressor Load, $\dot{W}_{comp}$	kW	1.176	1.914	1.031	1.775	0.886	1.637
Pump Load, $\dot{W}_{pump}$	kW	0.0073	0.007	0.011	0.011	0.020	0.019
Coefficient of performance, *COP*		2.429	2.25	2.339	2.051	2.183	1.94
Pressure ratio, R_p		2.018	2.018	1.87	1.87	1.731	1.731
Exergy destruction, $\dot{E}_{D,total}$	kW	2.503	2.829	2.436	2.774	2.428	2.745
Exergetic efficiency, η_{II}		.4227	.4017	0.449	0.4313	0.4894	0.4687

6.3.5 Section Summery

This section of the analysis presents a comprehensive investigation into enhancing the efficiency of absorption refrigeration systems by introducing a novel single-effect absorption framework that integrates ejector-injection and recompression technologies within (RE-RAC and VI-RAC). Unlike traditional cascading methods discussed in previous sections, this innovation permits the stand-alone RAC systems to operate at lower evaporator temperatures due to ejector-injection incorporation at the refrigerant side while simultaneously achieving a higher COP due to recompression technology employed in the generator.

Further, the section delves into the development and analysis of these improved stand-alone recompression sub-systems: Refrigerant Ejector Enhanced Recompression Absorption Cycle (RE-RAC) and Vapor Injection Enhanced Recompression Absorption Cycle (VI-RAC) systems. These systems enhance efficiency by replacing the conventional single-valve expansion with ejector and vapor injection techniques, thus recovering lost energy and allowing refrigerant to enter the absorber at higher pressures. Furthermore, this section conducts a detailed analysis comparing proposed recompression absorption systems to conventional ones under various operating conditions, focusing on key performance metrics like *COP*, Ex_{eff}, exergy destruction, compressor load, and heat requirements. It examines the impact of different parameters on system performance, enhancing understanding of the advanced stand-alone RAC systems. Additionally, it utilizes an ANN model combined with a Genetic Algorithm for multi-objective optimization, identifying optimal operational conditions to explore feasibility and set the stage for further research. The results of the thorough theoretical investigation based on 1st and 2nd law of thermodynamics and the multi-objective optimization are as follows:

- Under similar operating conditions the *COP* of RE-RAC and VI-RAC is 76% and 63% higher than the conventional RAC system, respectively. Compared to SE-RAC, they show a 28% and 19% *COP* increase. Although RE-RAC needs more $\dot{Q}_{gen,ext}$ to operate, its higher *COP* is due to VI-RAC's added compressor and much greater $\dot{W}_{comp}$ requirement.

- As T_{gen} rises, *COP* rapidly increases to an optimal value, then declines in a slower rate. Higher T_{evp} results in a lower optimal T_{gen}, with a steeper *COP* decrease rate. Conversely, a lower T_{evp} raises the optimal T_{gen} value. The peak *COP* advantage of RE-RAC over VI-RAC is at this optimal T_{gen}.

- As T_{evp} drops, system *COP* declines. The decrease is sharper for lower T_{gen}, with a surge in required $\dot{Q}_{gen}$ leading to a significant *COP* fall below a certain T_{evp}. At higher T_{gen}, *COP*'s decline is gradual, and its critical point occurs at a notably lower T_{evp}. The *COP* advantage of RE-RAC over VI-RAC also diminishes with decreasing T_{evp}. For T_{gen} = 67°C, RE-RAC has a 35% higher COP than VI-RAC at T_{evp} = 8°C, but this narrows to 5% at -10°C T_{evp}.

- Adjusting P_{gen} identifies an optimal value for peak *COP*. As T_{gen} and T_{evp} decreases, this optimal value of P_{gen} drops. Lower T_{gen} offers better *COP* but decreasing T_{evp} and increasing

P_{gen} complicates low T_{gen} systems. Moreover, for lower T_{evp}, the optimal P_{gen} is also lower. Increasing P_{gen} further results in rapid *COP* drop. Additionally, RE-RAC's advantage over VI-RAC lessens with increasing P_{gen}.

- Lowering ε or increasing *NPR* reduces *COP*. For systems with lower T_{gen} or T_{evp}, this decline is more pronounced. Higher ε systems have a lower optimal T_{gen}. The rate of *COP* decrease with ε is faster for systems with lower T_{evp}. RE-RAC's advantage over VI-RAC also diminishes as ε drops.

- As *NPR* increases, *COP* drops. Lower NPR systems experience a steeper *COP* decline with rising T_{gen} and falling T_{evp}. The most significant *COP* variance between *NPR* systems is at optimal T_{gen} and highest T_{evp}, where RE-RAC outperforms VI-RAC the most. This advantage diminishes with increasing NPR.

- RE-RAC has lower $\dot{E}x_{D,tot}$ than VI-RAC due to fewer components. As T_{gen} rises, both systems' $\dot{E}x_{D,tot}$ and the gap $\Delta\dot{E}x_{D,tot}$ between them grow. Higher T_{gen} shifts optimal values for P_{gen} and T_{evp} for minimal $\dot{E}x_{D,tot}$. The difference in $\Delta\dot{E}x_{D,tot}$ between systems is most pronounced at optimal conditions.

- With a fixed operating condition, rising ε boosts $\dot{E}x_{D,tot}$, but RE-RAC's $\dot{E}x_{D,ejector}$ incremental rate is notable, narrowing the gap ($\Delta\dot{E}x_{D,tot}$) with VI-RAC. Meanwhile, higher *NPR* increases both systems' $\dot{E}x_{D,tot}$ and their difference.

Chapter 7: Conclusion

This comprehensive study signifies a notable advancement in refrigeration technology, particularly within the domain of cascade compression-absorption refrigeration systems and the advancement of Absorption Refrigeration Cycles (ARC). The primary aim of the research is **"to enable the absorption system to operate at reduced evaporator temperatures with higher performance"**. To accomplish this goal, initially the study focuses on the development and simulation of sophisticated cascade compression-absorption refrigeration setups. Hence, a modified Absorption Refrigeration Cycle (ARC) is combined with an improved Vapor Compression Refrigeration (VCR) system, leading to the development of advanced systems like the Ejector injection compression absorption cycle (EICAC) and Ejector compression absorption cycle (ECAC) systems. A detailed analysis is presented in **Section 6.1**. Further exploration into cascaded compression absorption systems involves integrating a Recompression Absorption System (RAC) with advanced VCRs equipped with ejectors, leading to the development of innovative systems like the Ejector injection recompression absorption cycle (EI-CRAC) and Ejector recompression absorption cycle (E-CRAC) systems. The thermal assessment and analysis are elaborated in **Section 6.2**. Furthermore, the study pioneers the feasible upgrade of single-effect standalone absorption frameworks, incorporating recompression technologies with ejector and injection setup, leading to the development of RE-RAC and VI-RAC systems. The following analysis is discussed thoroughly in **Section 6.3**. The thorough analysis of each subsection comprises of thermal parametric and comparative assessment with multi-objective optimization to find optimal range of operating conditions for performance maximization.

These advancements collectively mark a significant leap forward in refrigeration technology. Summary of each analysis is discussed in the corresponding subsections of result and discussion. The key findings are stated below for further clarity with limitations and future recommendations.

7.1 Key Findings

- The study highlights that both ARC based proposed cascaded systems: EICAC and ECAC systems, using R41-LiBr/H2O as refrigerant, outperform traditional systems in terms of COP by approximately 15% and 6% respectively under various conditions. Additionally, EICAC and ECAC show significant improvements in exergy efficiency, up to 20% and 10%

respectively, with optimal performance around 77℃, indicating a stronger impact of generator temperature on exergetic efficiency compared to COP.

- It also reveals that while COP increases linearly with the T_{evp} for all systems, exergy efficiency decreases, with absorption cycles proving more effective at low temperatures. EICAC in particular demonstrates lower exergy destruction and about 9% higher exergy efficiency than ECAC. The study further identifies that the optimal generator temperature increases with $T_{cond.}$ Also, this optimum value varies 5-6℃ from energy and exergy perspective, whereas the optimal performance is gained at an evaporator temperature of -21℃ nearly.

- The study also explores RAC based proposed cascaded proposed systems: one basic CRAC and two advanced configurations as: E-CRAC and EI-CRAC. They significantly outperform the traditional CARC system, with the COP being nearly three times higher. EI-CRAC and E-CRAC show a COP enhancement of about 10% and 20%, respectively, along with an increase in Exergy Efficiency (Exeff) of 15% and 25% over CRAC, indicating superior efficiency in cooling operations.

- Optimal operating conditions, such as pressure (ΔP) and generator temperature (T_{gen}), play a crucial role in system performance. EI-CRAC exhibits remarkable stability and minimal sensitivity to pressure variations compared to E-CRAC, demonstrating its superior performance under varying conditions. Both systems achieve higher COP and Ex_{eff} at certain T_{gen} but their performance declines near same rate beyond these optimal points. With increasing T_{evp}, although *COP* rises, Ex_{eff} diminishes. Despite EI-CRAC exhibiting higher Ex_{eff}, its rate of decrease with rising T_{evp} is more pronounced. Proving EI-CRAC more effective at lower cooling applications.

- EI-CRAC shows a more efficient exergy performance with a lower total exergy destruction rate compared to E-CRAC. Also, optimal operation is achieved at specific T_{gen} and T_{evp} values, with maximum *COP* at the lowest T_{abs}, T_{evp}, and P_{cond} but highest ΔT_{chx}, and maximum Ex_{eff} under the inverse conditions of highest T_{evp}, indicating a strategic balance between operational parameters for optimal efficiency.

- Finally, this research introduces novel stand-alone recompression absorption refrigeration systems integrating ejector-injection setup to replace expansion valves (RE-RAC and VI-

RAC). RE-RAC and VI-RAC significantly outperform conventional ARC and RAC systems. The COP of RE-RAC and VI-RAC is 76% and 63% higher than the conventional RAC system, respectively despite RE-RAC requiring more external heat generation due to VI-RAC's additional compressor demands.

- Optimal performance conditions (peak COP) for both RE-RAC and VI-RAC are influenced by T_{gen}, T_{evp}, ε, P_{gen} and *NPR* with RE-RAC maintaining an advantage over VI-RAC with lower sensitivity to changes across various operating conditions. Optimal T_{gen} is influenced by T_{evp}, where a higher T_{evp} leads to a lower optimal T_{gen}. But lower T_{evp} system cannot operate in low T_{gen}, also for T_{evp} increasing COP increases. Whereas, adjusting P_{gen} reveals an optimal range for peak COP, which decreases with lower T_{gen} and T_{evp}. RE-RAC shows maximum COP advantage at optimal T_{gen}, however, this advantage narrows as T_{evp} decreases or P_{gen} increases.
- The total exergy destruction rate ($\dot{E}x_{D,tot}$) is lower in RE-RAC compared to VI-RAC, attributed to its simpler configuration with fewer components. Optimal operating conditions for minimal $\dot{E}x_{D,tot}$ involve careful balancing of T_{gen}, T_{evp}, ε, and *NPR*, with the gap in performance ($\Delta\dot{E}x_{D,tot}$) between RE-RAC and VI-RAC widening or narrowing based on these parameters.

7.2 Limitations and Future Recommendations

While the proposed advanced cascaded compression absorption systems (ECAC, EICAC, E-CRAC, EICRAC) and standalone RAC systems (RE-RAC & VI-RAC) demonstrate significant potential for efficiency gains in cooling operations, it is crucial to acknowledge the limitations inherent to this numerical study. These limitations underscore the need for further empirical research and development to fully realize the potential of these innovative systems.

7.2.1 Limitations

- Model assumptions: The study relies on several simplifying assumptions to facilitate model simulation. While these assumptions are commonly used in refrigeration system modeling, they may not perfectly reflect real-world conditions. Future work could refine the model by incorporating more detailed considerations of heat dissipation, pressure drops, and component inefficiencies.

- Limited scope of simulation and optimization parameters: The computational model primarily focuses on certain operational parameters and may not account for all practical aspects of real-world implementation, such as long-term wear and tear, system scaling, and economic factors.
- Requirement of adaptable control system: The efficiency metrics (*COP* and Ex_{eff}) of the systems are highly dependent on the optimal generator and evaporator's temperatures and pressure, which vary under different operational conditions. This highlights the need for adaptable control systems capable of dynamically adjusting to these variations to maintain optimal performance.
- Lack of experimental testing: The findings are based on theoretical modeling and computational analysis, and experimental validation through prototype testing is required to confirm their real-world performance.

7.2.2 Future Recommendations

In order to expand upon the valuable insights gained from this study and effectively tackle its identified limitations, a comprehensive set of recommendations is proposed, aimed at guiding and enriching future research endeavors in this field.

- Empirical testing and validation: Future research should aim to empirically test these systems to validate the theoretical findings and adapt them for real-world applications.
- Multi-objective optimization: While this study focused on maximizing both COP and exergy efficiency, future research could explore multi-objective optimization considering additional factors such as cost, environmental impact, and noise generation.
- Dynamic control strategies: Development and implementation of adaptive control strategies could enable the proposed systems to operate under varying conditions and maintain optimal performance across a wider range of scenarios.
- Long-term performance analysis: Studies focusing on the long-term durability and maintenance requirements of these systems would provide valuable insights for practical applications.

- Expansion of simulation parameters: Further research could expand the range of simulation parameters to include economic analysis, scalability, and environmental impact, offering a more holistic view of system performance.
- Integration with renewable energy sources: Exploring the integration of these advanced refrigeration systems with renewable energy sources could pave the way for even more sustainable and energy-efficient cooling solutions.
- Extensive cost analysis: Conducting comprehensive cost analyses that take environmental factors into account would provide a clearer understanding of the economic viability of these systems and their environmental benefits.
- Real-life implementation: Implementing these systems in real-life scenarios, such as power plants and various industries (e.g., textile, manufacturing, steel), could enhance the utilization of waste heat. The proposed systems ability to achieve lower evaporator and generator temperatures with higher performance than conventional systems make it suitable for using the lowest grades of energy efficiently.

Chapter 8: Publications From This Thesis

1. **Yasin Khan,** Md Walid Faruque, Mahdi Hafiz Nabil, M Monjurul Ehsan. "Ejector and Vapor Injection Enhanced Novel Compression-Absorption Cascade Refrigeration Systems: A Thermodynamic Parametric and Refrigerant Analysis",
   Energy Conversion and Management (2023): Volume 289, 2023, 117190, ISSN 0196-8904.
   Impact factor-11.53, Cite Score-19.1, SJR rank-Q-1
   https://www.sciencedirect.com/science/article/abs/pii/S0196890423005368

2. **Yasin Khan,** S. M. Naqib-Ul-Islam, Md Walid Faruque, M Monjurul Ehsan. " Advanced Cascaded Recompression Absorption System Equipped with Ejector and Vapor-Injection Enhanced Vapor Compression Refrigeration System: ANN Based Multi-Objective Optimization."
   Thermal Science and Engineering Progress (2024): Volume 49, 2024, 102485, ISSN 2451-9049.
   Impact factor-4.56, Cite Score-7.1, SJR rank-Q-1
   https://www.sciencedirect.com/science/article/pii/S2451904924001033

3. **Yasin Khan,** S. M. Naqib-Ul-Islam, M Monjurul Ehsan. "Performance Evaluation of Novel Advanced Recompression Absorption Refrigeration Systems Equipped with Ejector and Vapor Injection Technology." **Thermal Science and Engineering Progress (2024): Under Review**
   Impact factor-4.56, Cite Score-7.1, SJR rank-Q-1

Chapter 9: Bibliography

[1] V. S. Chakravarthy, R. K. Shah, and G. Venkatarathnam, "A review of refrigeration methods in the temperature range 4-300 K," *J Therm Sci Eng Appl*, vol. 3, no. 2, Jul. 2011, doi: 10.1115/1.4003701/469408.

[2] "Industrial Application of Refrigeration | ARANER." Accessed: May 25, 2024. [Online]. Available: https://www.araner.com/blog/industrial-refrigeration-applications-district-cooling

[3] "The Future of Cooling," *The Future of Cooling*, May 2018, doi: 10.1787/9789264301993-EN.

[4] U. Desideri, S. Proietti, and P. Sdringola, "Solar-powered cooling systems: Technical and economic analysis on industrial refrigeration and air-conditioning applications," *Appl Energy*, vol. 86, no. 9, pp. 1376–1386, Sep. 2009, doi: 10.1016/J.APENERGY.2009.01.011.

[5] S. B. Riffat and C. W. Wong, "Gas-driven absorption/recompression system," *Heat Recovery Systems and CHP*, vol. 14, no. 2, pp. 165–171, Mar. 1994, doi: 10.1016/0890-4332(94)90007-8.

[6] H. Selvnes, Y. Allouche, R. I. Manescu, and A. Hafner, "Review on cold thermal energy storage applied to refrigeration systems using phase change materials," *Thermal Science and Engineering Progress*, vol. 22, p. 100807, May 2021, doi: 10.1016/J.TSEP.2020.100807.

[7] D. Enescu and E. O. Virjoghe, "A review on thermoelectric cooling parameters and performance," *Renewable and Sustainable Energy Reviews*, vol. 38, pp. 903–916, Oct. 2014, doi: 10.1016/J.RSER.2014.07.045.

[8] "Thermoelectric cooling - Wikipedia." Accessed: Mar. 16, 2024. [Online]. Available: https://en.wikipedia.org/wiki/Thermoelectric_cooling

[9] "Magnetic refrigeration - Wikipedia." Accessed: Mar. 16, 2024. [Online]. Available: https://en.wikipedia.org/wiki/Magnetic_refrigeration

[10] M. E. H. Tijani and Technische Universiteit Eindhoven., "Loudspeaker-driven thermo-acoustic refrigeration," 2001.

[11] M. Walid Faruque, Y. Khan, M. Hafiz Nabil, M. Monjurul Ehsan, and A. Karim, "Thermal Performance Evaluation of a Novel Ejector-Injection Cascade Refrigeration System," *Thermal Science and Engineering Progress*, p. 101745, Feb. 2023, doi: 10.1016/J.TSEP.2023.101745.

[12] M. W. Faruque, Y. Khan, M. H. Nabil, and M. M. Ehsan, "Parametric analysis and optimization of a novel cascade compression-absorption refrigeration system integrated with a flash tank and a reheater," *Results in Engineering*, vol. 17, p. 101008, Mar. 2023, doi: 10.1016/J.RINENG.2023.101008.

[13] Z. Zhang, X. Feng, D. Tian, J. Yang, and L. Chang, "Progress in ejector-expansion vapor compression refrigeration and heat pump systems," *Energy Convers Manag*, vol. 207, p. 112529, Mar. 2020, doi: 10.1016/j.enconman.2020.112529.

[14] X. Wang, J. Yu, and M. Xing, "Performance analysis of a new ejector enhanced vapor injection heat pump cycle," *Energy Convers Manag*, vol. 100, pp. 242–248, Aug. 2015, doi: 10.1016/J.ENCONMAN.2015.05.017.

[15] "Refrigeration Cycle 101 - MEP Academy." Accessed: May 25, 2024. [Online]. Available: https://mepacademy.com/refrigeration-cycle-101/

[16] C. Park, H. Lee, Y. Hwang, and R. Radermacher, "Recent advances in vapor compression cycle technologies," *International Journal of Refrigeration*, vol. 60, pp. 118–134, Dec. 2015, doi: 10.1016/J.IJREFRIG.2015.08.005.

[17] "Difference between Vapour Compression and Vapour Absorption | PDF." Accessed: May 25, 2024. [Online]. Available: https://dizz.com/difference-between-vapour-compression-and-vapour-absorption-refrigeration-system-pdf-2/

[18] C. Cimsit and I. T. Ozturk, "Analysis of compression–absorption cascade refrigeration cycles," *Appl Therm Eng*, vol. 40, pp. 311–317, Jul. 2012, doi: 10.1016/J.APPLTHERMALENG.2012.02.035.

[19] Y. Khan, M. W. Faruque, M. H. Nabil, and M. M. Ehsan, "Ejector and Vapor Injection Enhanced Novel Compression-Absorption Cascade Refrigeration Systems: A Thermodynamic Parametric and Refrigerant Analysis," *Energy Convers Manag*, vol. 289, p. 117190, Aug. 2023, doi: 10.1016/J.ENCONMAN.2023.117190.

[20] S. Salehi, M. Yari, S. M. S. Mahmoudi, and L. G. Farshi, "Investigation of crystallization risk in different types of absorption LiBr/H2O heat transformers," *Thermal Science and Engineering Progress*, vol. 10, pp. 48–58, May 2019, doi: 10.1016/J.TSEP.2019.01.013.

[21] S. T. Kadam *et al.*, "Thermo-economic and environmental assessment of hybrid vapor compression-absorption refrigeration systems for district cooling," *Energy*, vol. 243, 2022, doi: 10.1016/j.energy.2021.122991.

[22] J. M. Asensio-Delgado, S. Asensio-Delgado, G. Zarca, and A. Urtiaga, "Analysis of hybrid compression absorption refrigeration using low-GWP HFC or HFO/ionic liquid working pairs," *International Journal of Refrigeration*, vol. 134, pp. 232–241, 2022, doi: 10.1016/j.ijrefrig.2021.11.013.

[23] L. Kairouani and E. Nehdi, "Cooling performance and energy saving of a compression-absorption refrigeration system assisted by geothermal energy," *Appl Therm Eng*, vol. 26, no. 2–3, pp. 288–294, 2006, doi: 10.1016/j.applthermaleng.2005.05.001.

[24] A. Razmi, M. Soltani, F. M. Kashkooli, and L. Garousi Farshi, "Energy and exergy analysis of an environmentally-friendly hybrid absorption/recompression refrigeration system," *Energy Convers Manag*, vol. 164, pp. 59–69, May 2018, doi: 10.1016/J.ENCONMAN.2018.02.084.

[25] A. Zarei, J. Zamani, L. Hooshyari, and S. Zaboli, "Energy and exergy analysis of a novel multi-pressure levels ejector absorption-recompression refrigeration system: Parametric study and optimization," *Thermal Science and Engineering Progress*, vol. 42, p. 101904, Jul. 2023, doi: 10.1016/J.TSEP.2023.101904.

[26] C. Park, H. Lee, Y. Hwang, and R. Radermacher, "Recent advances in vapor compression cycle technologies," *International Journal of Refrigeration*, vol. 60, pp. 118–134, Dec. 2015, doi: 10.1016/J.IJREFRIG.2015.08.005.

[27] B. O. Bolaji and Z. Huan, "Ozone depletion and global warming: Case for the use of natural refrigerant - A review," *Renewable and Sustainable Energy Reviews*, vol. 18, pp. 49–54, 2013, doi: 10.1016/j.rser.2012.10.008.

[28] R. A. Kerr, "Global warming is changing the world," *Science (1979)*, vol. 316, no. 5822, pp. 188–190, Apr. 2007, doi: 10.1126/science.316.5822.188.

[29] A. Mota-Babiloni, J. R. Barbosa, P. Makhnatch, and J. A. Lozano, "Assessment of the utilization of equivalent warming impact metrics in refrigeration, air conditioning and heat

pump systems," *Renewable and Sustainable Energy Reviews*, vol. 129, 2020, doi: 10.1016/j.rser.2020.109929.

[30] S. E. Hosseini and M. A. Wahid, "Hydrogen production from renewable and sustainable energy resources: Promising green energy carrier for clean development," *Renewable and Sustainable Energy Reviews*, vol. 57, pp. 850–866, 2016, doi: 10.1016/j.rser.2015.12.112.

[31] S. Bista, S. E. Hosseini, E. Owens, and G. Phillips, "Performance improvement and energy consumption reduction in refrigeration systems using phase change material (PCM)," *Appl Therm Eng*, vol. 142, pp. 723–735, 2018, doi: 10.1016/j.applthermaleng.2018.07.068.

[32] N. Johnson, J. Baltrusaitis, and W. L. Luyben, "Design and control of a cryogenic multi-stage compression refrigeration process," *Chemical Engineering Research and Design*, vol. 121, pp. 360–367, 2017, doi: 10.1016/j.cherd.2017.03.018.

[33] A. Rai and S. A. Tassou, "Environmental impacts of vapour compression and cryogenic transport refrigeration technologies for temperature controlled food distribution," *Energy Convers Manag*, vol. 150, pp. 914–923, Oct. 2017, doi: 10.1016/J.ENCONMAN.2017.05.024.

[34] J. A. Dopazo and J. Fernández-Seara, "Experimental evaluation of a cascade refrigeration system prototype with CO2 and NH3 for freezing process applications," *International Journal of Refrigeration*, vol. 34, no. 1, pp. 257–267, Jan. 2011, doi: 10.1016/J.IJREFRIG.2010.07.010.

[35] M. Walid Faruque, M. Hafiz Nabil, M. Raihan Uddin, M. Monjurul Ehsan, and S. Salehin, "Thermodynamic assessment of a triple cascade refrigeration system utilizing hydrocarbon refrigerants for ultra-low temperature applications," *Energy Conversion and Management: X*, vol. 14, p. 100207, May 2022, doi: 10.1016/J.ECMX.2022.100207.

[36] A. A. Kornhauser, "Purdue e-Pubs The Use of an Ejector as a Refrigerant Expander", Accessed: Aug. 18, 2022. [Online]. Available: http://docs.lib.purdue.edu/iracc/82

[37] D. M. Nasution, M. Idris, N. A. Pambudi, and Weriono, "Room air conditioning performance using liquid-suction heat exchanger retrofitted with R290," *Case Studies in Thermal Engineering*, vol. 13, Mar. 2019, doi: 10.1016/J.CSITE.2018.11.001.

[38] A. Mota-Babiloni, J. Navarro-Esbrí, V. Pascual-Miralles, Á. Barragán-Cervera, and A. Maiorino, "Experimental influence of an internal heat exchanger (IHX) using R513A and

R134a in a vapor compression system," *Appl Therm Eng*, vol. 147, pp. 482–491, Jan. 2019, doi: 10.1016/J.APPLTHERMALENG.2018.10.092.

[39] M. Elakhdar, B. M. Tashtoush, E. Nehdi, and L. Kairouani, "Thermodynamic analysis of a novel Ejector Enhanced Vapor Compression Refrigeration (EEVCR) cycle," *Energy*, vol. 163, pp. 1217–1230, Nov. 2018, doi: 10.1016/J.ENERGY.2018.09.050.

[40] J. Heo, M. W. Jeong, C. Baek, and Y. Kim, "Comparison of the heating performance of air-source heat pumps using various types of refrigerant injection," *International Journal of Refrigeration*, vol. 34, no. 2, pp. 444–453, Mar. 2011, doi: 10.1016/J.IJREFRIG.2010.10.003.

[41] X. Shuxue, M. Guoyuan, L. Qi, and L. Zhongliang, "Experiment study of an enhanced vapor injection refrigeration/heat pump system using R32," *International Journal of Thermal Sciences*, vol. 68, pp. 103–109, Jun. 2013, doi: 10.1016/J.IJTHERMALSCI.2012.12.014.

[42] D. Yang, Y. Li, J. Xie, and J. Wang, "Exergy destruction characteristics of a transcritical carbon dioxide two-stage compression/ejector refrigeration system for low-temperature cold storage," *Energy Reports*, vol. 8, pp. 8546–8562, Nov. 2022, doi: 10.1016/J.EGYR.2022.06.066.

[43] X. Cao, X. Liang, L. Shao, and C. Zhang, "Performance analysis of an ejector-assisted two-stage evaporation single-stage vapor-compression cycle," *Appl Therm Eng*, vol. 205, p. 118005, Mar. 2022, doi: 10.1016/J.APPLTHERMALENG.2021.118005.

[44] M. Q. Zeng, Q. Y. Zheng, X. L. Zhang, F. Y. Mo, and X. R. Zhang, "Thermodynamic analysis of a novel multi-target temperature transcritical CO2 ejector-expansion refrigeration cycle with vapor-injection," *Energy*, vol. 259, p. 125016, Nov. 2022, doi: 10.1016/J.ENERGY.2022.125016.

[45] R. Nikbakhti, X. Wang, A. K. Hussein, and A. Iranmanesh, "Absorption cooling systems – Review of various techniques for energy performance enhancement," *Alexandria Engineering Journal*, vol. 59, no. 2, pp. 707–738, Apr. 2020, doi: 10.1016/J.AEJ.2020.01.036.

[46] M. R. Islam, "Field guidelines," *Reservoir Development*, pp. 737–843, Jan. 2022, doi: 10.1016/B978-0-12-820053-7.00004-4.

[47] X. Liao and R. Radermacher, "Absorption chiller crystallization control strategies for integrated cooling heating and power systems," *International Journal of Refrigeration*, vol. 30, no. 5, pp. 904–911, Aug. 2007, doi: 10.1016/J.IJREFRIG.2006.10.009.

[48] W. Wu, B. Wang, W. Shi, and X. Li, "Crystallization Analysis and Control of Ammonia-Based Air Source Absorption Heat Pump in Cold Regions," *Advances in Mechanical Engineering*, vol. 2013, 2013, doi: 10.1155/2013/140341.

[49] J. S. Talpada and P. V. Ramana, "A review on performance improvement of an absorption refrigeration system by modification of basic cycle," *International Journal of Ambient Energy*, vol. 40, no. 6, pp. 661–673, Aug. 2019, doi: 10.1080/01430750.2017.1423379.

[50] A. Shirazi, R. A. Taylor, S. D. White, and G. L. Morrison, "A systematic parametric study and feasibility assessment of solar-assisted single-effect, double-effect, and triple-effect absorption chillers for heating and cooling applications," *Energy Convers Manag*, vol. 114, pp. 258–277, Apr. 2016, doi: 10.1016/J.ENCONMAN.2016.01.070.

[51] A. M. Abed, M. A. Alghoul, R. Sirawn, A. N. Al-Shamani, and K. Sopian, "Performance enhancement of ejector–absorption cooling cycle by re-arrangement of solution streamlines and adding RHE," *Appl Therm Eng*, vol. 77, pp. 65–75, Feb. 2015, doi: 10.1016/J.APPLTHERMALENG.2014.12.003.

[52] S. Raghuvanshi and G. Maheshwari, "Analysis of Ammonia-Water (NH3-H2O) Vapor Absorption Refrigeration System based on First Law of Thermodynamics," *Int J Sci Eng Res*, vol. 2, no. 8, 2011, Accessed: Oct. 13, 2023. [Online]. Available: http://www.ijser.org

[53] R. Gomri, "Second law comparison of single effect and double effect vapour absorption refrigeration systems," *Energy Convers Manag*, vol. 50, no. 5, pp. 1279–1287, May 2009, doi: 10.1016/J.ENCONMAN.2009.01.019.

[54] D. Colorado and W. Rivera, "Performance comparison between a conventional vapor compression and compression-absorption single-stage and double-stage systems used for refrigeration," *Appl Therm Eng*, vol. 87, pp. 273–285, Aug. 2015, doi: 10.1016/J.APPLTHERMALENG.2015.05.029.

[55] M. U. Arshad, M. Zaman, M. Rizwan, and A. Elkamel, "Economic optimization of parallel and series configurations of the double effect absorption refrigeration system," *Energy Convers Manag*, vol. 210, p. 112661, Apr. 2020, doi: 10.1016/J.ENCONMAN.2020.112661.

[56] R. Maryami and A. A. Dehghan, "An exergy based comparative study between LiBr/water absorption refrigeration systems from half effect to triple effect," *Appl Therm Eng*, vol. 124, pp. 103–123, Sep. 2017, doi: 10.1016/J.APPLTHERMALENG.2017.05.174.

[57] M. Azhar and M. A. Siddiqui, "Optimization of operating temperatures in the gas operated single to triple effect vapour absorption refrigeration cycles," *International Journal of Refrigeration*, vol. 82, pp. 401–425, Oct. 2017, doi: 10.1016/J.IJREFRIG.2017.06.033.

[58] A. Solanki and Y. Pal, "Energy and exergy evaluation of triple-effect H2O/LiBr absorption cooling system," *International Journal of Ambient Energy*, Dec. 2022, doi: 10.1080/01430750.2020.1831598.

[59] A. Dousti, L. G. Farshi, and N. Asadi, "Thermodynamic and crystallization analysis of absorption-recompression system and comparison with conventional absorption cycle," *Mech. Eng. Dept*, 2015, Accessed: Oct. 13, 2023. [Online]. Available: https://www.researchgate.net/publication/320182667

[60] A. R. Razmi, A. Arabkoohsar, and H. Nami, "Thermoeconomic analysis and multi-objective optimization of a novel hybrid absorption/recompression refrigeration system," *Energy*, vol. 210, p. 118559, Nov. 2020, doi: 10.1016/J.ENERGY.2020.118559.

[61] C. Vereda, R. Ventas, A. Lecuona, and R. López, "Single-effect absorption refrigeration cycle boosted with an ejector-adiabatic absorber using a single solution pump," *International Journal of Refrigeration*, vol. 38, no. 1, pp. 22–29, Feb. 2014, doi: 10.1016/J.IJREFRIG.2013.10.010.

[62] X. Liang, S. Zhou, J. Deng, G. He, and D. Cai, "Thermodynamic analysis of a novel combined double ejector-absorption refrigeration system using ammonia/salt working pairs without mechanical pumps," *Energy*, vol. 185, pp. 895–909, Oct. 2019, doi: 10.1016/J.ENERGY.2019.07.104.

[63] A. Dhahi Gharir, L. Garousi Farshi, and S. M. S. Mahmoudi, "Performance evaluation of a novel ejector absorption refrigeration cycle combined with two flash tanks," *Journal of the Brazilian Society of Mechanical Sciences and Engineering*, vol. 45, no. 3, pp. 1–22, Mar. 2023, doi: 10.1007/S40430-023-04093-1/METRICS.

[64] J. M. Asensio-Delgado, S. Asensio-Delgado, G. Zarca, and A. Urtiaga, "Analysis of hybrid compression absorption refrigeration using low-GWP HFC or HFO/ionic liquid working

pairs," *International Journal of Refrigeration*, vol. 134, pp. 232–241, Feb. 2022, doi: 10.1016/J.IJREFRIG.2021.11.013.

[65] S. T. Kadam *et al.*, "Thermo-economic and environmental assessment of hybrid vapor compression-absorption refrigeration systems for district cooling," *Energy*, vol. 243, p. 122991, Mar. 2022, doi: 10.1016/J.ENERGY.2021.122991.

[66] W. Han, L. Sun, D. Zheng, H. Jin, S. Ma, and X. Jing, "New hybrid absorption-compression refrigeration system based on cascade use of mid-temperature waste heat," *Appl Energy*, vol. 106, pp. 383–390, 2013, doi: 10.1016/J.APENERGY.2013.01.067.

[67] M. Yu, P. Cui, Y. Wang, Z. Liu, Z. Zhu, and S. Yang, "Advanced Exergy and Exergoeconomic Analysis of Cascade Absorption Refrigeration System Driven by Low-Grade Waste Heat," *ACS Sustain Chem Eng*, vol. 7, no. 19, pp. 16843–16857, Oct. 2019, doi: 10.1021/ACSSUSCHEMENG.9B04396/ASSET/IMAGES/MEDIUM/SC9B04396_0011.GIF.

[68] C. Cimsit and I. T. Ozturk, "Analysis of compression–absorption cascade refrigeration cycles," *Appl Therm Eng*, vol. 40, pp. 311–317, Jul. 2012, doi: 10.1016/J.APPLTHERMALENG.2012.02.035.

[69] C. Cimsit, I. T. Ozturk, and O. Kincay, "Thermoeconomic optimization of LiBr/H2O-R134a compression-absorption cascade refrigeration cycle," *Appl Therm Eng*, vol. 76, pp. 105–115, Feb. 2015, doi: 10.1016/J.APPLTHERMALENG.2014.10.094.

[70] Y. Xu, F. S. Chen, Q. Wang, X. Han, D. Li, and G. Chen, "A novel low-temperature absorption–compression cascade refrigeration system," *Appl Therm Eng*, vol. 75, pp. 504–512, Jan. 2015, doi: 10.1016/J.APPLTHERMALENG.2014.10.043.

[71] Y. Chen, W. Han, and H. Jin, "Proposal and analysis of a novel heat-driven absorption–compression refrigeration system at low temperatures," *Appl Energy*, vol. 185, pp. 2106–2116, Jan. 2017, doi: 10.1016/J.APENERGY.2015.12.009.

[72] A. Razmi, M. Soltani, and M. Torabi, "Investigation of an efficient and environmentally-friendly CCHP system based on CAES, ORC and compression-absorption refrigeration cycle: Energy and exergy analysis," *Energy Convers Manag*, vol. 195, pp. 1199–1211, Sep. 2019, doi: 10.1016/J.ENCONMAN.2019.05.065.

[73] A. Razmi, M. Soltani, F. M. Kashkooli, and L. Garousi Farshi, "Energy and exergy analysis of an environmentally-friendly hybrid absorption/recompression refrigeration system," *Energy Convers Manag*, vol. 164, pp. 59–69, May 2018, doi: 10.1016/J.ENCONMAN.2018.02.084.

[74] C. Cimsit and I. T. Ozturk, "Analysis of compression–absorption cascade refrigeration cycles," *Appl Therm Eng*, vol. 40, pp. 311–317, Jul. 2012, doi: 10.1016/J.APPLTHERMALENG.2012.02.035.

[75] O. Kaynakli and M. Kilic, "Theoretical study on the effect of operating conditions on performance of absorption refrigeration system," *Energy Convers Manag*, vol. 48, no. 2, pp. 599–607, Feb. 2007, doi: 10.1016/J.ENCONMAN.2006.06.005.

[76] Y. Cengel, M. Boles, and M. Kanoğlu, *Thermodynamics: an engineering approach*. 2011. Accessed: Dec. 01, 2022. [Online]. Available: https://www.academia.edu/download/55284132/Solution_Manual_8th_Ed.pdf

[77] H. Ghaebi, T. Parikhani, H. Rostamzadeh, and B. Farhang, "Thermodynamic and thermoeconomic analysis and optimization of a novel combined cooling and power (CCP) cycle by integrating of ejector refrigeration and Kalina cycles," *Energy*, vol. 139, pp. 262–276, Nov. 2017, doi: 10.1016/J.ENERGY.2017.07.154.

[78] C. Aktemur, I. T. Ozturk, and C. Cimsit, "Comparative energy and exergy analysis of a subcritical cascade refrigeration system using low global warming potential refrigerants," *Appl Therm Eng*, vol. 184, p. 116254, Feb. 2021, doi: 10.1016/J.APPLTHERMALENG.2020.116254.

[79] Z. Sun, Q. Wang, Z. Xie, S. Liu, D. Su, and Q. Cui, "Energy and exergy analysis of low GWP refrigerants in cascade refrigeration system," *Energy*, vol. 170, pp. 1170–1180, Mar. 2019, doi: 10.1016/J.ENERGY.2018.12.055.

[80] A. Bejan, G. Tsatsaronis, and M. Moran, *Thermal design and optimization*. 1995. Accessed: Dec. 01, 2022. [Online]. Available: https://books.google.com/books?hl=en&lr=&id=sTi2crXeZYgC&oi=fnd&pg=PA1&dq=Thermal+design+and+optimization&ots=IdahfnBtRd&sig=TfcMiHdnc2J2VfuMYwr2YH3qv8A

[81] T. Avanessian and M. Ameri, "Energy, exergy, and economic analysis of single and double effect LiBr–H2O absorption chillers," *Energy Build*, vol. 73, pp. 26–36, Apr. 2014, doi: 10.1016/J.ENBUILD.2014.01.013.

[82] S. M. Alirahmi, S. Rahmani Dabbagh, P. Ahmadi, and S. Wongwises, "Multi-objective design optimization of a multi-generation energy system based on geothermal and solar energy," *Energy Convers Manag*, vol. 205, p. 112426, Feb. 2020, doi: 10.1016/J.ENCONMAN.2019.112426.

[83] H. Nami and A. Arabkoohsar, "Improving the power share of waste-driven CHP plants via parallelization with a small-scale Rankine cycle, a thermodynamic analysis," *Energy*, vol. 171, pp. 27–36, Mar. 2019, doi: 10.1016/J.ENERGY.2018.12.168.

[84] D. Colorado-Garrido, "Advanced Exergy Analysis of a Compression-Absorption Cascade Refrigeration System," *Journal of Energy Resources Technology, Transactions of the ASME*, vol. 141, no. 4, Apr. 2019, doi: 10.1115/1.4042003/368161.

[85] A. Razmi, M. Soltani, F. M. Kashkooli, and L. Garousi Farshi, "Energy and exergy analysis of an environmentally-friendly hybrid absorption/recompression refrigeration system," *Energy Convers Manag*, vol. 164, pp. 59–69, May 2018, doi: 10.1016/J.ENCONMAN.2018.02.084.

[86] S. Somesh, S. K. Shaw, and P. Mahendru, "A comprehensive review on LiBr–H2O based solar-powered vapour absorption refrigeration system," *Lecture Notes in Mechanical Engineering*, pp. 343–352, 2019, doi: 10.1007/978-981-13-6577-5_32/COVER.

[87] M. A. I. El-Shaarawi and A. A. Al-Ugla, "Unsteady analysis for solar-powered hybrid storage LiBr-water absorption air-conditioning," *Solar Energy*, vol. 144, pp. 556–568, Mar. 2017, doi: 10.1016/J.SOLENER.2016.12.054.

[88] A. A. S. Lima *et al.*, "Absorption refrigeration systems based on ammonia as refrigerant using different absorbents: Review and applications," *Energies (Basel)*, vol. 14, no. 1, Jan. 2021, doi: 10.3390/EN14010048.

[89] L. T. Chen, "A new ejector-absorber cycle to improve the COP of an absorption refrigeration system," *Appl Energy*, vol. 30, no. 1, pp. 37–51, Jan. 1988, doi: 10.1016/0306-2619(88)90053-0.

[90] F. Táboas, M. Bourouis, and M. Vallès, "Analysis of ammonia/water and ammonia/salt mixture absorption cycles for refrigeration purposes in fishing ships," *Appl Therm Eng*, vol. 66, no. 1–2, pp. 603–611, May 2014, doi: 10.1016/J.APPLTHERMALENG.2014.02.065.

[91] H. Li, F. Cao, X. Bu, L. Wang, and X. Wang, "Performance characteristics of R1234yf ejector-expansion refrigeration cycle," *Appl Energy*, vol. 121, pp. 96–103, May 2014, doi: 10.1016/J.APENERGY.2014.01.079.

[92] K. Sumeru, H. Nasution, and F. N. Ani, "A review on two-phase ejector as an expansion device in vapor compression refrigeration cycle," *Renewable and Sustainable Energy Reviews*, vol. 16, no. 7, pp. 4927–4937, Sep. 2012, doi: 10.1016/J.RSER.2012.04.058.

[93] J. Sarkar, "Ejector enhanced vapor compression refrigeration and heat pump systems—A review," *Renewable and Sustainable Energy Reviews*, vol. 16, no. 9, pp. 6647–6659, Dec. 2012, doi: 10.1016/J.RSER.2012.08.007.

[94] Y. Liu, M. Yu, and J. Yu, "An improved 1-D thermodynamic modeling of small two-phase ejector for performance prediction and design," *Appl Therm Eng*, vol. 204, p. 118006, Mar. 2022, doi: 10.1016/J.APPLTHERMALENG.2021.118006.

[95] A. Sözen and M. Özalp, "Performance improvement of absorption refrigeration system using triple-pressure-level," *Appl Therm Eng*, vol. 23, no. 13, pp. 1577–1593, Sep. 2003, doi: 10.1016/S1359-4311(03)00106-6.

[96] A. Sohani, H. Sayyaadi, and S. Hoseinpoori, "Modeling and multi-objective optimization of an M-cycle cross-flow indirect evaporative cooler using the GMDH type neural network," *International Journal of Refrigeration*, vol. 69, pp. 186–204, Sep. 2016, doi: 10.1016/J.IJREFRIG.2016.05.011.

[97] A. K. Jain, Jianchang Mao, and K. M. Mohiuddin, "Artificial neural networks: a tutorial," *Computer (Long Beach Calif)*, vol. 29, no. 3, pp. 31–44, Mar. 1996, doi: 10.1109/2.485891.

[98] A. Krogh, "What are artificial neural networks?," *Nat Biotechnol*, vol. 26, no. 2, pp. 195–197, Feb. 2008, doi: 10.1038/nbt1386.

[99] A. Karthikeyan, M. E. Cimen, A. Akgul, A. F. Boz, and K. Rajagopal, "Persistence and coexistence of infinite attractors in a fractal Josephson junction resonator with unharmonic current phase relation considering feedback flux effect," *Nonlinear Dyn*, vol. 103, no. 2, pp. 1979–1998, Jan. 2021, doi: 10.1007/s11071-020-06159-4.

[100] B. Işcan, "ANN modeling for justification of thermodynamic analysis of experimental applications on combustion parameters of a diesel engine using diesel and safflower biodiesel fuels," *Fuel*, vol. 279, p. 118391, Nov. 2020, doi: 10.1016/j.fuel.2020.118391.

[101] A. Farsi, I. Dincer, and G. F. Naterer, "Multi-objective optimization of an experimental integrated thermochemical cycle of hydrogen production with an artificial neural network," *Int J Hydrogen Energy*, vol. 45, no. 46, pp. 24355–24369, Sep. 2020, doi: 10.1016/j.ijhydene.2020.06.262.

[102] F. Yang, H. Cho, H. Zhang, J. Zhang, and Y. Wu, "Artificial neural network (ANN) based prediction and optimization of an organic Rankine cycle (ORC) for diesel engine waste heat recovery," *Energy Convers Manag*, vol. 164, pp. 15–26, May 2018, doi: 10.1016/j.enconman.2018.02.062.

[103] A. Konak, D. W. Coit, and A. E. Smith, "Multi-objective optimization using genetic algorithms: A tutorial," *Reliab Eng Syst Saf*, vol. 91, no. 9, pp. 992–1007, Sep. 2006, doi: 10.1016/j.ress.2005.11.018.

[104] A. Sohail, "Genetic Algorithms in the Fields of Artificial Intelligence and Data Sciences," *Annals of Data Science*, vol. 10, no. 4, pp. 1007–1018, Aug. 2023, doi: 10.1007/s40745-021-00354-9.

[105] W. Zhang, A. Maleki, M. A. Rosen, and J. Liu, "Sizing a stand-alone solar-wind-hydrogen energy system using weather forecasting and a hybrid search optimization algorithm," *Energy Convers Manag*, vol. 180, pp. 609–621, Jan. 2019, doi: 10.1016/j.enconman.2018.08.102.

[106] A. I. Turja, M. M. Hasan, M. M. Ehsan, and Y. Khan, "Multi-objective performance optimization & thermodynamic analysis of solar powered supercritical CO2 power cycles using machine learning methods & genetic algorithm," *Energy and AI*, vol. 15, p. 100327, Jan. 2024, doi: 10.1016/J.EGYAI.2023.100327.

[107] C. Maschio, A. C. Vidal, and D. J. Schiozer, "A framework to integrate history matching and geostatistical modeling using genetic algorithm and direct search methods," *J Pet Sci Eng*, vol. 63, no. 1–4, pp. 34–42, Dec. 2008, doi: 10.1016/J.PETROL.2008.08.001.

[108] S. Diyaley, P. Shilal, I. Shivakoti, R. K. Ghadai, and K. Kalita, "PSI and TOPSIS Based Selection of Process Parameters in WEDM," *Periodica Polytechnica Mechanical Engineering*, vol. 61, no. 4, p. 255, Sep. 2017, doi: 10.3311/PPme.10431.

[109] F. Musharavati, S. Khanmohammadi, A. Pakseresht, and S. Khanmohammadi, "Waste heat recovery in an intercooled gas turbine system: Exergo-economic analysis, triple objective optimization, and optimum state selection," *J Clean Prod*, vol. 279, p. 123428, Jan. 2021, doi: 10.1016/j.jclepro.2020.123428.

[110] H. R. Shahhosseini, M. Farsi, and S. Eini, "Multi-objective optimization of industrial membrane SMR to produce syngas for Fischer-Tropsch production using NSGA-II and decision makings," *J Nat Gas Sci Eng*, vol. 32, pp. 222–238, 2016, doi: 10.1016/j.jngse.2016.04.005.

[111] B. Modi, A. Mudgal, and B. Patel, "Energy and Exergy Investigation of Small Capacity Single Effect Lithium Bromide Absorption Refrigeration System," *Energy Procedia*, vol. 109, pp. 203–210, Mar. 2017, doi: 10.1016/J.EGYPRO.2017.03.040.

[112] M. M. Talbi and B. Agnew, "Exergy analysis: an absorption refrigerator using lithium bromide and water as the working fluids," *Appl Therm Eng*, vol. 20, no. 7, pp. 619–630, May 2000, doi: 10.1016/S1359-4311(99)00052-6.

[113] G.-Y. Ma and H.-X. Zhao, "Experimental study of a heat pump system with flash-tank coupled with scroll compressor," *Energy Build*, vol. 40, no. 5, pp. 697–701, Jan. 2008, doi: 10.1016/j.enbuild.2007.05.003.

[114] J. Aman, D. S. K. Ting, and P. Henshaw, "Residential solar air conditioning: Energy and exergy analyses of an ammonia–water absorption cooling system," *Appl Therm Eng*, vol. 62, no. 2, pp. 424–432, Jan. 2014, doi: 10.1016/J.APPLTHERMALENG.2013.10.006.

[115] A. R. Razmi, A. Arabkoohsar, and H. Nami, "Thermoeconomic analysis and multi-objective optimization of a novel hybrid absorption/recompression refrigeration system," *Energy*, vol. 210, p. 118559, Nov. 2020, doi: 10.1016/J.ENERGY.2020.118559.

[116] A. Mota-Babiloni, J. Navarro-Esbrí, V. Pascual-Miralles, Á. Barragán-Cervera, and A. Maiorino, "Experimental influence of an internal heat exchanger (IHX) using R513A and R134a in a vapor compression system," *Appl Therm Eng*, vol. 147, pp. 482–491, Jan. 2019, doi: 10.1016/j.applthermaleng.2018.10.092.

[117] S. Elbel and P. Hrnjak, "Experimental validation of a prototype ejector designed to reduce throttling losses encountered in transcritical R744 system operation," *International Journal of Refrigeration*, vol. 31, no. 3, pp. 411–422, May 2008, doi: 10.1016/J.IJREFRIG.2007.07.013.

[118] S. M. Alirahmi, M. Rostami, and A. H. Farajollahi, “Multi-criteria design optimization and thermodynamic analysis of a novel multi-generation energy system for hydrogen, cooling, heating, power, and freshwater,” *Int J Hydrogen Energy*, vol. 45, no. 30, pp. 15047–15062, May 2020, doi: 10.1016/j.ijhydene.2020.03.235.